UNIVERSIDADE FEDERAL DO PARÁ
INSTITUTO DE GEOCIÊNCIAS
PROGRAMA DE PÓS-GRADUAÇÃO EM GEOLOGIA E GEOQUÍMICA

TESE DE DOUTORADO Nº 136

GEOLOGIA, ALTERAÇÃO HIDROTERMAL E GÊNESE DO DEPÓSITO IOCG CRISTALINO, PROVÍNCIA MINERAL DE CARAJÁS, BRASIL

Tese apresentada por:

GUSTAVO SOUZA CRAVEIRO

Orientador: Prof. Dr. Raimundo Netuno Nobre Villas (UFPA)
Coorientador: Prof. Dr. Roberto Perez Xavier (UNICAMP)

BELÉM
2018

Universidade Federal do Pará
Instituto de Geociências
Programa de Pós-Graduação em Geologia E Geoquímica

GEOLOGIA, ALTERAÇÃO HIDROTERMAL E GÊNESE DO DEPÓSITO IOCG CRISTALINO, PROVÍNCIA MINERAL DE CARAJÁS, BRASIL
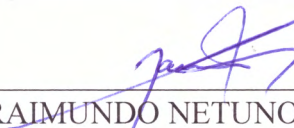
TESE APRESENTADA POR:

GUSTAVO SOUZA CRAVEIRO
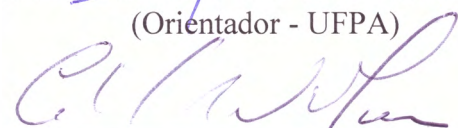
Como requisito parcial à obtenção de Grau de Doutor em Ciências na Área de **GEOLOGIA**

Data da Aprovação: 22 / 10 / 2018

Banca Examinadora:

_____
Prof. Dr. RAIMUNDO NETUNO NOBRE VILLAS
(Orientador - UFPA)

_____
Prof. Dr. CANDIDO AUGUSTO VELOSO MOURA
(Membro - UFPA)

_____
Prof. Dr. JOSÉ HAROLDO DA SILVA SÁ
(Membro - UFBA)

_____
Prof. Drª. LENA VIRGÍNIA SOARES MONTEIRO
(Membro - USP)

_____
Prof. Dr. RÉGIS MUNHOZ KRÁS BORGES
(Membro - UFPA)

Aos meus pais.

AGRADECIMENTOS

O autor agradece a todas as pessoas e entidades que concorreram para a realização deste trabalho, em especial:

- Ao Programa de Pós-Graduação em Geologia e Geoquímica da Universidade Federal do Pará, pelo fornecimento de infraestrutura e apoio financeiro;

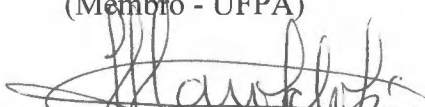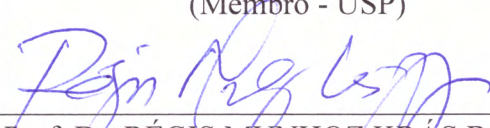- Ao CNPq pela concessão da bolsa de estudo de doutoramento. E ao INCT de Geociências da Amazônia pelo suporte financeiro;

- Ao Grupo de Metalogênese do Instituto de Geociências, pelo suporte técnico-científico;

- Ao Laboratório de Inclusões Fluidas do Instituto de Geociências da Universidade Federal do Pará, em especial ao Professor Régis Munhoz Krás Borges;

- Ao Laboratório de Microscopia Eletrônica de Varredura e Microanálises da Universidade Federal do Pará, em especial ao Professor Claudio Lamarão e à geóloga Gisele Tavares, pela presteza e aquisição de dados de química mineral.

- Ao Centro Regional para o desenvolvimento Tecnológico e Inovação da Universidade Federal de Goiás, em especial ao Professor José Affonso Brod, pela presteza e aquisição de dados de química mineral.

- Á geóloga Antonia Railine, pelo companheirismo, suporte técnico-científico e pelo incentivo incondicional.

- Aos meus pais, pelo alicerce e amor incomensurável.

- Ao professor Roberto Xavier, pelo suporte técnico-científico, e pela ajuda e por ter acreditado neste projeto.

- Por fim, ao Professor Netuno Villas, pelo exemplo como professor, pesquisador e amigo. Pelo incentivo, e que, incansável, sempre esteve disponível a ajudar e nunca deixou de acreditar em mim.

"Não vemos as coisas como elas são, mas como nós somos"

(Anais Nin)

RESUMO

O depósito Arqueano de cobre-ouro Cristalino está localizado a 40 km oeste da mina do Sossego, na terminação oeste da Zona de Cisalhamento Regional Carajás, na região da Serra do Rabo. Suas rochas hospedeiras são principalmente as rochas vulcânicas máficas da Formação Parauapebas, e subordinadamente, as FFB da Formação Carajás. Trabalhos de campo, dados petrográficos apoiados por MEV-EDS, somados a análises de microssonda eletrônica e dados de inclusões fluidas e sistemática de isótopos estáveis (O, H, C e S), permitiram caracterizar um sistema hidrotermal que foi responsável pelo desenvolvimento de sucessivas zonas de alteração na rocha encaixante. O metassomatismo sódico (650°C $\geq$ T > 400°C, and P > 1.8 Kbar) formou albita quase pura, turmalina schorlítica, minerais ricos em ETRL (alanita-Ce, monazita) associados a menores quantidades de calcita e quartzo. Foi seguido por alteração cálcico-férrica penetrante, onde foram produzidas abundante actinolita (X_{Mg} = 0.9-0.7, com até 0,6 % em peso de Cl), alanita-Ce (com até 0,6 % em peso de Cl) e magnetita, associados a disseminação de sulfeto e a corpos de substituição similares a brecha, compostos por calcopirita-pirita-magnetita-Au (associação mineral precoce). Localmente, em substituição à assembleia cálcico-férrica ocorre Fe-edenita (X_{Mg}=0.7 - 0.4, Cl com até 2.9 % em peso), produto de halos restritos de alteração sódico-cálcica. De 410°C para 220°C e 1.8 Kbar > P > 0.6 Kbar, assembleias de alterações anteriores foram superpostas por alterações potássica (K-feldspato, e subordinadamente biotita) e propilítica/carbonática (epidoto, clorita, calcita) nesta ordem. K-feldspato é praticamente estequiométrico, mas com elevados conteúdos de BaO (até 1,2 % em peso). Entre os minerais, clorita mostra maiores variações composicionais, parecendo ser controlada pelo tipo de rocha hospedeira, química do fluido hidrotermal e temperatura. Ambas chamosita e clinocloro (X_{Fe}=0.4-0.8) estão presentes, sendo a primeira variedade mais abundante. Conteúdos de cloro são, em geral, < 0,02 % em peso, sendo um pouco mais significantes em cloritas que substituem albitas com textura tabuleiro de xadrez (com até 0,06 % em peso). A associação de minério tardia (calcopirita±Au±pirita±hematita) é contemporânea com as alterações potássica e propilítica, gerando evidencias de que o sistema Cristalino evoluiu para os estágios finais com o aumento da fugacidade de oxigênio. O fluido mineralizante foi quente (>550°C), hipersalino e quimicamente próximo ao sistema H_2O-NaCl-$CaCl_2$-CO_2±$MgCl_2$±$FeCl_2$. Salinidades excederam 55.1% em peso equiv. de NaCl nos estágios precoces, mas diminuiu progressivamente para 7,9 % em peso equiv. de NaCl a partir de 250°C após a incursão de água superficial no sistema. Inicialmente enriquecido de ^{18}O e depletado em D ($\delta^{18}O_{vsmow}$

=+9,7 para +6,5 ‰; δD_{vsmow}= -30,8 para -40,2 ‰) e possivelmente derivado de fontes magmáticas, o fluido se tornou depletado em 18 O e enriquecido em D ($\delta^{18}O_{vsmow}$ =+5.57 to -0.28‰; δD_{vsmow}= -19.15 to -22.24‰) como resultado de diluição causada pela mistura com água meteórica. Valores de $\delta^{13}C_{VPDB}$ para calcita de veios e brechas (-6.5 para -3.8‰) são consistentes com fontes profundas de CO_2, provavelmente liberadas de câmaras magmáticas subjacentes. Valores de $\delta^{34}S_{VCDT}$ para calcopirita mostram uma estreita variação (+1.6 para +3.5 ‰) e indicam reservatórios homogêneos para o enxofre, certamente de origem ígnea. Embora a maioria das amostras apontam para uma filiação magmática, poucas revelam significante influência de rochas sedimentares em suas composições isotópicas. Principalmente transportados por complexos de cloro (>350°C), Cu e Au precipitaram em resposta a redução de temperatura e atividade de Cl$^-$ e aumento de pH. Um fluido aquoso e frio (200-150°C) e menos salino (21 – 3,1 % em peso equiv. de NaCl) parece ter circulado na área do depósito Cristalino, sendo aprisionadas em inclusões fluidas secundárias. Apesar de desconhecida, sua origem pode ter relação com intrusões graníticas Paleoproterozoicas próximas. Em comparação com outros depósitos IOCG Arqueanos de Carajás, particularmente aqueles que jazem no setor sul do Domínio Carajás, o depósito Cristalino mostra varia similaridades enquanto a composição dos fluidos e evolução, assim como assinaturas isotópicas de sulfetos e carbonatos.

Palavras-chave: Química mineral. Inclusões fluidas. Isótopos estáveis. Depósitos IOCG. Província Mineral de Carajás. Depósito Cristalino.

ABSTRACT

The Archean Cu-Au Cristalino deposit is located 40 km east from Sossego mine in the eastern end of the regional WNW-ESW Carajás shear zone, in the Serra do Rabo region. Its host rocks are mainly the mafic volcanic rocks of the Parauapebas Formation, and subordinately the BIF of the Carajás Formation. Field-work, petrographic data seconded by SEM-EDS, in addition to microprobe analysis and fluid inclusion and stable isotope (O, H, C and S) systematics, allowed characterizing a hydrothermal system that was responsible for the development of successive alteration zones in the wall rocks. Sodic metasomatism (650°C ≥ T > 400°C, and P > 1.8 Kbar) formed near pure albite, schorlitic tourmaline, REE-rich minerals (allanite-Ce, monazite) and minor calcite and quartz. It was followed by a more pervasive calcic-ferric alteration which produced abundant actinolite (X_{Mg} = 0.9-0.7 and up to 0.6 wt. % Cl), allanite-Ce (up to 0.6 wt. % Cl) and magnetite, associated with sulfide disseminations and replacement breccia-like bodies composed of chalcopyrite-pyrite-magnetite-Au (early ore association). Locally, Fe-edenite (X_{Mg}=0.7-0.4, Cl up to 2.9 wt. %) replaced calcic-ferric assemblages within restrict sodic-calcic alteration halos. From 410° down to 220° C and 1.8 Kbar > P > 0.6 Kbar, the previous alteration assemblages were overprinted by potassic (K-feldspar, minor biotite) and propylitic/carbonatic (epidote, chlorite, calcite) alterations, in this order. K-feldspar is practically stoichiometric, but with high contents of BaO (up to 1.2 wt. %). Chlorite shows the greatest compositional variation among all minerals and seems to have been controlled by the type of host rock, chemistry of the hydrothermal fluid and temperature. Both chamosite and clinochlore (X_{Fe}=0.4-0.8) are present, the former being more common. Chlorine contents are in general < 0.02 wt. % and a little more significant in chlorites that replaced chessboard albite (up to 0.06 wt. %). The late ore association (chalcopyrite±Au±pyrite±hematite) is contemporaneous with the potassic and propylitic alterations and bears evidence that the Cristalino system evolved to the final stages with increase in oxygen fugacity. The ore fluid was hot (> 550°C), hypersaline and chemically approached by the system H_2O-NaCl-$CaCl_2$-CO_2±$MgCl_2$±$FeCl_2$. Salinity exceeded 55.1 wt. % NaCl equiv. in the early stages but decreased progressively to 7.9 wt. % NaCl equiv. from 250° C on, after incursion of surficial water into the system. Initially ^{18}O-enriched/D-depleted ($\delta^{18}O_{vsmow}$ =+9.7 to +6.5 ‰; δD_{vsmow}= -30.8 to -40.2 ‰) and most likely derived from magmatic sources, the fluid became relatively ^{18}O-depleted/D-enriched ($\delta^{18}O_{vsmow}$ =+5.57 to -0.28‰; δD_{vsmow}= -19.15 to -22.24‰) as result of dilution caused by mixing with meteoric water. $\delta^{13}C_{VPDB}$ values for vein and breccia calcite (-6.5 to -3.8‰) are consistent with a deep

source for CO_2, which was probably released from an underlying magma chamber. The $\delta^{34}S_{VCDT}$ values for chalcopyrite show narrow variation (+1.6 to +3.5 ‰) and indicate a homogeneous reservoir for sulfur, which was likely of igneous origin. Although most data point to a magmatic affiliation, a few samples reveal significant influence of sedimentary rocks on their isotope composition. Mostly transported as chloride complexes (>350ºC), Cu and Au precipitated in response to decrease in temperature and Cl⁻ activity and increase in pH. An aqueous, colder (200-150º C) and less saline (21-3.1 wt. % NaCl equiv.) fluid appears to have circulated in the Cristalino deposit area, being trapped as secondary fluid inclusions. The origin is unknown, but it could be related to a nearby Paleoproterozoic granitic intrusion. The data presented here support previous interpretations that consider Cristalino as of IOCG typology. In comparison with other Archean Carajás IOCG deposits, particularly those that lie in the southern sector of the Carajás Domain, the Cristalino deposit shows many similarities regarding ore fluid composition and evolution, as well as the isotopic signature of sulfides and carbonates.

Keywords: Mineral Chemistry. Fluid Inclusion. Stable Isotopes. IOCG deposit. Carajás Mineral Province. Cristalino deposit.

LISTA DE ILUSTRAÇÕES

1. INTRODUÇÃO

2. THE CRISTALINO IOCG DEPOSIT: AN EXAMPLE OF MULTI-STAGE EVENTS OF HYDROTHERMAL ALTERATION AND COPPER MINERALIZATION

3. MINERAL CHEMISTRY AND GEOTHERMOMETRY OF ALTERATION ZONES, IOCG CRISTALINO DEPOSIT, CARAJÁS MINERAL PROVINCE, BRAZIL.

4. A FLUID INCLUSION AND STABLE ISOTOPE (O, H, S AND C) STUDY OF THE ARCHEAN IOCG CRISTALINO DEPOSIT, CARAJÁS PROVINCE, BRAZIL: IMPLICATIONS TO ORE GENESIS.

LISTA DE TABELAS

3. MINERAL CHEMISTRY AND GEOTHERMOMETRY OF ALTERATION ZONES, IOCG CRISTALINO DEPOSIT, CARAJÁS MINERAL PROVINCE, BRAZIL.

4. A FLUID INCLUSION AND STABLE ISOTOPE (O, H, S AND C) STUDY OF THE ARCHEAN IOCG CRISTALINO DEPOSIT, CARAJÁS PROVINCE, BRAZIL: IMPLICATIONS TO ORE GENESIS.

SUMÁRIO

1 INTRODUÇÃO

1.1 APRESENTAÇÃO

As reservas de cobre no Brasil são da ordem de 11 Mt (ca. 1.5% das reservas mundiais), 85% das quais concentradas na Província Mineral de Carajás. Depósitos de cobre são abundantes no Domínio Carajás e podem ser divididos em depósitos de óxido de ferro-cobre-ouro, IOCG na sigla em inglês, e depósitos de cobre-polimetálicos. Os depósitos IOCG contêm as maiores tonelagens e teores (da ordem de 1 Gt e até 1,4 % Cu e até 0,8 g/t Au; Hunh *et al*.1999b, Lancaster-Oliveira 2002, Tallarico *et al*. 2005, Pinto 2012). A despeito dessa imensa riqueza, os estudos até aqui realizados ainda são insuficientes para responder questões importantes ligadas à fonte dos fluidos mineralizantes, metais e enxofre, bem como à idade das mineralizações e ao papel de corpos graníticos na evolução do sistema hidrotermal.

Ressente-se da falta de dados estruturais, isotópicos (radiogênicos e estáveis), microtermométricos e de química mineral, dentre outros, embora disponíveis, em certa medida, para os depósitos Igarapé Bahia, Salobo, Sossego e Visconde. (Réquia & Xavier 1995, Dreher *et al*. 2007, Monteiro *et al*. 2008, Silva *et al*. 2015).

Com esta tese buscou-se ampliar a base de dados existentes sobre depósitos IOCG da Província Mineral de Carajás ao se investigar o depósito Cristalino, um dos maiores do Domínio Carajás. Foram definidas suas principais características geológicas, tipos de alteração hidrotermal e estilos de mineralização, além de se prover dados de química mineral, de isótopos estáveis (O, H, C e S) e de inclusões fluidas com vista ao entendimento de seu arcabouço metalogenético.

A tese foi elaborada segundo o modelo de integração de artigos científicos. Três artigos foram preparados, um deles submetido a periódico nacional e os outros dois a periódicos internacionais. Esses artigos, sumarizados abaixo, compõem capítulos e são precedidos por um texto integrador (conforme normas do Programa de Pós-graduação em Geologia e Geoquímica-PPGG).

Capítulo 2 – Artigo 1 - The Cristalino IOCG deposit: an example of multi-stage events of hydrothermal alteration and copper mineralization. Submetido para publicação à revista Brazilian Journal of Geology. Apresenta dados geológicos da área do depósito e petrográficos dos litotipos que hospedam a mineralização, modos de ocorrência do minério e sequência paragenética das zonas de alteração com os minerais que as tipificam. Em particular, foram

identificados dois principais estágios de mineralização, um mais precoce e rico em magnetita, formado a maiores profundidades e em regime dúctil-rúptil, e outro mais tardio, com hematita, gerado em níveis crustais mais rasos sob condições rúpteis.

Capítulo 3 – Artigo 2 - Mineral chemistry and geothermometry of alteration zones, IOCG Cristalino Deposit, Carajás Mineral Province, Brazil. Submetido para a publicação à revista Journal of South American Earth Sciences. O artigo apresenta dados de química mineral de silicatos selecionados que permitiram apontar a influência relativa das rochas hospedeiras e dos fluidos em sua composição, além de definir microambientes geoquímicos em que eles se formaram. Tratou também da obtenção de dados geotermométricos que subsidiaram o conhecimento da história termal do sistema hidrotermal Cristalino.

Capítulo 4 – Artigo 3 - A fluid inclusion and stable isotope (O, H, S and C) study of the Archean IOCG Cristalino deposit, Carajás Province, Brazil: Implications to ore genesis, que foi submetido à publicação na revista Ore Geology Reviews. Nele são apresentados dados microtermométricos e de isótopos estáveis, com os quais foi caracterizado composicionalmente o fluido mineralizador, balizadas as condições de P-T, apontadas fontes potenciais e sugerida uma evolução ao longo da história termal do sistema Cristalino. Foram também inferidos reservatórios para carbono e enxofre presentes, respectivamente, na calcita e calcopirita de veios e brechas.

Em seguida, são apresentadas as conclusões e as referências bibliográficas utilizadas na elaboração desta tese.

1.2 LOCALIZAÇÃO E ACESSO AO DEPÓSITO CRISTALINO

O acesso ao município de Curionópolis, região sudeste do Pará, onde está localizado o depósito Cristalino (Fig. 1A) se dá, por via terrestre, a partir de Belém, pelas rodovias BR 316 e BR 010 até a cidade de Dom Eliseu, BR 222 até a cidade de Marabá, PA-155 até a cidade Eldorado de Carajás, PA-275 até a cidade de Parauapebas e, por fim, PA-160 até a Vila Planalto. Vias privadas e não pavimentadas dão acesso à área do depósito Cristalino, bem como às instalações do Projeto Cristalino de propriedade da mineradora Vale.

O depósito Cristalino está integrado ao contexto estrutural da terminação leste da Falha Carajás, na região da Serra do Rabo, sudeste do Pará. Dista 40 km a leste da mina do Sossego e está imediatamente ao sul do depósito de Cu-polimetálico Estrela, e a cerca de 10 km a nordeste do depósito IOCG Borrachudo (Fig. 1B).
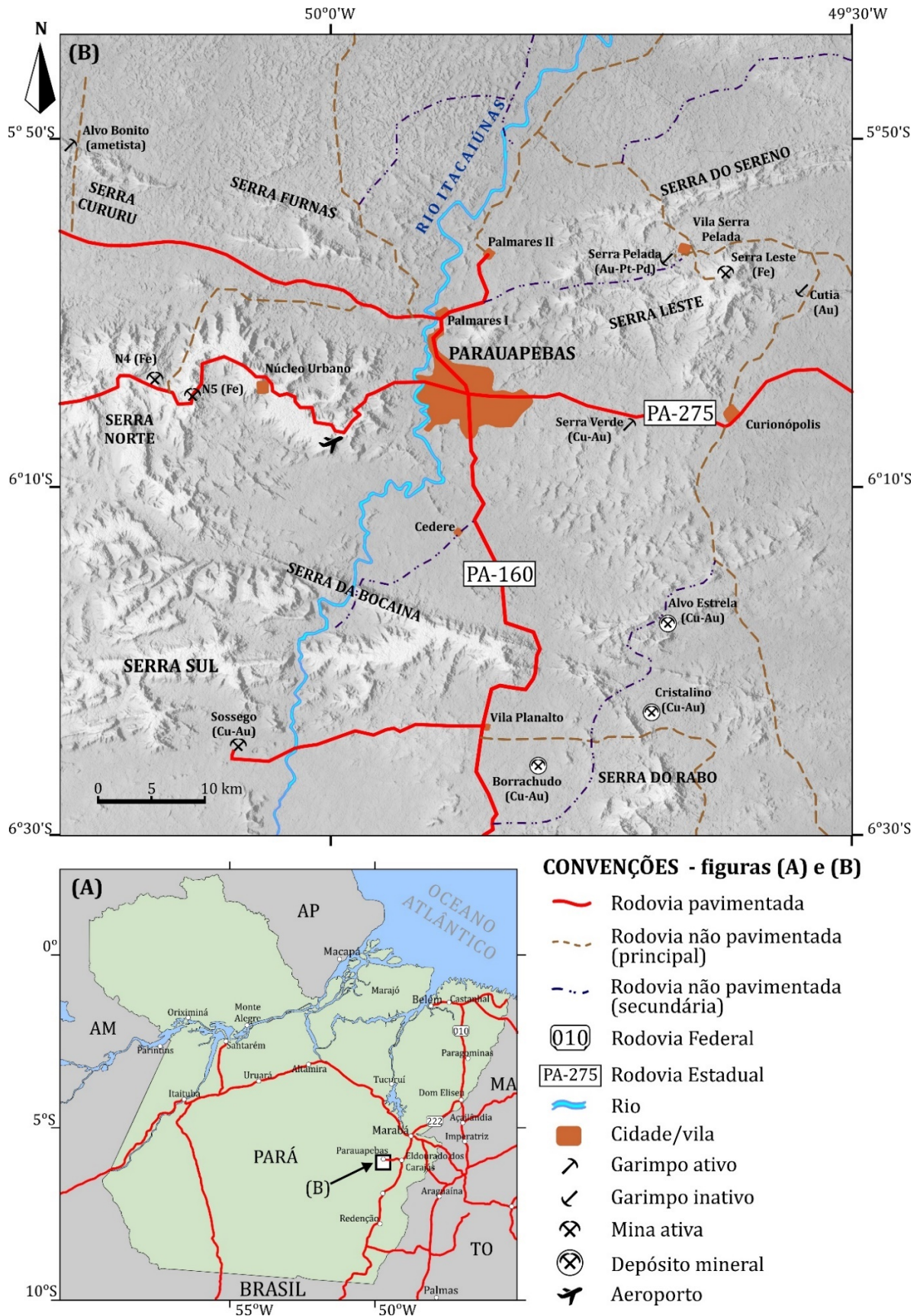
Figura 1- (A) Localização e vias de acesso à área do depósito Cristalino no Estado do Pará. (B) Imagem de relevo sombreado ASTER GDEM, onde estão representadas as principais feições geomorfológicas da porção nordeste do Domínio Carajás com a localização do depósito Cristalino.

1.3 CONTEXTO TECTÔNICO E GEOLOGIA REGIONAL DA PROVÍNCIA MINERAL DE CARAJÁS

O Cráton Amazonas é um extenso segmento crustal constituído e estruturado no Arqueano e Mesoproterozoico, tendo alcançado estabilidade tectônica em torno de 1,0 Ga (Brito Neves & Cordani, 1991). Os modelos de evolução e compartimentação tectônica mais aceitos são os de Santos *et al*. (2000, 2004, 2006) e Tassinari & Macambira (1999, 2004), e ambos defendem, com base em dados geocronológicos, que o desenvolvimento e evolução do Cráton se deu por sucessivos episódios de acresção continental a partir de um Protocráton arqueano. As principais diferenças entre os dois modelos residem em denominações e definições dos limites das províncias tectônicas. Na interpretação de Santos *et al*. (2000), adotada neste trabalho (Fig. 2) em virtude do maior volume de dados geocronológicos U-Pb (dados mais robustos), o Cráton é dividido em sete províncias tectônico-geocronológicas (Figura 1): Carajás (3000 – 2500 Ma), Transamazonas (2030 – 1990 Ma), Tapajós – Parima (2030 – 1860 Ma), Amazônia Central (1900 - 1860 Ma), Rondônia – Juruena (1850 – 1540 Ma), Rio Negro (1820 – 1520 Ma) e Sunsás (1450 – 1000 Ma). Em uma revisão mais recente, Vasquez *et al*. (2008) sugeriram, baseado no trabalho de Santos (2003), novos limites entre os domínios Tapajós-Parima e Amazonas Central, e a inclusão do Domínio Santana Central na Província Transamazonas, desmembrado da Província Carajás. A Província Mineral de Carajás está inserida na Província Carajás, especificamente no Domínio Carajás, e representa uma das mais importantes províncias minerais do mundo, especialmente pelas grandes concentrações de Fe, Cu, Au, além de Mn, Ni, Cr, Zn, entre outros, descobertas na área desde o final da década de 70.

A Província Carajás (Fig. 3) está situada na porção leste-sudeste do Cráton Amazonas, no Estado do Pará. É limitada ao Norte e Sul pela Província Transamazonas (domínios Bacajá e Santana do Araguaia, respectivamente), a oeste pela Província Amazônia Central, e a leste pelo Cinturão Araguaia (Província Tocantins). É dividida em dois domínios distintos (Vasquez *et al*. 2008): o Domínio Rio Maria (DRM) ao sul, e o Domínio Carajás (DC) ao norte.
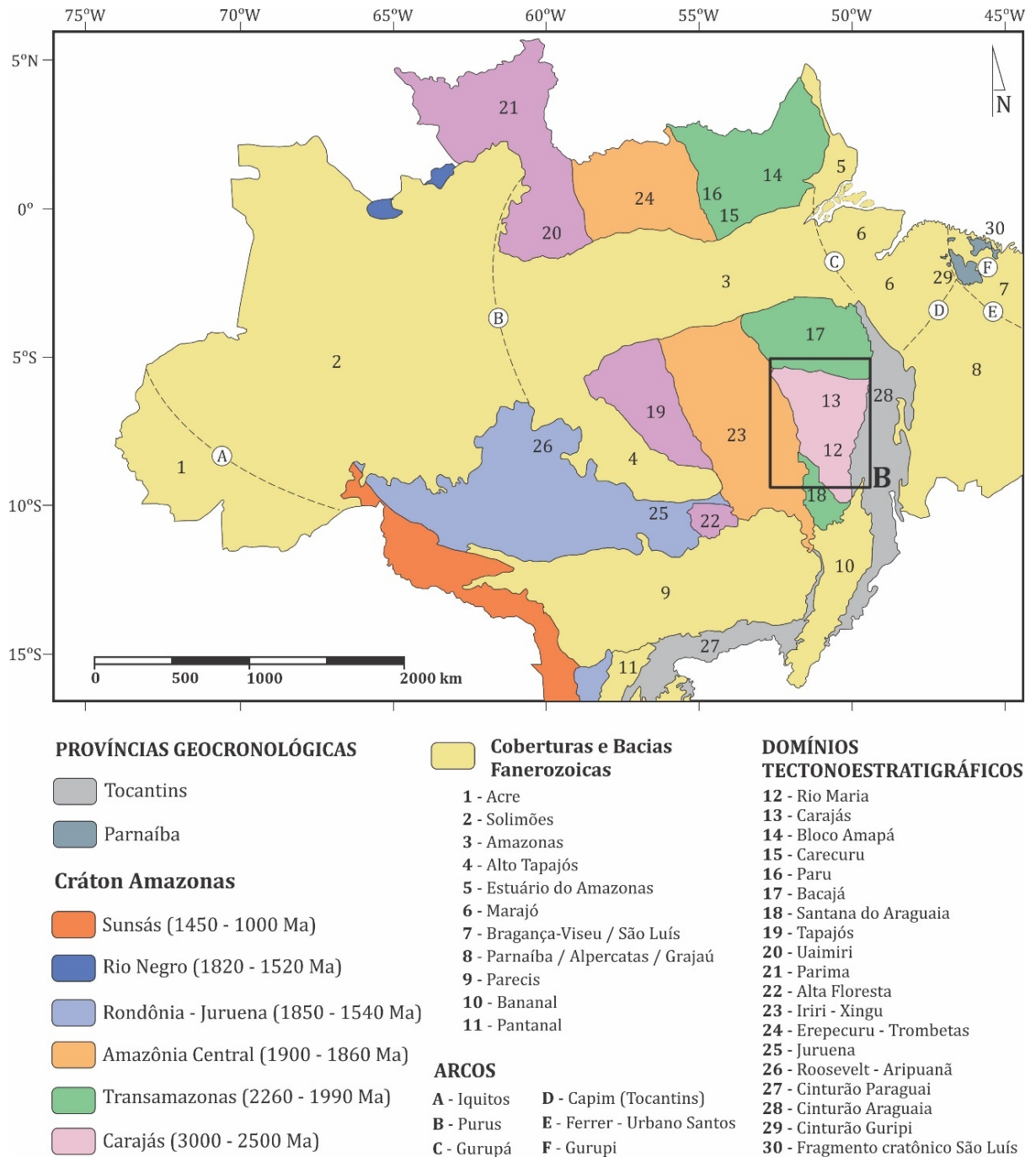
Figura 2. Cráton Amazônico e a compartimentação em províncias tectônico-geocronológicas segundo Santos *et al.* (2000).

O Domínio Rio Maria (DRM) é composto por *greenstone belts* (3,0-2,90 Ga; Macambira & Lafon 1995, Souza *et al.* 2001) e diversos granitoides colocados em período relativamente curto (120 Ma). Esses granitoides compreendem uma série TTG antiga (2,98-2,93 Ga; Macambira & Lancelot 1996, Althoff *et al.* 2000, Leite *et al.* 2004, Almeida *et al.* 2011), a suíte sanukitoide Rio Maria (~2,87 Ga; Macambira & Lancelot 1996, Oliveira *et al.* 2009, 2010), uma série TTG mais jovem (~2,87-2,86 Ga; Leite *et al.* 2004, Almeida *et al.*

2011), uma suíte leucogranodiorito-granítica (~2,87 Ga; Almeida *et al.* 2010) e leucogranitos de afinidade cálcio-alcalina com alto potássio (~2,87-2,86 Ga; Leite *et al.* 1999, 2004). A estruturação principal do DRM é resultado de processos de encurtamento colisional/acrescional N-S durante o Mesoarqueano (Althoff *et al.* 2000), embora também afetados pelo tectonismo vertical de "domos e quilhas" (Rosière *et al.* 2006).

Comparativamente ao DRM, o Domínio Carajás mostra evolução mais complexa, tendo sido subdividido em dois subdomínios distintos (Dall'Agnol *et al.* 2006). Ao Norte está a Bacia Carajás (Neoarqueano), enquanto ao sul está o sub-domínio de Transição, dominado por granitoides mesoarqueanos a neoarqueanos que têm sido incluídos nos complexos Xingu e Pium, assim como na Suíte Plaquê (Feio *et al.* 2013). Como o sub-domínio de Transição não representa uma crosta arqueana tectonicamente homogênea, uma divisão adicional tem sido proposta baseada em novos dados geoquímicos e geocronológicos (Dall'Agnol *et al.* 2013): o Domínio Canaã do Carajás na porção norte, composto de rochas granitoides Mesoarqueanas, e o Domínio Sapucaia ao sul, constituído por rochas correlacionadas geoquimicamente à suíte sanukitoide do DRM.

À despeito desses avanços recentes, o limite entre o DC e o DRM ainda permanece indefinido, embora Vasquez *et al.* (2008) aceitem que este esteja na região de Sapucaia. Ademais, a origem tectônica do sub-domínio de Transição não é consensual, sendo argumentado tanto como uma extensão do DRM retrabalhado durante os eventos neoarqueanos que afetaram a bacia Carajás (Dall'Agnol *et al.* 2006) ou um bloco tectônico independente sem relação com o DRM (Feio *et al.* 2013).

1.3.1 Evolução tectônica do Domínio Carajás

O Domínio Carajás mostra um embasamento arqueano (>2,83 Ga) recoberto discordantemente por sequencias sedimentares metavulcânicas (de 2,76 a 2,72 Ga), sendo ambos cortados por intrusões ígneas Neoarqueanas (2,76-2,70 Ga; Machado *et al.* 1991, Barros *et al.* 2004, Sardinha *et al.* 2006, Feio *et al.* 2012). Zircões detríticos forneceram idades U-Pb de até 3,2 Ga, sugerindo participação de crosta paleoarqueana na composição do Domínio Carajás (Galarza & Macambira 2002, Dall'Agnol *et al.* 2005).

A aglutinação da assembleia de embasamento ocorreu em 3,08 - 2,93 Ga e 2,87 - 2,83 Ga, relacionado a processos acrecionários e colisionais envolvendo segmentos crustais consolidados (Feio *et al.* 2013). Entre 2,76 e 2,70 Ga, o DC foi submetido a nova atividade tectônica, marcada tanto por deposição das sequencias vulcanossedimentares do Supergrupo

Itacaiúnas (Docegeo 1988), quanto por plutonismo. A deposição dessas rochas ocorreu em uma bacia cuja origem tem sido atribuída a riftes intracontinentais (Gibbs *et al.* 1986, Docegeo 1988, Macambira 2003, Tallarico *et al.* 2005) ou a um arco magmático (Meirelles & Dardenne 1991, Teixeira 1994, Lindenmayer *et al.* 2005, Lobato *et al.* 2005).

As estruturas mais importantes do Domínio Carajás são consideradas contemporâneas às intrusões tipo-A de 2,76 a 2,71 Ga (Barros *et al.* 2001, 2009, Feio *et al.* 2013, Dall'Agnol *et al.* 2013). Tais estruturas são resultantes de encurtamento crustal de direção NE-SE associado a zonas de cisalhamento obliquas contidas nas rochas do Supergrupo Itacaiúnas e evidenciadas por foliação vertical E-W nas unidades do embasamento. Reativações ocorreram pelo menos três vezes, do Arqueano ao Paleoproterozoico (Costa *et al.* 1995, Araújo *et al.* 1988, Pinheiro e Holdsworth 2000).

1.3.2 Síntese da Litoestratigrafia do Domínio Carajás

As rochas do embasamento do Domínio Carajás (DC), usualmente representadas pelos complexos Pium e Xingu, têm sido nos últimos anos, conforme os estudos avançam, desmembradas em diversos corpos arqueanos.

O Complexo Pium, originalmente descrito como uma associação granulítica (Docegeo 1988, Araújo & Maia 1991), tem suas melhores exposições ao longo do Rio Cateté. O mapeamento detalhado e trabalhos de petrografia levaram a separação dos verdadeiros granulitos, atualmente incluídos na unidade Ortogranulito Chicrim-Cateté, de gabros e noritos não metamorfisados aflorantes ao longo do rio Pium. Estes têm sido incluídos na unidade Diopsídeo Norito Pium (Ricci & Carvalho 2003, Vasquez *et al.* 2008). O Complexo Pium, por outro lado, foi primeiramente descrito como sendo constituído por gnaisses migmatíticos, granulitos, granitoides e rochas supracrustais (Silva *et al.* 1974), se estendendo além dos limites do Domínio Carajás. Mais recentemente, trabalhos detalhados (Gomes e Dall'Agnol 2007, Vásquez *et al.* 2008, Feio 2011, Moreto *et al.* 2011, 2015, Feio *et al.* 2012, 2013) individualizaram diversos granitoides arqueanos, como o Tonalitos Bacaba (3,0 Ga), o Trondhjemito Rio Verde (2,93; 2,86 Ga), o Granito Canaã dos Carajás (2,95 – 2,93 Ga), o Tonalito Campina Verde (2,87 – 2,85 Ga), e os granitos Bom Jesus, Cruzadão (2,86 – 2,85 Ga) e Serra Dourada (2,85 – 2,83 Ga). Como resultado, sua área de exposição tem sido drasticamente reduzida, tornando-se restrita essencialmente a ortognaisses e migmatitos.

Granitos alcalinos a cálcio-alcalinos, representados pelas suítes Plaquê e Planalto, intrudem o embasamento do Domínio Carajás. A Suíte Plaquê consiste de corpos

leucoganíticos, alongados na direção E-W, que exibem diversas variedades texturais e caráter sin-colisional (Macambira *et al.* 1996). Na região de Tucumã, esses granitos revelaram idades de 2729 ± 29 e 2736 ± 24 Ma (Pb-Pb evaporação em zircão; Avelar *et al.* 1999). A Suíte Planalto compreende o granito Planalto, próximo à região da Serra do Rabo, e outros corpos, todos deformados e alongados na direção E-W. Essa suíte é representada por sieno a monzogranitos, metaluminosos a fracamente peraluminosos, e álcali-feldspato granitos de afinidade alcalina (Hunh *et al.* 1999b, Gomes 2003). Idades de cristalização de 2747 ± 2 Ma (Pb-Pb evaporação em zircão; Hunh *et al.* 1999b) e 2738 ± 2 e 2730 ± 5 Ma (U-Pb SHRIMP em zircão; Feio *et al.* 2012) foram determinadas para esses granitos.

A bacia Carajás é essencialmente preenchida por rochas metavulcanossedimentares que formam o Supergrupo Itacaiúnas (2,76 - 2,73 Ga) e são superpostas pelas rochas siliciclásticas da Formação Águas Claras, além de serem cortadas por corpos máfico-ultramáficos neoarqueanos e granitos neoarqueanos e paleoproterozoicos. O Supergrupo Itacaiúnas é dividido nos grupos Grão Pará, Igarapé Salobo, Igarapé Bahia e Igarapé Pojuca (Docegeo 1988) que são composicionalmente similares, mas distintos em relação ao grau de deformação e metamorfismo. Esses grupos hospedam a maioria dos depósitos de Fe, Cu e Au que são conhecidos na Província Mineral de Carajás (Villas e Santos 2001).

O Grupo Grão Pará consiste de espessa pilha (~400m) de jaspilito (Formação Carajás; Beisiegel *et al.* 1973) intercalada por unidades vulcânicas (metabasaltos e metariolitos), denominada como Formação Parauapebas (Meireles *et al.* 1984). A Formação Carajás é o protólito das enormes reservas de minério de Fe de alto teor da PMC. Datações U-Pb do Grupo Grão Pará forneceram idade de 2758 ± 39 Ma (Wirth *et al.* 1986), 2758 ± 39 Ma (Olszewski *et al.* 1989) e 2759 ± 2 Ma (Machado *et al.* 1991).

O Grupo Igarapé Salobo ocorre na terminação norte da zona de cisalhamento Cinzento. Essa unidade foi primeiramente definida por Docegeo (1988) como uma sequência vulcanossedimentares com variado grau de metamorfismo (xisto verde baixo a granulito), sendo constituída por clorita quartzo xistos, anfibólio ± faialita ± magnetita xisto, formações ferríferas bandadas e granada ± silimanita quartzito. Datações U-Pb em zircão em rochas vulcânicas forneceram a idade de 2761 ± 3 Ma (Machado *et al.* 1991). Vasquez *et al.* (2008) redefiniram o Grupo Igarapé Salobo, incluindo no mesmo apenas as rochas metavulcanossedimentares, com mineralização polimetálica (Cu-Fe ± Au ± Mo ± Co ± U), expostas na Serra do Salobo. Esses autores excluíram as rochas metamórficas de alto grau desse grupo e, de acordo com essa nova classificação, o Grupo Igarapé Salobo seria composto

dominantemente de rochas metaclásticas (quartzo-clorita xistos, granada-biotita xistos e quartzitos), e, subordinadamente, rochas metavulcânicas máficas e intermediárias, com foliação vertical WNW-ESSE e feições de intensa transposição.
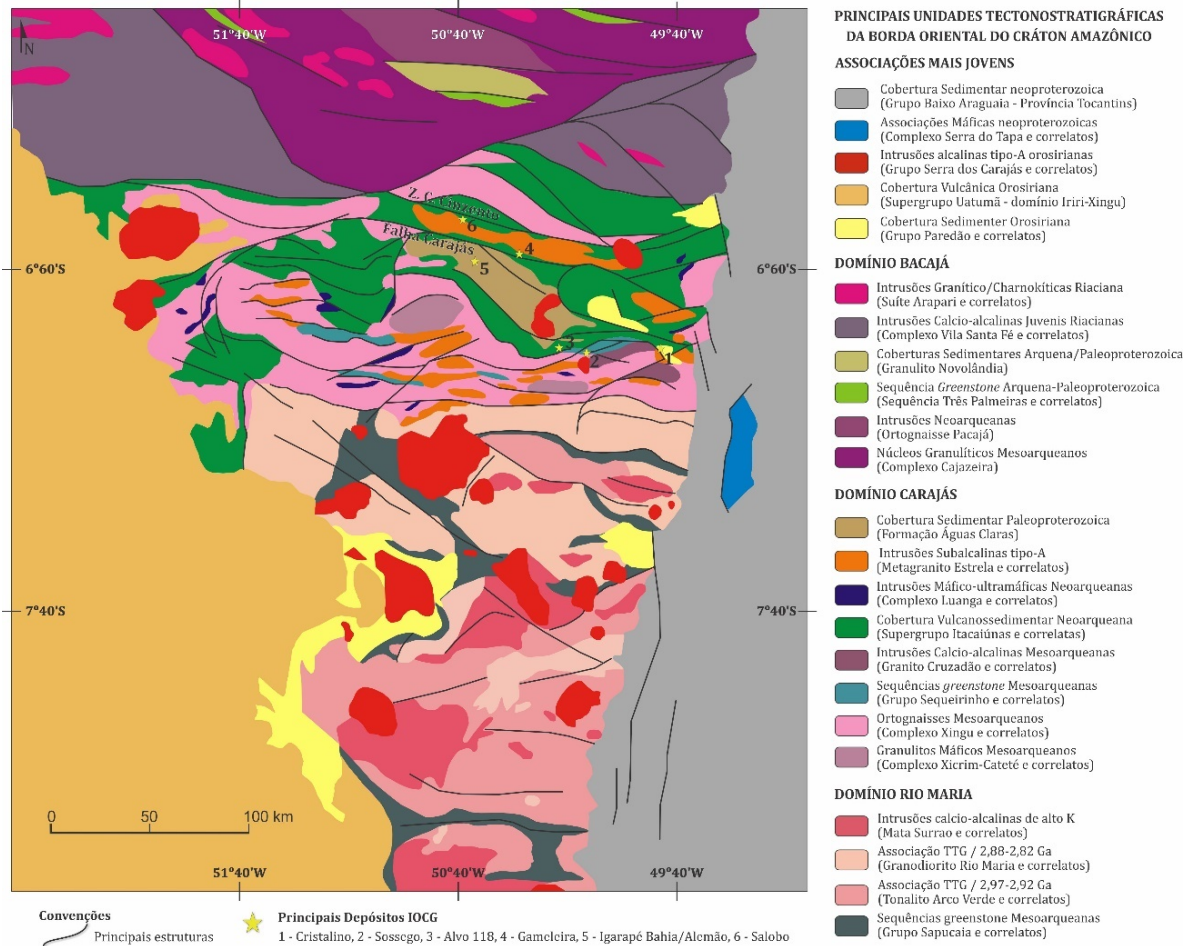
Figura 3- Principais unidades tectonoestratigráficas da borda leste do Cráton Amazônico (compilado e modificado de Vasquez *et al.* 2008, Xavier *et al.* 2012, Dall'Agnol *et al.* 2013, Feio *et al.* 2013, Tavares 2015).

O Grupo Igarapé Bahia é descrito como uma pilha subvertical de rochas metavulcanossedimentares, subdividida em unidade inferior, representada por rochas metavulcânicas máficas intercaladas com formações ferríferas bandadas, e unidade superior, com rochas metapiroclásticas intermediárias a félsicas e metassedimentares clásticas e químicas (Soares *et al.* 1999, Ronzê *et al.* 2000). A estruturas primárias, ígneas e sedimentares estão em sua maioria preservadas, a despeito da intensa alteração hidrotermal a que foram submetidas (Soares *et al.* 1999, Ronzê *et al.* 2000, Tallarico *et al.* 2005, Galarza *et al.* 2008). Brechas hidrotermais ocorrem concordantemente entre as unidades e são as hospedeiras dos principais corpos de minério de Cu-Au conhecidos (Almada e Villas 1999,

Ronzê *et al.* 2000, Tavaza e Oliveira 2000, Dreher *et al.* 2007, Tallarico *et al.* 2005). Datações de rochas vulcânicas forneceram idade de 2748 ± 34 Ma (U-Pb SHRIMP em zircão, Tallarico *et al.* 2005) a 2776 ± 12 Ma (Pb-Pb evaporação em zircão, Galarza *et al.* 2008).

O Grupo Igarapé Pojuca (Docegeo 1988) consiste de unidade vulcanossedimentar que de direção NW-SE, metamorfisada em condições de fácies xisto verde baixo a anfibolito, intercalada com rochas metassedimentares psamo-pelíticas e formação ferrífera bandada (Medeiros Neto e Villas 1985; Docegeo 1988; Lindenmayer *et al.* 2001; Vasquez *et al.* 2008), sendo hospedeiras do primeiro depósito de sulfeto contendo esfalerita descoberto na PMC. Uma idade U-Pb de 2732 ± 3 Ma, determinada em monocristal de zircão em anfibolitos (Machado *et al.* 1991), foi interpretada como idade do metamorfismo regional.

O Grupo Rio Novo (Araújo e Maia 1991, Oliveira 1994) é contemporâneo ao Supergrupo Itacaiúnas e suas melhores exposições estão na região de Serra Pelada, tendo sido primeiramente descrito como sequência metavulcanossedimentar por Hirata *et al.* (1982) e Meireles *et al.* (1984). É composto por metamáficas, meta-ultramáficas, metaquartzitos, formações ferríferas bandadas, mica-xistos e metapelitos ricos em grafita, manganês e ferro (Vasquez *et al.* 2008). Como essas rochas são intrudidas pelo Complexo máfico-ultramáfico Luanga (2736 ± 7 Ma, Machado *et al.* 1991) e o Complexo granítico Estrela (2736 ± 7 Ma, Pb-Pb evaporação em zircão; Barros *et al.* 2004), essa é considerada como idade mínima do Grupo Rio Novo.

Historicamente, o Grupo Buritirama tem sido também incluído no Supergrupo Itacaiúnas (Docegeo 1988). Em uma interpretação diferente, Vasquez *et al.* (2008) redefiniram essa unidade como Formação Buritirama, que junto com a Formação Taparipe, formam o Grupo Vila União no domínio Bacajá, tendo o Complexo Cajazeiras como seu embasamento.

A Suíte Serra Leste (Ferreira Filho *et al.* 2013) consiste de um grupo de intrusões máfico-ultramáficas (Complexos Luanga, Formiga e Lago Grande) mineralizadas em EGP (Elementos dos Grupo da Platina), localizados na porção leste do DC. Esses complexos máfico-ultramáficos são intrusivos em rochas gnáissicas do Complexos Xingu e em rochas vulcanossedimentares do Grupo Grão Pará. Os Complexos Luanga e Lago Grande, corpos melhor investigados (Mansur e Ferreira Filho 2016; Teixeira *et al.* 2015), foram datados em 2736 ± 3 Ma (Machado *et al.* 1991) e 2722 ± 53 Ma (Teixeira *et al.* 2015), respectivamente, indicando que um magmatismo Neoarqueano sobrepõe o vulcanismo bimodal do Grupo Grão Pará. A assembleia metamórfica encontrada nos complexos Lago Grande e Luanga é

compatível com metamorfismo em fácies anfibolito, que resultou na substituição ampla dos minerais ígneos primários em ambos os complexos (Teixeira *et al.* 2015; Mansur e Ferreira Filho 2016).

A Suíte Intrusiva Cateté (Macambira e Vale 1997) corta as rochas do Complexo Xingu e é formada por corpos máfico-ultramáficos alongados nas direções E-W e N-S, e se diferenciam dos complexos Luanga e Lago Grande pela ausência de deformação e metamorfismo. É constituída por intrusões como Serra da Onça, Serra do Puma, Serra do Jacaré, Serra do Jacarezinho, Igarapé Carapanã, Fazenda Maginco, Ourilândia, Vermelho, entre outros.

O Complexo Vermelho compreende uma intrusão máfico-ultramáfica NE-SW, hospedeira de minério de Ni e localizada cerca de 2 km a NW da cidade Canaã dos Carajás, na região de Serra Leste. É composto por dunitos, harzburgitos, gabronoritos, noritos (zona inferior) e um ortopiroxenito contendo cromitito que gradaciona verticalmente para dunitos-harzburgitos (zona superior) (Siepierski 2016).

Os granitos subalcalinos de alto potássio arqueanos Complexo Estrela, Serra do Rabo, Igarapé Gelado e Old Salobo intrudem somente as unidades da bacia Carajás (Feio 2011) e possuem idades de cristalização variando de 2763 a 2573 Ma.

A Formação Águas Claras consiste de cobertura sedimentar na porção centro-leste da bacia Carajás, disposta discordantemente sobre as rochas do Supergrupo Itacaiúnas. Considerada como um depósito costeiro (Nogueira *et al.* 1995), inclui metapelitos, meta-arenitos e raros metaconglomerados fluviais. Sua idade de deposição permanece incerta, mas posicionado entre 2,70 a 2,65 Ga, de acordo com idades U-Pb em zircão monocristais de diques intermediários e máficos que cortam essa unidade (Mougeot *et al.* 1996, Dias *et al.* 1996, Trendall *et al.* 1998).

Equivalente à Formação Águas Claras, a Formação Rio Fresco está disposta discordantemente sobre o Grupo Rio Novo, e hospeda o depósito de Au-EGP de Serra Pelada que tem sido interpretado como de origem epigenética (Grainger *et al.* 2008).

Outras coberturas sedimentares em Carajás incluem o Grupo Paredão e a Formação Caninana. Essas unidades representadas por brechas, conglomerados polimíticos e arenitos (Pereira *et al.* 2009) relacionados a ambientes de leques aluviais e fluvial entrelaçado. Zircões detríticos da Formação Caninana forneceram idades máximas deposição em 2,01 Ga (Pereira *et al.* 2009).

O Paleoproterozoico é representado por diversos granitos (Serra dos Carajás, Cigano e Pojuca) que cortam o embasamento e as sequencias metavulcanossedimentares (Dall'Agnol *et al.* 2005, Vasquez *et al.* 2008). Esses granitos revelam idades U-Pb que variam de 1883 ± 2 a 1874 ± 2 Ma (Machado *et al.* 1991, Rämö *et al.* 2002, Dall'Agnol *et al.* 2005). São granitos não deformados, tipo-A, metaluminosos a peraluminosos (Dall'Agnol *et al.* 2005), agrupados na Suíte Intrusiva Serra dos Carajás (Dall'Agnol *et al.* 2005). Outros granitos têm sido associados com a suíte, como os granitos Rio Branco e Breves. Este último hospeda mineralização de Cu ± Au ± (Mo, W, Sn), cujo sistema hidrotermal foi descrito como híbrido, envolvendo fluidos magmáticos e meteóricos, que interagiram com rochas oxidadas pré-existentes (Botelho *et al.* 2005).

Os Granito Formiga, Gabro Rio da Onça, Diabásio Rio Pajeú, além de diques máficos, são registros importantes de atividade magmática do Neoproterozoico no DC. Localizado a 2 km nordeste do depósito de Au-EGP de Serra Pelada, o Granito Formiga é um *stock* de álcali-feldspato granito cristalizado a cerca de 600 Ma, hospedeiro de minério de Au-(Cu) geneticamente ligado ao mesmo (Grainger *et al.* 2008). Descrito a primeira vez por Docegeo (1988), o Gabro Rio da Onça ocorre na porção sudeste da bacia Carajás como diques máficos (piroxênio-olivina gabros) de direção preferencial NNW-SSE, localmente deformados. Datações K-Ar de diques de gabros próximos à borda da Província Carajás e subparalelo ao Cinturão Araguaia forneceram idades de 507 ± 29 Ma (Gomes *et al.* 1975). Por outro lado, Macambira *et al.* (2013) descreveram um dique de diabásio não deformado (Diabásio Rio Pajeú) que exibem a mesma direção e foram correlacionados pelos autores ao magmatismo máfico Jurássico-Triássico que afetou a porção norte do Brasil.

1.4   REVISÃO DE DEPÓSITOS IOCG

Proposta por Hitzman *et al.* (1992), a classe de depósitos proterozoicos de óxido de Fe (Cu-U-Au-ETR) passou a ser conhecida mundialmente pelo acrônimo IOCG (*Iron-oxide copper gold*) (William & Skirrow 2000, Sillitoe 2003, William *et al.* 2005, Groves *et al.* 2010) para se referir a depósitos de altos teores e tonelagens em que óxidos de Fe são comumente associados a Cu, Au, Ag, U, Ba, F e elementos terras raras leves (ETRL). São da Província Carajás os primeiros depósitos IOCG de idade arqueana que foram descobertos.

Enquanto classe genética, os depósitos IOCG ainda permanecem em debate, embora agrupem um conjunto de depósitos com várias características em comum. Dentre essas características Williams *et al.* (2005) e Groves *et al.* (2010) destacam: *1)* Cu e Au como metais econômicos; *2)* notáveis zonas de alteração hidrotermal e forte controle estrutural,

sendo comum o desenvolvimento de brechas; *3)* abundante magnetita pobre em Ti e/ou silicatos de Fe; *4)* enriquecimento em ETRL e sulfetos que incluem calcopirita-bornita-calcocita e pirrotita; *5)* ausência de veios de quartzo durante a sulfetação, e alteração que resulta em decréscimo no conteúdo de SiO_2 das rochas encaixantes, e; *6)* uma relação temporal com atividade magmática, mas sem necessidade de relação espacial com intrusões que poderiam ser fontes diretas.

Os depósitos IOCG diferem em idade, tamanho, razão Cu/Au, rochas hospedeiras, assembleia de alteração, estilos de mineralização, assinatura geoquímica, e propriedades físico-química dos fluidos. Importantes exemplos são os depósitos Neoarqueanos Salobo, Cristalino, Sossego (corpo Sequeirinho), Igarapé Bahia/Alemão e Paleoproterozoicos, tais como o corpo Sossego e Alvo 118, na Província Mineral de Carajás (Brasil), os mesoproterozoicos Olympic Dam e Enerst Henry na Australia, e os mesozoicos Candelaria, Manto Verde e Raúl-Condestable, no Chile (Haller & Fontboté 2009, Groves *et al.* 2010, Moreto *et al.* 2015).

Vários modelos genéticos têm sido propostos para os depósitos IOCG, sem que ainda haja consenso entre os autores. Os maiores questionamentos concernem à natureza da fonte dos fluidos, sendo que alguns autores defendem fontes magmáticas, enquanto outros argumentam fontes não-magmáticas (Barton & Johnson 2004, Williams *et al.* 2005).

Os modelos magmáticos defendem a liberação de fluidos oxidados, salinos, ricos em metais e pobres em S a partir de magmas contemporâneos, com deposição posterior do minério causada pela mistura com fluido externo (por exemplo, meteórico). As fontes são inferidas como tendo componentes de arcos magmáticos cálcio-alcalinos (Pollard *et al.* 1998, Sillitoe 2003) ou magmas fortemente alcalinos a carbonatíticos (Groves *et al.* 2010). Da mesma forma, a presença de CO_2 pode influenciar o particionamento dos álcalis entre os magmas silicáticos e os fluidos, e a potencial geração de salmouras com altas razões Na/K as quais podem ser responsáveis pela alteração sódica presente em muitos depósitos IOCG (Pollard 2001).

Os modelos não-magmáticos sugerem fluidos derivados de bacias rasas ou aqueles que evoluíram em ambientes metamórficos de média-crosta. Ambos os tipos requerem ambientes especializados com disponibilidade de cloro não magmático. Intrusões podem agir como fonte termal da convecção e mobilização das salmouras não magmáticas, como aquelas que derivam de água superficial evaporada ou pela interação com depósitos evaporíticos pré-existentes (Barton & Johnson 1996) ou mesmo pela quebra de silicatos que contenham Cl em

sua composição, como a escapolita. Vale lembrar que os modelos metamórficos não necessitam uma fonte de calor ígnea, mas intrusões contemporâneas podem estar presentes e contribuir tanto com calor quanto com componentes (por exemplo, Fe, Cu) ao fluido (William *et al.* 2005).

Outros aspectos críticos acerca da gênese dos IOCG, além do fluido mineralizante, têm relação com a fonte dos metais e outros componentes vitais do sistema mineralizador, tal como Cl e S. São também ainda debatidos seu ambiente geológico e a associação tempo-espaço com as suítes graníticas, especialmente no caso dos exemplos pré-cambrianos.

No Domínio Carajás, a maioria dos depósitos IOCG conhecidos está agrupada em dois setores ao longo ou próximo a zonas de cisalhamento regionais. Ao longo da zona de cisalhamento Cinzento está o Cinturão Norte do Cobre compreendendo os depósitos Salobo, Igarapé Bahia-Alemão, Gameleira, Paulo Afonso, Furnas, Polo e Igarapé Cinzento/Alvo GT46. O Cinturão Sul do Cobre se estende pelo contato entre as rochas do Supergrupo Itacaiúnas e do embasamento do Domínio Carajás, aproximadamente alinhados à zona de cisalhamento Carajás. Inclui os depósitos Sossego, Cristalino, Alvo 118, Bacaba, Castanha, Visconde, Jatobá e Bacuri (Augusto *et al.* 2008, Grainger *et al.* 2008, Monteiro *et al.* 2008, Torresi *et al.* 2012, Xavier *et al.* 2012, Moreto *et al.* 2015).

Na tentativa de sistematizar os sistemas de mineralização de cobre no Domínio Carajás, eles foram divididos em depósitos de óxido de ferro-cobre-ouro (IOCG) e depósitos de cobre-polimetálicos. Depósitos como Gameleira, Breves, Estrela, Tarzan, entre outros, diferem dos IOCG por apresentarem menores tonelagens, menores teores e suítes metálicas mais diversas, tais como Cu, Au, Li, Be, Sn, W, Mo, Bi e Co, além das idades, notadamente paleoproterozoicas (Xavier *et al.* 2017).

Muitas idades têm se concentrado entre 2,76 Ga e 2,57 Ga (Huhn *et al.* 1999a, Pimentel *et al.* 2003, Tallarico *et al.* 2005, Neves *et al.* 2006, Galarza *et al.* 2008) e de 1,90 a 1,88 Ga (Moreto *et al.* 2015). A integração de dados geocronológicos mais recentes sugere que os sistemas IOCG de Carajás foram gerados durante múltiplos episódios hidrotermais, agrupados, segundo Xavier *et al.* (2017), em três intervalos: (i) 2,72 a 2,68 Ga, representados pelos corpos Sequeirinho-Pista (depósito Sossego, 245 Mt @ 1.1 % em peso de Cu; 0.28 g/t Au, Lanscaster-Oliveira *et al.* 2000) e depósito Cristalino (379 Mt @ 0.66% em peso Cu; 0.3 g/t Au; Pinto 2012); (ii) ca. 2,56 Ga registrado no depósito Salobo (1,11 Gt @ 0,69 % em peso Cu; 0,86 g/t Au, Pinto 2012) e Igarapé Bahia/Alemão (219 Mt @ 1.4% em peso Cu, 0.86 g/t Au) no setor sul do Domínio Carajás; (iii) 1.90 a 1.88 Ga, tendo com exemple os corpos

Sossego-Curral (depósito Sossego) e depósito Alvo 118 (*ca.* 100 Mt @ 1,0 % em peso Cu/ 0.3 g/t Au, Pinto 2012), todos no setor sul do Domínio Carajás.

O intervalo mais antigo, entre 2,72 e 2,68 Ga é, em parte, sincrônico à colocação da Suíte Planalto (2,74-2,72 Ga), o que sugere participação desses granitoides como fonte termal (>500°C) e possível contribuição de fluidos hipersalinos (salmouras com contribuição magmática) (Soares *et al.* 2001, Tassinari *et al.* 2003, Silva *et al.* 2005, Galarza *et al.* 2008, Silva *et al.* 2012, 2015, Moreto *et al.* 2015). A idade de 2,56 Ga pode ter relação com um evento transpressivo destral que gerou as zonas de cisalhamento regional Carajás-Cinzento (ca. 2,6-2,5 Ga; Pinheiro & Holdsworth, 2000) assim como a intrusão do Granito Old Salobo (2573 ± 2 Ma) (Tallarico *et al.* 2005).

O intervalo mais jovem (1,90 a 1,88 Ga) é mais facilmente associado à granitogênese tipo A de 1,88 Ga que ocorreu em domínios da Província Carajás. As intrusões granitoides podem ter funcionado como fontes de calor, causando circulação regional de fluidos hidrotermais em descontinuidades crustais reativadas, levando ao desenvolvimento de zonas de alteração hidrotermal e mineralização durante o Paleoproterozoico (Grainger *et al.* 2008, Moreto *et al.* 2015).

Apesar de todos os avanços nos estudos desses depósitos, os dados metalogenéticos e petrogenéticos ainda são insuficientes para definir precisamente a relação entre as mineralizações e os eventos intrusivos e/ou metamórficos. De acordo com Groves *et al.* (2010), sistemas IOCG pré-cambrianos, tais como Salobo e Cristalino, envolvem na constituição de suas salmouras, fluidos exsolvidos de magmas ricos em voláteis, formados a grandes profundidades. Neste sentido, admite-se a participação líquidos advindos de manto litosférico sub-crustal metassomatizado. Xavier *et al.* (2012) sugerem que, à despeito da origem dúbia dos fluidos hidrotermais (magmático, metamórfico ou ambos), a transição para um regime estrutural rúptil e rúptil-dúctil atuante na bacia Carajás favoreceu a diluição e resfriamento do sistema hidrotermal pelo influxo de fluidos superficiais.

1.5   APRESENTAÇÃO DO PROBLEMA

A descoberta do depósito australiano de cobre e ferro Olympic Dam, em 1975 desencadeou debates sobre depósitos de óxido de ferro cobre-ouro. Em seguida à publicação do artigo de Hitzman *et al.* (1992), o entendimento desses depósitos se beneficiou grandemente dos trabalhos de Barton & Johnson (1996), Pollard (2001), Williams *et al.* (2005) entre outros. Estes autores apontam como característica principal comum a assinatura

geoquímica marcada por abundante óxido de ferro associado a quantidades variáveis de Cu, Au, Ag, U, Ba, F e ETRL. Apontam também a variedade de rochas encaixantes, fluidos aquosos de alta salinidade, geralmente canalizados por sistemas controlados estruturalmente e responsáveis por intenso metassomatismo sódico e sódico-cálcico regional, e potássico e/ou hidrolítico (sericita - clorita) proximal às zonas mineralizadas, a depender do nível crustal (Williams *et al.* 2005, Groves *et al.* 2010, Xavier *et al.* 2010). Apesar dos importantes avanços, ainda não há consenso sobre questões críticas, tais como a origem dos fluidos hidrotermais, enxofre e metais.

Atualmente, há dois modelos principais para explicar a gênese de depósitos de IOCG, que se distinguem por envolver ou não fluidos magmáticos (Barton e Johnson 2004). No modelo magmático-hidrotermal, as mineralizações estariam relacionadas ao escape de salmouras oxidadas, metalíferas e pobres em enxofre, advindas de magmas em fracionamento, contemporâneos à deposição do minério. Os magmas podem ser cálcico-alcalinos primitivos de arco magmático (Sillitoe 2003) ou magmas graníticos dos tipos I ou A, em ambiente intracratônico ou de arco magmático distal (Pollard 2006).

O modelo que envolve fluidos essencialmente não magmáticos pode ser dividido em dois subtipos: (1) fluidos derivados principalmente de fontes superficiais (meteóricas e/ou bacinais); (2) fluidos de origem profunda e gerados por reações metamórficas. Ambos os subtipos precisam de disponibilidade de cloreto não magmático para constituir a fase fluida. No primeiro subtipo, intrusões magmáticas atuariam como fonte térmica para ativar a convecção dos fluidos e a interação com leitos evaporíticos. No modelo metamórfico, a desestabilização de minerais hidratados seria a principal fonte de fluidos hidrotermais, contudo, uma fonte de calor magmática não é indispensável, embora intrusões contemporâneas possam ocorrer associadas e contribuir com calor, fluidos e metais (Barton & Johnson 2004, Williams *et al.* 2005).

A gênese dos depósitos de IOCG localizados na Província Carajás também não é consensual. Similar aos análogos mundiais, independente das idades, segue também a polêmica sobre a fonte dos fluidos hipersalinos. Xavier *et al.* 2008 identificaram assinatura evaporítica marinha com base em isótopos de boro ($^{11}B/^{10}B$) em turmalina associada ao minério cupro-aurífero dos depósitos de Igarapé Bahia, Salobo e Sossego, entretanto, a participação de fluidos magmáticos, embora não predominante, não tenha sido descartada.

A deposição das sequencias vulcanossedimentares do Supergrupo Itacaiúnas por volta de 2,76 Ga em ambiente marinho raso pode ter iniciado o ciclo metalogenético do cobre no

Domínio Carajás. Depósitos IOCG neoarqueanos e paleoproterozoicos exibem um geral controle estrutural relacionado à zona de cisalhamento WNW-ESSE Carajás, que marca o limite entre as unidades supracrustais e as rochas do embasamento mesoarqueano (2,85 a 3,00 Ga). Esses depósitos também exibem relação espacial e temporal com o magmatismo tipo-A, félsico, de idade 2, 76 a 2,73 Ga, e 2,57 Ga (*e.g*, Granito Old Salobo), e para os congêneres paleoproterozoicos, relação temporal com o magmatismo tipo-A 1,88 Ga.

Diferentes estilos de mineralização cuprífera na escala de depósitos, no entanto, têm sido descritos, indicando que corpos de minério podem ser formados a condições e idades diferentes. Tal superposição de sistemas IOCG foi registrada no depósito Sossego (Monteiro *et al.* 2008, Moreto *et al.* 2015) em que idades neoarqueanas e paleoproterozoicas foram obtidas para diferentes corpos de minério (Sequeirinho e Salobo). Os depósitos IOCG Borrachudo (Previato 2016) e Grota Funda (Hunger 2017) também apresentam diferentes associações de minério que se formaram durante estágios de alteração bem distintos, o que, na falta de dados geocronológicos, pode ser interpretado como evidências indiretas de possível superposição de eventos hidrotermais de idades e níveis crustais distintos.

O atual conhecimento sobre depósitos IOCG em Carajás permite concluir que: (1) depósitos IOCG são produtos de múltiplos eventos hidrotermais controlados estruturalmente e colocados a diferentes níveis crustais, durante o Arqueano e o Paleoproterozoico; (2) os fluidos mineralizantes são em geral resultado da mistura de fluidos quentes, hipersalinos e metalíferos com outros tipos de fluidos, e que essa mistura poderia desencadear, pelo menos em parte, a precipitação de minerais de minério.

Nesse contexto, o estudo sobre a geologia do depósito Cristalino, definição das assembleias paragenéticas, química de minerais e composição e fonte de fluidos hidrotermais podem contribuir para a compreensão dos processos de formação desse depósito e do sistema IOCG de Carajás como um todo. Adicionalmente, a comparação do depósito Cristalino com outros depósitos IOCG trará subsídios para a geração de modelos de mineralização de Cu-Au regional em Carajás.

São listadas abaixo algumas questões ainda em aberto sobre a gênese dos depósitos IOCG de Carajás:

1. Haveria influência do magmatismo granítico na formação dos depósitos? Quais granitoides/suítes intrusivas no Domínio Carajás seriam adequados para fornecer fluidos e metais para os depósitos IOCG? De acordo com as conclusões de Tallarico *et al.* (2005), seriam os granitos Jovem Salobo e Itacaiúnas, de idade 2,57 Ga, capazes de mobilizar

quantidades de fluidos hidrotermais suficientes para provocar mineralizações cupro-auríferas em Carajás?

2. Quais fluidos alimentam os sistemas hidrotermais relacionados aos depósitos IOCG de Carajás? Há contribuições de fluidos de fontes diversas? Qual a fonte dos fluidos hipersalinos responsáveis pelas alterações sódica e sódico-cálcica precoces registradas em todos os depósitos IOCG de Carajás?

3. Quais as fontes do enxofre, carbono e metais? As rochas encaixantes e nas cercanias dos depósitos seriam reservatórios potenciais para fornecê-los? Ou haveria fontes distais envolvidas no processo? Revisões sobre o tema (Grainger *et al.* 2008, Xavier *et al.* 2012, Xavier *et al.* 2017) sustentam que intrusões graníticas, apesar da relação espacial ou mesmo temporal com mineralizações IOCG em Carajás, não são provedoras de metais. Groves *et al.* (2010) apontam magmas de derivação mantélica, máficos e ultramáficos, ricos em voláteis, como fonte de metais e fluidos para depósitos IOCG.

4. Quais as condições de formação e mecanismos de precipitação do minério? Em Carajás, a maioria dos sistemas hidrotermais que resultou em mineralização cupro-aurífera parece ter evoluído de ambientes rúptil-dúcteis a francamente rúpteis associados à infiltração de água de derivação externa e à queda de temperatura. Seria essa uma condição necessária? Qual o papel do pH, f_{O2}, f_{S2} na estabilidade dos complexos que transportam Cu, Au e outros metais?

1.6   OBJETIVOS

Como objetivo principal, a presente tese visa a: (1) reconhecer os principais litotipos hospedeiros do minério; (2) identificar e estabelecer relações espaciais e temporais entre as várias zonas de alteração hidrotermal; (3) avaliar o controle que as rochas hospedeiras/ou fluidos possam ter tido na composição química de minerais hidrotermais; (4) estimar as condições P e T de formação das zonas de alteração e do minério; (5) caracterizar composicionalmente os fluidos hidrotermais e apontar suas fontes potenciais, extensivas ao carbono e enxofre; (6) contribuir para o entendimento da gênese do depósito; e (7) estabelecer comparações com outros depósitos IOCG de Carajás, especialmente aqueles localizados no setor sul do Domínio Carajás.

1.7   MATERIAIS E MÉTODOS

Durante o desenvolvimento dessa pesquisa, e com o intuito de alcançar os objetivos propostos, foram adotados os seguintes procedimentos metodológicos:

1.7.1. Pesquisa Bibliográfica

Ocorreu de maneira contínua, enfocando em tópicos relacionados aos temas abordados, dentre eles: a) principais características de depósitos tipo IOCG em nível mundial e de Carajás; b) trabalhos acerca de processo hidrotermais, tais como reações químicas, processos físicos associados ao transporte e precipitação de metais, processos físico-químicos condicionantes, bem como outros pontos considerados cruciais para a determinação de modelos genéticos; c) a evolução do contexto geológico da Província Mineral de Carajás (PMC); d) teoria e aplicação dos métodos e técnicas utilizadas em metalogenia, incluindo petrografia, minerografia, química mineral, inclusões fluidas e isótopos estáveis.

1.7.2. Atividades de Campo

Foram realizadas duas etapas de campo, uma em outubro de 2013, e outra em agosto de 2014, quando foram visitados os galpões do Projeto Cristalino e da mina do Sossego. Nestas oportunidades, foram descritos e fotografados nove testemunhos de sondagem (FD-58, FD-96, FD-107, FD-155, FD-209, FD-224, FD-266, FD-325 e DH-00003), perfazendo aproximadamente 5000 m de testemunhos descritos, que atravessam as principais rochas encaixantes do minério e das zonas hidrotermalizadas. Desses testemunhos foram coletadas amostras representativas dos principais litotipo, tipos de alteração e das zonas mineralizadas, para a condução dos estudos metalogenéticos subsequentes.

1.7.3. Petrografia

Foram preparadas cerca de 120 seções delgadas-polidas de amostras dos testemunhos. Os dados petrográficos foram obtidos em microscópio Zeiss, de luz transmitida e refletida, modelo Axioplan 40, do Laboratório de Metalogênese do IG-UFPA. O foco foi a descrição dos aspectos primários ainda preservados nas rochas hospedeiras, a definição dos principais tipos de alteração, suas assembleias paragenéticas, e as relações entre os estágios, bem como a definição da assembleia de sulfetos (minério) e seus modos de ocorrência.

1.7.4. Microscopia Eletrônica de Varredura (MEV-EDS)

Esta técnica foi utilizada para refinar o exame petrográfico por meio de imagens de elétrons retroespalhados e análises químicas semi-quantitativas (por meio do EDS - Espectroscopia por energia dispersiva) em minerais selecionados. O intuito foi o refinamento

da assembleia de minerais metálicos, da assembleia de minerais hidrotermais acessórios, tais como inclusões de minerais de ETR. As análises foram realizadas em equipamento modelo LEO-1430, no Laboratório de Microscopia Eletrônica de Varredura da UFPA (LABMEV), sob a supervisão do Prof. Dr. Cláudio Lamarão.

1.7.5. Química Mineral

Após os trabalhos petrográficos e de MEV, e, partindo das considerações acerca das questões paragenéticas, foram selecionadas 12 lâminas delgadas e polidas, representativas das rochas alteradas do depósito Cristalino para a análises de microssonda. Foram analisados os minerais feldspatos, anfibólios, alanita, turmalina e clorita.

As análises e imagens de elétrons retroespalhados foram obtidos no Centro Regional de Tecnologia e Inovação (CRTI) da Universidade Federal do Pará, e no Laboratório de Microanálises do Instituto de Geociências da Universidade Federal do Pará, ambos utilizando Microssonda Eletrônica modelo JEOL JXA-8230.

As análises foram realizadas em seções polidas metalizadas com carbono, empregando técnica dispersiva de comprimento de onda, com voltagens de 15 kV, com corrente na sonda de 20 nA e um diâmetro de feixe de $10\mu m$. Uma variedade de padrões foram utilizados para a calibração dos elementos, incluindo albita, barita, celestina, coríndon, diopsídio, Fe_2O_3, fluorita, microclina, Mn-ortoclásio, olivina, jadeíta, quartzo, rutilo, sodalita e wolastonita naturais, e os padrões sintéticos A-128, A-408, AN_100, CaF_2 e CeO_2, Cl_Scap, $LaPO_4$, $NdPO_4$, $PrPO_4$, $SmPO_4$, $ThSiO_4$, UO_2, e YAG.

Foram obtidos de 60 a 190 pontos de análises nos cristais de feldspato, anfibólio, alanita, turmalina e clorita, e suas composições catiônicas foram recalculadas com base em 8, 23, 12,5, 24,5 e 28 átomos de oxigênio, respectivamente. Para alanita e turmalina, foram utilizadas as recomendações de Ercit (2002) e Tindle et al. (2002). As concentrações de Fe^{3+} e Li, especificamente para turmalina foram estimadas com base em cálculos estequiométricos.

As condições de temperatura para a formação de actinolita foram estimadas por meio do geotermômetro plagioclásio-anfibólio (Holland & Blundy 1994). Para os cálculos, foram usadas 158 composições de actinolita, as quais cumprem as seguintes exigências: $Ca^B > 1,50$, (1,70 – 2,11 apfu) $(Na+K)_A < 0,50$ apfu (0,07 – 0,30) e $Al^{vi} < 0,7$ apfu (0,06 - 0,60 apfu), em uma pressão estimada de 2 Kbar para os estágios precoces de alteração no Depósito Cristalino (Craveiro et al. submetido c). A composição do plagioclásio foi fixada em $X_{Ab} = 0,98$ e $X_{an} = 0,01$ e correspondem à média de 57 análises dos feldspatos no depósito Cristalino.

As temperaturas de formação da clorita foram baseadas em 187 análises pontuais, usando a equação empírica proposta por Cathelineau & Nieva (1985), com as correções de Al^{iv} com o aumento da razão Fe/(Fe+Mg) (Kranidiotis & MacLean 1987).

1.7.6. Estudo de Inclusões Fluidas

Foram confeccionadas mais de 20 lâminas bipolidas para o estudo de inclusões fluidas (IF), de amostras representativas das zonas mineralizadas e hidrotermalizadas. Foi realizada petrografia de IFs em lâminas de quartzo e calcita da massa rochosa e de veios e brechas mineralizados.

A sistemática utilizada na petrografia e testes para a organização dos grupos de IFs seguiu as recomendações Shepherd *et al.* (1985), Goldstein & Reynolds (1994), van den Kerkhof & Hein (2001), Wilkinson (2001) e Samson *et al.* (2003), entre outros. Os testes microtermométricos para obtenção das temperaturas de mudanças de fase foram conduzidos em platina Linkam THSMG600, capaz de alcançar temperaturas de -180 a + 650 °C, do Laboratório de Metalogênese, do Instituto de Geociências, da Universidade Federal do Pará.

Foram feitos testes de calibração periódico, usando o ponto tríplice do CO_2 puro (-56,6ºC) e da H_2O (0,0 ºC). As composições (sistema) dos fluidos foram estimadas a partir das temperaturas de eutéticos, com base nos dados experimentalmente definidos para sistemas simples por Borisenko (1977, 1982), Davis *et al.* (1990) e Spencer *et al.* (1990).

1.7.7. Isótopos Estáveis

Foram selecionadas amostras de minerais hidrotermais, representativos dos estágios de alteração do depósito Cristalino e provenientes de rochas vulcânicas alteradas e veios e brechas mineralizadas, para a determinação das composições isotópicas. Foram 12 amostras de silicatos, 10 de carbonatos, 10 de sulfetos e 5 de óxidos, totalizando 37 amostras. Após terem sido fragmentadas com martelo e grau de ágata, as frações de amostras foram separadas manualmente, com auxílio de lupa binocular, e imã de mão. Para algumas análises as amostras foram também pulverizadas.

As análises isotópicas em actinolita, turmalina, clorita (oxigênio e hidrogênio), quartzo, epidoto, magnetita (oxigênio) e calcopirita (enxofre) foram realizadas no Queen's Facilities for Isotope Research (QFIR), do Departamento de Ciências Geológicas, Queen's University, no Canadá. Já as análises de carbono e oxigênio em calcitas foram realizadas no Laboratório de Isótopos Estáveis (LABISE) do Departamento de Geologia da Universidade

Federal de Pernambuco. As análises de isótopos estáveis consistem de uma linha de extração dos elementos a partir do mineral por aquecimento, seguida de separação do elemento desejado por meio de armadilhas físicas e químicas, e por fim, a detecção dos isótopos em espectrômetro de massa. Os resultados são expressos na notação convencional delta (δ), per mil (‰).

A extração do oxigênio a partir da estrutura dos silicatos foi feita por meio do aquecimento das amostras a cerca de 550-600°C, seguindo o método desenvolvido por Clayton & Mayeda (1963), e a composição isotópica determinada em espectrômetro de massa Thermo-Finnigan Delta^{Plus} XP. Para as análises de hidrogênio, foi seguida a metodologia de Kyser & O'Neil (1984). As amostras foram aquecidas a 100°C em cápsulas de prata por uma hora, e em seguida carregadas em amostrador automatizado. A composição isotópica foi medida usando um analisador elementar de termo-combustão Thermo-Finnigan thermo-combustion elemental analyzer (TC/EA) associado a um espectrômetro de massa para isótopos estáveis de fluxo contínuo Thermo-Finnigan Delta^{Plus} (CF-IRMS). Os valores de δ^{18}O e δD são apresentados em relação ao padrão V-SMOW (*Vienna Standard Mean Ocean Water*), e possuem precisão de 0,1‰.

A composição isotópica de enxofre foi obtida usando um espectrômetro Finningan MAT 253 com o espectrômetro de massa Costech ECS 4010 acoplado. Os valores de δ^{34}S são apresentados em relação ao padrão V-CDT (*Vienna Canyon Diablo Troilite*), e possuem reprodutibilidade de 0,2 ‰.

E as composições de δ^{18}O e δ^{13}C em calcita foram determinadas a partir da reação com H$_3$PO$_4$ @ 100% a 25°C por12 horas, seguidas de evaporação e análise no espectrômetro de modelo Finnigan Delta-E. Os valores são dados em relação aos padrões V-PDB (*Vienna Pee Dee Belemnite*) e, no caso do δ^{18}O, também ao V-SMOW.

2 THE CRISTALINO IOCG DEPOSIT: AN EXAMPLE OF MULTI-STAGE EVENTS OF HYDROTHERMAL ALTERATION AND COPPER MINERALIZATION

Gustavo Souza Craveiro

Roberto Perez Xavier

Raimundo Netuno Nobre Villas

Brazilian Journal of Geology - Manuscript ID BJGEO-2018-0015

1 mensagem

Tatiana Alonso <onbehalfof@manuscriptcentral.com> 6 de março de 2018 16:34
Responder a: secretaria@zeppelini.com.br
Para: craveiro@ufpa.br
Cc: craveiro@ufpa.br, xavier@ige.unicamp.br, netuno@ufpa.br

06-Mar-2018

Dear Mr. Craveiro:

Your manuscript has been screened for possible publication in the Brazilian Journal of Geology and was forwarded to the Associated Editor, who will handle the peer-review process.

Please note that this message constitutes a confirmation of submission for manuscript ID BJGEO-2018-0015, entitled "The Cristalino IOCG deposit: an example of multi-stage events of hydrothermal altera-tion and copper mineralization", to the Brazilian Journal of Geology.

Please mention the above manuscript ID in all future correspondence or when calling the office for questions. If there are any changes in your street address or e-mail address, please log in to ScholarOne Manuscripts at https://mc04.manuscriptcentral.com/bjgeo-scielo and edit your user information as appropriate.

You can also view the status of your manuscript at any time by checking your Author Center after logging in to https://mc04.manuscriptcentral.com/bjgeo-scielo.

Thank you for submitting your manuscript to the Brazilian Journal of Geology.

Sincerely,
Brazilian Journal of Geology Editorial Office

The Cristalino IOCG deposit: an example of multi-stage events of hydrothermal alteration and copper mineralization

Gustavo Souza Craveiro[a], Roberto Perez Xavier[b], Raimundo Netuno Villas[a]
[a]Instituto de Geociências, Universidade Federal do Pará.
[b]Instituto de Geociências, Universidade Estatual de Campinas.

Abstract

The Cristalino deposit is located 40 km east of Sossego mine, Carajás. The orebody lies along a NW-SE-striking shear zone and is mainly hosted by the Neoarchean bi-modal volcanics of the Grão Pará Group. Field works, and petrographic data seconded by SEM-EDS analysis allowed recognizing an early sodic metasomatism that was followed by calcic-ferric, potassic and propylitic alterations, and finally by carbonation. The volcanic rocks were altered under deformation regimes that changed from ductile-brittle to brittle. The deposit resulted from two mineralizing stages. The early stage took place at a greater depth and produced an ore association composed chiefly of chalcopyrite, pyrite, and magnetite as disseminations, breccia, and veins particularly in Ca-Fe altered rocks. The later stage occurred at a shallower depth and formed a practically magnetite-free ore association, consisting essentially of chalcopyrite-hematite±pyrite in breccias and veins generated mostly during the potassic alteration. These ore associations indicate that the hydrothermal system evolved with temperature decrease and increase in fO_2, Cu/Fe ratio and sulfur activity, suggesting their precipitation from two distinct fluids. Cristalino is conceived as a multi-stage IOCG deposit like others lying in the Carajás E-W corridor of IOCG systems.

Keywords: IOCG, metallogenesis, hydrothermal system, Neoarchean, Carajás Province.

Resumo

O depósito Cristalino localiza-se a 40 km leste da mina do Sossego, Carajás. O corpo de minério jaz ao longo de zona de cisalhamento regional NW-SE e, está principalmente hospedado nas rochas vulcânicas bimodais Neoarqueanas do Grupo Grão Pará. Trabalhos de campo, dados petrográficas apoiados por análises MEV-EDS permitiram reconhecer um metassomatismo sódico precoce, que foi seguido por alterações cálcico-férrica, potássica, propilítica e finalmente, carbonatação. As rochas vulcânicas foram alteradas sob regime deformacional que mudou de rúptil-dúctil para rúptil. O depósito resultou de dois estágios de mineralização. O estágio precoce, gerado a grandes profundidades, produziu a associação de minério composta principalmente por calcopirita-pirita-magnetite, como disseminações,

brechas e veios, particularmente em rochas afetadas por metassomatismo cálcico-férrico. O estágio tardio, formado a profundidades mais rasas, apresenta associação de minério praticamente livre de magnetita, com calcopirita-hematita±pirita, em brechas e veios, gerados especialmente durante a alteração potássica. Tais associações de minério revelam que o sistema hidrotermal evoluiu com o aumento na fO_2, Cu/Fe e atividade de enxofre, associadas ao arrefecimento da temperatura, sugerindo que suas precipitações derivam de dois fluidos distintos. O Cristalino é considerado como um depósito IOCG multiestágio, similar a outros sistemas IOCG que jazem no corredor Leste-Oeste de Carajás.

Palavras-chave: IOCG, metalogênese, sistema hidrotermal, Neoarqueano, Província Carajás.

INTRODUCTION

Copper reserves in Brazil are in the order of 11 Mt (1.5% of the world) (Xavier *et al.* 2017), ca. 85% of which concentrated in copper systems of the Carajás Province, an Archean crustal segment in the southeastern Amazon Craton, northern Brazil. This province is divided into two tectonic domains: Rio Maria Domain in the south and Carajás Domain (CD) in the north (Fig. 1A).

A variety of copper deposits occur in the CD and may be broadly divided into two systems (Xavier *et al.* 2017): (1) iron oxide-copper-gold (IOCG), the most economically important deposits; and (2) copper–polymetallic. These copper systems are structurally controlled by regional-scale WNW-ESE–striking brittle-ductile shear zones (e.g., Carajás and Cinzento in the northern sector and Canaã in the southern sector), particularly close to the contact between the basement and supracrustal units of the CD (Xavier *et al.*, 2012; Fig. 1B).

Geochronological data reveal that the Carajás IOCG systems were emplaced during multiple hydrothermal episodes during the Neoarchean and Paleoproterozoic with the ore-forming events having occurred at: (i) 2.72 – 2.68 Ga, represented by the Sequeirinho - Pista ore bodies, Sossego deposit (245 Mt @ 1.1 wt.% Cu, 0.28 g/t Au), and its satellite deposits, including Bacuri, Bacaba, Castanha, Visconde and Pedra Branca, all in the southern sector (Moreto *et al.* 2015a,b); (ii) 2.60-2.53 Ga recorded at the Salobo mine (1.11 Gt at 0.69 % Cu and 0.43 g/t Au), Igarapé Bahia/Alemão (219 Mt @ 1.4 wt.% Cu, 0.86 g/t Au) and Grota Funda deposits in the northern sector (Réquia *et al.* 2003; Tallarico *et al.* 2005; Hunger 2017); and iii) 1.90-1.88 Ga, having as examples the Sossego-Curral ore bodies (Sossego deposit) and Alvo 118 (ca. 170 Mt @ 1.0% Cu and 0.3 g/t Au) deposit, also in the southern sector of the CD (Grainger *et al.* 2008; Moreto *et al.* 2015a). Mesoarchean basement

gneisses/granitoids and Neoarchean metavolcano-sedimentary units of the Itacaiúnas Supergroup as well as gabbros/diorites, quartz-feldspar porphyries, and A2-type anorogenic granites may be hosts to the IOCG systems (Xavier *et al.* 2012).

The Neoarchean 2.72–2.68 Ga and 2.60-2.53 Ga IOCG systems were generally emplaced at deeper crustal levels and display distal Na-Ca alteration (albite - scapolite – hastingsite - actinolite – epidote) followed by variable combinations of more proximal and structurally-controlled calcic-ferric (actinolite - magnetite - apatite), iron-rich (almandine - grunerite – tourmaline – magnetite), potassic-ferric (K-feldspar and biotite - magnetite), and/or chlorite – epidote - carbonate alteration types (Xavier *et al.* 2017). The copper ore zones are represented by chalcopyrite - pyrite - siegenite - magnetite - actinolite - chlorite - apatite - allanite breccias in the southern sector (e.g., Sequeirinho – Pista ore bodies, Visconde and Pedra Branca deposits). In the northern sector, copper ore zones include massive magnetite lenses containing disseminated bornite–chalcocite (e.g. Salobo), magnetite – chalcopyrite - actinolite breccias (e.g., Igarapé Bahia/Alemão, Grota Funda), chalcopyrite - bornite - magnetite veins, stockworks and breccias (e.g., Furnas) or chalcopyrite disseminations along the mylonitic foliation (e.g., GT46).

Comparatively with the Neoarchean examples, the Paleoproterozoic IOCG systems represent hydrothermal systems developed at shallower crustal levels and controlled predominantly by brittle structures. These systems are generally characterized by absent or poorly developed sodic-calcic or calcic-ferric alteration, but commonly display strong and pervasive potassic - ferric (K-feldspar and biotite with magnetite) alteration (Tallarico 2003, Torresi *et al.* 2011, Xavier *et al.* 2017) commonly overprinted by extensive zones dominated by chlorite - epidote - calcite or sericite that host the copper-gold ore. The ore forms breccia (Sossego-Curral) and vein systems (Alvo 118) containing quartz, calcite, actinolite, magnetite/hematite, apatite, and sulfides (chalcopyrite – pyrite - siegenite). In both Neoarchean and Paleoproterozoic IOCG systems, the Fe-Cu-Au association is generally accompanied by variable concentrations of P-LREE-U-Ni-Co-Pd.

The Cristalino deposit is located about 40 km east of Sossego mine and immediately south of the Estrela copper-polymetallic deposit at the eastern termination of Carajás fault, in the Serra do Rabo region (Fig. 1B). It is a world-class Cu-Au (379 Mt @ 0.66 wt.% Cu; 0.3 g/t Au; Pinto 2012) deposit of the southern sector of the CD that probably belongs to the 2.72–2.68 Ga IOCG group (2700 ± 29 Ma, Pb-Pb in sulfide, Soares *et al.* 2001). Despite its economic importance and possibility to become a mine in the near future, none of the few

available studies (Huhn *et al*. 1999, Soares *et al*. 2001 and Ribeiro *et al*. 2009 among others) have fully investigated the temporal evolution of the Cristalino hydrothermal system and associated copper mineralization.
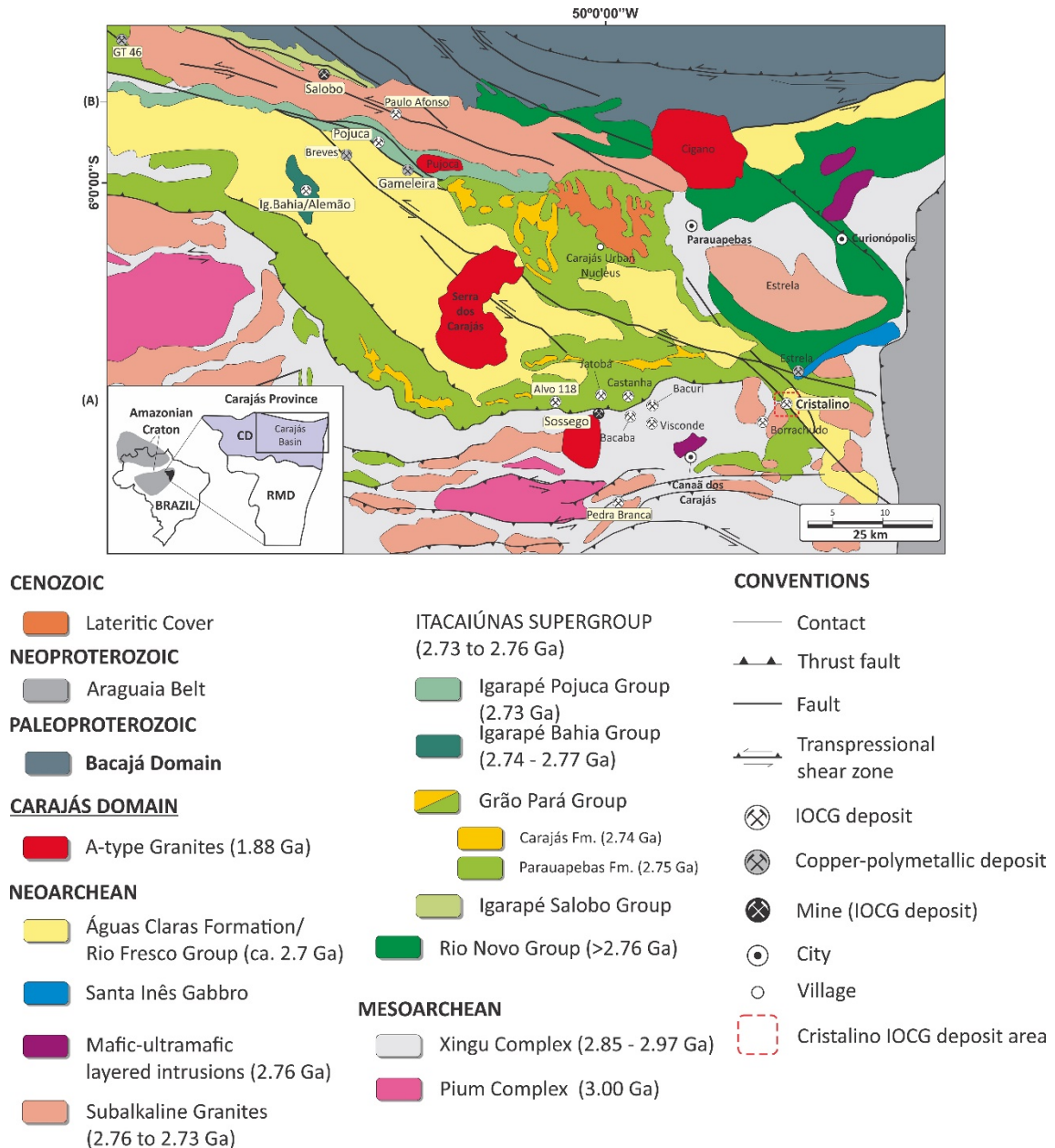
Figure 1. (A) Location of the Carajás Domain (CD) in the Amazon Craton (Santos *et al*. 2000); (B) Geological map of the Carajás Domain showing the location of important IOCG and Cu-polymetallic systems (modified from Vasquez *et al*. 2008). The inset area represents the site of the Cristalino IOCG deposit. *Abbreviations*: *CD*: Carajás domain; *RMD*: Rio Maria domain.

The main goal of this work is to characterize the host rocks and the alteration zones of the Cristalino deposit, as well as to present a consistent paragenetic sequence of the hydrothermal minerals resulting from the alteration processes. In addition, it aims to point out possible evidence of overlapping of different mineralization styles at Cristalino, as described

recently in other IOCG systems of the CD (Moreto *et al.* 2015a,b, Melo *et al.* 2017, Xavier *et al.* 2017), with implications on physico-chemical variations of the fluid regime and copper deposition during the evolution of the hydrothermal system.

GEOLOGICAL SETTING OF THE CARAJÁS DOMAIN

The Carajás Domain is made up of Mesoarchean (3.0-2.83 Ga) basement rocks, with TTG-like gneisses-migmatites, orthogranulites and calc-alkaline granitoids overlain by Neoarchean metavolcano-sedimentary sequences of the Rio Novo Group (>2.76 Ga) and Itacaiúnas Supergroup (2.76-2.73 Ga) as well as metasiliciclastic rocks of the Águas Claras Formation (> 2.65 Ga) (Fig. 1B; Vasquez *et al.* 2008).

The Rio Novo Group is a mafic/ultramafic volcano-sedimentary sequence with banded iron formations (BIF) and metapelites (Araújo and Maia 1991, Oliveira 1994, Vasquez *et al.* 2008) which outcrops in the Serra Pelada region. It has a minimum age of 2763 ± 7 Ma, the dating of the intrusive Luanga mafic-ultramafic and the Estrela granitic complexes (Machado *et al.* 1991, Barros *et al.* 2001).

The Itacaiúnas Supergroup encompasses the following groups: Igarapé Salobo, Igarapé Pojuca, Grão Pará and Igarapé Bahia. Their lower units are dominantly composed of bi-modal volcanic rocks, whereas the intermediate units comprise thick layers of BIF. Dominantly of sedimentary nature, the upper units are made up of metasiltstones, metargilites and BIF intercalated with metabasalts (DOCEGEO 1988, Soares *et al.* 1999, Ronzê *et al.* 2000, Lindenmayer *et al.* 2001, Vazquez *et al.* 2008).

Mafic-ultramafic layered igneous intrusions crosscut the basement rocks and the Itacaiúnas Supergroup, being represented by the Serra Leste and the Cateté Intrusive suites. They consist of clusters of elongated bodies mineralized with PGE-, Cr- or Ni (Macambira and Vale 1997, Mansur and Ferreira Filho, 2016, Siepierski 2016). As part of the Serra Leste Suite, the chromite-bearing Luanga and Lago Grande complexes have been dated at 2763 ± 7 Ma (Machado *et al.* 1991) and 2722±53 Ma (Teixeira *et al.* 2015), respectively, overlapping the Neoarchean bimodal magmatism of the Grão Pará Group.

High potassium subalkaline granites, namely the Estrela Complex, Serra do Rabo, Igarapé Gelado and Old Salobo bodies, have been emplaced in the Carajás basin rocks (Feio *et al.* 2013) with emplacement ages spanning from 2763 to 2573 Ma.

Archean sedimentary covers include the marine coastal Águas Claras Formation, which overlies unconformably the Itacaiúnas Supergroup (Nogueira *et al.* 1995) and by the

Rio Fresco Formation, which overlies the Rio Novo Group and hosts the epigenetic Au-PGE Serra Pelada deposit (Grainger *et al*. 2008). Their deposition age is uncertain, ranging from 2.70 to 2.30 Ga, according to U-Pb dating on zircon monocrysts from crosscutting mafic dikes (Dias *et al*. 1996, Mougeot *et al*. 1996, Santos 2002).

The Paleoproterozoic is essentially represented by non-deformed metaluminous to peraluminous A-type granites that crosscut the basement and the meta-volcano-sedimentary sequences (Dall'Agnol *et al*. 2005, Vasquez *et al*. 2008) with ages varying from 1883±2 to 1874±2 Ma (Machado *et al*. 1991, Rämö *et al*. 2002, Dall'Agnol *et al*. 2005).

The tectonic setting of the supracrustal units has been attributed to a ca. 2.76 Ga intracontinental rift (Wirth *et al*. 1986; Gibbs *et al*. 1986, DOCEGEO 1988, Macambira 2003) or volcanic arc (Meirelles and Dardenne 1991, Teixeira 1994, Lindenmeyer *et al*. 2005, Lobato *et al*. 2005) built over the > 2.83 Ga Mesoarchean basement. Between 2.76 and 2.70 Ga, the Carajás Domain in marked by the deposition of the volcano-sedimentary sequences of the Itacaiúnas Supergroup (DOCEGEO 1988) and mafic-ultramafic and granitic plutonism. The most remarkable CD structures are considered coeval with the 2.76-2.71 Ga type-A granite intrusions (Barros *et al*. 2001, 2009), a hypothesis also defended by Feio *et al*. (2013) and Dall'Agnol *et al*. (2013). These structures have resulted from a NE-SE crustal shortening, which is associated with strike-slip and oblique shear zones in the Itacaiúnas Group rocks and evidenced by an E-W subvertical foliation in the basement units. Tectonic reactivation took place at least three times from the Archean to the Paleoproterozoic (Costa *et al*. 1995, Araújo *et al*. 1988, Pinheiro and Holdsworth 2000).

MATERIALS AND METHODS

During field work in the Cristalino deposit area, nine drill-holes (FD-58, FD-96, FD-107, FD-155, FD-209, FD-224, FD-266, FD-325 and DH-00003) were described and several core samples collected for analysis in laboratories housed at the Geosciences Institute of the Federal University of Pará (IG-UFPA). Approximately 100 polished thin sections were prepared for petrographical study under transmitted and reflected light, using a Zeiss Axioplan 40 microscope. Selected thin sections were coated with carbon and then analyzed by scanning electron microscopy coupled with energy dispersive X-ray spectrometry (EDS). The equipment was a MEV Zeiss LEO-1430 with EDS IXRF model Sirius-SD that operated under the following analytical conditions: electron beam = 90 µA; constant acceleration voltage =

20 kV; working distance =15 mm; and counting time to analyze the elements = 30 s. Samples were carbon coated by the metallizer Quorum model Q150T-ES.

RESULTS

Main lithotypes and structures in the Cristalino copper-gold deposit area

The main lithotypes identified in the Cristalino deposit area may be grouped into: (1) basement rocks; (2) a volcano-sedimentary sequence; and (3) mafic/felsic intrusions (Fig. 2 and 3).

Mesoarchean basement rocks do not outcrop at the Cristalino deposit area and are recognized only along drill cores. These rocks are mainly represented by the Cruzadão Granite (Fig. 4A) with age of 2857±8 Ma (U-Pb in zircon, LA-MC-ICPMS, Feio *et al*. 2013). This granite is granular to moderately foliated (Fig. 4A) with local cataclastic and recrystallized domains (Fig. 4C). It is mainly composed of plagioclase, quartz and rare K-feldspar (Fig. 4B). Scapolite, sericite, chlorite, epidote, titanite and hematite are the main alteration minerals. Scapolite (Fig. 4B) replaces selectively plagioclase while sericite tends to overprint both primary and secondary minerals. Chlorite, epidote, titanite and hematite are derived from the biotite alteration.

The volcano-sedimentary sequence in the area consists predominantly of mafic volcanic rocks, generally interlayered with BIF (Fig.4D, E) and felsic units of rhyolitic composition (Fig. 4F). The mafic and felsic volcanic units are stratigraphically correlated with the Parauapebas Formation (2760±11 Ma - 2757±7Ma; Trendall *et al*. 1988) whereas the BIF is part of the Carajás Formation. Both the Parauapebas and Carajás formations belong to the Grão Pará Group.

At the deposit scale, the mafic volcanics are dark gray to dark green and show different degrees of shearing and hydrothermal alteration that obliterate up to 70% of their original magmatic mineral assemblages. Actinolite, albite, chlorite, quartz and magnetite are the main hydrothermal products, which have replaced most primary minerals in these rocks (Fig. 4F, G). The texture varies from fine- and medium-grained to porphyritic with plagioclase phenocrysts immersed in a microcrystalline matrix. Albite and quartz commonly fill rounded cavities interpreted as vesicles (Fig.4G). Apatite, allanite, and monazite are subordinate alteration minerals.
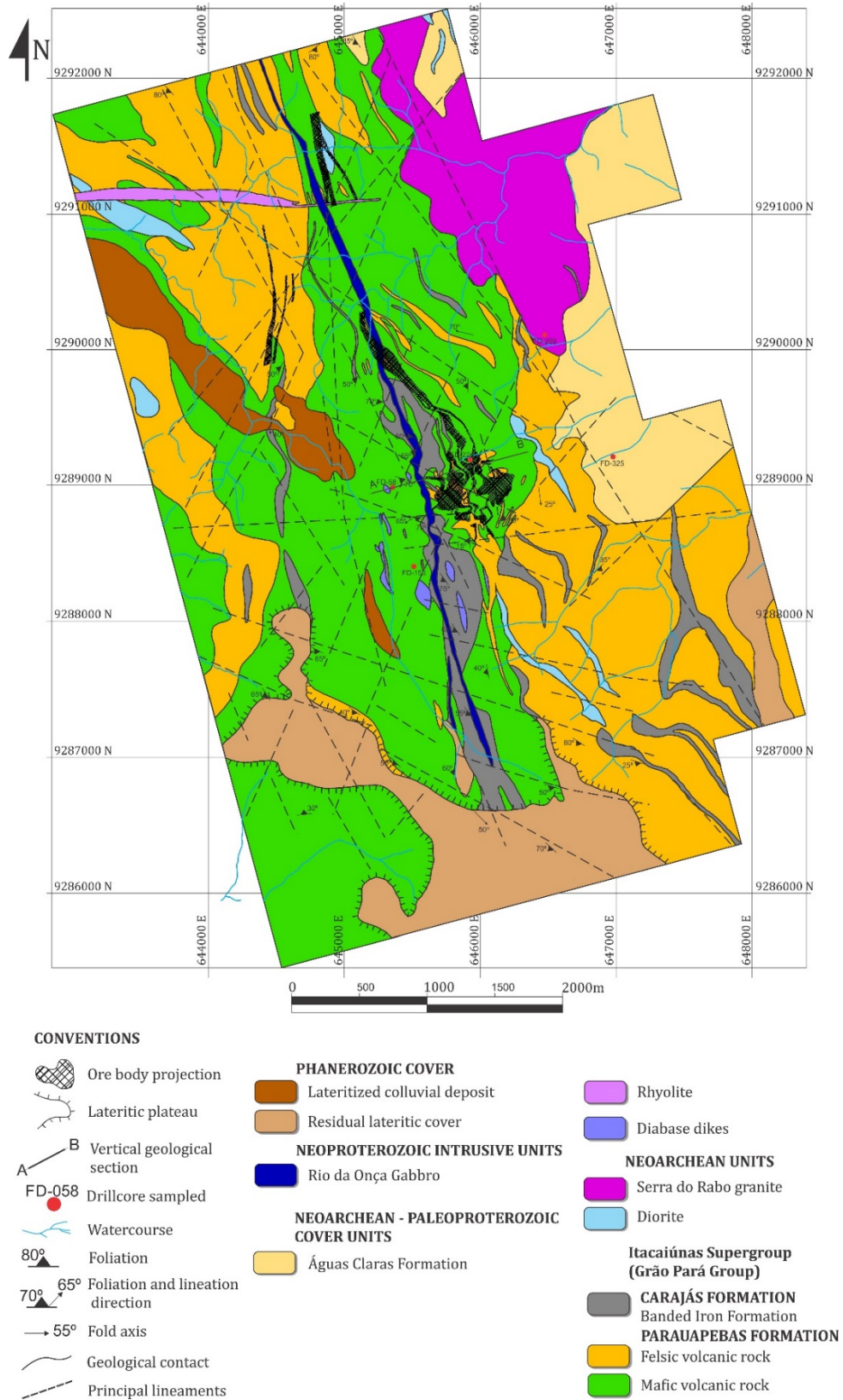
Figure 2. Geological map of the Cristalino deposit area, modified from Soares *et al*. (2001) and Vale (2003).
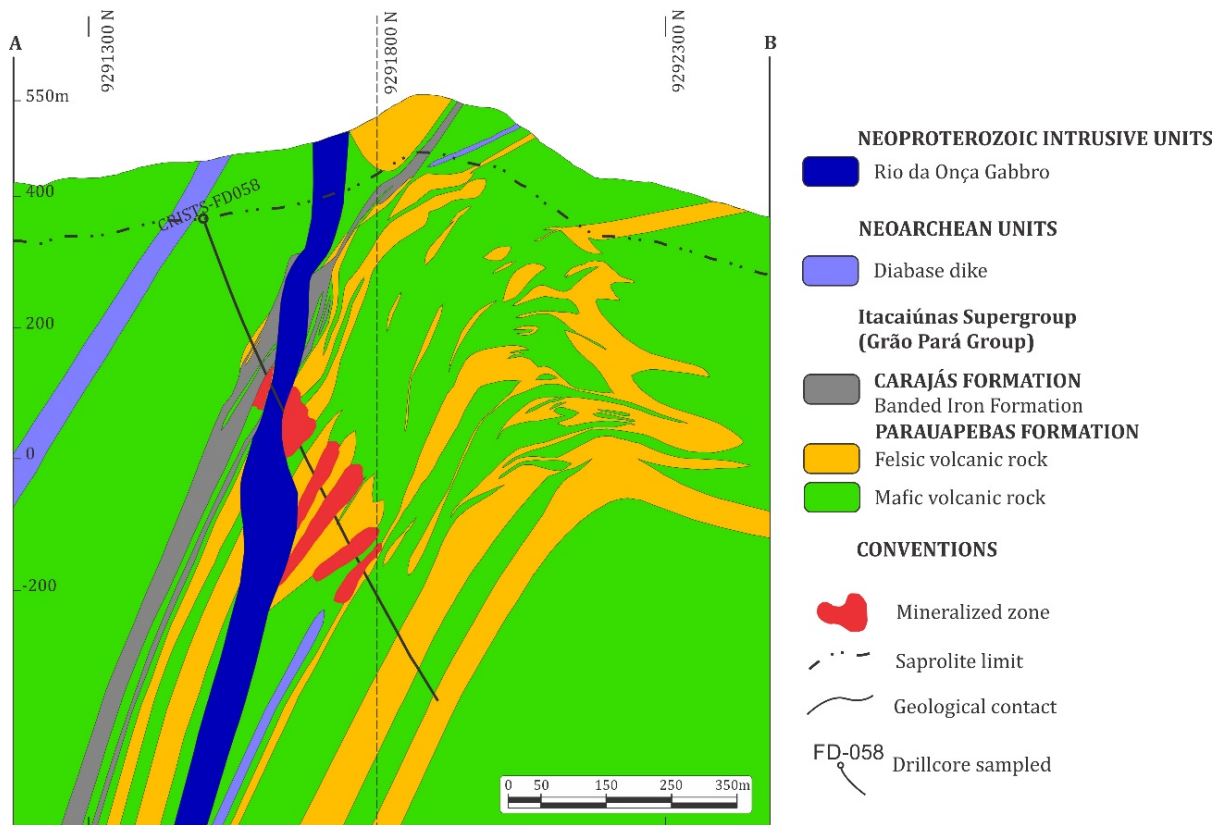
Figure 3. N75°E geological section across the mineralized zone of the Cristalino deposit (A-B line in figure 2), modified from Vale (2003).

The more felsic varieties (Fig. 4H) are not abundant in the deposit. They form irregular bodies with thickness up to a few tens of meters. These rocks are greenish gray to reddish green and display a fine-grained isotropic to slightly foliated matrix, commonly porphyritic. The less altered varieties are composed of K-feldspar (30-40%), plagioclase (10-20%) and quartz (30-40%) and have been classified as rhyolite (Fig. 4I). Commonly quartz occurs as bluish phenocrysts immersed in the rock matrix.

At the regional scale, BIF form 150 up to 350 m-thick sequences that sustain hills and extend over 3,500 m along the E-W strike (Fig. 2; Vale, 2003). These units are characterized by folded and faulted quartz-rich bands finely interbedded with magnetite-rich bands (Fig. 4D). Calcite and chlorite form several generations of veins that crosscut randomly the BIF. Chalcopyrite (Fig. 4E) and pyrite also occur as alteration products but are spatially related to the interface between BIF and mafic volcanic rocks.
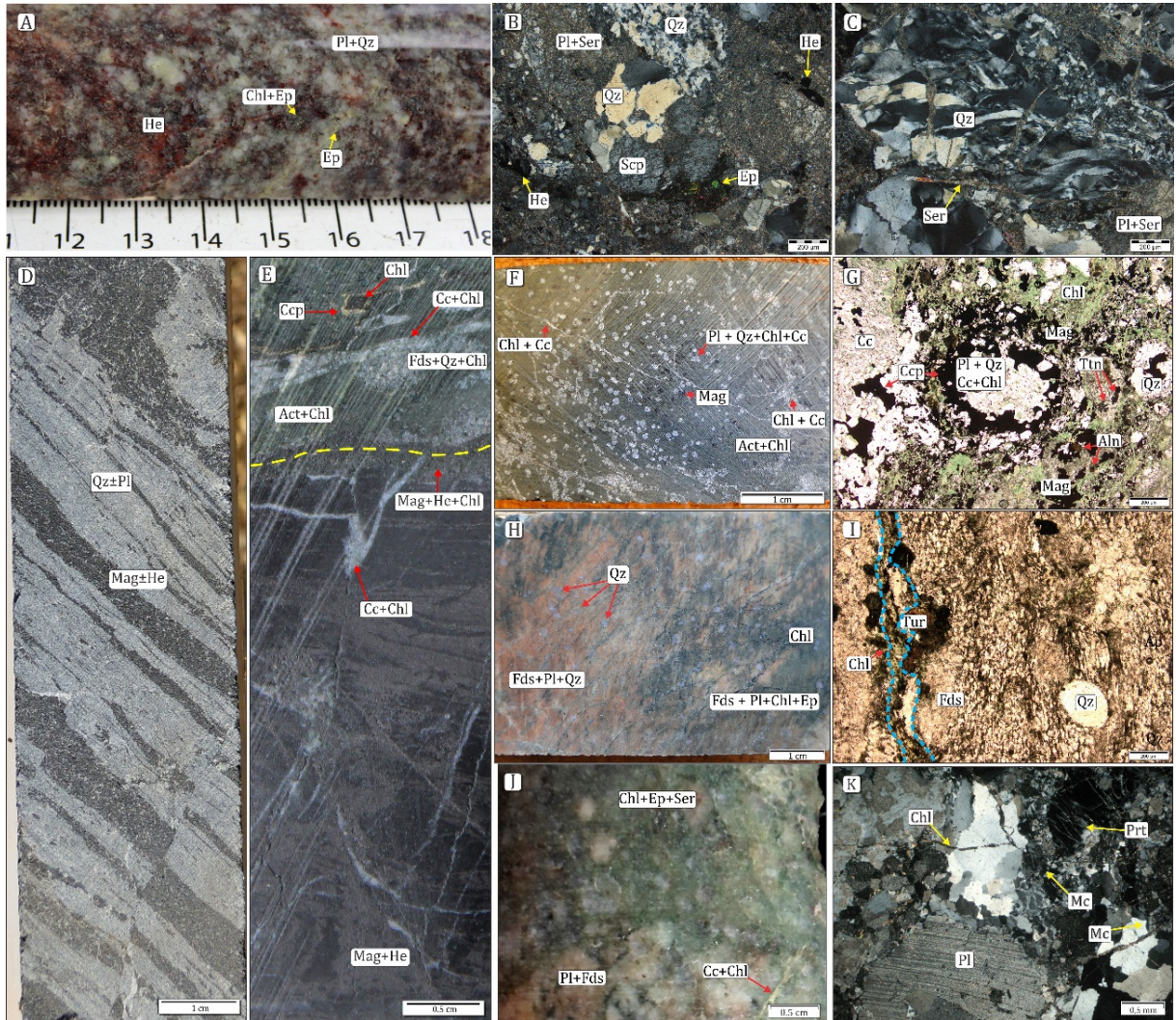
Figure 4. Main lithotypes of the Cristalino deposit area: (A) Cruzadão granite showing typical granular texture. The red spots correspond mostly to hematite-stained plagioclase and quartz, whilst the light-grey and dark-grey spots are, respectively, plagioclase and quartz, and chlorite-hematite±epidote. Scale is in cm. (B) Photomicrograph (transmitted light - XPL) of the Cruzadão metagranite strongly altered to sericite, although a few plagioclase crystals are still recognizable. Quartz occurs as anhedral crystals some forming microcrystalline aggregates. Epidote and hematite occur as fine interstitial crystals. (C) Same as B, showing the strained portions of Cruzadão granite, with deformed and fragmented quartz crystals. (D) Banded iron formation showing disrupted and fractured quartz-rich bands interleaved with magnetite-hematite-rich bands. (E) Sharp contact (dashed line) between strongly altered volcanic rock (upper part) and BIF (lower part); (F) Hydrothermally-altered mafic volcanic rock composed of quartz, actinolite, plagioclase, chlorite, and magnetite. Note the presence of vesicles (white spots), filled with plagioclase, quartz, chlorite, and calcite; (G) Photomicrograph (transmitted light – PPL) of altered mafic volcanic rock depicted in F showing chlorite as the main alteration mineral. Chalcopyrite replaces selectively vesicular minerals. Magnetite and allanite are alteration minerals, and both are corroded by chlorite; (H) Potassic-altered rhyodacite with bluish-quartz phenocrysts and fractures filled by chlorite. (I) Photomicrograph (transmitted light –PPL) of altered rhyodacitic rock depicted in H, showing relic feldspar, quartz, and tourmaline, with chlorite and calcite filled veinlet (between dashed lines); (J) Coarse-grained Serra do Rabo granite with green (chlorite-sericite-epidote) and the pink patches that represent, respectively, strongly, and less altered portions of the rock. (K) Photomicrograph (transmitted light –XPL) of the Serra do Rabo granite showing oligoclase, microcline/perthite and quartz as essential minerals. Sericite and chlorite are the most common alteration minerals. The scale in A photograph is in centimeter. Act: actinolite; BIF:

banded iron formation; Cc: calcite; Ccp: chalcopyrite, Chl: chlorite; Ep: epidote; Fds: feldspar; He: hematite; Mag: magnetite; Mc: microcline; Pl: plagioclase; Pr: perthite; Qz: quartz; Ser: sericite; Scp: Scapolite; Ttn: titanite.

The volcano-sedimentary sequence is crosscut by the Serra do Rabo Granite and NW-SE-striking gabbro/diabase dikes. The Serra do Rabo Granite was dated at 2743 ± 1.6 Ma (U-Pb in zircon LA-ICPMS, Sardinha *et al.* 2006) and in the deposit area is restricted to the NE sector. This granitic rock shows an hypidiomorphic granular texture with medium to coarse, weakly oriented crystals (Fig. 4J). Graphic texture is locally present. It is mainly composed of plagioclase (40-30%), quartz (30-40%) and microcline (10-30%) and classified as syeno- to monzogranite. No primary mafic mineral is observed. Most plagioclase (An_{20-28}) crystals are subhedral and medium- to coarse-grained, and show bookshelf micro-fractures, irregular to recrystallized borders and intra-granular deformation. In general, quartz developed medium- to fine-grained crystals that commonly exhibit undulose extinction, sutured contacts, and recrystallized borders. Microcline develops fine- to medium-grained crystals, some showing flame perthite (Fig. 4K).

Shearing affected both primary and early alteration minerals, yielding wavy primary quartz that coexists with elongated and rotated tourmaline (Fig. 5A) and allanite crystals (Fig. 5C). Late stages of alteration, however, tend to occur preferably in brittle deformed portions, where cm-thick veins are filled with tourmaline (Fig. 5D), K-feldspar (Fig.5E) and/or chlorite-calcite-epidote (Fig. 5F).

Hydrothermal Alteration

Mafic and felsic volcanic rocks, correlated to the Parauapebas Formation, are the main hosts to the copper-gold mineralization at the Cristalino deposit. These rocks have been subjected to strong hydrothermal alteration that includes an early sodic alteration characterized by widespread formation of albite and local occurrence of scapolite that was subsequently overprinted by a calcic-ferric alteration dominated by actinolite, allanite and magnetite. The ensuing potassic alteration is structurally controlled and observed especially in ductile-brittle sheared domains. It is represented by K-feldspar, biotite, and minor magnetite and hematite. Propylitic alteration, characterized mainly by chlorite, epidote and calcite, took place next under more brittle conditions, overprinting the previous assemblages. The infill stage was the last event of the Cristalino hydrothermal history and is recorded by K-feldspar- and calcite-rich veins that intercept each other, but ambiguously.

Sodic Alteration

This alteration type occurs mainly in distal portions of the deposit and is marked by the development of chessboard albite (Fig.6A). It confers to the rock a pale-yellow to light-rose tint, best recognized in the felsic volcanic varieties. This albitization occurs as a textural retentive alteration, leaving residual crystals of primary K-feldspar associated with decalcified plagioclase (An<10) with turbid aspect, suggesting that this process was accompanied by an incipient sericitization. Quartz and REE minerals, such as allanite (Fig. 6B) and monazite (Fig. 6C), are also seen associated with hydrothermal albite.

Scapolite was only observed away from the mineralized zones in the Cruzadão granite where it shows deformed crystals (Fig. 4B). It is considered a product of the sodic alteration as it is in other copper-gold deposits of the Carajás Province (*i.e*, Visconde and Borrachudo; Silva *et al.* 2015, Previato 2016).

Calcic-ferric alteration

This is best developed in the mafic volcanic rocks, where it severely obliterates the primary mineral assemblages by forming actinolite and magnetite. The common light to dark green color acquired by these rocks results from the lesser or greater abundance of actinolite (Fig. 6D, 7B, 7D) that replaced preferably ferromagnesian minerals and was later replaced by chlorite (Fig. 7A). Actinolite forms fine- to coarse-grained aggregates, being locally represented by acicular crystals. In turn, magnetite appears disseminated or as cm-thick clusters, closely associated with the actinolite-rich zones (Fig. 6D, 7B).

Allanite is subordinate but of common occurrence in the calcic-ferric alteration assemblages, in contact with magnetite or intergrown with actinolite (Fig. 6D). It forms fine-grained aggregates or coarse-grained zoned crystals that present metamitic halos and borders that normally grade to epidote. Additionally, rare uraninite occurs associated with allanite.

Apatite and epidote (Fig. 6C) occur as subordinate constituents of the calcic-ferric assemblage and seem to be later than the actinolite-magnetite-allanite association. They are normally observed replacing early hydrothermal minerals, including monazite of the sodic alteration.

Locally, hastingsite/edenite, associated with quartz, occurs as fine-grained crystals that replace actinolite aggregates, particularly in portions of mafic volcanic rocks, implying a second generation of hydrothermal amphibole.
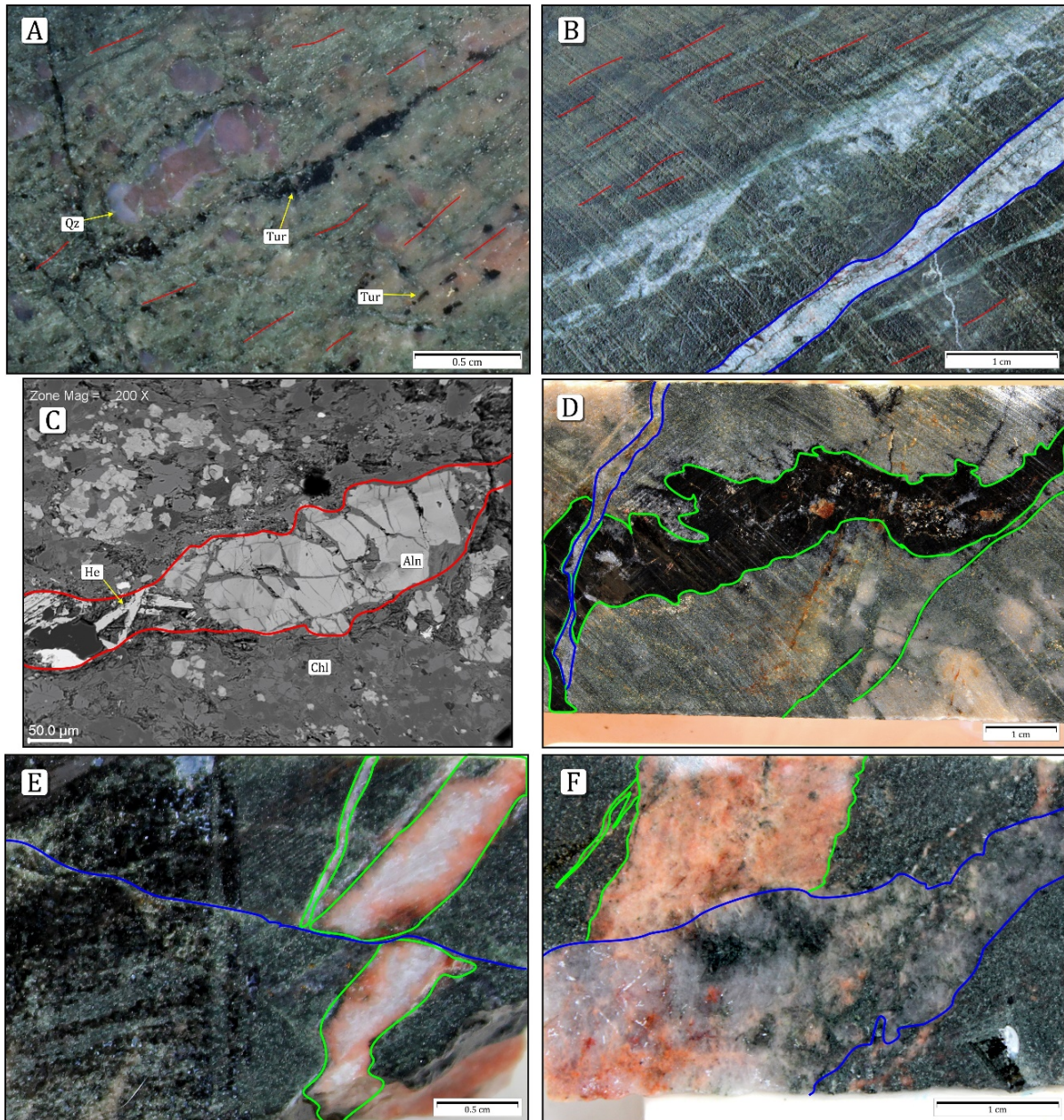
Figure 5. Main types of microstructures observed in the host rocks of Cristalino deposit. Photographs of borehole samples, except in C. (A) Mineral lineation (highlighted as red lines) defined by deformed blue quartz and oriented strings of tourmaline in a chloritized felsic volcanic rock. (B) Centimeter shear zone developed in chloritized mafic volcanic rock (shear zone sense highlighted as red lines). In the lower right corner, dilatant fracture (between blue lines) filled mostly by calcite. (C) Back-scattered electron image showing an oriented, deformed and cracked allanite crystal, defining a mineral lineation (lineation sense highlighted as red lines). (D) Tourmaline-rich vein (green lines) with diffuse borders crosscut by a calcite veinlet (blue lines). (E) Faulted K-feldspar-quartz-calcite vein (between green lines) crosscutting the chloritized felsic volcanic rock. The fault plain is filled with chlorite and calcite (blue line). (F) K-feldspar vein (between green lines) crosscut by quartz-calcite-K-feldspar-chlorite vein (between blue lines) in volcanic rock. Aln: allanite; Chl: chlorite; He: hematite; Qz: quartz; Tur: tourmaline.
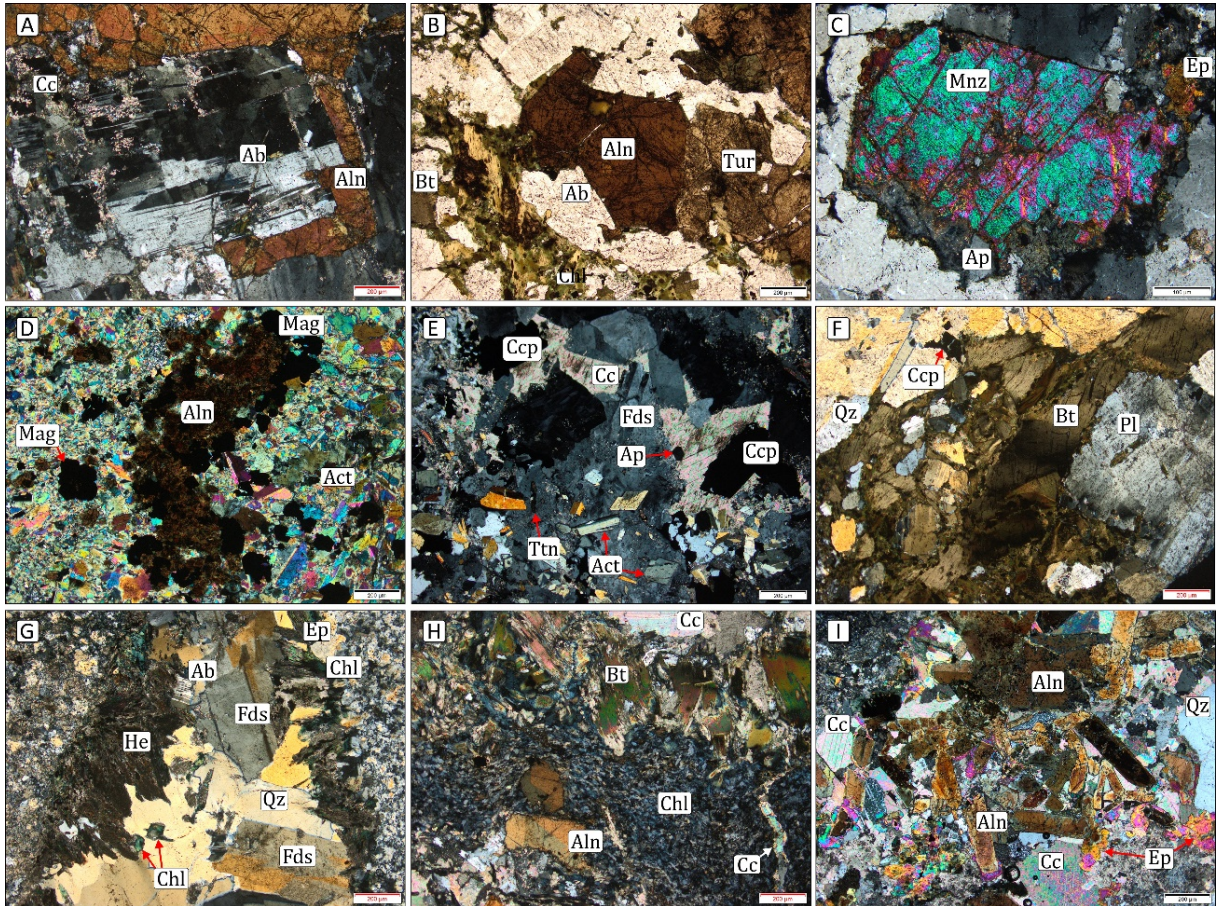
Figure 6. Photomicrographs (transmitted light) of the main types of hydrothermal alteration at the Cristalino deposit. (A) Altered felsic volcanic rock displaying chessboard albite and coarse-grained allanite, partially taken by late calcite (XPL). (B) Albitized felsic volcanic rock with late medium-grained allanite, tourmaline and chlorite (PPL). (C) A monazite crystal in felsic volcanic rock matrix replaced by apatite and epidote along the borders (XPL). (D) Abundant actinolite ± magnetite produced during Ca-Fe alteration in mafic volcanic rock. Actinolite occurs as fine- to medium-grained crystals and microcrystalline aggregates coexisting with magnetite and chalcopyrite (PPL). E) Felsic volcanic rock with subhedral actinolite crystals engulfed by secondary K-feldspar and chalcopyrite. Calcite is the last mineral to precipitate (XPL). (F) Potassic alteration represented by hydrothermal biotite in a felsic volcanic rock (PPL). (G) Sericitized volcanic rock crosscut by a veinlet composed of K-feldspar, quartz, hematite, chlorite and minor epidote and albite (PPL). (H) Chlorite mass replacing allanite and biotite in a mafic volcanic rock (XPL) and crosscut by a calcite veinlet (lower right corner). (I) Portion of a calcite-veinlet (carbonate stage) with high concentration of allanite and epidote that crosscuts an altered felsic volcanic rock (XPL). Ab: albite. Act: actinolite; Aln: allanite; Ap: apatite; Bt: biotite; Cc: calcite; Ccp: chalcopyrite; Chl: chlorite; Ep: epidote; Fds: K-feldspar; He: hematite; Mag: magnetite; Qz: quartz; Ser: sericite; Tur: tourmaline; Ttn: titanite.

Potassic alteration

The sodic and calcic-ferric alteration assemblages are partially overprinted by potassic alteration, which is characterized by K-feldspar and, to a lesser extent, biotite. The potassic alteration and infill are better developed along lithological contacts, foliation planes, fault gashes and fractures. A second and less important potassic alteration marks the final stage of

the hydrothermal alteration at the Cristalino deposit. It is fissure-controlled and has K-feldspar as the only potassic mineral.

Biotite (Fig. 6F, 7C) grew over sodic and calcic-ferric alteration minerals without showing distinct halos of biotitization. Locally, it coexists with magnetite (Fig. 7H) and is also recognized as fine lamellae on mylonitic foliation planes where it is partially altered by chlorite.

Hydrothermal K-feldspar forms centimeter-sized aggregates (Fig. 7E) that partially replace actinolite, albite, and apatite. Commonly, hydrothermal K-feldspar presents reddish coloration in hand specimens (Fig. 7E, 7K, 7N) and turbid crystals in thin-sections probably due to the very minute hematite inclusions (Fig. 6E).

Veins related to the potassic alteration II transect lithological contacts and foliation planes, as well as zones previously affected by sodic and calcic-ferric alterations. A few show mm- to cm-thick halos and are composed of K-feldspar, quartz and minor albite, hematite, titanite and sulfides (Fig. 5E, 5F, 6D, 6G, 7K).

Tourmaline Formation

The temporal relationships of the different generations of tourmaline are not always straightforward, but at least two tourmaline generations are defined with a good degree of confidence.

The early event is especially recorded in sodic and calcic-ferric altered samples. Tourmaline occurs as green to dark brown, medium- to coarse-grained crystals, with several quartz inclusions, associated with chessboard albite, allanite and monazite. It is a textural retentive alteration, in which tourmaline crystals were probably formed at the expense of primary plagioclase of the wall rocks. In deformed domains, tourmaline crystals show undulose extinction and microfractures and are oriented along with bluish quartz and allanite crystals, defining a mineral lineation (Fig.5A, 7I).

The other generation, relatively more expressive, is spatially associated with potassic altered felsic volcanic rocks. Along with quartz and minor albite, tourmaline forms centimeter clusters of fine- to medium-grained zoned crystals that replace earlier minerals (Fig. 4I, 6B). Locally tourmaline may exceed 60% of the wall rock minerals.

Unpublished data on the chemistry of these tourmalines (Craveiro *et al*. submitted) reveal that those of schorlitic composition are more common in association with sodic and calcic-ferric alteration, whereas those of dravitic composition grew mainly during the main tourmaline-forming event.

Propylitic alteration

Developed at the vicinity and along shear zones, lithological contacts and fracture planes, the propylitic alteration clearly overprints the potassic zones and most of the previous mineral assemblages. This alteration is represented by the chlorite-epidote-calcite assemblage (Fig. 6H, 7A) and by an array of veinlets composed mostly of calcite (Fig.7F) with variable amounts of chlorite, epidote and sulfides, and minor contents of albite, hematite, allanite and titanite (Fig. 6I, 7J, 7I). It seems that the propylitic alteration grades into carbonation. Calcite is by far the most abundant veinlet constituent, so that the latter mode of occurrence should be more properly attributed to carbonation, thus recording one of the latest hydrothermal processes in the Cristalino system.

The growth of the chlorite-epidote-calcite assemblage was a texture destructive process and was best developed in mafic volcanic rocks as the result of the partial (Fig. 7E and 7N) to total replacement of the groundmass minerals. Locally, the calcite-rich veinlets generated breccias bodies (Fig. 7J and 7L) with multi-mineral matrix and supported angular lithic clasts. Musketovite (magnetite after hematite) is confined to the veinlets and breccia matrix associated with chlorite, epidote, calcite and, chalcopyrite (Fig.8G). Carbonates (mainly calcite and minor dolomite and siderite, Fig. 7H, 7I, 7J, 8D) were the last minerals to be formed during both the pervasive propylitic alteration and veining stage.

Locally, portions that formerly underwent chloritization are partially taken over by a new generation of K-feldspar. Likewise, breccias hosted by felsic volcanic rocks exhibit chloritized lithic clasts that are rimmed by K-feldspar-rich aureoles (Fig.8G).

Cu-Au mineralization styles and ore mineral associations

The Cu-Au mineralization at the Cristalino deposit is dominantly hosted by volcanic rocks of the Grão Pará Group and based on their modes of occurrence may be grouped in the following types: (1) disseminated; (2) breccias (magnetite-chalcopyrite and chalcopyrite–hematite-rich); and (3) sulfide-bearing veins.

Disseminated type

The disseminated mineralization occurs preferably along shear zones, close to contacts between the Parauapebas and Carajás Formations, where it is commonly involved by zones of calcic-ferric and potassic alteration I (Vale 2003).

FD-107 profile representation
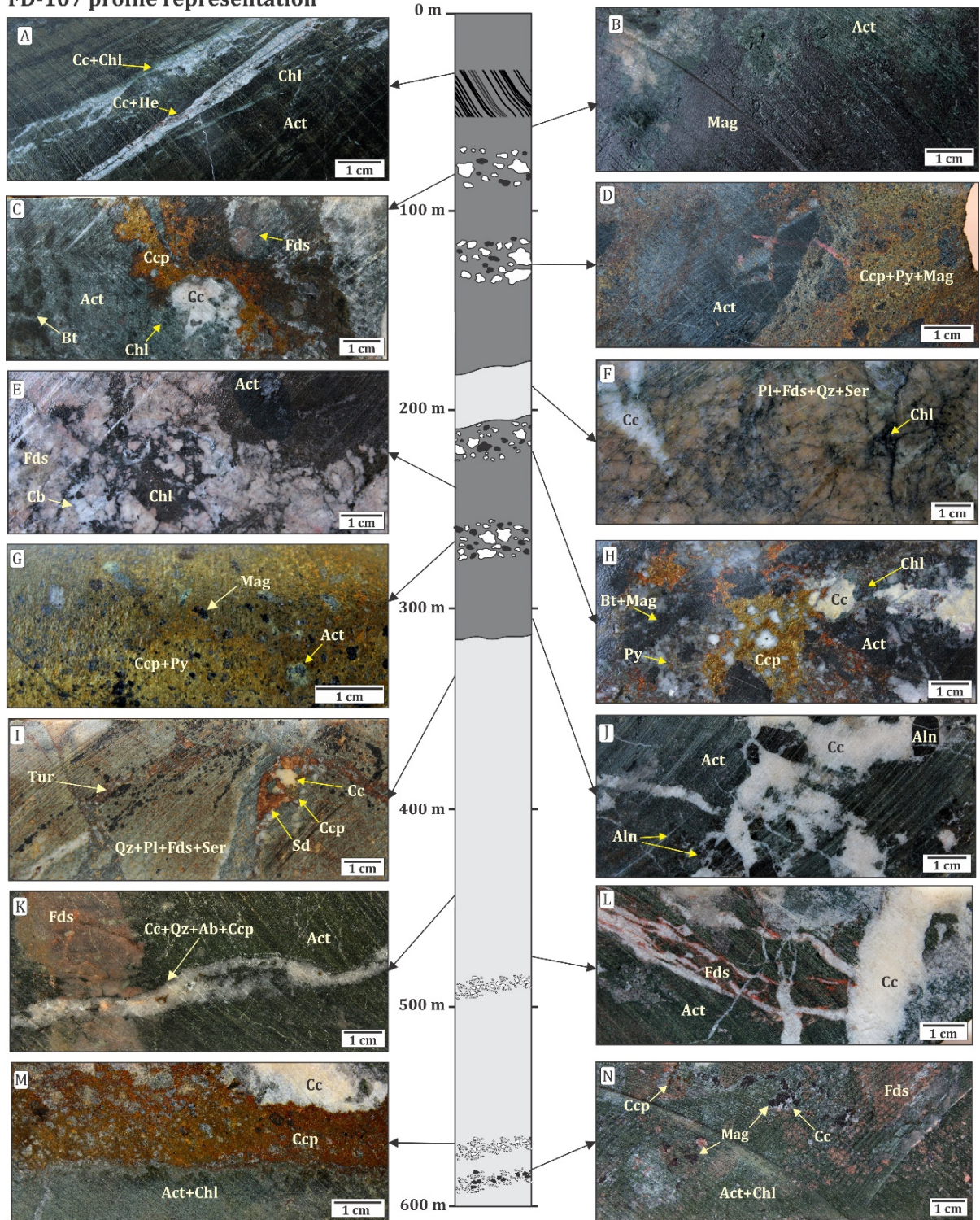
Figure 7. Main features of the hydrothermal alteration and mineralization in mafic and felsic volcanics at the Cristalino deposit based on observations of drill-core FD-007. (A) Sheared and chloritized actinolite-rich mafic volcanic rock with calcite-chlorite and calcite-hematite veinlets parallel to the foliation planes. (B) Mafic volcanic rock totally replaced by actinolite and magnetite, typifying zone of calcic-ferric alteration. (C) Chalcopyrite aggregate displaying Ca-Fe alteration (responsible for the overall green coloration of the sample) overprinted by potassic alteration (biotite and K-feldspar). Observe, close to the chalcopyrite aggregate, chlorite and calcite replacing previous hydrothermal minerals as part of the propylitic alteration. (D) Actinolite-magnetite-rich rock merging gradually to mineralized breccia zone with matrix filled with. (E) Overprinting of different alteration types: actinolite-rich zones partially replaced by K-feldspar and later by chlorite-calcite alteration. (F) Albitized felsic volcanic rock crosscut by different generations of essentially monomineralic chlorite- and calcite-veinlets. (G) Highly mineralized breccias containing chalcopyrite- and pyrite-rich matrix and clasts with actinolite, magnetite and allanite. (H) Chalcopyrite-magnetite-pyrite breccia, in actinolite-altered (Ca-Fe alteration) rock, affect by biotite (potassic alteration), and later overprinted by a chlorite-calcite assemblage. Note that chalcopyrite is a late phase and engulfs actinolite-rich and calcite-chlorite-rich fragments. (I) Tourmaline strings concordant to foliation planes of a sericitized felsic volcanic rock. The sample is also crosscut by veinlets of chlorite, calcite and, locally, siderite. (J) Actinolite-rich rock resulted from Ca-Fe alteration crosscut by calcite-allanite veins. (K) Actinolite-rich felsic volcanic rock crosscut by a K-feldspar-rich veinlet and both transected by a veinlet composed of calcite, quartz, albite, and chalcopyrite. (L) Array of calcite veinlets in felsic volcanic most likely developed by hydraulic fracturing under a brittle-dominated regime. The host rock has been previously affected by Ca-Fe and potassic alteration. (M) Chalcopyrite-rich veinlet associated with calcite in felsic volcanic rock that has been strongly altered to actinolite and chlorite. (N) Felsic volcanic rock altered by Ca-Fe alteration with actinolite and magnetite, later affected by potassic alteration (K-feldspar), chlorite-epidote-calcite alteration with minor chalcopyrite dissemination. Act: actinolite; Aln: allanite; Bt: biotite; Cb: carbonate; Cc: calcite; Ccp: chalcopyrite; Chl: chlorite; Fds: potassic feldspar; He: hematite; Mag: magnetite; Py: pyrite; Qz: quartz; Ser: sericite; Sd: siderite; Tur: tourmaline.

Two types of disseminated ore could be distinguished: (1) chalcopyrite, pyrite, and magnetite (up to 50%) with minor amounts of millerite and galena, and rare gold inclusions in sulfides. It generally occurs in mafic volcanic rocks affected by Ca-Fe alteration, in both isotropic (Fig.8A, 9A) and deformed portions along shear zones (Fig.8B). Locally, this type of ore is found in felsic volcanic rocks affected by potassic alteration with biotite; and (2) chalcopyrite (ca. 80%) with minor pyrite and almost magnetite-free (Fig.8C, 9B), present in the felsic volcanic rocks affected by potassic alteration I and propylitic alteration (Fig.7M). Moreover, when present, the scarce magnetite is partially replaced by hematite (martite).

In both cases, the sulfides precipitated during most of the calcic-ferric and potassic alterations, the final stages recording exclusively chalcopyrite (Fig.9B). Although generally formed earlier than sulfides, some allanite crystals from the Ca-Fe alteration present ambiguous textural relationships with chalcopyrite, suggesting intergrowth between these two minerals. Locally, covellite and digenite, present in both disseminated ore types, have resulted from weathering processes on chalcopyrite (Fig. 9E).
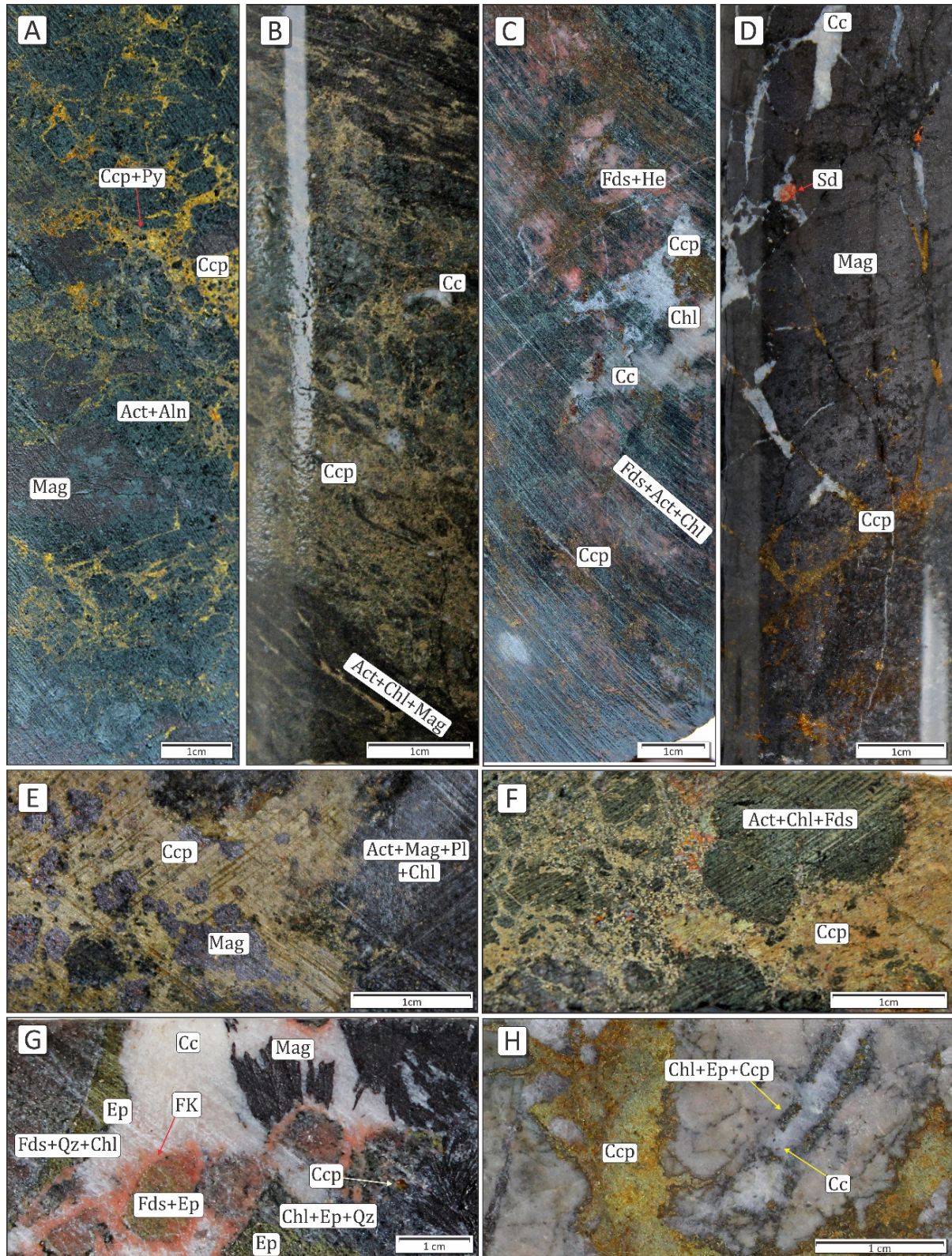
Figure 8. Photographs of mineralized samples of boreholes from the Cristalino deposit. (**A**) Mafic volcanic-hosted sulfide-rich breccia with clasts containing actinolite, magnetite and allanite and essentially with chalcopyrite and pyrite. (**B**) Disseminated chalcopyrite-pyrite along shear zones, in actinolite-magnetite-allanite (Ca-Fe alteration) in mafic volcanic rock. (**C**) Disseminated chalcopyrite in mafic volcanic rock altered by actinolite (Ca-Fe alteration), K-feldspar hematite (potassic alteration) and chlorite-calcite (propylitization/carbonation). (**D**) Magnetite alteration in mafic volcanic rock, near

banded iron formation contact, invaded and fractured by calcite-chalcopyrite rich veins. (**E**) Chalcopyrite-magnetite breccia type, in Ca mafic volcanic rock affected by Ca-Fe alteration. (**F**) Chalcopyrite-rich type breccia, in deeply altered felsic volcanic rock, affected by Ca-Fe and potassic with K-feldspar alteration. (G) Felsic volcanic rocks affect by superposition of potassic alteration with K-feldspar and propylitic alteration. This portion in crosscut by calcite-musketovite±chalcopyrite vein. Lithic clasts coated by K-feldspar within calcite-rich veins suggest a local superposition of calcite-vein over K-feldspar vein. (**H**) Felsic volcanic rock transected by multidirectional calcite-chlorite-epidote veins and later chalcopyrite-rich veins. Act: actinolite; Cc: calcite; Ccp: chalcopyrite; Chl: chlorite; Ep: epidote; Fds: K-feldspar (group); He: hematite; Mag: magnetite; Py: pyrite, Qz: quartz, Ser: sericite.

Breccias

Mineralized breccias are generally located in central portions of disseminated zones or preferably along lithological contacts and dilatant structures as well. Two types of breccia could be distinguished: (1) Chalcopyrite – pyrite - magnetite bodies; and (2) chalcopyrite±pyrite±hematite bodies.

The cm-thick chalcopyrite-pyrite-magnetite bodies (Fig.8E) formed under ductile-brittle conditions (dominance of shear zones over fractures) at the vicinity of zones enriched in magnetite and are generally hosted by mafic volcanic rocks that were prior affected by calcic-ferric alteration. Chalcopyrite and pyrite occur in different proportions replacing the wall rock that is currently represented by mm-thick, fine to medium-sized clasts containing magnetite (up to 30%), actinolite, allanite and other calcic-ferric minerals (Fig. 7G, 9B). These mineralized breccias grade into disseminated chalcopyrite-pyrite ore bodies.

The chalcopyrite±pyrite±hematite bodies (Fig. 8F) formed under dominantly brittle conditions (abundance of fractures) and occur particularly in felsic volcanic rocks that were affected by potassic alteration I, followed by propylitization/carbonation. Chalcopyrite is the principal constituent of the matrix, which shows practically neither pyrite nor magnetite, but instead contains hematite. These breccias vary from clast- to matrix-supported, with altered rock clasts composed of K-feldspar, hematite, allanite, epidote, chlorite, calcite, and quartz. These breccia bodies grade into an array of multidirectional chalcopyrite-rich veinlets.

As the textural relationships suggest and similarly to the dissemination types, chalcopyrite is the latest sulfide to form in the breccias, replacing partially pyrite (Fig. 9D) and most of the previous alteration minerals. Even when pyrite is the dominant matrix sulfide, chalcopyrite occurs interstitially (Fig. 9F). Some allanite grains from the Ca-Fe alteration (Fig. 9C), however, are apparently neoformed and occur in textural equilibrium with the sulfide matrix. Minor millerite, galena and rare uraninite (Fig. 9I) are seen in massive chalcopyrite of type 1 breccias.
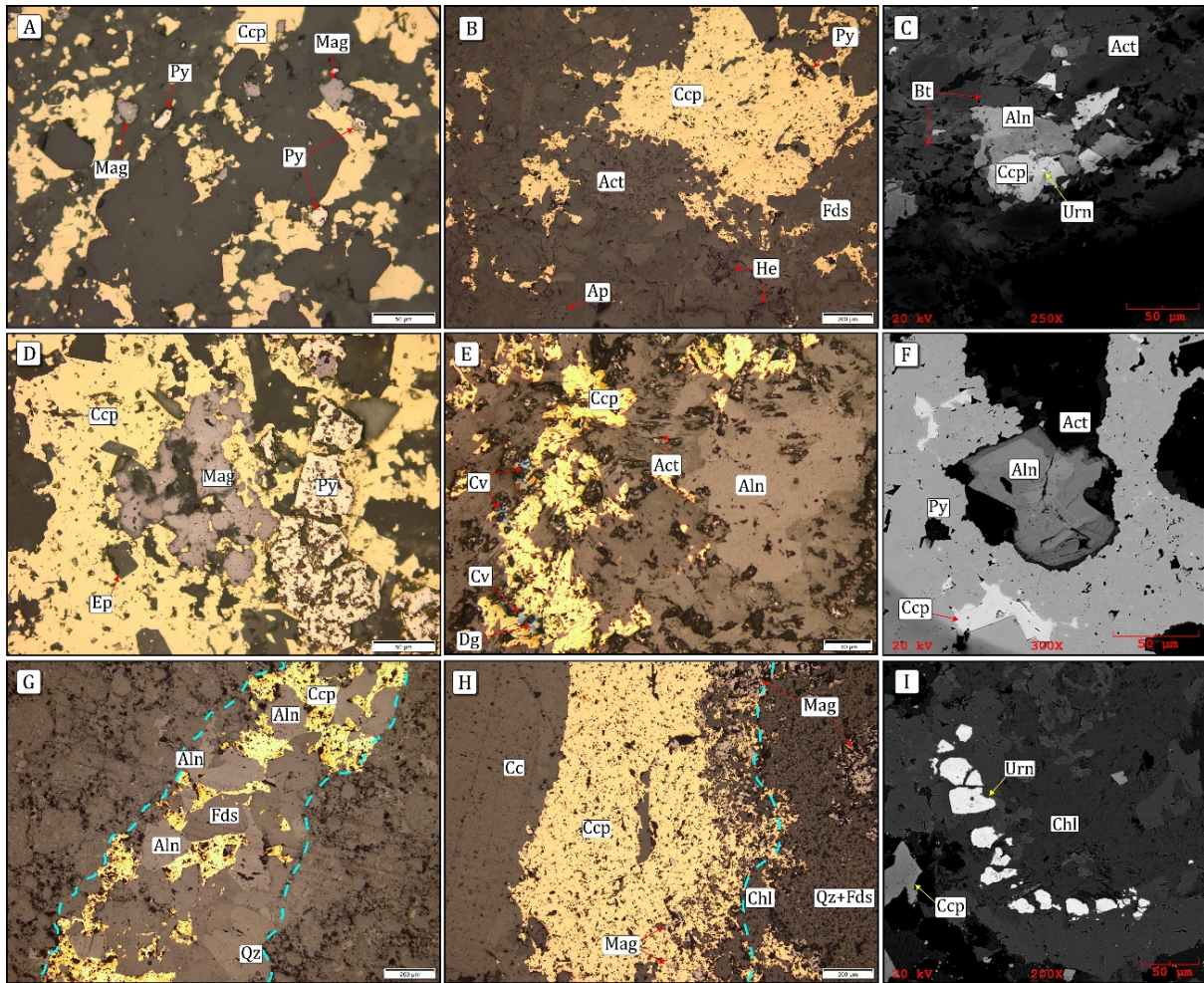
Figure 9. Photomicrographs of the Cu-Au mineralization types of the Cristalino deposit. All images are taken under reflected light and PPL, except for C, F, and I which are back-scattered electron microscope images. (A) Disseminated type **w**ith chalcopyrite and pyrite in an altered mafic volcanic rock. Magnetite crystals present minute inclusions of chalcopyrite, suggesting a generation of sulfide prior to the precipitation of the iron oxide. (B) disseminated type with chalcopyrite only, in felsic volcanic rock altered by actinolite-apatite (Ca-Fe alteration) and K-feldspar (potassic alteration). (C) Crystals of allanite and chalcopyrite in a mafic volcanic rock exhibiting equilibrium contact, and uraninite inclusions in chalcopyrite. (D) Sulfide-rich breccia within the Ca (actinolite) – Fe (magnetite) alteration zone in volcanic rock. Magnetite and pyrite are partially to totally replaced by chalcopyrite. (E) Covellite and digenite resulting from the supergene alteration of chalcopyrite in an actinolite-magnetite-allanite altered mafic volcanic rock. (F) Allanite immersed in a pyrite-rich mass within a mafic volcanic rock. Chalcopyrite is included in pyrite. (G) K-feldspar-rich veinlet (late potassic alteration) with comb-like quartz, allanite and chalcopyrite. Dashed lines highlight the vein walls. (H) Calcite-rich vein with chalcopyrite in a felsic altered volcanic rock. The contact of chalcopyrite with the wall rock is diffuse, creating an alteration halo. The dashed line traces the vein wall. (I) A string of uraninite crystals in a chloritized mafic volcanic rock. Act: actinolite; Aln: allanite; Ap: apatite, Bt: biotite, Cc: calcite, Ccp: chalcopyrite; Cv: covellite; Dg: digenite; Ep: epidote, Fds: K-feldspar, He: hematite; Mag: magnetite; Py: pyrite; Qz: quartz, Urn: uraninite.

Sulfide-bearing veins

Most sulfide-bearing veins are discordant to lithological contacts and mylonitic foliation developed in high strain shear zones at the Cristalino deposit. These veins can be divided into three main types according to their prevalent mineral composition: (1) K-feldspar-rich veins; (2) calcite-rich veins; and (3) chalcopyrite-rich veins. Relatively to the other types, calcite-rich veins are the most abundant and generally crosscut the K-feldspar-veins, while the chalcopyrite-rich veins are the scarcest and locally crosscut the other two types.

K-feldspar-rich veins fill millimeter-thick fractures and faults and may represent the late stage of the potassic alteration. In addition to K-feldspar and scarce chalcopyrite (Fig. 9G), the veins consist of fine-grained hematite, quartz, allanite, epidote, titanite, albite, and calcite.

Calcite-rich veins belong to the late stages of propylitization/carbonation and resulted from the filling of millimeter-thick dilatant structures. They generally display sharp walls and crosscut all varieties of volcanic rock (Fig.8D, G, H). Other mineral constituents include variable amounts of chalcopyrite and pyrite both in equilibrium with hematite and musketovite (Fig. 8G). Locally, millimeter-sized allanite grains can be found in these veins.

Millimeter-thick chalcopyrite-rich veins (Fig. 8H, 9H) show a non-uniform spatial distribution and are essentially composed of chalcopyrite. These veins/veinlets are probably a subcategory of the calcite-rich veins, in which sulfides replace, and seldom crosscut, calcite and other vein minerals.

DISCUSSION

The volcanic rocks that host the Cristalino deposit show no evidence of regional metamorphism, although Ribeiro *et al*. (2009) argue that they are metamorphosed at the greenschist to amphibolite facies conditions. In fact, the volcanic rocks are affected by centimeter- to meter-thick brittle-ductile shear zones, causing them to acquire protomylonitic texture. Most likely, the complex history of the region involving deformation, hydrothermal alteration and reactivation along the Carajás fault has led to the false interpretation that these rocks have been submitted to a regional metamorphism.

Zones affected by sodic and calcic-ferric alterations present deformed and mosaic-like crystals of allanite (Fig. 5C) and early tourmaline, whilst zones of potassic alteration show not only oriented biotite lamellae within local shear zones but also K-feldspar-bearing veins. In

the later alteration stages, the assemblage chlorite-epidote-calcite tends to be associated with dilatant structures. These features may suggest that the deformational environment changed from ductile-brittle to dominantly brittle throughout the evolution of the hydrothermal system.

The regional circulation of hot and hypersaline fluids through the CD units brought about most likely the sodic alteration and the input of metals leached from the rocks. As a result, these fluids became metalliferous and were ultimately responsible for the formation of Archean IOCG deposits. The origin of this hypersaline fluid is debatable. Some authors consider it of magmatic origin and related to Neoarchean granitoids (Tallarico *et al.* 2005, Grainger *et al.* 2008), whereas others defend a hybrid hydrothermal system in which marine-evaporitic beds played an important role as source of the fluid halogens and alkalis (Xavier *et al.* 2008, 2012, Moreto *et al.* 2015a,b).

The ensuing calcic-ferric alteration overprinted the sodic mineral assemblage in the mineralized zones of Cristalino area. Especially recognized in mafic volcanic rocks, the allanite continued to precipitate, signalizing a possible transition between sodic and calcic-ferric alterations. The ductile-brittle regime persisted during this transition, but at different physico-chemical conditions that allowed precipitating calcic minerals and magnetite. After most magnetite has been formed, chalcopyrite and pyrite started to precipitate as disseminations. Towards the end of the Ca-Fe alteration, chalcopyrite-pyrite-magnetite breccia-like bodies were also developed with diffuse contacts, suggesting the replacement of the wall rocks by sulfides

This ore association marks the first mineralization stage (Fig.10-A) that has been recognized in the Cristalino deposit. The source of iron is uncertain, although the host rocks may be the most important reservoir. Despite the pervasive character of the calcic-ferric alteration, magnetite concentrates in mafic volcanic rocks, possibly due to its ferromagnesian primary minerals, which were partly destabilized to form hydrothermal iron oxides. On the other hand, little magnetite was observed in the Ca-Fe altered felsic rocks, showing actinolite marginally associated with iron oxide.

As the calcic-ferric minerals stabilized, the solutions had reached a level of temperature that may have allowed a local formation of the hastingsite-quartz assemblage. It may represent a discrete calcic-sodic alteration that is evidently later than the calcic-ferric alteration, since it acted upon rocks previously altered to actinolite-magnetite-allanite.

Later on, a new mineralization stage came into scene, generating the chalcopyrite±pyrite±hematite ore association with practically no magnetite, especially in

breccias and veins. This virtually magnetite-free ore represents a second mineralization stage (Fig.10-B) in the Cristalino area. Its formation coincides with the potassic alteration that affected the host rocks, notably the felsic volcanic rocks. It is dubious the temporal relationship between biotite and K-feldspar (Fig. 6E), the diagnostic minerals of the potassic alteration. However, if the hydrothermal system evolved with increasing f_{O2}, the precipitation of the biotite-magnetite pair should have preceded the K-feldspar-hematite pair.
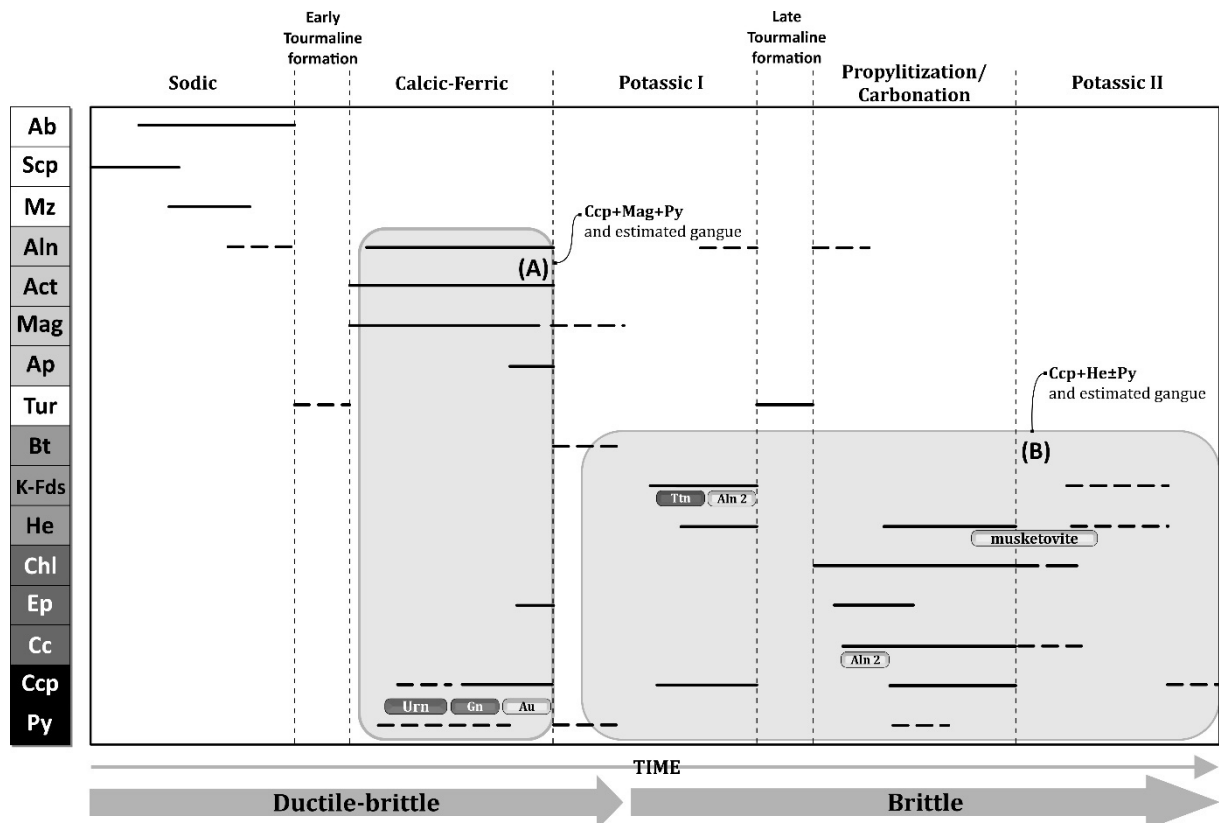
Figure 10. Paragenetic sequence of the hydrothermal alteration at the Cristalino deposit. (A) First mineralizing stage marked by a chalcopyrite+magnetite+pyrite±uraninite±galena±Au assemblage spatially associated with Ca–Fe alteration zones; (B) Second mineralizing stage, with chalcopyrite-hematite±pyrite associated in part with potassic alteration and epidote – calcite - chlorite alteration. Ab: albite, Act: actinolite, Aln: allanite, Ap: apatite, Bt: biotite, Cc: calcite, Ccp: chalcopyrite, Chl: chlorite, Ep: epidote, Fds: K-feldspar, Gn: galena, He: hematite, Mag: magnetite, Mz: monazite, Py: pyrite, Scp: scapolite, Tur: tourmaline, Urn: uraninite.

Based on the identified ore associations, it is plausible to assume that the fluid was initially less oxidizing and with lower Cu/Fe ratio and became more oxidizing (precipitation of hematite) and with higher Cu/Fe inhibiting largely the pyrite formation. Moreover, given that the brittle conditions are more prone to exist at shallower depths, the infiltration of surficial waters might have also contributed to the f_{O2} increase during the second mineralizing stage, allowing the formation of hematite.

As alteration advanced, the fluid became K-depleted due to the formation of K-feldspar and biotite, whereas calcium and carbonate species, among other components, had their concentrations relatively increased. These new chemical conditions combined with the progressive fall in temperature brought about the deposition of chlorite, epidote, and calcite. This mineral association commonly includes hematite or martite, representing a low temperature alteration assemblage marked by an overall loss of silica (abundance of chlorite), under oxidizing and acidic conditions. This propylitic alteration evolved to carbonation. Apparently, the solutions were still reactive to remove Ca from the host rocks and to precipitate it especially as calcite, with minor chalcopyrite, on multi-directional fracture planes. The second mineralization stage seems to extend over the propylitic and carbonation stages, mostly with chalcopyrite as part of the calcite-chlorite-epidote-hematite infill assemblage. The hydrothermal history of the Cristalino deposit ended with a discrete precipitation of K-feldspar in veins, characterizing a local and new potassic infill stage.

The chalcopyrite-pyrite-magnetite and the chalcopyrite-hematite ore paragenesis reflect distinct oxidation state of the mineralizing fluid, but also availability of iron. The magnetite formed plentifully during the calcic-ferric alteration, but was inexpressive in the subsequent alterations, when hematite became the major iron oxide without being, nonetheless, abundant.

The differences regarding the ore associations, redox conditions and Cu/Fe ratios of the fluid, and the crustal levels where the mineralization took place are suggestive that two IOCG systems may be superimposed at Cristalino. At a greater depth, sulfides (chalcopyrite, pyrite, with minor millerite and galena) alongside magnetite, monazite, allanite and minor apatite and uraninite, initially precipitated during the calcic-ferric alteration, whereas the younger sulfide generation, chiefly represented by chalcopyrite-rich breccias and veins, precipitated mainly during the potassic alteration when rocks had been significantly exhumed.

The log f_{O2} vs. log $a_{\Sigma S}$ diagram, at 2 kbar and 350 ºC, depicted in Figure 11, summarizes possible conditions of the mineralization stages in the Cristalino deposit.

A few multistage IOCG deposits have been described in the Carajás Province in the last decade and they seem to be confined to the southern sector of the Carajás Domain. The first mineralization stage of the Cristalino deposit is comparable to those of the Neoarchean Sossego (Sequerinho orebody), Bacaba, Visconde, and Castanha IOCG systems (Monteiro *et al*. 2008, Moreto *et al*. 2015a,b, Xavier *et al*. 2017). The Pb-Pb age of 2700 ± 29 Ma obtained on sulfides of a chalcopyrite-magnetite breccia from the Cristalino deposit (Soares *et al.*

2001) supports its formation in Neoarchean times, despite the high uncertainties of the analytical method used. On the other hand, the second mineralization stage is comparable to the Paleoproterozoic IOCG systems that have been described at the Sossego (Sossego orebody) and Alvo 118 deposits.
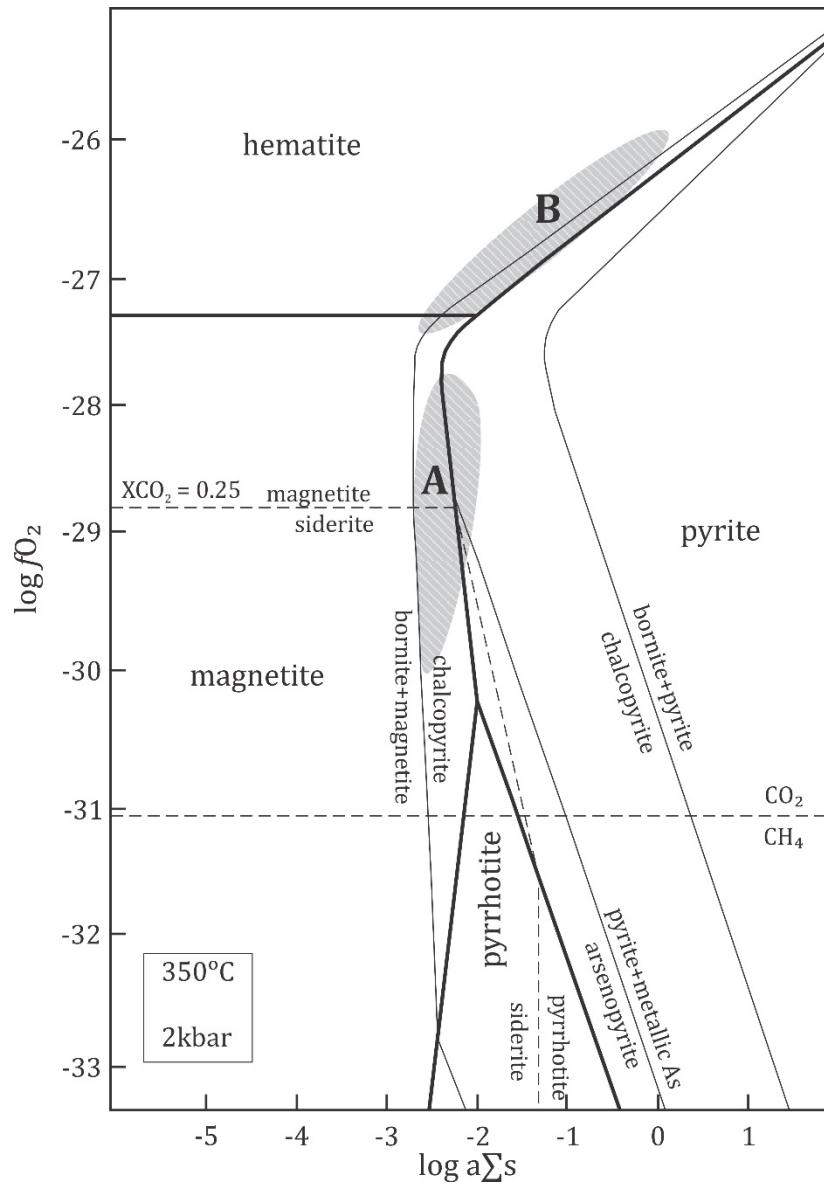
Figure 11. log $a_{\sum S}$ − log f_{O2} diagram at 350ºC and 2 kbar (modified from Mikucki and Ridley, 1993). (A) Suggested conditions for the first mineralization stage, with formation of chalcopyrite, pyrite and magnetite at relatively lower oxygen fugacity (f_{O2}) and sulfur activity (a_{S2}). (B) Suggested conditions for the second mineralization stage, at higher f_{O2} and a_{S2}, allowing the formation of chalcopyrite-hematite with minor pyrite and practically no magnetite.

The neighboring Borrachudo IOCG deposit also presents two mineralization stages (Previato 2016). The first copper mineralization was incipient and assumed to be Neoarchean. It consists of chalcopyrite-magnetite ore with abundant apatite formed in a brittle-ductile

deformational environment. The second and most economic copper mineralization, dated at 2.01 Ga (U-Pb in titanite, Previato 2016), is composed mainly of chalcopyrite (up to 90%) and associated with low-temperature minerals (chlorite-epidote-calcite). Magnetite is scarce. The proximity and similarities between the mineralization stages of both Cristalino and Borrachudo deposits suggest that they might be co-genetic and part of the E-W corridor of Neoarchean IOCG systems in Carajás.

CONCLUSIONS

The Cruzadão Granite is first described in the Cristalino deposit are and is the oldest unit there. The host rocks of the deposit are mainly the bimodal volcanic rocks of the Parauapebas Formation that have been subjected to an early and regional sodic alteration and deformed locally by shear zones. It was followed by pervasive calcic-ferric, potassic I, and propylitic alterations. The propylitic type grades to carbonation, which is represented by an array of calcite-rich veins. The hydrothermal history in the Cristalino area ends with a new but discrete potassic alteration (II). These metasomatic processes affected rocks subjected to deformational regimes that evolved from ductile-brittle to brittle, the transition occurring between the calcic-ferric and the potassic alteration I.

The Cristalino deposit is characterized by a major ~N15ºW-trending ore body that resulted from two mineralizing stages. The earlier stage took place at a greater depth and produced an ore association composed of chalcopyrite, pyrite, and magnetite, minor monazite and allanite, and subordinate amounts of uraninite, millerite, galena, and gold, yielding a Cu-Fe-Ni-Au-U-Pb-REE signature. Sulfides precipitated initially as disseminations and then in breccia matrix and veins particularly in Ca-Fe altered rocks. The later stage occurred at a shallower crustal level, where a practically magnetite-free ore association, consisting essentially of chalcopyrite-hematite±pyrite, was formed. The main modes of occurrence are in breccias and veins generated during the potassic and succeeding alterations. These ore associations are indicative that the hydrothermal system evolved with temperature decrease and increase in fO_2, and Cu/Fe ratio. However, $fO2$ decreased locally to give rise to Musketovite.

By comparison with similar Carajás copper-gold deposits, the first mineralization stage would be equivalent to the Neoarchean Sossego (Sequeirinho orebody), Castanha, Bacaba, Visconde deposits. The 2700 ± 29 Ma (Pb-Pb in sulfide) age determined for the magnetite-rich ore in the Cristalino deposit supports this interpretation. The second

mineralization stage, with chalcopyrite-rich and hematite-bearing ore in breccias is comparable to the Paleoproterozoic Alvo 118 and Sossego (Sossego-Curral orebody) deposits. Cristalino would be then another example of a multi-stage deposit lying in the E-W corridor of Neoarchean IOCG systems in Carajás.

Acknowledgements

References

Araújo, O.J.B., Maia, R.G.N., Jorge-João, X.S. Costa, e J.B.S. 1988. A megaestruturação da folha Serra dos Carajás. In: Congresso Latino Americano de Geologia, *Anais*...SBG, **7:**324-333.

Araújo, O.J.B. and Maia, R.G.N. 1991. Serra dos Carajás: folha SB.22-Z-A. Estado do Pará. Escala 1:250.000. Texto explicativo. Brasília: DNPM/CPRM,1991.164p.il. Programa Levantamentos Geológicos Básicos do Brasil (PLGB).

Augusto, R.A., Monteiro, L.V.S., Xavier, R.P., Souza Filho, C.R. 2008. Zonas de alteração hidrotermal e paragênese do minério de cobre do Alvo Bacaba, Província Mineral de Carajás (PA). *Revista Brasileira de Geociências*, **38:**263–277.

Barros, C.E.M., Barbey, P., Boullier, A.M. 2001. Role of magma pressure, tectonic stress and crystallization progress in the emplacement of the sysntectonic granites. The A-type Estrela Granite Complex (Carajás Mineral Province, Brazil). *Tectonophysics*, **343:**93–109.

Barros, C.E.M., Sardinha, A.S., Barbosa, J.P.O., Macambira, M.J.B., Barbey, P., Boullier, A.M. 2009. Structure, petrology, geochemistry and zircon U/Pb and Pb/Pb geochronology of the sinkinematic Archean (2.7 Ga) A-type granites from the Carajás Metallogenic Province, northern Brazil. *Canadian Mineralogist*. **47:**1423–1440.

Costa J.B.S., Araújo O.J.B., Santos, A., Jorge João, X.S., Macambira, M.J.B., Lafon, J.M. 1995. A Província Mineral de Carajás: aspectos tectono-estruturais, estratigráficos e geocronológicos. *Boletim do Museu Paraense Emílio Goeldi*, **7:**199-235.

Craveiro, G.S, Villas, R.N. da Costa Silva. A.R. 2012. Depósito Visconde, Carajás (PA): geologia e alteração hidrotermal das rochas encaixantes. *Revista Brasileira de Geociências*, **42:**453-470.

Craveiro, G.S., Xavier, R.P., Villas, R.N.N. 2018. Mineral chemistry and Geothermometry of alteration zones, IOCG Cristalino Deposit, Carajás Mineral Province, Brazil. *Manuscript submitted for publication*.

Dall'Agnol, R., Oliveira, D., Guimarães, F.V., Gabriel, E.O., Feio, G.R.L, Lamarão, C.N., Althoff, F.J., Santos, P.A., Teixeira, M.F.B, Silva, A.C., Rodrigues, D.S., Santos, M.J.P, Silva, C.R.P., Santos, R.D., Santos, P.J.L. 2013. Geologia do Subdomínio de Transição do Domínio Carajás: Implicações para a evolução arqueana da Província Carajás – Pará. In: 13° Simpósio Geologia da Amazônia. *Proceedings...* 2013. Belém, Pará. Brazil.

Dall'Agnol, R., Teixeira, N.P., Rämö, O.T., Moura, C.A.V., Macambira, M.J.B., Oliveira, D.C. 2005, Petrogenesis of the Paleoproterozoic, rapakivi, A-type granites of the Archean Carajás Metallogenic Province, Brazil. *Lithos*, **80:**101–129.

Dias, G.S., Macambira, M.B., Dall'Agnol, R., Soares, A.D.V., Barros, C.E.M. 1996, Datações de zircões de sill de metagabro: comprovação de idade arqueana da Formação Águas Claras, Carajás, Pará. In: SBG, 5° Simpósio de Geologia da Amazônia, Belém, *Anais*. pp. 376-378.

DOCEGEO, 1988. Revisão litoestratigráfica da Província Mineral de Carajás – Litoestratigrafia e principais depósitos minerais. *In*: Congresso Brasileiro de Geologia, 35. Belém, *Expanded abstract*, 11-54.

Feio, G.R.L., Dall'Agnol. R., Dantas, E.L., Macambira, M.J.B, Santos, J.O.S, Althoff, F.J., Soares, J.E.B. 2013. Archean granitoid magmatism in the Canaã dos Carajás área: Implications for crustal evolution of the Carajás Province, Amazonian craton, Brazil. *Precambrian Research*, **227:**15 –185.

Gibbs, A.K., Wirth, K.R., Hirata, W.K., Olszewski Jr., W.J. 1986. Age and composition of the Grão Pará Group volcanics, Serra dos Carajás. *Revista Brasileira de Geociências*, **16:**201–211.

Grainger, C.J., Groves, D.I., Tallarico, F.H.B., Fletcher, I.R. 2008. Metallogenesis of the Carajás Mineral Province, southern Amazon Craton: Varying styles of Archean through Paleoproterozoic to Neoproterozoic base- and precious-metal mineralization. *Ore Geology Reviews*, **33:**451-489.

Huhn, S.R.B., Souza, C.I.J., Albuquerque, M.C., Leal, E.D., Brustolin, V. 1999. Descoberta do depósito Cu (Au) Cristalino: Geologia e mineralização associada região da Serra do Rabo - Carajás – PA. *In*: SBG/NO, Simpósio de Geologia da Amazônia, Manaus, *Proceedings...* **6:**140–143.

Hunger, R.B. 2017. O depósito de óxido de ferro cobre-ouro (IOCG) Grota Funda, Domínio Carajás (PA): alteração hidrotermal, regime de fluidos e idade da mineralização. Masters dissertation. IG-UNICAMP, 182p.

Lindenmayer, Z. G., Fleck, A., Gomes, C.H., Santos, A.B.S., Caron, R., Paula, F.C., Laux, J.H., Pimentel, M.M., Sardinha, A.S. 2005. Caracterização geológica do alvo estrela (Cu-Au), Serra dos Carajás, Pará *In*: Marini, J.O.; Queiróz, E.T.; Ramos, W.B. (eds.), *Caracterização de distritos mineiros da Amazônia*. DNPM-CT/Mineral-ADIMB, Brasília 2005, cap. IV, 1, 137-205.

Lindenmayer, Z. G., Fleck, A., Gomes, C.H., Santos, A.B.S., Caron, R., Paula, F.C., Laux, J.H., Pimentel, M.M., Sardinha, A.S. 2005. Caracterização geológica do alvo estrela (Cu-Au), Serra dos Carajás, Pará In*: Caracterização de Depósitos Minerais em Distritos*

Mineiros da Amazônia. DNPM, CT-Mineral / FINEP, ADIMB, Brasília, 2005, cap. IV, 1, 137-205.

Lindenmayer, Z.G., Laux, J.H., Teixeira, J.B.G. 2001. Considerações sobre a origem das Formações Ferríferas da Formação Carajás, Serra dos Carajás. *Revista Brasileira de Geociências*, **31(1)**:21-28.

Lobato, L.M., Rosière, C.A., Silva, R.C.F., Zucchetti, M., Baars, F.J., Seoane, J.C.S., Rios, F.J., Pimentel, M., Mendes, G.E., Monteiro, A.M. 2005. A mineralização hidrotermal de ferro da Província Mineral de Carajás - controle estrutural e contexto na evolução metalogenética da Província. *In*: Marini, J.O.; Queiróz, E.T.; Ramos, W.B. (eds.), *Caracterização de distritos mineiros da Amazônia*. DNPM-CT/Mineral-ADIMB, Brasília 2005. Cap II, 25–92.

Macambira, E.M.B. and Vale, A.G. 1997. Programa Levantamentos Geológicos Básicos do Brasil: São Felix do Xingu, Folha SB.22-Y-B. Estado do Pará: Brasília, Departamento Nacional de Produção Mineral-Companhia de Pesquisa de Recursos Minerais (DNPM/CPRM), 384 p.

Macambira, J.B. 2003. O ambiente deposicional da Formação Carajás e uma proposta de modelo evolutivo para a Bacia Grão Pará. Doctoral thesis, IG-UNICAMP, 217p.

Machado, N., Lindenmayer, Z.G., Krogh, T.E., Lindenmayer, D. 1991. U–Pb geochronology of Archean magmatism and basement reactivation in the Carajás area, Amazon shield, Brazil. *Precambrian Research*, **49:**329–354.

Mansur, E.T. and Ferreira Filho, C.F. 2016. Magmatic structure and geochemistry of the Luanga mafic-ultramafic complex: Further constraints for the PGE-mineralized magmatism in Carajás, Brazil. *Lithos*, **266-267:**28–43.

Meirelles, M.R. and Dardenne, M.A. 1991. Vulcanismo basáltico de afinidade shoshonítica em ambiente de arco arqueano, Grupo Grão Pará, Serra dos Carajás, PA. *Revista Brasileira de Geociências*, **21:**41-50.

Melo, G.H.C., Monteiro, L.V.S., Xavier, R.P., Moreto. C.P.N., Santiago, E.S.B., Dufrane, S.A., Aires, B. 2017. Temporal Evolution of the giant Salobo IOCG deposit, Carajás Province (Brazil): constraints from paragenesis of hydrothermal alteration and U-Pb geochronology. *Mineralium Deposita*, **52:**709–732.

Monteiro, L.V.S., Xavier, R.P., Carvalho, E.R., Hitzman, M.W., Johnson, C.A., Souza Filho, C.R., Torresi, I. 2008. Spatial and temporal zoning of hydrothermal alteration and mineralization in the Sossego iron oxide- copper-gold deposit, Carajás Mineral Province, Brazil: Parageneses and stable isotope constraints. *Mineralium Deposita*, **43:**129−159.

Moreto, C.P.N., Monteiro, L.V.S., Xavier, R.P., Creaser, R.A., Dufrane, S.A., Melo, G.H.C., Delinardo da Silva, M.A., Tassinari, C.C.G., Sato, K. 2015a. Timing of multiple hydrothermal events in the iron oxide–copper–gold deposits of the Southern Copper Belt, Carajás Province, Brazil. *Mineralium Deposita*, **50:**517–546.

Moreto, C.P.N., Monteiro, L.V.S., Xavier, R.P., Creaser, R.A., Dufrane, S.A., Tassinari, C..CG., Sato, K., Kemp, A.I.S., Amaral, W.S. 2015b. Neoarchean and Paleoproterozoic iron oxide-copper-gold events at the Sossego deposit, Carajás Province, Brazil, Re-Os and U-Pb geochronological evidence. *Economic Geology*, **110**:809–835.

Mougeot, R., Respaut, J.P., Briqueu, L., Ledru, P., Milesi, J.P., Lerouge, C., Marcoux, E., Huhn, S.B., Macambira, M.J.B. 1996. Isotope geochemistry constrains for Cu, Au

mineralizations and evolution of the Carajás Province (Para, Brazil). In: SBG, Congresso Brasileiro de Geologia, Salvador. *Anais...*, **7:**321–324.

Mukicki, E.J. and Ridley, J.R. 1993. The hydrothermal fluid of Archean lode-gold deposits at different metamorphic grades: composition constrains from ore and wallrock alteration assemblages. *Mineralium Deposita*, **28:**469–481.

Nogueira, A.C.R., Truckenbrodt, W., Pinheiro, R.V.L. 1995. Formação Águas Claras, Pré-cambriano da Serra dos Carajás: redescrição e redefinição litoestratigráfica. *Boletim do Museu Paraense Emílio Geoldi*, **7:**177–197.

Oliveira, J.R.1994. Programa Levantamentos Geológicos Básicos do Brasil: Folha Serra Pelada (Folha SB.22-Z-A). Estado do Pará. Brasília, DNPM/CPRM, 248p.

Pestilho, A.L.S. 2011. Sistemática de isótopos estáveis aplicada à caracterização da evolução dos paleo-sistemas hidrotermais associados aos depósitos cupríferos Alvo Bacaba e Alvo Castanha, Província Mineral de Carajás, PA. Masters dissertation, University of Campinas.

Pestilho, A.L.S. and Monteiro, L.V.S. 2008. Caracterização petrográfica das zonas de alteração hidrotermal e paragêneses do minério de cobre e ouro do Alvo Castanha, Província Mineral de Carajás; *In*: IV Simpósio de Vulcanismo e Ambientes Associados, Foz do Iguaçu, Proceedings, Sociedade Brasileira de Geologia [CD-ROM].

Pinheiro, R.V.L. and Holdsworth, R.E. 2000. Evoluão tectonoestratigráfica dos sistemas transcorrentes Carajás e Cinzento, Cinturão Itacaiúnas, na borda leste do Cráton Amazônico, Pará. *Revista Brasileira de Geociências*, **30(4):**597-606.

Pinto, A. 2012. Salobo Copper Mine Feasibility in Carajás, Pará State. *In*: ADIMB, V Brazilian Symposium on Mineral Exploration. 2012. Ouro Preto - MG, Brazil.

Previato, M., 2016. Evolução paragenética e regime de fluidos hidrotermais no sistema Borrachudo: Implicações para a metalogênese e cobre na Província Carajás. Masters dissertation.IG-USP. 131p.

Rämö, O.T. Dall'Agnol, R., Macambira, M.J.B., Leite, A.A.S., Oliveira, D.C. 2002. 1.88 Ga Oxidized A-type Granites of the Rio Maria Region, Eastern Amazonian Craton, Brazil: Positively Anorogenic! *The Journal of Geology*, **110:** 603 – 610.

Réquia, K., Stein, H., Fontboté, L., Chiaradia, M. 2003. Re–Os and Pb–Pb geochronology of the Archean Salobo iron oxide copper–gold deposit, Carajás Mineral Province, northern Brazil. *Mineralium Deposita*, **38:**727–738.

Ribeiro, A.A., Suíta, M.T.F., Sial, A.N., Fallick, A.E., Eli F., Goulard, A.E. 2009. Geoquímica de isótopos estáveis (C, S e O) das rochas encaixantes e do minério de Cu (Au) do depósito Cristalino, Província Mineral de Carajás, Pará. *Geochimica Brasiliensis*, **23:** 159-176.

Ronzê, P.C., Soares, A.D.V., Santos, M.G.S. dos., and Barreira, C.F., 2000. Alemão copper-gold (U-REE) deposit, Carajás, Brazil, *in* Porter, T.M., ed., *Hydrothermal iron-oxide copper-gold and related deposits: A global perspective*. Adelaide, PGC Publishing, v. 1, p. 191−202.

Santos, J.O.S., Hartmann, L.A., Gaudette, H.E., Groves, D.I., Macnaughton. N.J., Fletcher, I.R. 2000. A new understanding of the Provinces of the Amazon Craton based of integration of field mapping and U-Pb and Sm-Nd geochronology. *Gondwana Research*, **4(3):** 453-488.

Santos, M.G.S. 2002. Estudo dos isótopos de Pb e Nd do Depósito de Cu-Au (U-ETR) Alemão, Província Mineral de Carajás (PA). Masters dissertation. IG/UFPA. 126p.

Sardinha, A.S., Barros, C.E.M. Krymsky, R. 2006. Geology, geochemistry and U–Pb geochronology of the Archean (2.74 Ga) Serra do Rabo granite stocks, Carajás Metallogenic Province, northern Brazil. *Journal of South American Earth Sciences*, **20:**327-339.

Siepierski, L. 2016. Geologia, petrologia e potencial para mineralizações magmáticas dos corpos máfico-ultramáficos da região de Canaã dos Carajás, Província Mineral de Carajás. Doctoral thesis, UnB, 158 f.

Silva, A.R, Villas, R.N., Lafon, J., Craveiro, G.S., Ferreira, V.P. 2015. Stable isotope systematics and fluid inclusion studies in the Cu-Au Visconde deposit, Carajás Mineral Province, Brazil: implications for fluid source generation. *Mineralium Deposita*, **50:**547-569.

Soares, A.D.V., Macambira, M.J.B., Santos, M.G.S., Vieira, E.A., Masotti, F.S., Souza, C.I.J., Padilha, J.L., Magni, M.C.V. 2001. Depósito Cu (Au) Cristalino, Serra dos Carajás PA: Idade da Mineralização com base em Análises Pv-Pb em sulfetos (Dados Preliminares). *In*: SBG, 7° Simpósio de Geologia da Amazônia, Belém, *Proceedings...* CD-ROM.

Soares, A.D.V., Ronzê, P.C., Santos, M. G.S., Leal, E.D., Barreira, C.F. 1999. Geologia e mineralizações do depósito de Cu-Au Alemão – Província Mineral de Carajás (PA). In: SBG, 5° Simpósio de Geologia da Amazônia, *Resumos expandidos...* Manaus:, p. 144-147.

Tallarico, F.H.B. 2003. O cinturão cupro-aurífero de Carajás, Brasil. Doctoral thesis. UNICAMP. 229p.

Tallarico, F.H.B., Figueiredo B.R., Groves D.I., Kositcin N., McNaughton N.J., Fletcher I.R., Rego J.L. 2005. Geology and SHRIMP U–Pb geochronology of the Igarapé Bahia deposit, Carajás copper–gold belt, Brazil: an Archean (2.57 Ga) example of iron–oxide Cu–Au–(U– REE) mineralization. *Economic Geology*, **100:**7–28.

Tavares, F.M. 2015. Evolução geotectônica do nordeste da Província Carajás. Doctoral thesis. IG-UFRJ. 115p.

Teixeira, A.S., Ferreira Filho, C.F., Giustina, M.E.S.D., Araújo, S.M., Silva, H.H.A.B. 2015. Geology, petrology and geochronology of the Lago Grande layered complex: evidence for a PGE-mineralized magmatic suite in the Carajás Mineral Province, Brazil. *Journal of South American Earth Sciences*, **64:**116-138.

Teixeira, J.B.G. 1994. Geochemistry, petrology, and tectonic setting of Archean basaltic and dioritic rocks from the N4 Iron deposit, Serra dos Carajás, Pará, Brazil. Doctoral thesis. IG-USP. 161p.

Torresi, I. Xavier, R.P., Bortholoto, D.F.A., Monteiro. L.V.S. 2012. Hydrothermal alteration, fluid inclusions and stable isotope systematics of the Alvo 118 iron oxide-copper-gold deposit, Carajás Mineral Province (Brazil); Implications for ore genesis. *Mineralium Deposita*, **47(3):**299–323.

Trendall, A.F., Basei, M.A.S., De Laeter, J.R., and Nelson, D.R. 1998. SHRIMP U-Pb constraints on the age of the Carajás formation, Grão Pará Group, Amazon Craton. *Journal of South American Earth Sciences*, **11:**265-277.

Vasquez, L.V., Rosa-Costa, L.R., Silva, C.G., Ricci, P.F., Barbosa, J.O., Klein, E.L., Lopes, E.S., Macambira, E.B., Chaves, C.L., Carvalho, J.M., Oliveira, J.G., Anjos, G.C., Silva, H.R., 2008. *Geologia e Recursos Minerais do Estado do Pará: Sistema de Informações Geográficas–SIG: Texto Explicativo dos Mapas Geológico e Tectônico e de Recursos Minerais do Estado do Pará. Organizadores*: M.L Vasquez, L.T. Rosa Costa. Scale1:1.000.000. Belém: CPRM.

Veloso, A.S.R., Monteiro, L.V.S,, Juliani, C. 2016. Depósito de cobre-(níquel) Jatobá, Província Carajás (PA): Evolução paragenética e fontes de enxofre. *In*: 48° Congresso Brasileiro de Geologia, *Proceedings...*, Porto Alegre, 2016.

Wirth, K.R., Gibbs, A.K., Olszewski, W.J. 1986. U-Pb ages of zircons from the Grão Pará group and Serra dos Carajás granite, Pará, Brazil. *Revista Brasileira de Geociências*, **16:**195 – 200.

Xavier, R.P., Monteiro, L.V.S., Moreto, C.P.N., Pestilho, A.L.S., Melo, G.H.C., Silva, M.A.D., Aires, B., Ribeiro, C., Silva, F.H.F. 2012. The iron oxide copper-gold system of the Carajás Mineral Province, Brazil. *Economic Geology, Special Publication*, 16, Chapter X.

Xavier, R.P., Moreto, C.P.N., de Melo, G.H.C., Toledo, P., Hunger, R., Delinardo, M., Faustinoni, J., Lopes, Ananda. 2017. Geology and metallogeny of Neoarchean and Paleoproterozoic copper systems of the Carajás Domain, Amazonian Craton, Brazil. *Proceedings* of the 14th Biennial SGA Meeting of the Society for Geology Applied to Mineral Deposits, Quebec, Canada. 20-23 August, pp.899-902.

Xavier, R.P., Wiedenbeck, M., Trumbell, R.B., Dreher, A.M., Monteiro, L.V.S., Rhede, D., Araújo, C.E.G., Torresi, I. 2008. Tourmaline B-isotopes fingerprint marine evaporites as the source of high-salinity ore fluids in iron-oxide-copper-gold deposits, Carajás Mineral Province (Brazil). *Geology*, **36:**743–746.

3 MINERAL CHEMISTRY AND GEOTHERMOMETRY OF ALTERATION ZONES, IOCG CRISTALINO DEPOSIT, CARAJÁS MINERAL PROVINCE, BRAZIL.

Gustavo Souza Craveiro

Raimundo Netuno Nobre Villas

Roberto Perez Xavier

Successfully received: submission Mineral chemistry and geothermometry of alteration zones, IOCG Cristalino Deposit, Carajás Mineral Province, Brazil. for Journal of South American Earth Sciences

1 mensagem

Journal of South American Earth Sciences <EviseSupport@elsevier.com> 28 de agosto de 2018 17:26
Responder a: sames@elsevier.com
Para: craveiro@ufpa.br

This message was sent automatically. Please do not reply.

Ref: SAMES_2018_321
Title: Mineral chemistry and geothermometry of alteration zones, IOCG Cristalino Deposit, Carajás Mineral Province, Brazil.
Journal: Journal of South American Earth Sciences

Dear Mr. Souza Craveiro,

Thank you for submitting your manuscript for consideration for publication in Journal of South American Earth Sciences. Your submission was received in good order.

To track the status of your manuscript, please log into EVISE® at: http://www.evise.com/evise/ faces/pages/navigation/NavController.jspx?JRNL_ACR=SAMES and locate your submission under the header 'My Submissions with Journal' on your 'My Author Tasks' view.

Thank you for submitting your work to this journal.

Kind regards,

Journal of South American Earth Sciences

Have questions or need assistance?
For further assistance, please visit our Customer Support site. Here you can search for solutions on a range of topics, find answers to frequently asked questions, and learn more about EVISE® via interactive tutorials. You can also talk 24/5 to our customer support team by phone and 24/7 by live chat and email.

Copyright © 2018 Elsevier B.V. | Privacy Policy

Elsevier B.V., Radarweg 29, 1043 NX Amsterdam, The Netherlands, Reg. No. 33156677.

Mineral Chemistry and Geothermometry of Alteration Zones, IOCG Cristalino Deposit, Carajás Mineral Province, Brazil.

Gustavo Souza Craveiro, Raimundo Netuno Nobre Villas, Roberto Perez Xavier.

Abstract

The Cristalino deposit, located in the Serra do Rabo region (Pará State, Brazil), is related to a hydrothermal system in which two major alteration stages could be distinguished most likely with the involvement of a hyper-saline fluid. The first stage (410-650º C) is characterized by a distal sodic metasomatism that produced almost pure chessboard albite, minor schorlitic tourmaline and REE-rich minerals (allanite-Ce, monazite). It was followed by a pervasive calcic-ferric alteration that generated abundant actinolite (X_{Mg}=0.87–0.69, Cl up to 0.59 wt. %) in addition to Ce-allanite and magnetite associated with sulfide disseminations and breccia-like bodies composed of chalcopyrite-pyrite-magnetite-Au (early ore association). Locally, Fe-edenite (X_{Mg}=0.67-0.42, Cl up to 2.94 wt. %) replaced calcic-ferric assemblages within restrict sodic-calcic alteration halos. From 410º down to 220º C, the previous alteration assemblages were overprinted by the hydrothermal products of the second stage. Potassic (K-feldspar, minor biotite) and propylitic (epidote, chlorite, calcite) alterations came into play successively. K-feldspar is practically stoichiometric, but it contains some impurities, notably BaO (up to 1.21 wt. %). Chlorite shows the greatest compositional variation among all minerals and its composition seems to have been particularly controlled by the type of host rock, chemistry of the hydrothermal fluid and temperature. Both chamosite and clinoclore (X_{Fe}=0.37-0.80) are present, the former being more common. Chlorine contents are in general < 0.02 wt. % and a little more significant in chlorites that replaced chessboard albite (up to 0.06 wt. %). Their formation temperature ranges from 220º to 360º C, the infill chlorites showing the highest values. The late ore association (chalcopyrite-Au±pyrite±hematite) is contemporaneous with the potassic and propylitic alterations and bears evidence that the Cristalino system evolved to the final stages with increase in oxygen fugacity. Comparatively to other IOCG deposits from the southern sector of the Carajás domain, especially the Sossego and Visconde deposits, two varieties of amphibole (mainly actinolite and edenite) have been formed, but the Cristalino chlorites, despite some overlapping, present very distinct populations not yet described in the other two deposits, confirming the diversity of IOCG systems in Carajás.

Keywords: Cristalino deposit, Iron oxide-copper-gold deposit, Carajás Mineral Province, Mineral Chemistry, Geothermometry

*G. S. Craveiro, e-mail: craveiro@ufpa.br;
G. S. Craveiro; R. N. N. Villas,
Graduate Program in Geology and Geochemistry, Geoscience Institute, Federal University of Pará-UFPA, Rua Augusto Corrêa, 01 Guamá, P.O. Box 1611, 66075-110 Belém, PA, Brazil.
R. N. N. Villas, e-mail: netuno@ufpa.br

R. P. Xavier, e-mail: xavier@ig.unicamp.br
Instituto de Geociências, Universidade Estadual de Campinas, R. João Pandiá Calógeras, 51, CEP 13083-970, Campinas, SP, Brazil

INTRODUCTION

In the Carajás Province (Amazonian Craton, northern Brazil) lie several economically important iron oxide-copper-gold deposit (IOCG) which make up reserves of 100–990 Mt @ 0.77–1.4% Cu and 0.28–0.86g/t Au (Xavier *et al.* 2017). These deposits belong to a broad copper system which is controlled by the regional-scale WNW-ESE–striking Cinzento and Carajás shear zones. The host rocks of the Carajás IOCG deposits are Mesoarchean gneisses and granitoids of the Xingu Complex, supracrustal units of the Carajás Domain (CD), especially the Neoarchean volcano-sedimentary Itacaiúnas Supergroup, as well as 2.7 Ga syntectonic alkaline granites and related gabbros and diorites (Grainger *et al.* 2008).

The Carajás IOCG deposits present intense hydrothermal alteration, marked by proximal potassic alteration with associated magnetite, surrounded by a regional sodic and sodic-calcic alteration in deeper or distal zones, and by an ore-related and late-stage chlorite-carbonate alteration. Sulfides generally post-date the iron-oxides and occur as disseminations, breccias, veins and stockwork. Chalcopyrite, pyrite, and bornite are the main ore minerals, along with Ni and Pb sulfides, being the Cu-U-Au-REE metal suite common for these deposits (Grainger *et al.* 2008, Moreto *et al.* 2015 a,b, Xavier *et al.* 2017).

The formation of the Carajás IOCG deposits spanned from the Neoarchean to the Paleoproterozoic and covered three distinct periods: (1) 2.72 - 2.68 Ga, confined to the southern sector of the CD and having as examples the Sossego (Sequeirinho - Pista ore bodies, 245 Mt @ 1.1 wt. % Cu, 0.28 g/t Au) and satellite deposits, including Bacuri, Bacaba, Castanha, Visconde and Pedra Branca (Moreto *et al.* 2015a, b); (2) 2.60 - 2.53 Ga, represented by deposits that lie in the CD northern sector such as Salobo (1.11 Gt at 0.69 % Cu and 0.43 g/t Au), Igarapé Bahia/Alemão (219 Mt @ 1.4 wt.% Cu, 0.86 g/t Au) and Grota Funda (Réquia *et al.* 2003, Tallarico *et al.* 2005, Hunger 2017); and (3) 1.90 - 1.88 Ga, recorded in deposits also located at the CD southern sector, comprising the Sossego ore body

(245 Mt @ 1.1 wt.% Cu, 0.28 g/t Au; Lancaster *et al.* 2000) and Alvo 118 (ca. 170 Mt @ 1.0% Cu and 0.3 g/t Au (Grainger *et al.* 2008; Xavier *et al.* 2017).

Field relationships and geochronological data allowed interpreting the genesis of the Carajás IOCG deposits as a result of multi-stage events related to the closure of the intracratonic Carajás Basin at ca. 2.7 Ga, as well as to successive reactivation of the Cinzento and Carajás shear zones around 2.6 Ga and 1.9 Ga, which brought about deep-seated fluid circulation and emplacement of Neoarchean and Paleoproterozoic Cu-Au systems in the CD (Xavier *et al.* 2017). A magmatic genetic link is more straightforward between the widespread 1.88 A-type granitic magmatism and the Paleoproterozoic IOCG deposits, but it is less obvious for older deposits. However, it is worth pointing out that the 2.7-2.5 Ga granitic magmatism (e.g. Plaquê and Planalto suite) may have played important role as heat, metal and fluid source, since it temporally overlaps with most Carajás IOCG deposits. Significantly, stable isotopic data support the development of hybrid hydrothermal systems with a magmatic component (Xavier *et al.* 2007, Monteiro *et al.* 2008a, Silva *et al.* 2015).

Despite the large amount of data already available on the Carajás IOCG deposits, their geological environment and time-space relationships with granite suites, particularly concerning the Neoarchean examples, have not yet been fully resolved. Another critical issue is the source of metals, fluids, and vital components for ore formation, such as S and Cl.

The Cu-Au Cristalino deposit (379 Mt @ 0.66 wt.% Cu; 0.3 g/t Au; Vale 2012) is an example of a multi-stage IOCG deposit (Craveiro *et al.* submitted), in which basalts, gabbros and rhyolites were converted by hydrothermal alteration mostly into amphibole-, K-feldspar- and chlorite-calcite-rich assemblages (Soares *et al.* 2001, Ribeiro *et al.* 2009). Data on the chemistry of hydrothermal minerals (Oberti *et al.* 1993, Léger *et al.* 1996, Gieré and Sorensen 2004, Monteiro *et al.* 2008b, Cunha *et al.* 2016) and estimates of their formation temperature (Kranidiotis and MacLean 1987, Holland and Blundy 1994) may set more strictly the different stages and shed some light on the evolution history of the Cristalino deposit.

This paper deals with the chemical composition of selected hydrothermal minerals and the application of geothermometers in order to constrain some conditions under which hydrothermal alteration took place in the Cristalino deposit. It is also sought to collect data that can subsidize answers to some of those critical issues, besides pointing out possible differences and similarities with other IOCG deposits present in the Carajás domain.

GEOLOGICAL SETTING OF THE CARAJÁS DOMAIN

Located in the east-southeast region of the Amazonian craton, Pará State, Brazil, the Carajás Province is divided into two crustal segments: the southern Rio Maria Domain and the northern Carajás Domain (Vasquez *et al*. 2008) (Fig. 1A)

The Carajás Domain (Fig. 1B) consists of the Mesoarchean (3.0 - 2.83 Ga) basement rocks, with TTG-like gneisses-migmatites, orthogranulites and calc-alkaline granitoids overlain by the Neoarchean metavolcano-sedimentary sequences of the Rio Novo Group (>2.76 Ga) and Itacaiúnas Supergroup (2.76 - 2.73 Ga) as well as the metasiliciclastic rocks of the Águas Claras Formation (> 2.65 Ga) (Fig. 1B; Vasquez *et al.* 2008).

The Rio Novo Group is a mafic/ultramafic volcano-sedimentary sequence containing banded iron formations (BIF) and metaquartzites (Araújo and Maia 1991, Oliveira 1994, Vasquez *et al*. 2008) which outcrops in the Serra Pelada region. It is intruded by the Luanga mafic-ultramafic and the Estrela granitic complexes, both dated at 2736 ± 3 Ma, value that constrains the minimum age of this group (Machado *et al*. 1991, Barros *et al*. 2001).

The Itacaiúnas Supergroup (2.77 - 2.73 Ga) is represented by the Igarapé Salobo, Grão Pará, Igarapé Bahia and Igarapé Pojuca groups which host several world-class metallic deposits. Their lower units are dominantly composed of bi-modal volcanic rocks, whereas the intermediate units comprise thick layers of BIF. Dominantly of sedimentary nature, the upper units are made up of metasiltstones, metargilites and BIF intercalated with metabasalts and metarhyolites, (DOCEGEO 1988, Soares *et al*. 1999, Ronzê *et al*. 2000, Lindenmayer *et al*. 2001, Vazquez *et al*. 2008).

During the Neoarchean, intense plutonic activity took place in the Carajás Domain and several intrusions were emplaced into the basement and the Itacaiúnas Supergroup rocks, varying from mafic-ultramafic to granitic in composition. The former is represented by the Serra Leste and Cateté Intrusive suites, which consist of elongated layered bodies that form clusters of PGE-, Cr- and Ni-bearing mafic-ultramafic rocks (Macambira and Vale 1997, Ferreira Filho *et al*. 2013, Siepierski 2016). The chromite-bearing Luanga and Lago Grande complexes belong to the Serra Leste Suite and have been dated, respectively, at 2763 ± 7 Ma (Machado *et al*. 1991) and 2722 ± 53 Ma (Teixeira *et al*. 2015). The granitic plutonism is mainly represented by the Estrela complex, Plaquê and Planalto suites, Igarapé Gelado and Old Salobo granites that span in age from 2.76 to 2.53 Ga (Machado *et al*. 1991, Barros *et al*. 2004, Sardinha *et al*. 2006, Feio *et al*. 2012).

The Archean sedimentary covers include the Águas Claras Formation, which overlies unconformably the Itacaiúnas Supergroup (Nogueira *et al.* 1995), and the Rio Fresco Formation, which in turn overlies the Rio Novo Group and hosts the epigenetic Au-PGE Serra Pelada deposit (Grainger *et al.* 2008). Águas Claras deposition age is uncertain, ranging from 2.70 to 2.65 Ga, according to U-Pb dating on zircon monocrysts from crosscutting mafic dikes (Dias *et al.* 1996), Mougeot *et al.* 1996, Trendall *et al.* 1998).

The Paleoproterozoic is essentially represented by several granitic intrusions that crosscut the basement and the metavolcano-sedimentary sequences with ages varying from 1883±2 to 1874±2 Ma (Machado *et al.* 1991, Rämö *et al.* 2002, Dall'Agnol *et al.* 2005). They are non-deformed metaluminous to peraluminous A-type granites that have been assembled in the Serra dos Carajás Intrusive Suite (Dall'Agnol *et al.* 2005) to which belong the Serra dos Carajás, Cigano and Pojuca granites. Other granites form also part of this suite, such as the Rio Branco and Breves granites. The latter intrusion hosts a Cu ± Au ± (Mo, W- Sn) mineralization that has resulted from a hybrid hydrothermal system with a complex evolution involving the interaction of magmatic and meteoric fluids with pre-existing oxidized rocks (Botelho *et al.* 2005).

Vestiges of a Paleoarchean crust in the Carajás Domain come from detrital zircon crystals that provided U-Pb ages up to 3.20 Ga (Galarza and Macambira 2002, Dall'Agnol *et al.* 2005). Accretional and collisional processes involving consolidated crustal segments ranging from 3.08-2.93 to 2.87-2.83 Ga are related to the agglutination of the basement assemblage (Feio *et al.* 2013). Between 2.76 and 2.70 Ga, the Carajás Domain underwent a new tectonic activity, marked by both the deposition of the volcano-sedimentary sequences of the Itacaiúnas Supergroup (Docegeo 1988) and by mafic/ultramafic and granitic plutonism. The rock deposition occurred in a basin whose origin has been attributed to an intracontinental rift (Gibbs *et al.* 1986, DOCEGEO 1988, Macambira 2003, Tallarico *et al.* 2005) or a magmatic arc (Meirelles and Dardenne 1991, Teixeira 1994, Lindenmayer *et al.* 2005, Lobato *et al.* 2005). The most remarkable Carajás Domain structures are considered coeval with the 2.76-2.71 Ga type-A granite intrusions (Barros *et al.* 2009), a hypothesis also defended by Feio *et al.* (2013) and Dall'Agnol *et al.* (2013). These structures have resulted from a NE-SE crustal shortening, which is associated with strike-slip and oblique shear zones in the Itacaiúnas Supergroup rocks and evidenced by an E-W sub-vertical foliation in the basement units. Reactivation took place at least three times from the Archean to the Paleoproterozoic (Costa *et al.* 1995, Araújo *et al.* 1988, Pinheiro and Holdsworth 2000).
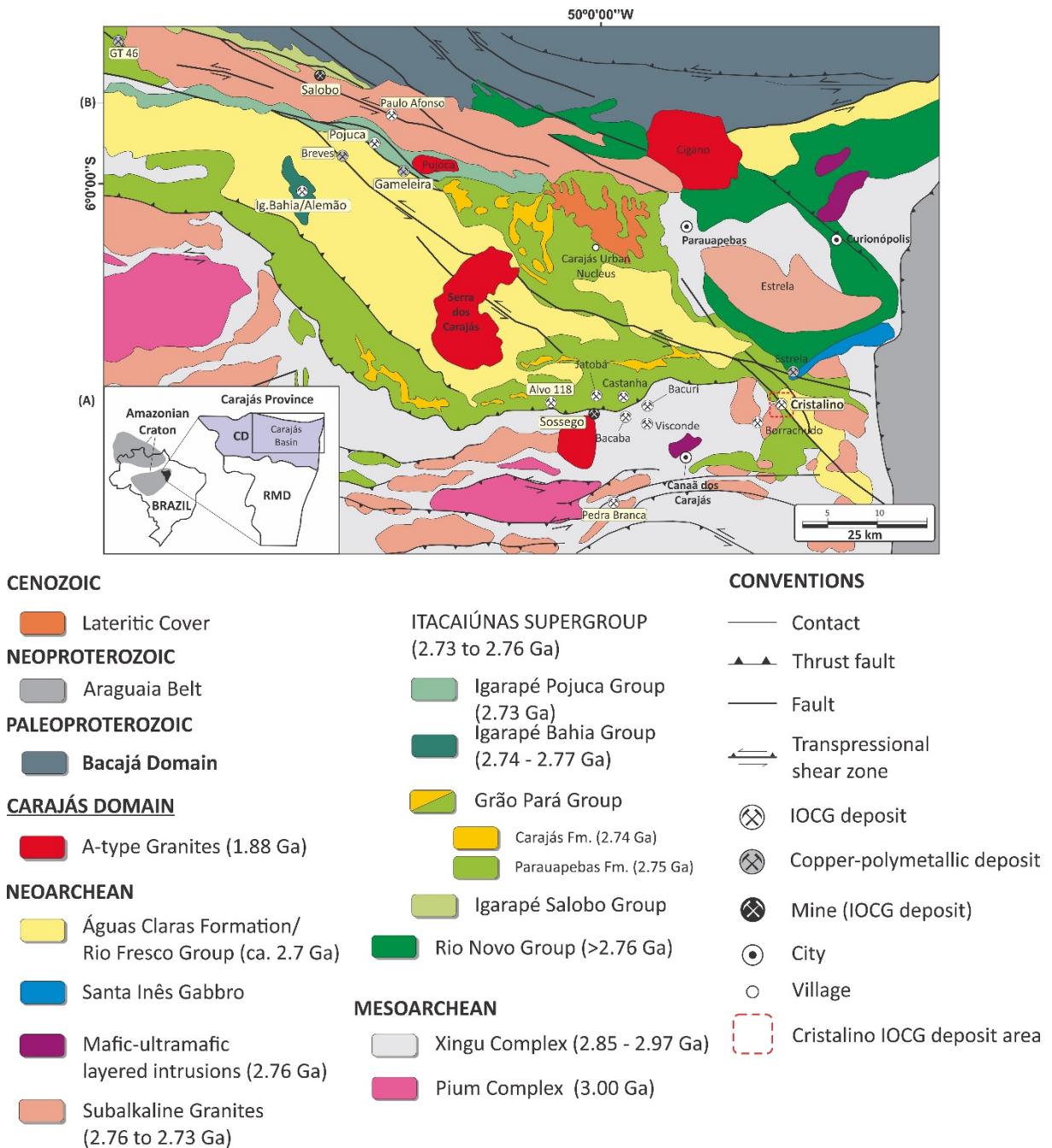
Figure 1. (A) Tectonic compartmentation of the Amazonian Craton (Santos et al. 2000); (B) Main tectono-stratigraphic units of the Carajás Domain (compiled and modified from Vasquez *et al*. 2008, Xavier *et al*. 2012, Dall'Agnol *et al*. 2013, Feio *et al*. 2013, Tavares 2015).

GEOLOGY OF CRISTALINO DEPOSIT

Main Lithological Units

The Cristalino deposit occurs in the eastern termination of the Carajás fault, in the Serra do Rabo region, being located about 40 km east of the Sossego mine and 9 km northeast of the Borrachudo deposit (Fig. 1B). The main lithotypes in the Cristalino deposit area are recognized as: (1) basement rocks; (2) a volcano-sedimentary sequence; and (3) mafic-felsic intrusions. (Huhn *et al.* 1999b, Soares *et al.* 2001, Ribeiro *et al.* 2009, Tavares 2015, Craveiro *et al.* accepted). The mineralization is hosted by the Grão Pará Group, mainly its lower felsic and mafic volcanic rocks (Parauapebas Formation) and, to a lesser extent, banded iron formations (Carajás Formation). The geological map and sections of the Cristalino deposit are depicted in figures 2A and 2B, respectively.

The Cruzadão Granite (2831 ± 6 Ma, 2848 ± 5 Ma, U-Pb in zircon, Moreto *et al.* 2011) does not crop out in the deposit area but has been intercepted by drill cores at depth. It represents the basement and it is observed in sharp contact with both the volcanic rocks of Parauapebas Formation and the Serra do Rabo Granite. The Serra do Rabo intrusion occurs in the NE portion of the deposit area and has been dated at 2743 ± 1.6 Ma (Sardinha *et al.* 2006).

The Cruzadão Granite is overlain discordantly by the Grão Pará Group, especially by the Parauapebas Formation rocks (Fig. 3) that include rhyolitic and basaltic varieties. This formation is the main host of the Cristalino deposit and varies texturally and in alteration intensity, being transected by mm- to cm-thicker shear zones and veins with variable compositions. The mafic volcanic rocks display aphanitic to vesicular texture (Fig. 3A, 3B) and are composed mostly of amphibole, magnetite, allanite, and chlorite (Fig. 3C, 3D). Less abundant than the mafic variety in the mineralized area, the felsic volcanic rocks show a rhyolitic composition (Fig. 3F) and have been altered by tourmaline (Fig. 3F, 3G, 3H), amphibole (Fig. 3G, 3H), K-feldspar, and chlorite-epidote-calcite. In cm-thick shear zones (Fig. 3H), tourmaline and elongated blue quartz crystals define a mineral lineation (Fig. 3H).

Both the volcanic rocks of the Grão Pará Group and the Serra do Rabo granite are crosscut by NNW-SSE-trending gabbro dikes, probably related to the Neoproterozoic Rio da Onça Gabbro (Tavares 2015).

Hydrothermal Alteration

The hydrothermal alteration is mainly observed along lithological contacts and NW-SE and NE-SW second order shear zones and is best developed in the volcanic rocks of the

Parauapebas Formation. It varies in intensity and typology, having evolved under ductile-brittle to dominantly brittle regime. The early stages are dominated by a distal sodic alteration and a proximal calcic-ferric alteration. Later on, the rocks experienced a proximal potassic alteration at essentially brittle conditions that was followed by a chlorite-epidote-calcite alteration (propylitization).
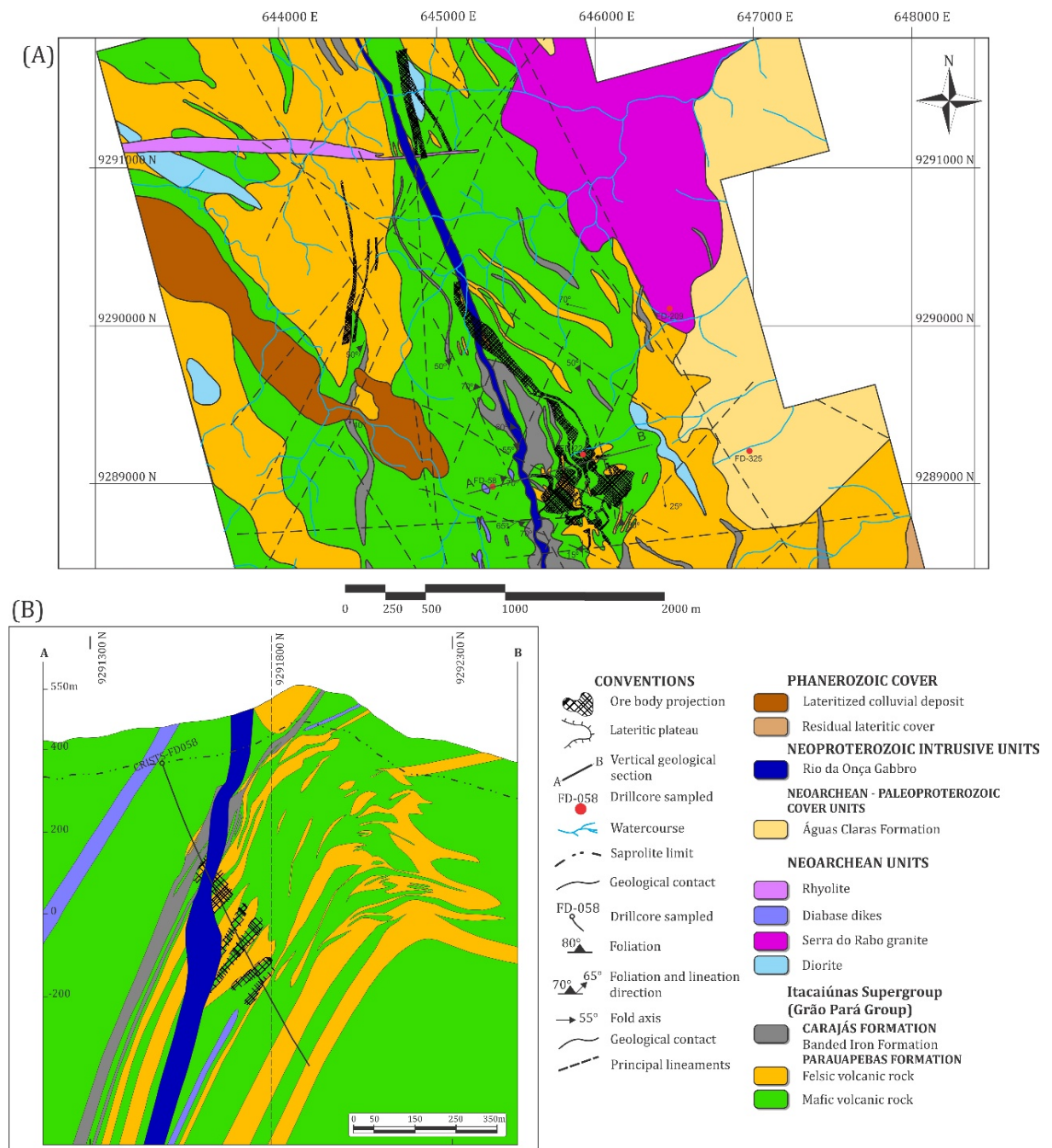
Figure 2. Geology of Cristalino deposit: (**A**) Geological map (1:5.000 scale), modified from Soares *et al.* (2001) and Vale (2003); (**B**) Geological section modified from vale 2003.
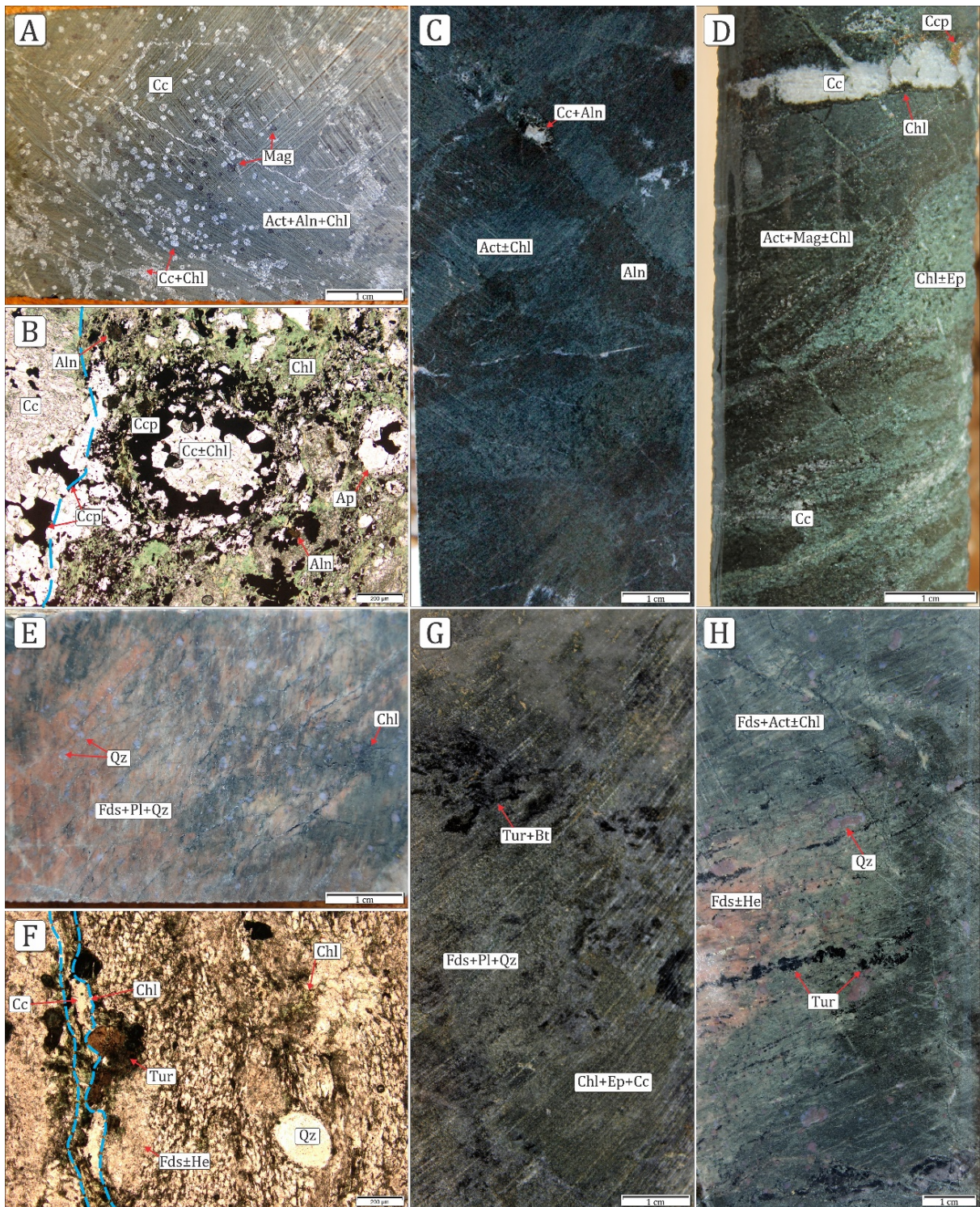
Figure 3. Petrographic aspects of volcanic rocks from the Parauapebas Formation, the main host rocks of the Cristalino deposit. All photographs represent drill core samples, except for B and F, which are photomicrographs in plane polarized light (PPL). (**A**) Chloritized aphanitic mafic volcanic rock plenty of vesicles transected by several calcite veinlets; (**B**) One of the vesicles depicted in Figure A filled by calcite-chlorite-chalcopyrite besides apatite and chalcopyrite; (**C**) Aphanitic mafic volcanic rock altered to actinolite (dark green) and allanite (dark brown); (**D**) Altered fine-grained volcanic rock crosscut by centimeter-thick shear zone. Within the shear zone, actinolite and magnetite are partially replaced by chlorite-calcite-epidote. In the upper part of the photograph, a calcite-chlorite-chalcopyrite

vein crosscuts the rock; (**E**) Fine-grained felsic volcanic rock with blue quartz. K-feldspar, plagioclase and quartz, the main constituents of the rock, are partially replaced by chlorite; (**F**) Slightly chloritized felsic volcanic rock showing turbid K-feldspar, probably impregnated with fine hematite, in addition to quartz and tourmaline. At left, a calcite-chlorite veinlet transects the rock; (**G**) Felsic volcanic rock affected by tourmaline, biotite, and chlorite-epidote-calcite alteration; (**H**) Deformed altered felsic volcanic rock made up of K-feldspar (stained by hematite), blue quartz, actinolite and minor chlorite, and tourmaline crystals defining mineral lineation along the shear zone. Act: actinolite; Aln: allanite; Ap: apatite, Bt: biotite; Cc: calcite; Ccp: chalcopyrite; Chl: chlorite; Ep: epidote; Fds: K-feldspar; He: hematite; Mag: magnetite; Pl; plagioclase; Qz: quartz; Tur: tourmaline.

The sodic metasomatism is characterized by the presence of chessboard albite developed at the expense of primary plagioclase of the volcanic rocks. Monazite and allanite, with minor quartz and calcite, occur associated with chessboard albite. Scapolite was only observed distally in outcrops of the Cruzadão Granite and is most likely also related to the sodic alteration.

The texture destructive calcic-ferric alteration is marked by the development of actinolite, magnetite and allanite over primary ferromagnesian minerals. Minor apatite, epidote, and rare uraninite are part of this alteration stage.

The Na- and Ca-Fe-rich assemblages were affected by potassic alteration during which small amounts of biotite initially formed in equilibrium with magnetite, followed then by K-feldspar growth along with hematite, quartz, and titanite.

Tourmaline is chiefly observed in felsic volcanic rocks and seems to have been formed: (1) earlier, in association with chessboard albite, allanite and monazite, during the sodic alteration; and (2) later, as tourmaline-bearing veins and aggregates, in zones formerly altered by hydrothermal K-feldspar.

The chlorite-epidote-calcite association overshadows all previous alteration stages, selectively growing over sodic, calcic and ferromagnesian minerals, and destroying pre-existing textures.

The infill stages are characterized by K-feldspar-rich and calcite-rich veins, both with variable proportions of quartz, allanite, chalcopyrite, hematite, chlorite and epidote. The former tends to form straight veins that show cm-thick alteration halos, while the latter, despite presenting alteration halo with variable thickness, is multi-directional and crosscuts most host rocks and structures, tending to evolve to breccias.

Cu-Au mineralization styles and ore association

The Cristalino deposit encompasses a major ~N15ºW-trending ore body, hosted in bi-modal volcanic rocks of the Parauapebas Formation with minor occurrences in banded iron formation (BIF) of the Carajás Formation. Three types of ore have been identified: (1) disseminations; (2) breccias; and (3) sulfide-bearing veins/veinlets.

Disseminations occur either as chalcopyrite and pyrite coexisting with magnetite (up to 50%) and minor allanite (Fig. 4G) and uraninite (Fig. 4J), chiefly in mafic volcanic rocks, or as chalcopyrite accompanied by minor hematite, pyrite, and practically no magnetite, in felsic volcanic rocks. The chalcopyrite-pyrite-magnetite-Au association is related to the late stages of the calcic-ferric alteration, whereas the chalcopyrite±Au±pyrite±hematite association is mainly related to the potassic and propylitic alterations.

The mineralized breccias form part of the main ore body and are preferably hosted in mafic volcanic rocks. Two types of breccias can be distinguished: (1) chalcopyrite-pyrite-magnetite breccia-like bodies (Fig. 4A, 4E, 4F), generally hosted by mafic volcanic rocks previously affected by calcic-ferric (actinolite-magnetite-allanite) and developed at the vicinity of magnetite-rich zones; and (2) chalcopyrite±hematite breccias (Fig. 4B, 4H), which occur particularly in felsic volcanic rocks affected by potassic alteration (K-feldspar) and followed by propylitization/carbonation.

Chalcopyrite-bearing veins and veinlets are often related to chalcopyrite±hematite breccia bodies and crosscut the volcanic rocks in multiple directions, varying in composition and proportion of sulfides. The most common assemblage is chalcopyrite-calcite±pyrite±hematite ±magnetite (musketovite?) (Fig. 4C, 4D, 4I) followed by less expressive chalcopyrite-K-feldspar±pyrite±hematite.

Based on the type of the iron oxide present in the ore assemblage, two parageneses have been distinguished (Craveiro *et al*. submitted): a) chalcopyrite-magnetite-pyrite occurring as disseminations and breccia-like bodies temporally and spatially related to the calcic-ferric alteration; and b) chalcopyrite±hematite±pyrite identified in breccias and sulfide-rich veins hosted mostly in felsic volcanic rocks that have been affected by potassic (K-feldspar) and propylitic alterations.
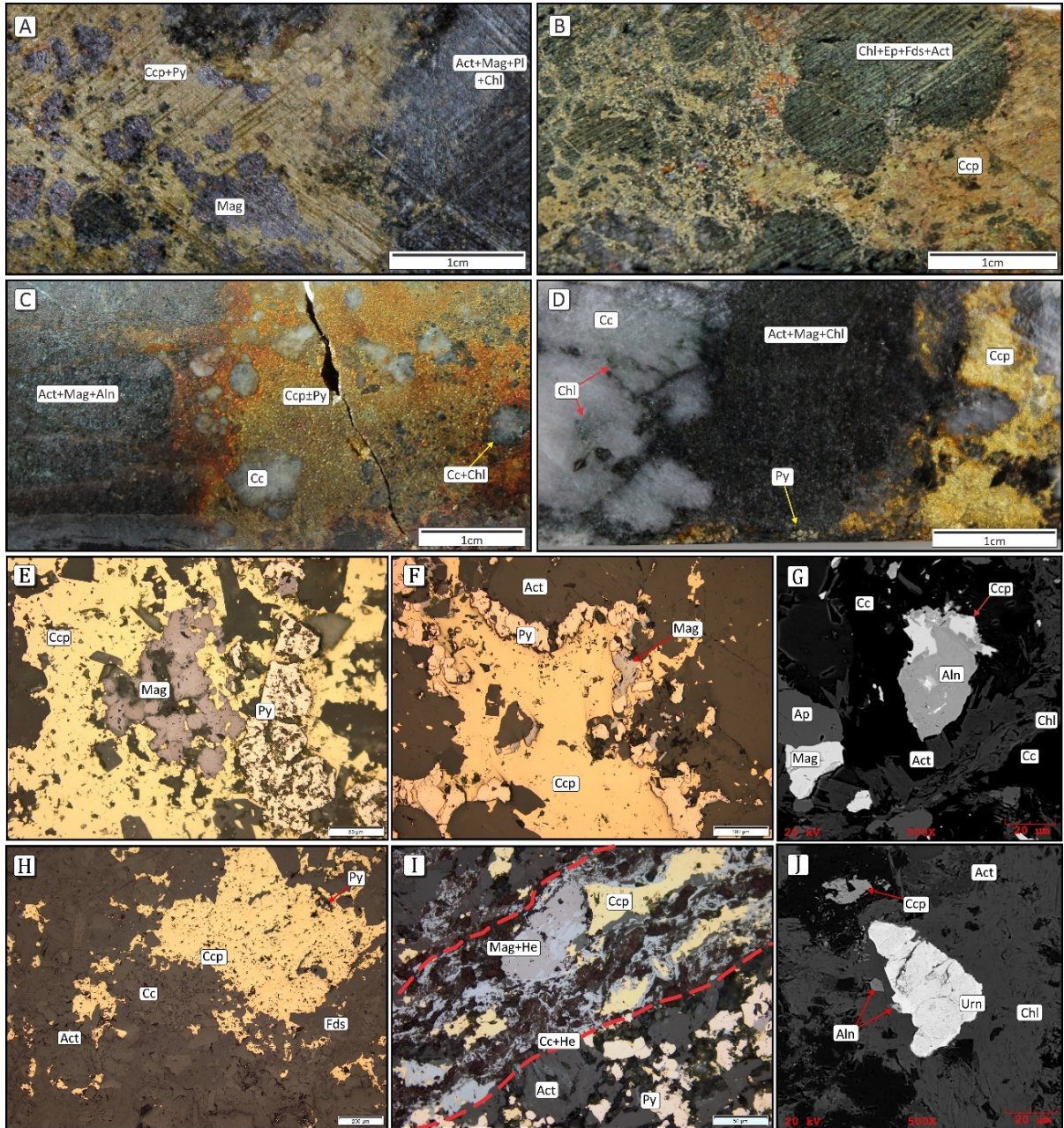
Figure 4. Main features of the Cristalino deposit ore. Photographs of drill-hole samples (A to D), photomicrographs under reflected light (E, F, H and I), and back-scattered electron images (G and J). (A) Chalcopyrite-pyrite-magnetite-Au breccia-like body in Ca-Fe altered mafic volcanic rock. (B) Chalcopyrite±Au±hematite±pyrite breccia and veinlets, in felsic volcanic rock harshly altered by chlorite-epidote, K-feldspar and actinolite. (C) Chalcopyrite-calcite breccia developed in a Ca-Fe altered mafic volcanic rock. (D) Calcite-chlorite-chalcopyrite±pyrite-rich veins crosscutting an altered mafic volcanic rock. (E) Magnetite and pyrite replaced by chalcopyrite in a chalcopyrite-magnetite breccia hosted by a mafic volcanic rock. (F) Actinolite-magnetite (remnant crystals) replaced by aggregate of chalcopyrite-pyrite in a mafic volcanic rock. (G) Crystal of allanite partially replaced by chalcopyrite in mafic volcanic rock that has been successively altered to a Ca-Fe assemblage (Act, Aln, Mag, Ap) and chlorite-calcite (propylitic alteration). (H) A magnetite-free, chalcopyrite-rich breccia in a felsic volcanic rock. (I) A calcite-chalcopyrite-hematite±magnetite veinlet, bounded by the dashed red lines, in a felsic volcanic rock. Magnetite crystals are partially martitized; (J) Anhedral crystal of uraninite in a chloritized mafic volcanic rock where fine crystals of chalcopyrite and allanite are also present. Act: actinolite; Aln: allanite, Cc: calcite, Ccp: chalcopyrite, Chl: chlorite, Fds: K-feldspar, He: hematite; Mag: magnetite; Py: pyrite; Qz: quartz, Urn: uraninite.

MATERIALS AND METHODS

Eleven representative samples of the host rocks of Cristalino deposit were selected for microprobe analysis after thorough petrographic work and paragenetic considerations. The samples came from four drill cores (FD-96, DH00003, FD-155, FD-107) and comprise felsic to mafic volcanic rocks of the Parauapebas Formation. Feldspar, amphibole, allanite, tourmaline and chlorite were analyzed.

Polished thin sections were submitted initially to a semi-quantitative chemical analysis by energy dispersive spectroscopy (EDS) in a LEO 1430 scanning electron microscope of the Microanalyses Laboratory of the Geosciences Institute of the Federal University of Pará. Mineral analyses and back-scattered electron images were obtained at the Regional Center of Technology and Innovation (Crti) of the Federal University of Goiás, and at the Microanalyses Laboratory of the Geosciences Institute of the Federal University of Pará, both in a JEOL JXA-8230 electron microprobe. The runs were performed in carbon coated thin sections, employing wavelength dispersive technique, with accelerating voltages of 15 kV, probe current of 20 nA and a beam diameter of 10μm. A variety of standards were used to calibrate all elements, including natural albite, barite, celestine, corundum, diopside, Fe_3O_4, fluorite, microcline, Mn-orthoclase, olivine, jadeite, quartz, rutile, sodalite, wollastonite, and the synthetics A-128, A-408, AN_100, CaF_2 and CeO_2, Cl_Scap, $LaPO_4$, $NdPO_4$, $PrPO_4$, $SmPO_4$, $ThSiO_4$, UO_2, and YAG.

Sixty to one hundred ninety spot analyses were carried out on crystals of feldspar, amphibole, allanite, tourmaline and chlorite, and their cationic composition was recalculated on basis of 8, 23, 12.5, 24.5 and 28 oxygen atoms, respectively. For allanite and tourmaline, the procedures recommended by Ercit (2002) and Tindle *et al.* (2002) were followed. Fe^{3+} and Li concentrations, specifically for tourmalines, were estimated with basis on stoichiometric calculations.

The thermal conditions for actinolite formation were estimated with the plagioclase-amphibole geothermometer (Holland and Blundy 1994). For the calculations, 158 actinolite compositions were used fulfilling the following requirements: $Ca^B > 1.50$, (1.70 − 2.11 apfu) $(Na+K)_A < 0.50$ apfu (0.07–0.30) and $Al^{vi} < 0.7$ apfu (0.06-0.60 apfu), at an estimated 2 kbar pressure for the early stages of the hydrothermal alteration in the Cristalino deposit area (Craveiro *et al.* unpublished data). The plagioclase composition was fixed at $X_{Ab}=0.98$ and $X_{an}=0.01$ and corresponds to the average of 57 analyses of this feldspar in the Cristalino deposit.

The temperatures of chlorite formation were based on 187 punctual analyses, using the empirical equation proposed by Cathelineau and Nieva (1985) as well as the correction for the Al^{iv} increase with Fe/(Fe+Mg) (Kranidiots and MacLean 1987).

RESULTS

Mineral Chemistry

Feldspars

Present in several IOCG deposits of Carajás, albite is commonly related to regional sodic alteration, which was controlled by first-order shear zones in ductile-brittle conditions. In the Cristalino area, the sodic metasomatism produced a textural retentive alteration which lends, locally, a pale-rose to pale-yellow coloration to the felsic volcanic rocks (Fig. 5A). Albite, the principal sodic alteration product, is normally associated with monazite, allanite (Fig. 5C) and minor quartz and calcite (Fig. 5A, 5B).

In turn, the hydrothermal K-feldspar is a potassic alteration product that has been interpreted to be contemporaneous with the main stage of IOCG mineralization in the Carajás Province (Réquia *et al.* 2003, Monteiro *et al.* 2008a,b, Torresi *et al.* 2011, Silva *et al.* 2015, Moreto *et al.* 2015a,b, Melo *et al.* 2017). In the Cristalino deposit, the K-feldspar shows a reddish coloration and occurs in the rock mass (Fig. 5D, F) and as infill phase (Fig. 5E). It seems to be contemporaneous with the late mineralization stage (chalcopyrite±pyrite±hematite).

The analyzed feldspar crystals are from: (1) a sodic altered mafic volcanic rock (sample 12-107, drill core FD-107 engulfed by calcic-ferric minerals; (2) an altered felsic volcanic rock (sample 13-96, drill core FD-96), partly mineralized and strongly affected by potassic alteration and; (3) a K-feldspar-rich vein (sample 17-107, drill core FD-107) that crosscuts a felsic volcanic rock.

Representative chemical compositions of plagioclase and K-feldspar are shown in table 1. No significant compositional differences were observed between decalcified plagioclase and chessboard albite, both occurring as fine- to medium-grained crystals in textural equilibrium with allanite, tourmaline, and rare monazite. Their compositions record $An_{0.02-0.00}$-$Ab_{0.99-0.97}$-$Or_{0.01-0.00}$ (Fig. 6A). Purer albite ($An_{0.00}$-$Ab_{1.00-0.99}$-$Or_{0.00}$) was found in contact with hydrothermal K-feldspar.

Formed after the stabilization of the calcic-ferric assemblages, the hydrothermal K-feldspar shows two modes of occurrence: (1) replacing primary minerals as medium-grained crystals (Fig. 5F), generally in association with titanite, hematite, allanite, and disseminated

sulfides (samples 13-96); and (2) in dilatant structures (sample 17-107) where it precipitated alongside with quartz, titanite, allanite, hematite, magnetite (tabular habit), with minor chalcopyrite and albite.

Table 1. Representative microprobe analyses of feldspars from Cristalino deposit.

Lithology	Felsic Volcanic Rock					Vein
Sample	107-12.3-2	107-12.1-5	107-12.3-5	13-96.2-3	13-96.1-10	17-107.4
SiO_2	68,37	68,14	68,24	63,94	64,15	64,36
TiO_2	19,60	19,35	19,62	0,00	18,49	18,38
Al_2O_3	0,00	0,00	0,00	18,04	0,00	0,00
FeO	0,08	0,02	0,08	0,01	0,03	0,02
MgO	0,00	0,00	0,00	0,00	0,00	0,00
CaO	0,38	0,10	0,27	0,00	0,00	0,00
Na_2O	11,88	11,88	11,78	0,71	0,27	0,29
K_2O	0,06	0,22	0,03	15,81	16,58	16,65
SrO	0,31	0,00	0,34	0,08	0,10	0,00
BaO	0,09	0,00	0,03	0,95	1,21	0,64
Total	100,77	99,72	100,37	99,54	100,81	100,34
Chemical formulae calculated based on 16 oxygens						
Si	2,985	2,991	2,980	2,992	2,977	2,987
Al^{iv}	0,015	0,009	0,020	0,008	0,023	0,013
Al^{vi}	0,984	0,992	0,990	0,987	0,988	0,992
Ti	0,000	0,000	0,000	0,000	0,000	0,000
Fe	0,007	0,001	0,002	0,001	0,001	0,001
Mn	0,000	0,000	0,000	0,000	0,000	0,000
Mg	0,000	0,000	0,000	0,000	0,000	0,000
Ca	0,011	0,005	0,013	0,000	0,000	0,000
Na	1,002	1,011	0,997	0,065	0,024	0,026
K	0,001	0,012	0,002	0,944	0,981	0,985
Sr	0,007	0,000	0,009	0,002	0,003	0,000
Ba	0,001	0,000	0,000	0,017	0,022	0,012
Anor	0,011	0,005	0,013	0,000	0,000	0,000
Ab	0,988	0,984	0,986	0,064	0,024	0,026
Or	0,001	0,012	0,002	0,936	0,976	0,974

K-feldspar approaches the stoichiometric composition ($An_{0.00}Ab_{0.06-0.10}Or_{0.93-0.98}$) (Fig. 6A) with negligible CaO amounts (< 0.02 wt. %). The main impurities refer to FeO_{total} (0.01 to 0.19 wt. %), BaO (up to 1.21 wt. %) and SrO (up to 0.49 wt. %). As shown in the diagram of Fig. 6B, the infill K-feldspar tends to present higher K/Ba ratios reflecting its generally lower Ba concentrations (0.01 to 0.71 wt. %).
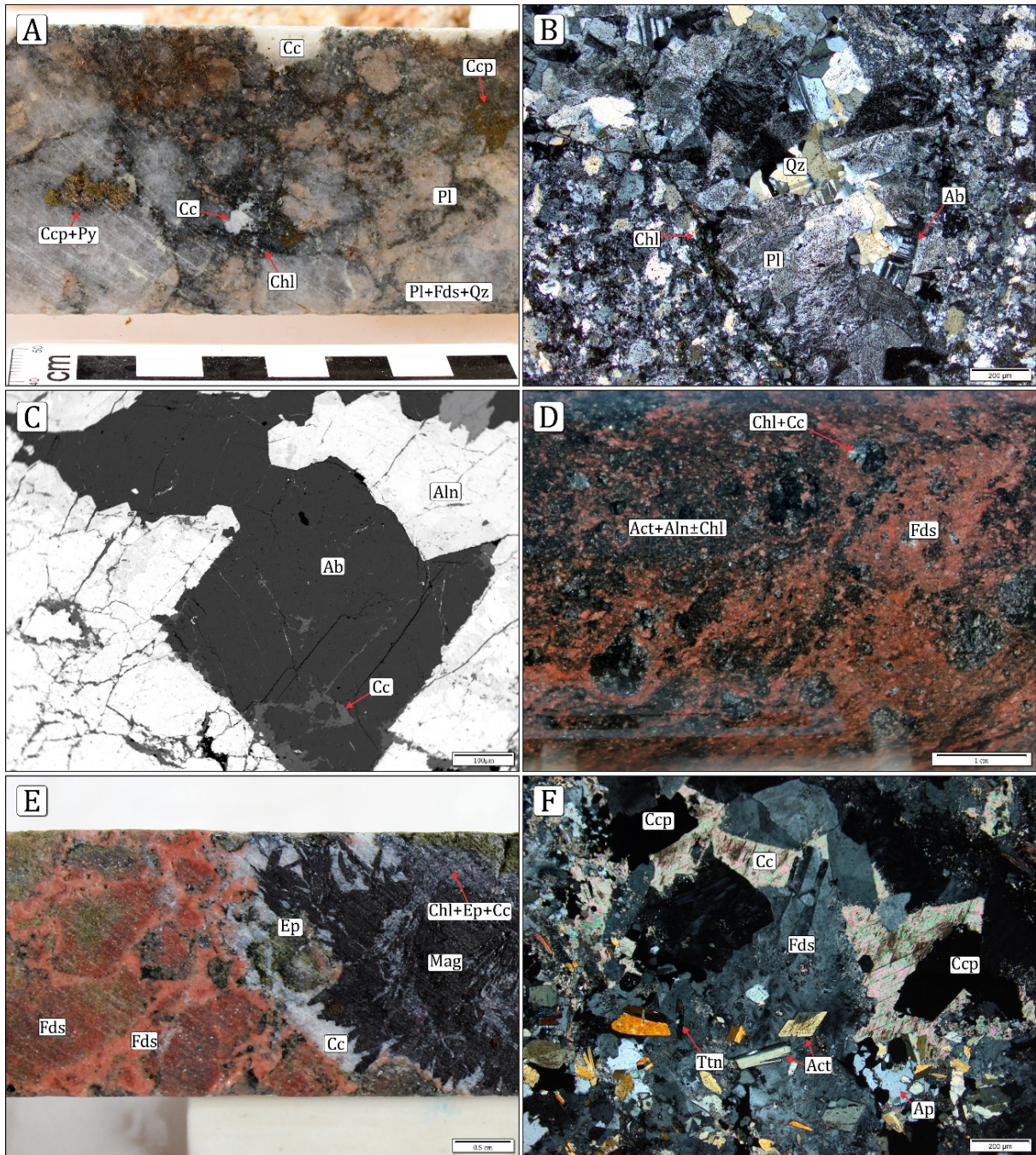
Figure 5. General characteristics of feldspars from the Cristalino deposit. (A) Photograph of drill core sample (altered felsic volcanic rock), in which albite-rich portions correspond to pale yellow/cream spots. Observe that chlorite and calcite coexist with disseminated chalcopyrite and pyrite; (**B**) Texture-retentive sodic alteration with chessboard albite associated with quartz in a felsic volcanic rock, in which chlorite fills micro-fractures (photomicrograph in crossed polarized light); (**C**) Albite and allanite in textural equilibrium presenting signs of minor alteration by calcite (back-scattered electron image); (**D**) Mafic volcanic rock previously altered by actinolite-allanite±chlorite and then affected by a texture-destructive potassic alteration dominated by K-feldspar (photograph of drill core sample); (**E**) K-feldspar-rich breccia matrix in sharp contact with chlorite-epidote-calcite and calcite-magnetite (musketovite?) (photograph of a drill core sample); (**F**) K-feldspar engulfing minerals of a felsic volcanic rock previously altered to actinolite and apatite. Ab: albite; Act: actinolite; Aln: allanite; Ap: apatite; Cc: calcite; Ccp: chalcopyrite; Chl: chlorite; Ep: epidote; Fds: K-feldspar; Mag: magnetite; Pl: plagioclase; Py: pyrite; Qz: quartz; Ttn: titanite.
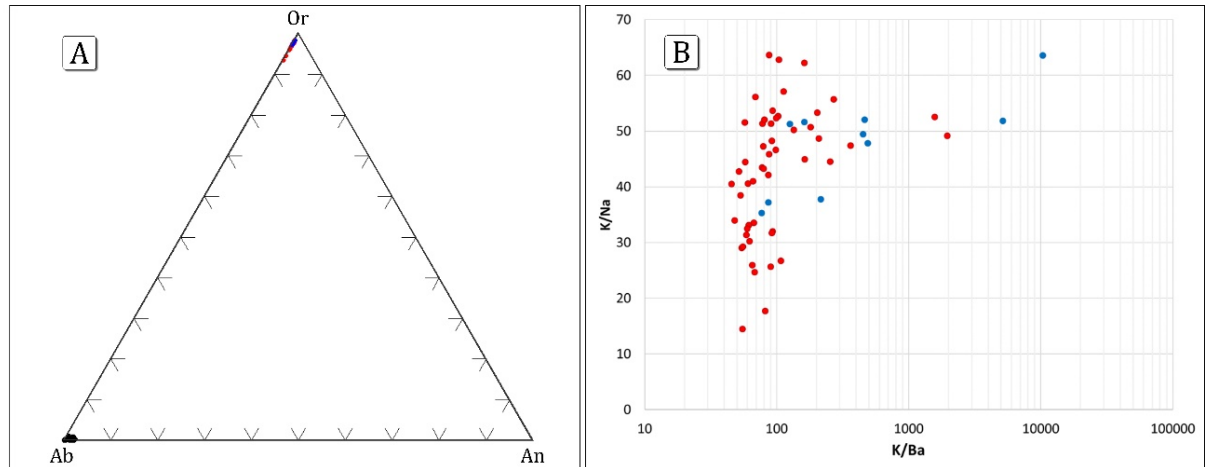
Figure 6. Hydrothermal feldspar compositions. (**A**) Ab-Or-An ternary diagram showing to be practically stoichiometric the composition of both K-feldspar and albite; and (**B**) K/Ba vs K/Na plot exhibiting a significant scattering of the analytical points with vein K-feldspar tending to have higher K/Ba ratios. Black dots: plagioclase; red dots: K-feldspar and; blue dots: vein K-feldspars.

Amphibole

Hydrothermal amphiboles are commonly found as gangue minerals in the Carajás IOCG deposits (e.g. Sequerinho ore body, Bacaba, Visconde, Bacuri, Borrachudo; Monteiro *et al*. 2008b, Augusto *et al*. 2008, Craveiro *et al*. 2012, Melo *et al*. 2014, Previato 2016). In the Cristalino deposit, mafic volcanic rocks have been largely replaced by amphibole mainly during the calcic-ferric alteration. Optically, most amphibole has been identified as actinolite that occurs as subhedral, medium- to fine-grained crystals, forming microcrystalline (Fig. 7A) and local fibrous aggregates.

The analyzed amphiboles are from: (1) a mineralized amphibole-rich zone (sample DH03-12, drill core DH-00003), developed in a mafic volcanic rock; (2) a felsic volcanic rock altered by amphibole and K-feldspar (Fig.8C) (sample 13-96, drill core FD-96); and (3) deformed zone (sample DH03-18, drill core DH-00003), in a mafic volcanic rock, affected by Ca-Fe alteration and propylitization.

Table 2 shows a representative set of chemical compositions of Cristalino amphiboles obtained from 185 microprobe spot analyses. All amphiboles belong to the calcic group (Leake *et al*. 1997), with Na^B <0.7 and $(Ca+Na)^B$ >1.7 (Fig.8A).

Actinolite (Fig. 7B-7E, 8B) was confirmed as the dominant variety [$K^A_{(0.01-0.07)}Na^A_{(0.00-0.19)}$] [$Ca^B_{(1.70-2.08)}Na^B_{(0.00-0.29)}Mn_{(0.01-0.06)}$][$Mg_{(2.24-3.53)}Fe^{3+}total_{(0.55-1.02)}Al^{vi}_{(0.08-0.58)}Ti_{(0.01-0.03)}$] [$Si_{(7.61-8.41)}Al^{iv}_{(0.00-0.39)}$] [$OH_{(1.84-2.00)} F_{(0.00)} Cl_{(0.00-0.16)}$], but Fe-edenite (Fig. 7D, 8B) was also locally identified [$K^A_{(0.21-0.49)}Na^A_{(0.30-0.61)}$][$Ca^B_{(1.76-2.09)}Na^B_{(0.00-}$

$_{0.23)}Mn_{(0.01)}][Mg_{(1.06-2.17)}Fe^{3+}total_{(1.08-2.17)}Al^{vi}_{(0.67-0.86)}Ti_{(0.12-0.13)}][Si_{(6.43-7.05)}Al^{iv}_{(0.95-1.57)}][OH_{(1.06-1.53)}F_{(0.00)}Cl_{(0.47-0.94)}]$. A few analytical points fall in the edenite and hastingsite fields.

There are no significant compositional differences between actinolites from mafic (Fig. 7A) and felsic (Fig. 7B) altered volcanic rocks. In both types #Mg varies from 0.69 to 0.87 and the average chlorine content records 0.15 wt. %. Fluorine was not detected.

In sulfide-rich breccias (Fig. 7C), actinolite presents chemical characteristics comparable to those of other Carajás IOCG deposits, namely #Mg (0.76-0.85, average= 0.83), Na^{B} ($0.04-0.25_{apfu}$, average= 0.10_{apfu}), chlorine content ($0.01-0.16_{apfu}$, average of 0.04_{apfu}, or 0.05-0.59 wt. %, average of 0.26 wt. %) and no fluorine.

A quartz- Fe-edenite assemblage locally invades actinolite-allanite-magnetite portions in altered mafic volcanic rocks. Fe-edenite occurs as fine-grained bluish to dark-green crystals (Fig.7D), in contact with quartz and chalcopyrite and shows Na < 0.6_{apfu}, (Na+K) > 0.50_{apfu}, (Ca+Na) > 1.34_{apfu} and Ti < 0.50_{apfu}. It presents also high chlorine content (1.62-2.94 wt. % or $0.47-0.94_{apfu}$) and no detectable fluorine. Additionally, it reveals potassium and titanium contents that reach up to 2.05 wt. % and 0.94 wt. %, respectively. The chlorine content shows a positive correlation with potassium and a negative one with #Mg (0.68-0.42).

Some actinolite crystals are zoned and show from core to edge (Fig. 7E) changes in Mg (3.10 to 2.50_{apfu}), Fe (0.60 to 1.0_{apfu}), Ca (1.80 to 2.0_{apfu}) and Al^{vi} (0.45 to 0.20_{apfu}) (Fig. 7F).

Allanite

Allanite is a REE-rich mineral commonly found in the orebodies of the Carajás IOCG deposits (Monteiro *et al*. 2008a,b, Xavier *et al*. 2012, Moreto *et al*. 2015a,b, Xavier *et al.* 2017), however it is still poorly described.

In the Cristalino area, allanite, though not abundant, is a hydrothermal mineral often observed in the volcanic rocks, near and within mineralized zones. It occurs as (1) fine- to coarse-grained crystals in textural equilibrium with chessboard albite (Fig. 9A) and actinolite (Fig. 9B) produced during the sodic and calcic-ferric alterations, respectively (samples 13-96, and 13-107); and (2) as constituent of K-feldspar-rich (Fig. 9C, sample 17-155) and calcite-rich veins (Fig. 9D) where it develops fine- to coarse-grained crystals.

Table 02. Representative microprobe analyses of amphiboles from Cristalino deposit.

Lithotype	Felsic volcanic rock				Ccp+Py+Mag breccia			Mafic Volcanic rock					
	13-96				DH03-12			DH03-18					
Sample	Core	Core	Rim	Rim								Fe-edenite	
	2.11	2.13	2.03	2.04	3.12	3.15	3.18	2.02	3.03	3.05	1.18	1.19	2.10
SiO_2	53,01	51,82	50,94	51,94	49,88	49,84	49,65	48,55	49,13	50,90	34,61	34,99	33,39
TiO_2	0,07	0,09	0,02	0,03	0,24	0,24	0,22	0,15	0,10	0,02	0,94	0,94	0,94
$Al2O_3$	1,79	2,35	0,40	1,00	3,40	3,60	3,45	3,04	3,36	0,43	10,45	10,38	10,09
Fe_2O_3	15,61	16,34	19,91	20,51	18,48	18,46	18,40	17,84	18,66	21,69	30,02	29,48	29,63
MnO	0,06	0,10	0,41	0,47	0,07	0,07	0,07	0,04	0,10	0,12	0,03	0,05	0,06
MgO	14,89	14,25	11,05	11,13	12,70	12,68	12,80	12,96	13,63	13,04	3,94	4,35	4,45
CaO	11,55	11,39	11,99	11,55	11,29	11,28	11,28	11,38	10,48	9,70	10,40	10,25	10,15
Na_2O	0,37	0,42	0,56	0,43	0,69	0,62	0,67	0,63	0,58	0,13	1,57	1,67	1,60
K_2O	0,08	0,17	0,04	0,07	0,23	0,23	0,22	0,19	0,17	0,05	1,76	1,57	1,67
F	0,00	0,00	0,00	0,00	0,00	0,00	0,00	0,00	0,00	0,00	0,00	0,00	0,00
Cl	0,12	0,21	0,02	0,01	0,29	0,32	0,34	0,20	0,16	0,03	2,78	2,54	2,57
Total	97,55	97,14	95,34	97,14	97,28	97,34	97,10	94,98	96,37	96,10	96,50	96,22	94,54
Chemical formulae calculated based on 23 oxygens (Cl, F, OH)													
Si	8,11	8,04	8,35	8,34	7,90	7,88	7,88	7,87	7,86	8,31	6,50	6,54	6,43
Al ^{IV}	0,00	0,00	0,00	0,00	0,10	0,12	0,12	0,13	0,14	0,00	1,50	1,46	1,57
Al^{VI}	0,32	0,43	0,08	0,19	0,53	0,55	0,52	0,45	0,49	0,08	0,81	0,82	0,71
Fe^{3+}_{total}	0,60	0,64	0,82	0,83	0,73	0,73	0,73	0,73	0,75	0,89	1,41	1,38	1,43
Ti	0,01	0,01	0,00	0,00	0,03	0,03	0,03	0,02	0,01	0,00	0,13	0,13	0,14
Mn	0,01	0,01	0,06	0,06	0,01	0,01	0,01	0,01	0,01	0,02	0,01	0,01	0,01
Mg	3,40	3,29	2,70	2,66	3,00	2,99	3,03	3,13	3,25	3,17	1,10	1,21	1,28
(B) Ca	1,89	1,89	2,11	1,99	1,92	1,91	1,92	1,98	1,80	1,70	2,09	2,05	2,09
(B) Na	0,10	0,09	0,00	0,00	0,08	0,08	0,07	0,02	0,19	0,29	0,00	0,00	0,00
(A) Ca	0,00	0,00	0,00	0,00	0,00	0,00	0,00	0,00	0,00	0,00	0,00	0,00	0,00
(A) Na	0,01	0,03	0,18	0,13	0,14	0,11	0,13	0,18	0,00	0,00	0,57	0,60	0,60
(A) K	0,02	0,03	0,01	0,01	0,05	0,05	0,04	0,04	0,03	0,01	0,57	0,60	0,60
Cation	15,97	15,94	16,00	16,00	15,92	15,91	15,91	15,94	15,96	15,99	15,12	15,20	15,16
Cl$^-$	0,03	0,06	0,00	0,00	0,08	0,09	0,09	0,06	0,04	0,01	0,88	0,80	0,84
F$^-$	0,00	0,00	0,00	0,00	0,00	0,00	0,00	0,00	0,00	0,00	0,00	0,00	0,00
Mg/Mg+Fe	0,85	0,84	0,77	0,76	0,80	0,80	0,81	0,81	0,81	0,78	0,44	0,47	0,47
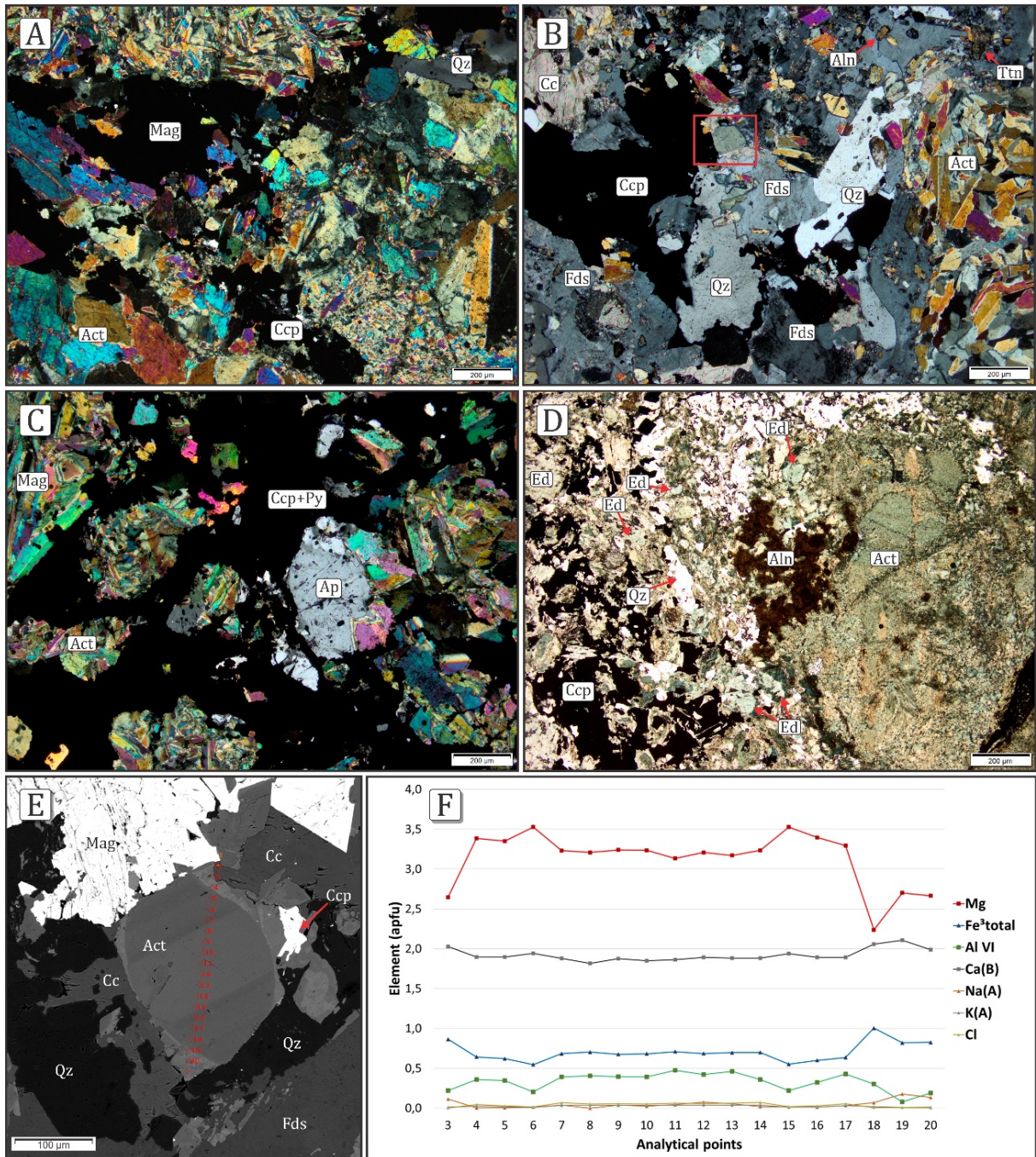
Figure 7. General characteristics of amphibole from Cristalino deposit. A-D (Photomicrographs) (A) An amphibole-rich zone composed of actinolite and magnetite that replaced totally the primary ferromagnesian minerals of a mafic volcanic rock (XPL); (B) Medium-grained, subhedral crystals of actinolite partially replaced by K-feldspar in felsic volcanic rock. The red square delimits the area of the back-scattered electron image depicted in Fig. E (XPL); (C) Sulfide-rich (chalcopyrite and pyrite) breccia in mafic volcanic rock, with abundant actinolite and less common apatite clasts (XPL); (D) Light-green to bluish fine- to medium-grained edenite crystals associated with quartz and chalcopyrite representing a front that partially replaced zones with actinolite and allanite in mafic volcanic rock (PPL); (E) Back-scattered electron image showing a zoned subhedral actinolite crystal depicted in Fig. B (red square). The red dots indicate spot-analysis; (F) Compositional variation of the zoned actinolite crystal that is depicted in Fig. C and zoomed in Fig. E. Abbreviations: Act: actinolite; Aln: allanite; Cc: calcite; Ccp: chalcopyrite; Ed: edenite; Fds: K-feldspar; Mag: magnetite; Qz: quartz; Ttn: titanite; PPL: plane polarized light; XPL: crossed polarized light.
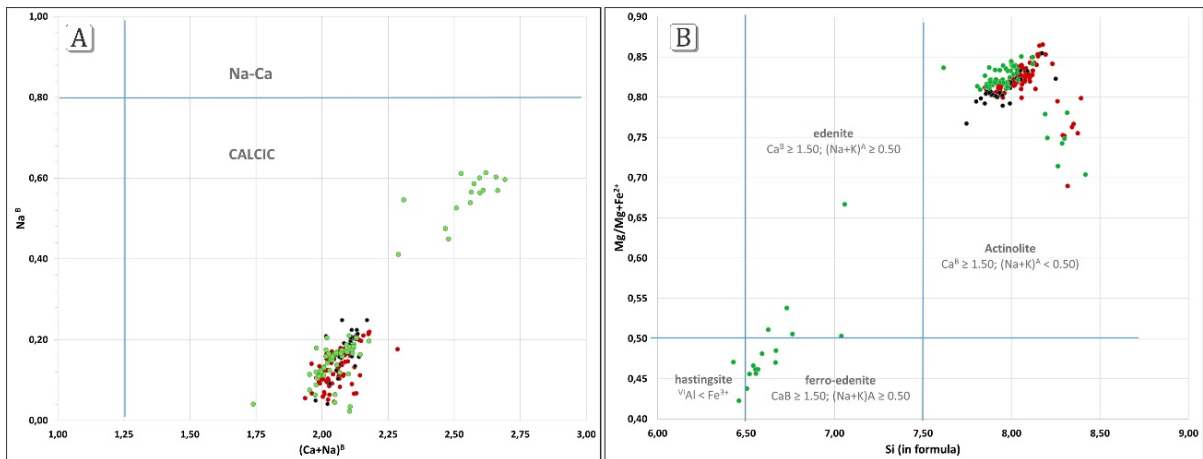
Figure 8. Distribution of the analytical points obtained for amphiboles of Cristalino rocks on diagrams proposed by Leake *et al.* (1997). (A) $(Ca+Na)^B$ vs Na^B plot showing that all points fall in the field of the calcic amphiboles. (B) Si_{apfu} vs $Mg/(Mg + Fe^{2+})$ plot. Most spot analyses record $Si_{apfu} > 7.5$ and $Mg/(Mg + Fe^{2+}) > 0.50$ corresponding to actinolite. A few show $Si_{apfu} < 7.5$, $Ca^B \geq 1.50$ and $(Na+K)^A \geq 0.50$ and are distributed in the fields of edenite, ferro-edenite and hastingsite. Conventions: Red dots: sample 13-96, altered felsic volcanic rock, Black dots: sample DH03-12, mineralized amphibole-rich zone in mafic volcanic rock; Green dots: sample DH03-18, altered mafic volcanic rock.

Over one hundred spot analyses were done on hydrothermal allanite crystals and the results are presented in Table 3. They reveal an average of 19.2 wt. % for $\sum_{REE}$, Ce being the dominant rare earth cation. It is therefore an allanite-Ce (Fig. 10A) according to Levinson (1966) and Ercit (2002) with the following structural formula: (1) groundmass allanite (Fig.9A, 9B) - $Ca^{A1}_{(0.83-1.62)}[Ca^{A2}_{(0.16-0.41)} Ce_{(0.30-0.42)}La_{(0.17-0.28)}Nd_{(0.07-0.15)}Th_{(0.000-0.004)}Y_{(0.01-0.05)}\square_{(0.00-0.14)}][(Al_{(1.47-1.97)}Fe^{2+}_{(0.50-1.00)}Fe^{3+}_{(0.03-0.59)}Mg_{(0.03-0.25} Mn_{0.01-0.07}](Si_2O_7)(SiO_4)O.[OH_{(0.90-0.99)}Cl_{(0.01-0.10)}F_{(0.00)}]$;   (2) and infill allanite (Fig.9C, 9D, 9E) - $Ca^{A1}_{(0.88-1.20)}[Ca^{A2}_{(0.23-0.88)}Ce_{(0.04-0.40)}La_{(0.01-0.24)}Nd_{(0.03-0.12)}Th_{(0.000-0.001)}Y_{(0.01-0.05)}\square_{(0.00-0.17)}] [(Al_{(1.77-2.10)}Fe^{2+}_{(0.78-1.06)}Fe^{3+}_{(0.00-0.23)}Mg_{(0.03-0.06)}Mn_{(0.00-0.05)}] (Si_2O_7)(SiO_4)O. [OH_{(0.99-1.00)}Cl_{(0.00-0.01)}F_{(0.00)}]$.

Although similar in overall composition, fine-grained groundmass allanite from felsic volcanic rocks (sample 13-96) presents higher MnO (average of 0.57 wt. %) and lower FeO_{total} values (average of 12.13 wt. %) in comparison with medium-grained groundmass allanite from mafic volcanic rocks (sample 13-107, Fig. 10C), which shows average contents of 0.08 wt.% and 14.94 wt.% for MnO and FeO_{total}. In turn, allanite from K-feldspar-rich veinlets (sample 17-155) presents MnO and FeO_{total} average values of 0.20 wt. % and 12.82 wt. %, respectively, and too low Cl content (0.01 wt. %) in comparison to averages of 0.34 wt.% and 0.14 wt.% for felsic and mafic rocks, respectively.

On the diagram ($Ca^{2+}+Al^{3+}+Fe^{3+}$) versus ($Ln^{3+}+Fe^{2+}+Mg+Mn$) compositional differences can be highlighted (Fig. 10B). Veinlet allanite presents lower Fe^{3+} and higher Ca and Al contents in comparison to the allanite from the altered rock mass. Their regression lines are similar, indicating high concentration of REE at lower $Ca+Al^{3+}$. The regression line of the veinlet allanite has a greater angular component and may suggest a tendency of change to epidote. Moreover, the veinlet allanite is often zoned and, according to its chemical profile (Fig. 9E, 9F), it changes to epidote, with antipathetic behavior between (REE + Y) and Ca or Fe^{2+} from core to edge.

On the ternary diagram $Ln+M3^{2+}-2^{A1}\square - {}^{A2}Ca+M3^{3+} - 2^{A1}\square - 4^{A1}$ (Fig. 10C) all the analyzed allanites, the composition of the core regions fall in allanite-(Ce),-(La),-(Y) field, while the edge regions stray towards the epidote-clinozoisite and vacancy epidote fields.

Tourmaline

Tourmaline as a common mineral related to the IOCG hydrothermal systems of Carajás (e.g., Xavier *et al.* 2008, Monteiro *et al.* 2008a,b, Moreto *et al.* 2015a,b), however no consensus exists about its paragenetic relationship with the ore. In the Cristalino deposit, tourmaline is best developed in felsic volcanic rocks of the Parauapebas Formation, in general distally in relation to the mineralized breccias. It shows two main modes of occurrence: (1) as isotropic, shattered or mildly deformed crystals (Fig. 11A, sample 17-96, of drill core FD-96); and (2) in cm-thicker veins that transect the volcanic rocks (Fig. 11B, sample 15-107 of drill core FD-107).

In sodic alteration assemblages, tourmaline forms fine- to medium-grained crystals that are in equilibrium with chessboard albite, allanite and monazite, but present a dubious textural relationship with magnetite (Fig. 11C). Relatively less abundant, tourmaline-rich veins (Fig. 11B) are found in zones previously affected by potassic alteration, where it develops medium- to coarse-grained crystals with a non-uniform zoning (Fig. 11E) associated with quartz and calcite (Fig. 11D).
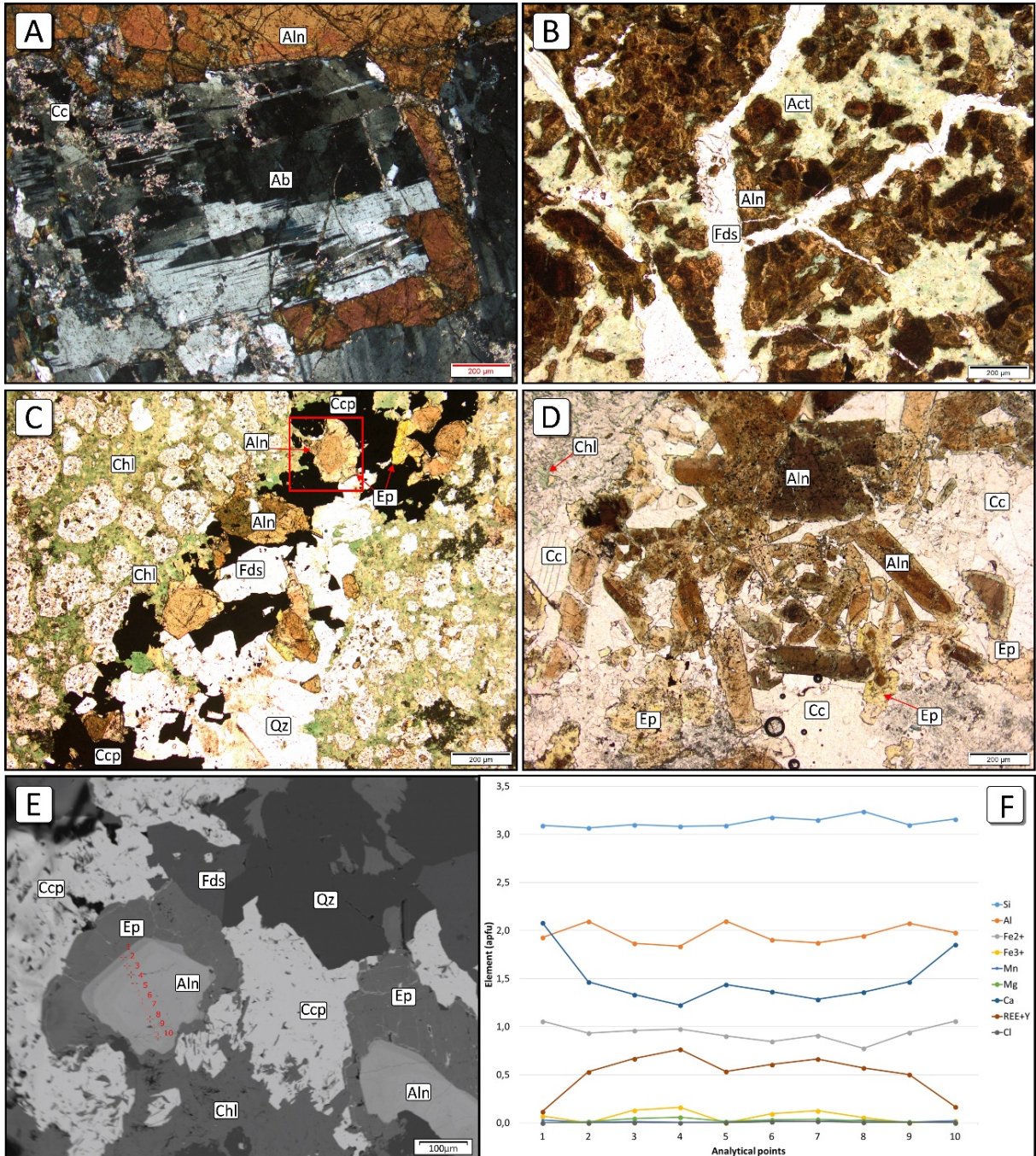
Figure 9. General characteristics of allanite from the Cristalino deposit. A-D (Photomicrographs). (A) Typical allanite crystal associated with actinolite aggregates, both altered by chlorite and chalcopyrite (XPL); (B) Mafic volcanic rock altered by actinolite and allanite which was then brecciated and invaded by K-feldspar-rich veins (PPL); (C) Chloritized felsic volcanic rock crosscut by a veinlet composed of albite, quartz, allanite (with occasional aureoles of epidote), chalcopyrite and chlorite (PPL). (D) Altered felsic volcanic rock crosscut by a vein made up of coarse-grained allanite and calcite. Some allanite crystals are surrounded by epidote in the form of replacement aureoles (PPL); (E) Back-scattered electron image showing a zoned subhedral allanite crystal surrounded by epidote. This zoned crystal occupies the center of the red square drawn in Fig. 6C; (F) Spot analysis showing the compositional variation of the zoned allanite crystal depicted in Fig. 6E. Abbreviations: Ab: albite, Act: actinolite, Aln: allanite, Cc: calcite, Ccp: chalcopyrite, Chl: chlorite; Ep: epidote, Fds: K-feldspar, Qz: quartz; PPL: plane polarized light; XPL: crossed polarized light.
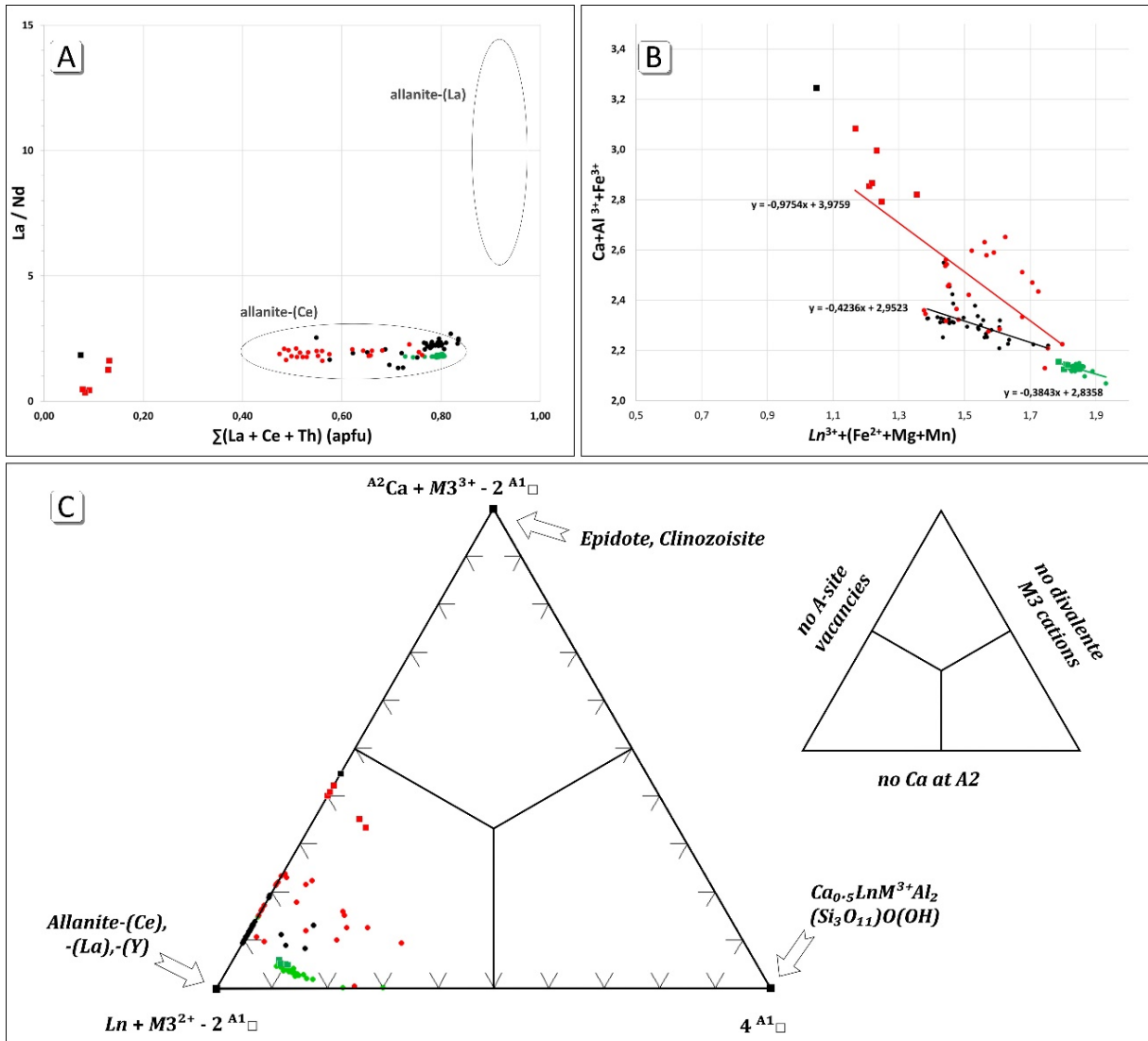
Figure 10. (A) La/Nd versus $\sum$ (La+Ce+Th) plot showing the concentration of the analytical points obtained on allanite crystals from the Cristalino deposit in the field of allanite-(Ce) (after Levinson, 1966); (B) Ca+Al^{3+}+Fe^{3+} versus Ln^{3+}+(Fe^{2+}+Mg+Mn) plot exhibiting distinct trend-lines for each analyzed sample. (C) Ternary Ln+M3^{2+}-2$^{A1}\square$ − ^{A2}Ca+M3^{3+} - 4 $^{A1}\square$ diagram (Peterson and MacFarlane, 1993) showing that crystal borders are less enriched in REE. Conventions - sample 13-96: black dots (core), black squares (rim); sample 13-107: green dots (core), green squares (rim); sample 17-155: red dots (core), red squares (rim).

A set of representative compositions, based on 64 microprobe spot analyses, is shown in table 4. The Cristalino tourmaline belongs to the alkali group (Fig. 12A) and presents schorlitic composition when present in the altered rock mass and schorlitic to dravitic composition when present in veins (Fig. 12B), as can be seen from their respective structural formulas: $[Ca_{(0.01-0.23)}$ $Na_{(0.52-0.72)}K_{(0.00-0.03)}\square_{(0.09-0.44)}]$ $[Li_{(0.06-0.34)}Mg_{(0.29-1.26)}Fe^{2+}_{(1.06-2.14)}Mn_{(<0.01)}Ti_{(0.01-0.25)}$ $Al_{(0.00-0.32)}]$ $[Al_{(5.04-6.34)}$ $Fe^{3+}_{(0.00-0.96)}]$ $[Si_{(6.03-6.16)}O_{18}]BO_3[OH_{(0.99-1.00)}Cl_{(0.00-0.01)}]$ and $[Ca_{(0.11-0.20)}Na_{(0.63-0.72)}K_{(0.01-0.02)}\square_{(0.10-0.20)}][Li_{(0.02-0.23)}Mg_{(1.66-1.75)}Fe^{2+}_{(1.06-1.27)}Mn_{(<0.01)}Ti_{(0.05-0.12)}][Al_{(5.52-5.81)}Fe^{3+}_{(0.13-0.48)}][Si_{(6.02-6.10)}O_{18}]BO_3[OH_{(0.99-1.00)}Cl_{(0.00-0.01)}F_{(0.00)}]$.

Table 03. Representative microprobe analyses of allanite from Cristalino deposit.

	Felsic volcanic rock			Mafic volcanic rock			Vein		
	core	rim	core	core	core	rim	rim	core	core
Sample	13-96. 5_21	13-96. 5_5	13-96. 5_22	13-107. 3_14	13-107. 3_17	13-107. 3_24	17-155. 6_11	17-155. 6_13	17-155. 6_23
SiO$_2$	32.04	31.87	31.38	30.63	30.73	30.35	34.74	30.55	32.11
Al$_2$O$_3$	13.11	13.50	12.44	14.26	14.15	14.23	18.52	16.31	15.32
FeO	11.34	12.47	11.97	14.69	15.30	14.25	15.49	13.42	12.57
MnO	0.82	0.74	0.77	0.07	0.06	0.09	0.46	0.16	0.20
MgO	0.34	0.29	0.33	0.47	0.45	0.44	0.15	0.30	0.25
CaO	11.48	12.26	11.87	10.32	10.49	10.36	20.89	13.55	13.55
Y$_2$O$_3$	0.12	0.19	0.14	0.31	0.25	0.27	0.84	0.22	0.43
La$_2$O$_3$	6.50	5.89	6.57	6.56	6.70	6.57	0.39	5.47	5.88
Ce$_2$O$_3$	11.08	10.30	11.11	11.20	11.19	11.19	1.05	9.65	9.55
Nd$_2$O$_3$	3.05	3.15	3.03	3.65	3.69	3.70	1.05	3.08	3.00
ThO$_2$	0.15	0.19	0.12	0.03	0.07	0.06	0.00	0.02	0.03
Cl$^-$	0.60	0.18	0.51	0.18	0.07	0.25	0.09	0.04	0.17
F$^-$	0.00	0.00	0.00	0.00	0.00	0.00	0.00	0.00	0.00
Total	90.62	91.02	90.24	92.37	93.15	91.73	93.68	92.76	93.06
Chemical formulae calculated based on 12.5 oxygens									
Si	3.263	3.229	3.241	3.116	3.113	3.109	3.094	3.019	3.145
Al	1.574	1.612	1.514	1.709	1.690	1.718	1.944	1.900	1.769
Fe^{2+}	0.540	0.669	0.548	0.959	0.986	0.938	1.098	1.009	0.798
Fe^{3+}	0.426	0.388	0.486	0.291	0.310	0.282	0.056	0.100	0.231
Mn	0.071	0.063	0.067	0.006	0.005	0.007	0.035	0.013	0.017
Mg	0.052	0.045	0.051	0.071	0.068	0.067	0.020	0.044	0.037
Ca	1.252	1.331	1.314	1.125	1.138	1.137	1.994	1.435	1.422
Y	0.007	0.010	0.008	0.017	0.014	0.015	0.040	0.012	0.022
La	0.244	0.220	0.250	0.246	0.250	0.248	0.013	0.199	0.212
Ce	0.413	0.382	0.420	0.417	0.415	0.420	0.034	0.349	0.342
Nd	0.111	0.114	0.112	0.133	0.133	0.135	0.034	0.109	0.105
Th	0.003	0.004	0.003	0.001	0.002	0.001	0.000	0.001	0.001
Cl	0.103	0.031	0.090	0.031	0.012	0.044	0.013	0.006	0.028
F	0.000	0.000	0.000	0.000	0.000	0.000	0.000	0.000	0.000
OH	0.897	0.969	0.910	0.969	0.988	0.956	0.987	0.994	0.972
∑M	2.662	2.777	2.667	3.036	3.058	3.013	3.152	3.066	2.852
A1 Ca	1.031	1.061	1.107	0.939	0.952	0.956	1.114	1.104	1.105
A1 VAC	0.000	0.000	0.000	0.061	0.048	0.044	0.000	0.000	0.000
A2 Ca	0.221	0.270	0.207	0.187	0.186	0.181	0.880	0.331	0.317
REE + Y	0.779	0.730	0.793	0.813	0.814	0.819	0.120	0.669	0.683
∑A	2.031	2.061	2.107	2.000	2.000	2.000	2.114	2.104	2.105

The T-site is fully occupied by Si (6.02-6.16$_{afpu}$) and the Z site is not completely taken over by Al. In fact, most the analyzed tourmalines are aluminum-deficient (Al^Z < 6$_{apfu}$), with Fe^{3+} filling the Z site irrespective of their mode of occurrence (Henry *et al*. 2011). Aluminum-rich tourmalines (Al^Z > 6$_{apfu}$) were observed only as groundmass constituent.

In some tourmaline crystals of veins (Fig. 11E), the light to dark green zoning is not concentric and presents a convoluted aspect. The lighter zones are enriched in Mg and slightly deficient in Al (6.01 to 5.93) while the darker zones present higher aluminum contents (Fig. 11E, 11F).

Table 4. Representative microprobe analyses of tourmalines from Cristalino deposit.

Sample	Early Tourmalines				Late Tourmalines		
	17-96-I2-3	17-96-I2-8	17-96-I2-14	17-96-I2-19	15.1-107-I1b-6	15.1-107-I1b-14	15.1-107-I2b-10
	Core	Core	Core	Core	Core	Core	Core
SiO_2	35,51	35,32	35,77	36,34	35,94	35,52	35,54
TiO_2	0,04	0,18	0,98	0,16	0,51	0,75	0,82
Al_2O_3	30,90	29,57	29,90	32,34	28,83	28,14	28,05
FeO	14,35	14,83	11,43	9,98	9,75	10,13	10,48
MnO	0,00	0,00	0,00	0,00	0,00	0,01	0,00
MgO	2,39	2,89	4,78	4,74	6,79	6,79	6,92
CaO	0,05	0,05	0,41	0,10	0,70	0,83	0,97
Na_2O	1,63	2,07	1,92	1,68	2,10	2,05	2,03
K_2O	0,03	0,04	0,03	0,01	0,02	0,03	0,04
Cl	0,01	0,00	0,00	0,00	0,01	0,01	0,03
F	0,00	0,00	0,00	0,00	0,00	0,00	0,00
Total	84,90	84,95	85,22	85,35	84,63	84,24	84,85
Chemical formulae calculated based on 24.5 oxygens and 3 B							
Si	6,087	6,094	6,048	6,046	6,086	6,067	6,045
Al total	6,242	6,013	5,959	6,342	5,754	5,667	5,623
Al (Z)	6,000	6,000	5,959	6,000	5,754	5,667	5,623
Al (Y)	0,242	0,013	0,000	0,342	0,000	0,000	0,000
Ti	0,005	0,023	0,125	0,020	0,065	0,096	0,105
Fe^{2+}	2,057	2,141	1,575	1,388	1,135	1,113	1,114
Fe^{3+}	0,000	0,000	0,041	0,000	0,246	0,333	0,377
Mn	0,000	0,000	0,000	0,000	0,000	0,001	0,000
Mg	0,611	0,744	1,206	1,176	1,713	1,729	1,754
Li	0,090	0,102	0,219	0,094	0,152	0,157	0,132
Ca	0,009	0,010	0,075	0,018	0,126	0,153	0,177
Na	0,541	0,694	0,630	0,542	0,688	0,680	0,670
K	0,006	0,009	0,006	0,003	0,005	0,005	0,008
Cl	0,003	0,000	0,001	0,001	0,002	0,004	0,007
F	0,000	0,000	0,000	0,000	0,000	0,000	0,000
X	0,556	0,713	0,711	0,563	0,819	0,838	0,855
VAC (X)	0,444	0,287	0,289	0,437	0,181	0,162	0,145
Y	2,910	2,898	2,781	2,906	2,848	2,843	2,868
Z	6,000	6,000	6,000	6,000	6,000	6,000	6,000
T	6,087	6,094	6,048	6,046	6,086	6,067	6,045
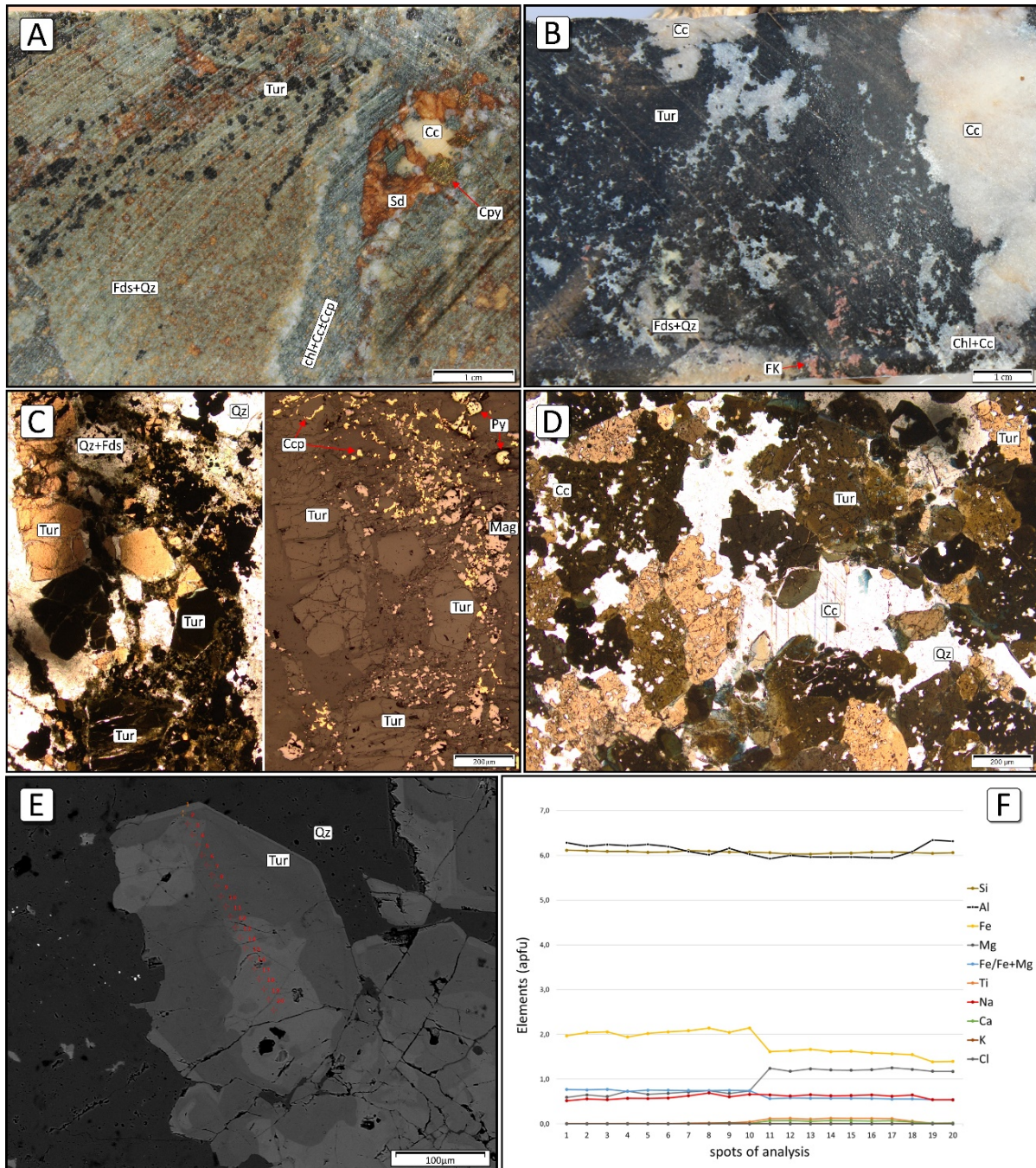
Figure 11. Main aspects of the tourmalines from the Cristalino deposit. (A) Photograph of a drill core sample with strings of tourmaline in slightly deformed felsic volcanic rock. At the right side, a vein composed of chlorite, calcite and minor amounts of chalcopyrite and siderite crosscuts the rock; (B) Photograph of a drill core sample showing a tourmaline vein with calcite-rich portions (right side) associated with millimetric spots of feldspar and quartz, chlorite-calcite and reddish K-feldspar; (C) Photomicrograph (PPL and reflected light) of slightly deformed and shattered tourmaline crystals, in association with magnetite. Observe micro-fractures in the tourmaline crystals filled by pyrite and chalcopyrite; (D) Photomicrograph of vein tourmalines in association with quartz and calcite. Note the fine quartz inclusions in tourmaline crystals (PPL); (E) Back-scattered electron image showing a zoned vein tourmaline crystal across which 20 spot analyses were done; (F) Compositional variation of the tourmaline crystal depicted in Fig. E. Elements are in atoms per formula unit (apfu). Abbreviations: Cc: calcite, Ccp: chalcopyrite, Chl: chlorite, Fds: feldspar group, FK: K-feldspar, Qz: quartz, Sd: siderite, Tur: tourmaline.
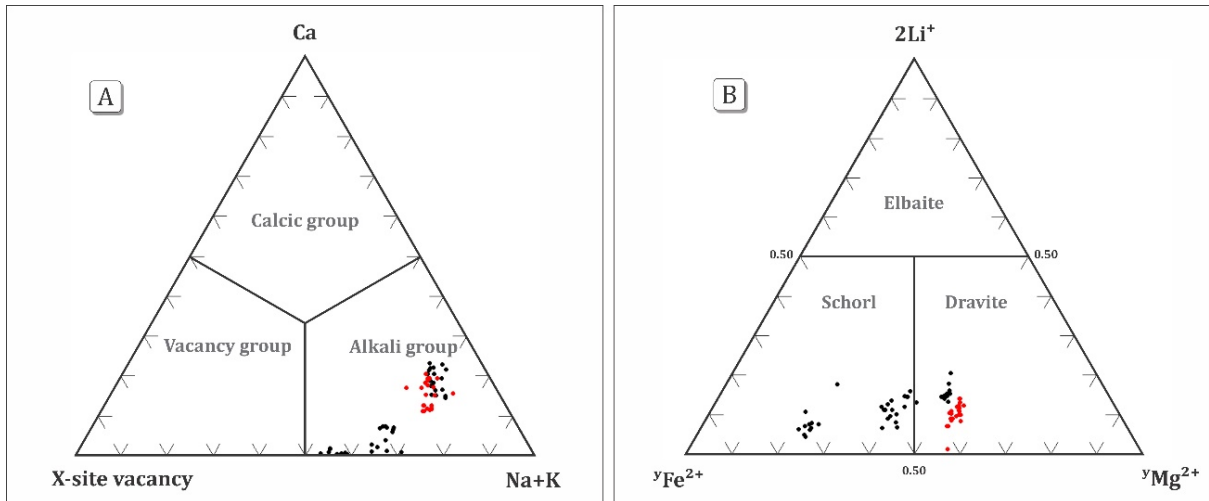
Figure 12. (A) X-site vacancy-Ca-(Na+K) diagram revealing the alkali nature of the Cristalino tourmalines; (B) $^yFe^{2+}$-$2Li^+$-$^yMg^{2+}$diagram (Henry *et al*. 2011) showing that most Cristalino tourmalines belong to the schorl variety. Black dots: groundmass tourmalines; Red dots: vein tourmaline.

Chlorite

Chlorite is a common mineral in most IOCG deposit of Carajás and tends to be developed in the late alteration stages, being often observed in breccia matrix. It is conspicuous in shallow IOCG deposits, such as Sossego orebody (Monteiro *et al*. 2008a, b), Alvo 118 (Torresi *et al*. 2011) amongst others. In the Cristalino area, chlorite occurs replacing primary and secondary minerals, and as an infill phase in veins and veinlets. Alongside with epidote and calcite, it forms part of a texture destructive assemblage, affecting almost all previously altered rocks.

The chlorites occur: (1) in felsic volcanic rocks, distally to the mineralized zones (sample 06-96, from drill core FD-96, Fig. 13A), near the lithological contact with banded iron formation, where fine flakes have taken over chessboard albite and are locally associated with chalcopyrite; (2) in felsic volcanic rocks, proximal to the mineralized zones, in which fine flakes and vermicular aggregates grew over feldspar (Fig. 13B), quartz, allanite and monazite, this condition being well documented in samples 13-155 and DH03-20, respectively from drill cores FD-155 and DH000003; (3) in mafic volcanic rocks, within the mineralized zones, where fine aggregates destabilized actinolite-rich clusters as seen in sample 13-107 from borehole FD-107 (Fig. 13C); and (4) in calcite-rich and K-feldspar-rich veins that crosscut felsic volcanic rocks (sample 15-107, drill core FD-107), growing as fine flakes in variable proportions accompanied by epidote, titanite, chalcopyrite, hematite and tabular magnetite (musketovite?) (Fig. 13D).

Representative chemical compositions of chlorites from the Cristalino deposit are shown in table 5. In felsic volcanic rocks, chlorite is essentially chamositic [$Fe^{2+}/(Fe^{2+}+Mg)$] = (0.48-0.68) and two distinct populations, FChl1 and FChl2 (Fig. 14A), can be identified, the former revealing higher X_{Fe} and, in general, lower Cl contents than the other. In the mafic volcanic rocks, the X_{Fe} of chlorite ranges from 0.37 to 0.56 characterizing two distinct varieties, MChl1 (clinoclore) and MChl2 (chamosite), the latter additionally with more elevated Al^{iv} values. Infill chlorite (VChl) is also chamositic but presents even higher $Fe^{2+}/(Fe^{2+}+Mg)$ ratios, reaching up to 0.8.
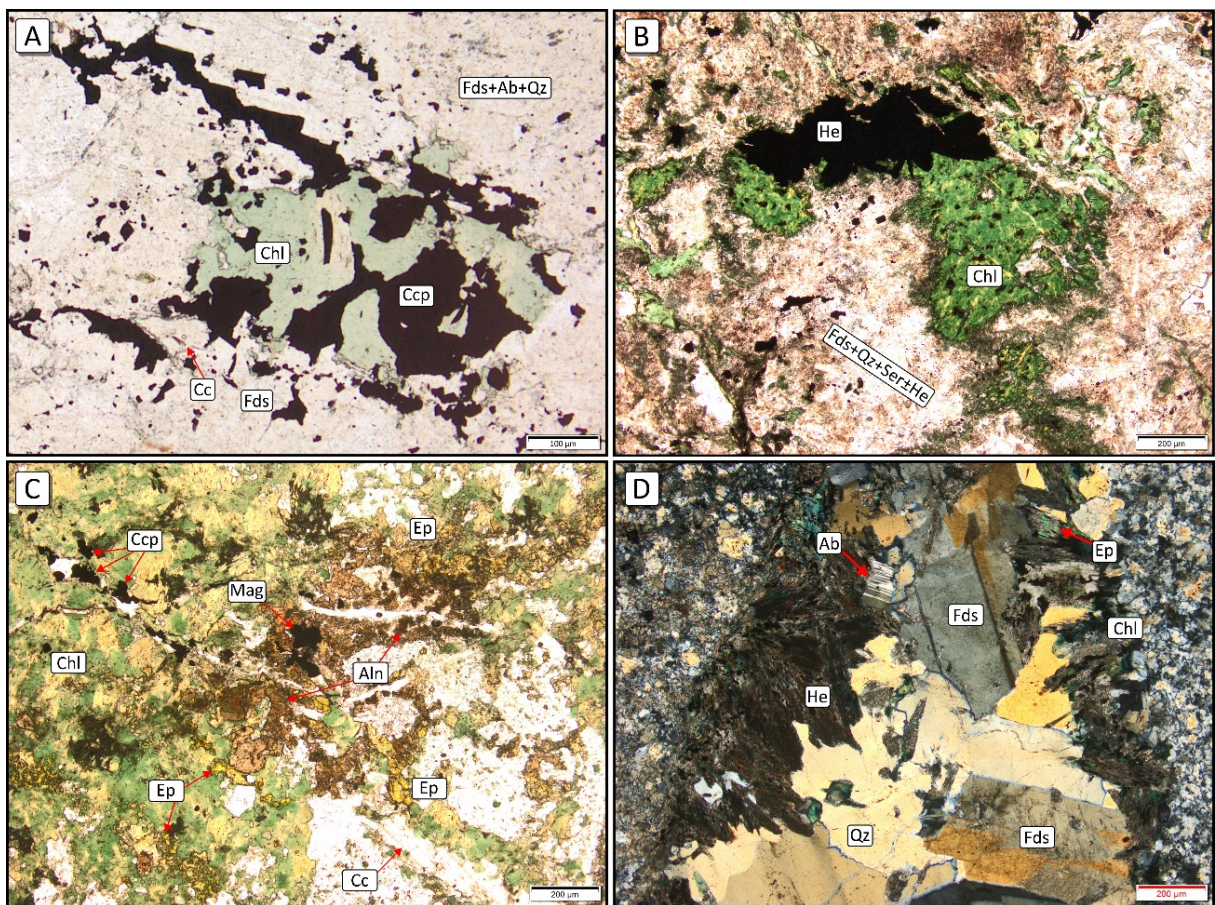
Figure 13. Photomicrographs of selected samples containing chlorite in the Cristalino deposit. (A) Chlorite associated with chalcopyrite, in felsic volcanic rock affected previously by sodic and potassic (K-feldspar) alterations (PPL); (B) Deeply sericitized felsic volcanic rock partially replaced by chlorite and hematite (PPL); (C) Chlorite-epidote-calcite making up a texture-destructive assemblage, in mafic volcanic rock previously affected by calcic-ferric alteration (PPL); (D) Chlorite, hematite and epidote bordering the walls of K-feldspar-quartz-rich vein, in felsic volcanic rock (XPL). Abbreviations: Ab: albite; Aln: allanite; Cc: calcite; Ccp: chalcopyrite; Chl: chlorite; Ep: epidote; Fds: K-feldspar; He: hematite; Mag: magnetite; Qz: quartz; Ser: sericite. PPL: plane polarized light; XPL: crossed polarized light.

Table 5. Representative microprobe analyses of chlorite form Cristalino deposit.

Lithology	Felsic Volcanic rock		Mafic Volcanic rock		Vein		Vein		Felsic Volcanic rock	
Sample	FD-69		FD-107				FD-155		DH-0000003	
	06.1-3	06.1-8	13.1-11	13.4-18	15.1.1.4	15.1.2-9	13.3-5	13.3-14	20.1-10	20.1-16
SiO_2	25,55	27,28	26,58	26,70	24,86	23,96	25,15	25,61	23,94	25,09
TiO_2	0,06	0,14	0,05	0,11	0,03	0,03	0,00	0,02	0,00	0,02
Al_2O_3	19,53	15,84	19,19	16,83	17,99	19,55	17,29	17,38	16,05	17,37
$FeO_{(total)}$	26,85	30,25	22,65	28,82	37,49	33,79	34,35	32,60	33,98	34,72
MnO	0,00	0,00	0,00	0,00	0,00	0,00	0,00	0,00	0,00	0,00
MgO	13,63	11,76	17,26	13,24	6,99	8,83	9,06	9,50	10,13	9,56
CaO	0,00	0,00	0,00	0,00	0,06	0,03	0,10	0,08	0,06	0,08
BaO	0,00	0,00	0,00	0,00	0,00	0,00	0,00	0,00	0,00	0,00
Na_2O	0,00	0,00	0,00	0,00	0,03	0,02	0,02	0,04	0,01	0,00
K_2O	0,00	0,00	0,00	0,00	0,00	0,00	0,00	0,00	0,00	0,00
Cl	0,15	0,62	0,07	0,09	0,01	0,02	0,01	0,02	0,01	0,04
F	0,00	0,00	0,00	0,00	0,00	0,00	0,00	0,00	0,00	0,00
Total	85,62	85,28	85,72	85,70	87,44	86,22	85,98	85,22	84,17	86,83
Chemical formulae calculated based on 28 oxygens										
Si	5,563	6,056	5,644	5,877	5,638	5,409	5,713	5,804	5,592	5,651
Ti	0,010	0,024	0,007	0,018	0,005	0,006	0,001	0,003	0,000	0,003
^{iv}Al	2,437	1,944	2,356	2,123	2,362	2,591	2,287	2,196	2,408	2,349
^{vi}Al	2,573	2,200	2,444	2,241	2,447	2,612	2,344	2,446	2,011	2,263
Fe^{2+}	4,888	5,616	4,021	5,303	7,112	6,378	6,526	6,181	6,243	6,453
Fe^{3+}	0,000	0,000	0,000	0,000	0,000	0,000	0,000	0,000	0,396	0,086
Mn	0,000	0,000	0,000	0,000	0,000	0,000	0,000	0,000	0,000	0,000
Mg	4,423	3,892	5,463	4,345	2,365	2,971	3,068	3,209	3,529	3,209
Ca	0,000	0,000	0,000	0,000	0,016	0,006	0,025	0,020	0,015	0,019
Ba	0,000	0,000	0,000	0,000	0,000	0,000	0,000	0,000	0,000	0,000
Na	0,000	0,000	0,000	0,000	0,012	0,011	0,011	0,018	0,004	0,000
K	0,000	0,000	0,000	0,000	0,000	0,000	0,000	0,000	0,000	0,000
Cl	0,056	0,234	0,025	0,033	0,006	0,007	0,004	0,009	0,003	0,014
F	0,000	0,000	0,000	0,000	0,000	0,000	0,000	0,000	0,000	0,000
OH	15,944	15,766	15,975	15,967	15,994	15,993	15,996	15,991	15,997	15,986

The Cristalino chlorite is thus compositionally very variable, as shown by the following structural formula: $(Mg_{2.09-6.25},Fe^{2+}_{3.79-7.25})^{vi}Al_{1.85-3.03},Fe^{3+}_{0.00-0.77}(Si_{5.56-6.31},{}^{iv}Al_{1.69-2.63})O_{10}(Cl_{0.00-0.23},F_{0.00},OH_{7.77-8.00})$. Al^{IV} contents vary from 1.59 to 2.63 apfu. The higher values are found in chlorites that replaced chessboard albite in felsic volcanic rocks as well as in infill chlorites. This distinguishes them from the other chlorites that replaced actinolite, allanite and locally tourmaline in mafic and felsic volcanic rocks and reveal lower Al^{IV} contents. Infill chlorites in mafic volcanic rocks tend to present an overall higher Al^{IV} value

(2.12-2.63 apfu), with higher average (2.50 apfu) relative to other occurrences. Chlorine presents very low contents, although in the chlorite that replaced chessboard albite they are a little more significant (Fig. 14B).

Disregarded the FChl2 population, a regression line is defined by all other analytical points (Fig. 14A), suggesting that VChl, FChl1, MChl1 and MChl2 groups may be contemporaneous but formed at different temperatures. FChl2 chlorites exhibit a poor correlation between Al^{IV} and Fe/(Fe+Mg) and most likely is an independent generation related to the replacement of chessboard albite in distal portions of the deposit.
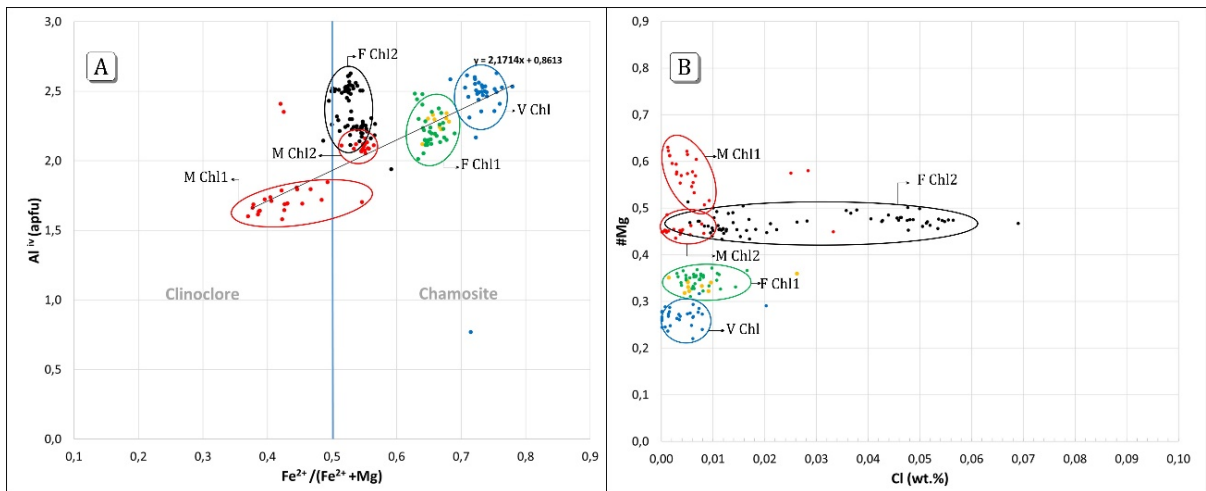
Figure 14. Compositional variations of chlorites from the Cristalino deposit. (A) $Fe^{2+}/(Fe^{2+}+Mg)$ vs Al^{iv} (apfu) diagram (Bailey, 1988) showing a regression line from which chlorites of sample 06-96 (FChl2) have been excluded; (B) Cl (wt.%) vs #Mg diagram showing that the Cl contents vary little no matter what the chlorite variety but vary more significantly at an almost constant #Mg in those replacing chessboard albite. Black dots: Sample FD-96/06); red dots: sample 13-107; yellow dots: sample 13-155; green dots: sample 20-DH03; and blue dots: sample 15-107.

Geothermometry

Plagioclase-Amphibole Geothermometer

The calculated temperature ranged from 645.4 to 413.0ºC (Fig. 15A). Values below 400 ºC were discarded due to the geothermometer constraints. Most temperatures fall in the 500-580ºC range and refer to the grain cores. Higher values (up to 645.4ºC) were obtained in actinolite-rich portions developed in mafic volcanic rock, near cm-thick shear zones. The zoned crystal depicted in Fig. 15B recorded temperatures that decrease from 540ºC to lower than 400ºC as the grey zones become increasingly darker. According to Trzcienski *et al.* (1984) and Féménia *et al.* (2006), it is coherent to expect appreciable temperature and pressure fluctuation in well-defined zoned crystals.
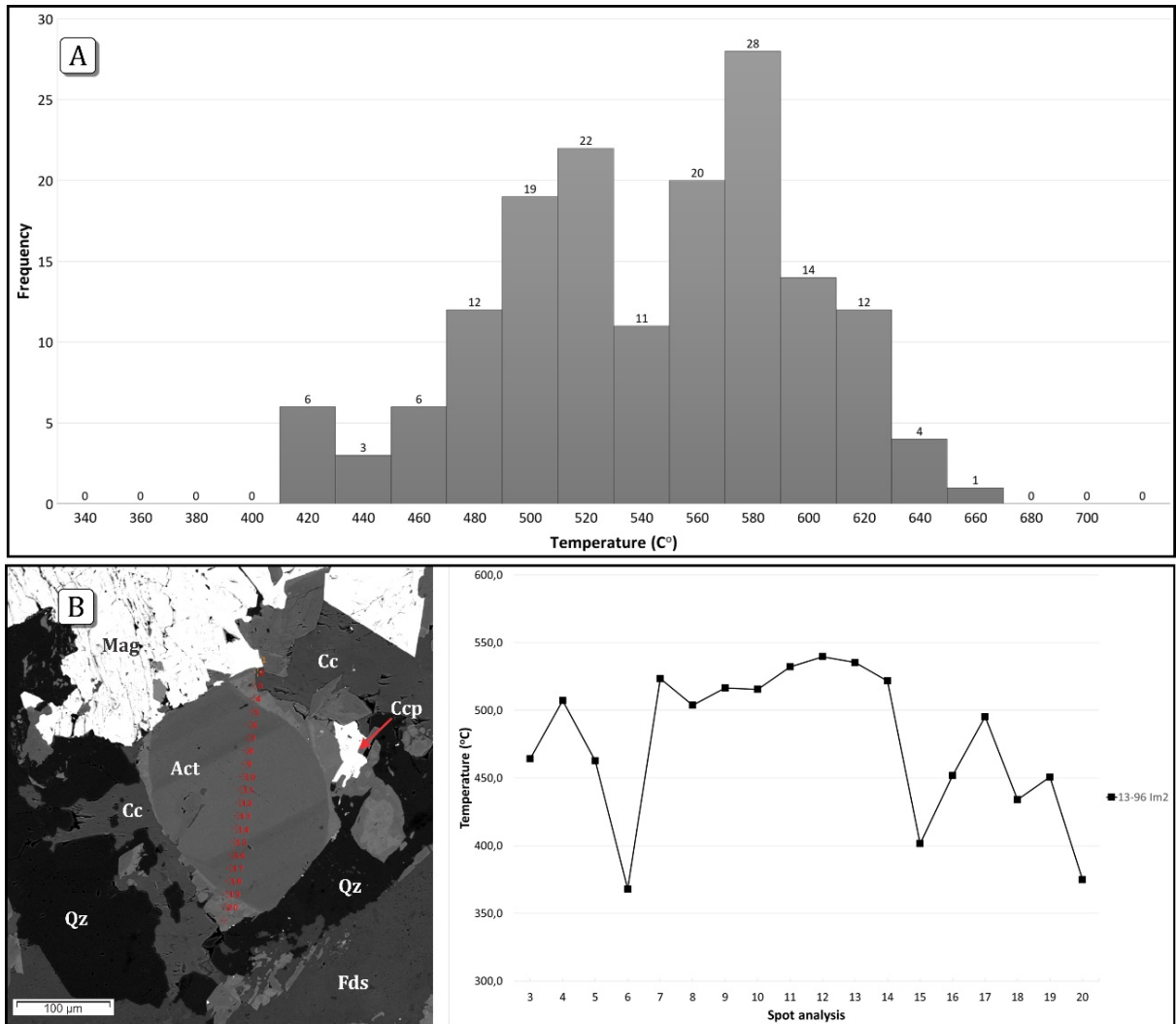
Figure 15. (A) Histogram of frequency for formation temperatures of actinolite from calcic-ferric alteration zones estimated according to the geothermometer of Holland and Blundy (1994). (B) Backscattered electron image of a zoned actinolite crystal and the corresponding temperature profile. Act: actinolite, Cc: calcite, Ccp: chalcopyrite, Fds: K-feldspar, Mag: magnetite, Qz: quartz.

Chlorite Geothermometer

In the propylitic stage of the alteration of the Cristalino deposit rocks, chlorites are closely related to epidote and calcite, and more strictly, to chalcopyrite and hematite of the late chalcopyrite±pyrite±hematite mineralization.

All analyzed chlorites present a positive correlation between Al^{IV} and Fe/(Fe+Mg) ratio (Fig. 14A), which mimics the chlorite behavior described by Cathelineau and Nieva (1985) and Kranidiotis and MacLean (1987), wherein the Al^{IV} and Fe^{VI} entrance is controlled by temperature. The plot Al^{IV} vs temperature (Fig. 15A) shows that all analyzed chlorites are Al^{IV} undersaturated, not presenting high Al^{IV}/Si substitution, a characteristic of high pressure

(2-6 kbar) systems (Kranidiotis and MacLean, 1987). This may suggest that the Cristalino chlorites formed at a low-pressure condition (ca. 1 kbar).

Using the equation T (°C) $= 106Al^{iv} + 18$ (Cathelineau and Nieva 1985) and the correction $Al^{iv}_{corrected} = Al^{iv}_{sample} \pm 0.7$ Fe/(Fe+Mg) proposed by Kranidiotis and MacLean (1987), the calculated temperature ranged from 217 to 353°C (Fig. 15B). The highest temperature was obtained in a vein chlorite and decreasing values were recorded in chlorites from sodic altered felsic volcanic rock, mafic volcanic rocks (330 to 270°C) and mineralized mafic volcanic rock (down to 220°C).
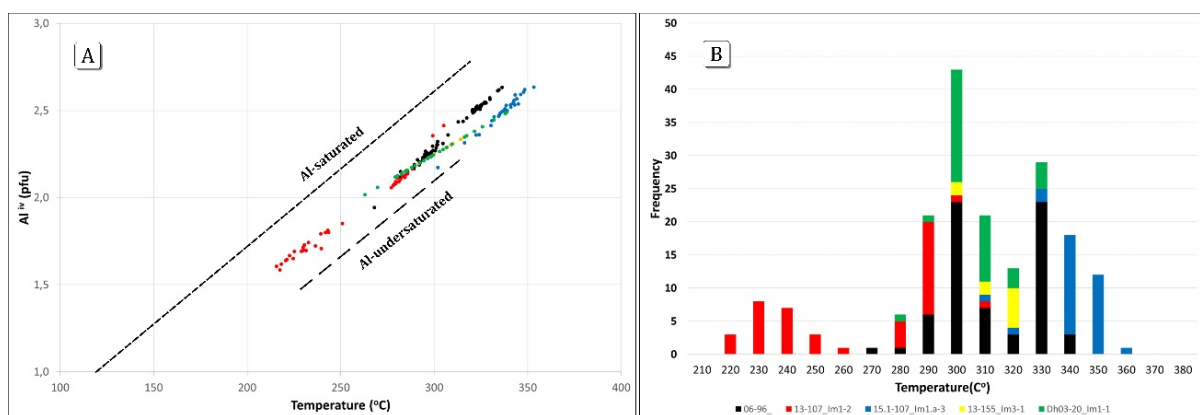
Figure 16. (A) Plot Al^{IV} vs Temperature with experimental regression lines for Al-saturated and Al-unsaturated chlorites (Kranidiotis and MacLean, 1987); (B) Histogram of temperatures calculated according to equations of Cathelineau and Nieva (1985) and Kranidiotis and MacLean (1987). Sample conventions as in figure 14.

DISCUSSION

Hydrothermal history of the Cristalino deposit

A striking feature of the Cristalino deposit is the overlapping of alteration stages that occurred during its hydrothermal history under ductile-brittle to brittle deformational regimes. Petrographical and mineral chemistry data indicate a sequence that can be separated into two major alteration stages, with different chemical trends and structural setting.

The sodic and calcic-ferric alterations belong to the first event, both developed under a ductile-brittle regime. The chalcopyrite-pyrite-magnetite assemblage, spatially and probably temporally related to calcic-ferric altered zones, marks the earliest ore association which evolved from disseminations to breccia-like bodies.

Not as intense as the former, the second stage took place in the transition from ductile-brittle to dominantly brittle environment when the potassic and propylitic alteration assemblages came into play. Spatially and temporally related to this alteration event is the chalcopyrite±pyrite±hematite ore association that occurs as breccia matrix and vein filling.

This sequence of alteration is repeated in several other IOCG systems worldwide. Similarly to other IOCG deposits, Cu-Au mineralization is also a late process and post-dates the main formation of iron oxides (Williams et al. 2005, Grainger *et al.* 2008, Groves *et al.* 2010).

Temperature conditions of the hydrothermal system

The hydrothermal alteration recorded in the wall-rocks of the Cristalino deposit seems to have evolved with an overall drop in temperature, from around 650º C to values as low as 220º C. Occasional fracturing, however, may have triggered new hydrothermal pulses interrupting this negative thermal gradient with local increases in temperature, as indicated by some vein chlorites (Fig. 14A). The sodic and calcic-ferric alterations and the first mineralization event developed at higher temperatures (> 410º C), whereas the potassic alteration, the second mineralization event and the propylitization/carbonation occurred at lower temperatures (< 410º C). Unfortunately, no data are available for the temperature at which the potassic alteration started forming biotite and/or K-feldspar. But as it developed between the calcic-ferric and the propylitic alteration stages, it is valid to state that 410º C > $T_{biot-KF}$ > 220º C, assuming a gradual cooling for the Cristalino hydrothermal system.

Main chemical trends of the hydrothermal system

The sodic alteration commonly observed in a number of Archean IOCG deposits of Carajás has been attributed to the interaction of the rocks with a hypersaline hydrothermal fluid of origin not yet fully understood (Monteiro *et al.* 2008a, Xavier *et al.* 2012, Silva *et al.* 2015, Moreto *et al.* 2015a,b, Melo *et al.* 2017). This fluid would be responsible for the stabilization of the diverse alteration assemblages found in the Cristalino rocks, the later ones having the participation of surficial water (Craveiro *et al.*, submitted). Apart from the sulfides and oxides, albite, actinolite, quartz, tourmaline, biotite, K-feldspar, allanite, epidote, chlorite and calcite are the main constituents of these assemblages, most having grown in distinct rocks and just a few replicated in more than one alteration stage.

The chemical data on each analyzed mineral reveal that there is, in most cases, no significant difference in its composition, no matter the rock in which it is present or the mode of occurrence. Chessboard albite and decalcified plagioclase are practically pure, and their formation appears to have been essentially controlled by the composition of the hypersaline

fluid, particularly by its high Na^+ activity. The former resulted from the replacement of primary alkali-feldspar and the latter from the removal of Ca from igneous plagioclase.

Actinolite, the main product of the Cristalino hydrothermal system, is confined to the calcic-ferric alteration zones and sulfide-rich breccias. The values of #Mg overlap greatly so that the average is about the same in both occurrences (0.82/0.83), although the range is greater in the rock mass actinolite. In turn, the average Cl content is almost two-fold in the actinolite that crystallized in the mineralized breccia (0.26 wt. %) than in the rock mass (0.15 wt. %). Apparently, the host rock played a less decisive role in the amphibole composition, but the physico-chemical conditions of the fluid and crystallochemical mechanisms seem to have been determinant.

In a few zoned crystals, it is observed that their borders are slightly impoverished in Mg (Fig. 7F). The iron leached from primary mafic minerals by a relatively low pH fluid may have helped forming magnetite and locally aureoles of calcic-amphiboles with higher X_{Fe}.

A residual portion of the fluid that initiated the process of alteration of the Cristalino rocks could be accounted for the local crystallization of ferro-edenite (Fig. 7D) in textural disequilibrium with calcic-ferric assemblages. Its high Cl (up to 2.78 wt. %) and Na (up to 1.70 wt. %) may be indicative that it crystallized from a high salinity fluid. In the particular case of chlorine, the edenite-hastingsite substitution [Al^{iv} + $(Na+K)_A$ ↔ Si + A-site vacancy] creates distortions in the unit cell sufficient to favor Cl^- entrance (Deer *et al.* 1986, Pe-Piper 1988). Similarly, the substitution of K and Fe onto the A and C sites of the amphibole lattice causes it to expand and thus appears to accommodate the Cl^- fixation (Giesting and Filiberto, 2015). There is then a positive correlation between K and Cl that is typical of amphiboles generated in Cl-rich media. This correlation is observed in the Cristalino amphiboles (Fig. 17D).

A negative correlation between #Mg and Cl content of amphiboles is distinguishable (Fig. 17C) which indicates that Mg-Cl avoidance mechanisms can control the incorporation of halogen in the amphibole structure, the substitution of Cl being more likely where Cl-bearing anion sites are enlarged (Rosenberg and Foit 1977, Makino *et al.* 1993, Deer *et al.* 1997, Henry and Daigle 2018).

It should be noted that coupled substitution mechanisms can induce compositional variations in minerals precipitating from a common Cl-rich fluid (Monteiro *et al.* 2008b). This condition may have led to the formation of both actinolite and ferro-edenite found in the Cristalino deposit.

The main production of allanite occurred during the ferric-calcic alteration stage, in both mafic and felsic rocks. The compositional differences are not significant, except for the contents of MnO and Cl, both tending to be much higher in the felsic type. FeO_{total} concentrations are slightly higher in the mafic variety. These minor differences may reflect the host rock composition. More expressive differences can be detected in the veinlet allanite, notably the contents of REE_{total} which tend to be lower in comparison to those of the allanite from the rock mass. Chlorine shows very low contents. Another important difference refers to the estimated Fe^{3+} content, higher in the rock mass allanite (up to 0.54 apfu) comparatively to the infill allanite (up to 0.23 apfu). The fixation of Fe^{3+} in the mineral lattice may indicate relatively high f_{O2} conditions, causing Al^{3+} and Ca^{2+} to give way to the accommodation of Ln^{3+} (REE + Y), according to the relation $Ca^{2+}+Al^{3+}+Fe^{3+}\leftrightarrow Ln^{3+}+Fe^{2+}+Mg+Mn$ (Ercti 2002). This complex exchange mechanism probably allowed the incorporation of Cl (up to 0.60 wt. %) in the infill allanite and the general absence of F in the mineral structure. This contradicts Gieré and Sorensen (2004) who maintain that F^- is the halogen that commonly substitutes for O^{2-} and is typically more abundant than Cl^- in Ce-allanite.

K-feldspar reveals an almost pure composition, and its reddish coloration could be due to fine hematite inclusions. However, the lack of specific analysis for Fe^{3+} does not allow such a conclusion. Ba^{2+} and Sr^{2+} are ions that can be easily accommodated in the K-feldspar lattice substituting for K^+. According to Ollila (1984), sulfates and carbonates (evaporite beds?) are the most important sources of Ba and Sr detected in K-feldspar precipitating from hydrothermal fluids.

The alkaline nature of the tourmalines was to be expected considering the Na-rich fluids supposed to have altered the rocks of the Cristalino deposit. In turn, the essential schorlitic character of tourmalines only changed to dravitic at the late stages of the Cristalino hydrothermal system when the fluids had already lost appreciable amounts of iron during the previous precipitation of magnetite. However, the remaining dissolved Fe was still at enough concentration to allow the formation of hematite and other iron minerals.

Among all the minerals analyzed, chlorite presents the greatest compositional variation, certainly resulting from the interplay of factors such as host rock composition, fluid composition and temperature. The formation of clinoclore (MChl1) in mafic rocks meets common sense, but the generation of chamosite (MChl2) in these same rocks certainly was more dependent on the composition of the hydrothermal fluid that altered them. Its higher Al^{iv} values may indicate additionally a hotter fluid. As far as the chamosites in felsic rocks (FChl1

and FChl2) are concerned, the thermal conditions appear to have been comparable, since they have similar Al^{iv} range. More determinant to their compositional difference seems to have been the fluid chemistry, FChl1 crystallizing at higher fluid a_{Fe2+}. VChl chlorites precipitated in the vein channels directly from the fluid at temperatures that reached up to $360°$ C. As the fluid moved out and interacted with the wall rocks, it lost heat and favored the growth of chlorites with lower Al^{iv} values such as those of chamositic composition, hence their lower formation temperatures.

During the early stages of hydrothermal alteration, f_{O2} of the Cristalino environment was high enough to provide Fe^{3+} to precipitate abundant magnetite and enter the structure of other minerals, in particular allanite. Later on, f_{O2} increased causing, from the potassic alteration onwards, a drastic reduction in magnetite production and the martitization of much of the pre-existing magnetite, as well as the formation of hematite. The precipitation of a new generation of sulfides may have resulted from the dilution of the hydrothermal fluid by meteoric waters, as suggested by the very low Cl contents of the younger chlorites. These waters may have supplied additional oxygen to the system becoming the hydrothermal fluid even more oxidizing.

It should be noted that the f_{O2} increase may not be vital for the martitization of magnetite. An alternative mechanism, as that proposed by Cannon (1976), for the transformation of magnetite into hematite could be via the reaction Fe_3O_4 (s) + $2H^+$ (aq) $\leftrightarrow$ Fe^{2+} (aq) + Fe_2O_3(s) + H_2O(l). Leaching of Fe^{2+} would require very acid solutions, and the martitization would occur in a non-conservative Fe condition. This temperature-independent and non-redox reaction (Ohmoto 2003) could account for the later formation of musketovite in the system as a phase of the propylitic assemblage.

Comparison with other Carajás IOCG deposits (southern sector): amphibole and chlorite chemistry

Two main types of amphiboles are recognized in several IOCG deposits of Carajás: (1) amphibole with $Ca_B \geq 1.50$, $(Na+K)_A < 0.50$, with lower Cl contents (from 0.1 to 0.6 apfu), with composition of actinolite, ferro-actinolite, and tremolite; and (2) $Ca_B \geq 1.50$; $(Na+K)_A \geq 0.50$, and $Al^{vi} < Fe^{3+}$, with higher Cl contents (up to 0.1.1 apfu), with composition of edenite, ferro-edenite, hastingsite, pargasite and ferro-pargasite (Gomes and Lindenmayer 2003, Dreher 2004, Monteiro et al. 2008b).

Comparison with the Archean Sequeirinho orebody (Sossego deposit) and the Visconde deposit (Fig. 17A-D), both located at the southern sector of the Carajás domain, makes it evident that their actinolites show a great compositional similarity. Very different is, however, the actinolite of the Paleoproterozoic Sossego orebody (Sossego deposit), although some similarity is found if the K-Cl relationship is considered (Fig. 17D). The contrasting chemical differences between the actinolites may be related to the shallower crustal level in which the Sossego orebody was formed.
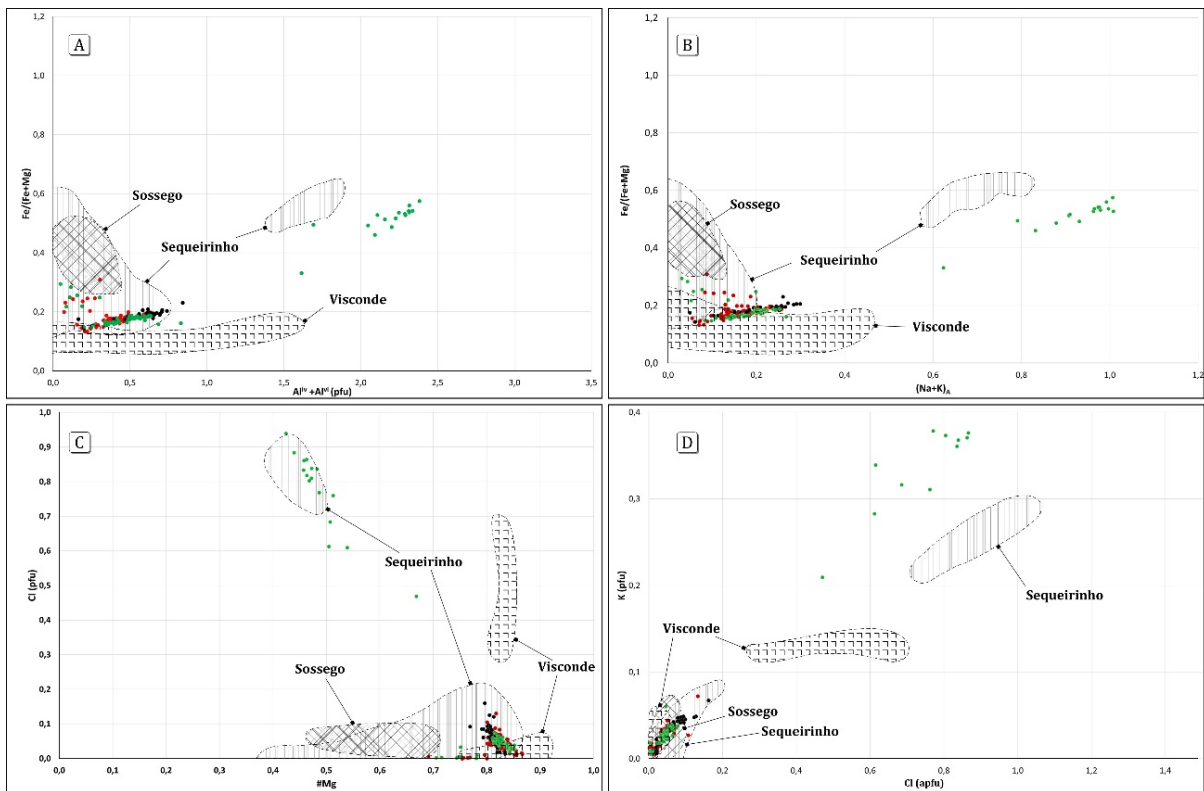
Figure 17. Chemical variation of amphiboles from the Cristalino deposit comparatively to those from the IOCG Sossego (Sequeirinho and Sossego orebodies) and Visconde deposits. (A) $(Al^{iv}+Al^{vi})$ *vs*. Fe/(Fe+Mg); (B) $(Na+K)_A$ *vs*. Fe/(Fe+Mg); (C) #Mg *vs*. Cl and; (D) Cl *vs*. K. Data sources: Sossego deposit: Monteiro *et al*. (2008b); Visconde deposit: (Craveiro *et al*. 2012); Cristalino deposit (this work). Symbols for the Cristalino deposit are the same as in figure 8.

On the other hand, the edenites (mostly ferro-edenites) of the Cristalino deposit occupy a distinct field on the diagrams X_{Fe}-Al_{total}, X_{Fe}-$(Na+K)_A$ and K-Cl (Fig. 17A, 17B, 17D), in view of their higher Al_{total}, $(Na+K)_A$ and K contents. This may suggest a particular chemical environment and/or fluid regime at the time of their formation in comparison to those of the Sossego (Sequeirinho orebody) and Visconde deposits, despite some overlapping on the #Mg-Cl diagram (Fig. 17C). In fact, it can be said that in each of these deposits a chemically different variety of edenite was produced, emphasizing that no chemical data are available on the Sossego orebody edenites.

Chlorites from the Carajás IOCG deposits present a broad spectrum of compositions reflecting mainly the nature of the host rocks, the fluid chemical characteristics and temperature. Concerning the Cristalino chlorites, their compositions are also highly variable especially in terms of parameters such as Al^{iv}, Al^{vi}, X_{Fe}, #Mg and Cl (Fig. 14).
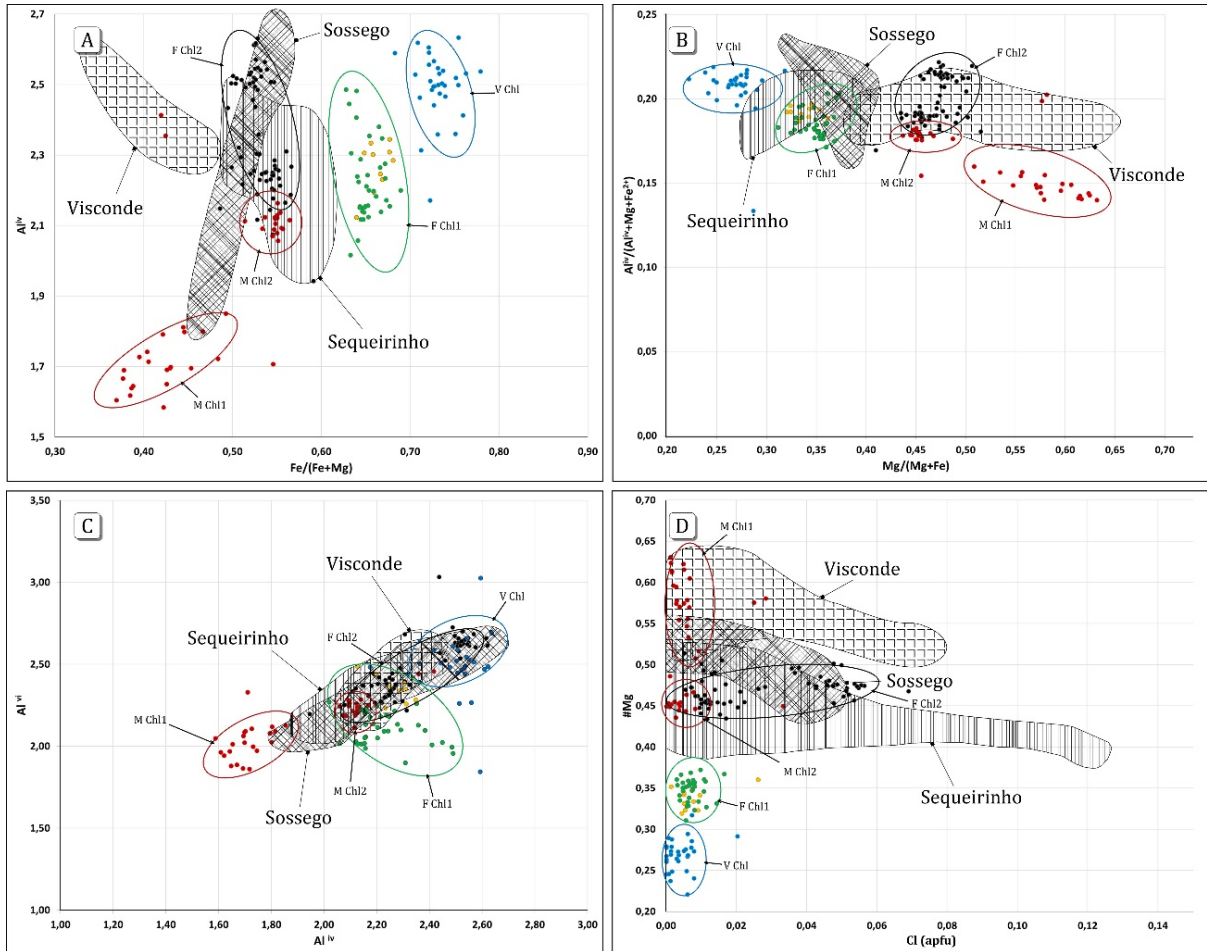
Figure 18. Chemical variation of chlorites from the Cristalino deposit comparatively to those from the IOCG Sossego (Sequeirinho and Sossego orebodies) and Visconde deposits. (A) Fe/(Fe+Mg) versus Al^{iv}; (B) Mg/(Mg+Fe) versus $Al^{iv}/(Al^{iv}+Mg+Fe^{2+})$; (C) Al^{iv} versus Al^{vi}; (D) Cl versus #Mg. Data sources: Sossego deposit: Monteiro *et al.* (2008b); Visconde deposit: (Craveiro *et al.* 2012); Cristalino deposit (this work). Symbols for the Cristalino deposit are the same as in figure 14.

Compared to the chlorites from the Sossego and Visconde deposits, the FChl1, MChl1 and vein chlorites constitute distinct groups (Fig. 18A, C and D) with practically no counterparts in these deposits. This may suggest that these chlorites grew under special conditions that were not recorded in the Sossego and Visconde deposits. In turn, the groups FChl2 and MChl2 are compositionally comparable to chlorites from these deposits, given the extensive overlapping they present (Fig. 18A-D), meaning that they most likely crystallized in environments reproduced in all three deposits. Relatively to Sossego, Sequeirinho orebodies and Visconde deposit, the lower content in Cl and wider #Mg (ca. 0.22 to 0.65, Fig. 18D)

seems to be characteristic of the chlorites from the Cristalino deposit. The lower Cl content in analyzed late minerals phases, such as allanites and chlorites, could be translated as diluted fluid derivation. At brittle conditions, and probably in a leaching-dominated system, the entrance of externally derived fluid, like meteoric fluids, is feasible.

CONCLUSIONS

The hydrothermal system related to the Cristalino IOCG deposit produced in the host rocks several alteration zones, recording successively sodic, ferric-calcic, potassic and propylitic/carbonation assemblages. Commonly, younger zones overprinted older ones.

In the Cristalino system two major alteration stages could be distinguished, according to the mineralogical assemblages, and thermal and deformational regimes. The first stage accounted for the sodic and calcic-ferric alterations that took place under ductile-brittle and higher temperature ($> 410°$ C) conditions, the latter associated with the earlier ore association (chalcopyrite-pyrite-magnetite-Au), which occurs as disseminations and breccia-like bodies. During the second stage, developed under essentially brittle regime and at lower temperatures ($< 410°$ C), potassic and propylitic assemblages were generated contemporaneously with the later ore association (chalcopyrite±Au±pyrite±hematite) present in breccia matrix and vein fillings.

The thermal history of the Cristalino hydrothermal system records a general drop of temperature, from around 650 °C to as low as 220°C. This negative thermal gradient seems to have been occasionally disrupted by new hydrothermal pulses with local temperature increase, as registered in some chlorite veins.

Almost pure chessboard albite is the most important product of the sodic metassomatism, together with some REE-rich minerals (allanite-Ce and monazite). Actinolite (X_{Mg}=0.87–0.69, Cl up to 0.59 wt. %) is the main mineral of the pervasive ferric-calcic zones where it is associated with Ce-allanite and magnetite, as well as with disseminations and breccia-like bodies of chalcopyrite-pyrite-magnetite (early ore association). Locally, Fe-edenite (X_{Mg}=0.67-0.42, Cl up to 2.94 wt. %) replaced calcic-ferric assemblages within restrict sodic-calcic alteration halos. The abundance of magnetite indicates that f_{O2} might have been relatively high at the prevalent temperatures, causing significant production of Fe^{3+}, some entering the structure of other minerals, in particular allanite.

Along the potassic alteration stage, biotite and K-feldspar formed at conditions bracketed by $410°$ C $> T_{Bt-Fds} > 220°$ C. K-feldspar is almost stoichiometric, despite impurities

such as BaO, FeO_{total} and SrO with contents of up to 1.21 wt. %, 0.19 wt. % and 0.49 wt. %, respectively.

Chlorite shows the greatest compositional variation among all minerals and its composition seems to have been particularly controlled by the type of host rock, chemistry of the hydrothermal fluid and temperature. Both chamosite and clinochlore (X_{Fe}=0.37-0.80) are present, the former being more common. Chlorine contents are in general < 0.02 wt. % and a little more significant in chlorites that replaced chessboard albite (up to 0.06 wt. %). Their formation temperature ranges from 220º to 360º C, the infill chlorites showing the highest values. The late ore association (chalcopyrite±Au±hematite±pyrite) is contemporaneous with the potassic and propylitic alterations and bears evidence that the Cristalino system evolved to the final stages with increase in oxygen fugacity.

Comparatively to other IOCG deposits from the southern sector of the Carajás domain, especially the Sossego and Visconde deposits, two varieties of amphibole (mainly actinolite and edenite) have been formed, but the Cristalino chlorites, despite some overlapping, present very distinct populations not yet described in the other two deposits, confirming the diversity of IOCG systems in Carajás.

REFERENCES

Araújo, O.J.B., Maia, R.G.N., Jorge-João, X.S. Costa, e J.B.S. 1988. A megaestruturação da folha Serra dos Carajás. *In*: SBG, Congresso Latino Americano de Geologia, *Proceedings...* **7:**324-333.

Augusto, R.A., Monteiro, L.V.S., Xavier, R.P., Souza Filho, C.R. 2008. Zonas de alteração hidrotermal e paragênese do minério de cobre do Alvo Bacaba, Província Mineral de Carajás (PA). *Revista Brasileira de Geociências*, **38:**263–277.

Barnes, H.L. (Ed). 1967. *Geochemistry of hydrothermal ore deposits*. Wiley, New York, 1967.

Barros, C.E.M., Macambira, M.J.B., Barbey, P., Scheller, T. 2004. Dados isotópicos Pb–Pb em zircão (evaporação) e Sm–Nd do Complexo Granítico Estrela, Província Mineral de Carajás, Brasil: implicações petrológicas e tectônicas. *Revista Brasileira de Geociências*, **34:**531–538.

Barros, C.E.M., Sardinha, A.S., Barbosa, J.P.O., Macambira, M.J.B., Barbey, P., Boullier, A.M. 2009. Structure, petrology, geochemistry and zircon U/Pb and Pb/Pb geochronology of the synkinematic Archean (2.7 Ga) A-type granites from the Carajás Metallogenic Province, northern Brazil. *The Canadian Mineralogist*, **47:**1423-1440.

Barros, C.E.M.; Macambira, M.J.B.; Barbey, P. 2001. Idade de zircão do Complexo Granítico Estrela: relações entre magmatismo, deformação e metamorfismo na Província Mineral de Carajás. *In*: Simpósio de Geologia da Amazônia, 7, Belém. Resumos Expandidos: SBG, 17-20.

Bonazzi, P. and Menchetti, S. 1994. Structural variations induced by heat treatment in allanite and REE-bearing piemontite. *American Mineralogist*, **79:**1176-1184.

Botelho, N.F., Moura, M, A., Teixeira, L.M., Olivio, G.R., Cunha, L.M., Santana, M.U. 2005. Caracterização geológica e metalogenética do depósito de Cu ± (Au, W, Wo, Sn) Breves, Carajás. In: Eds. Marini, O.J, Queiroz, E.T, Ramos, B.W. *Caracterização de depósitos minerais em distritos mineiros da Amazônia*, Brasília: DNPM – CT/MINERAL – ADIMB, 2005. 339-387.

Cannon, W.F. 1976. Hard iron ore of the Marquette Range, Michigan: *Economic Geology*, **71:**1012–1028.

Costa, J.B.S., Araújo, O.J.B., Santos, A., Jorge João, X.S., Macambira, M.J.B., Lafon, J.M. 1995. A Província Mineral de Carajás: aspectos tectono-estruturais, estratigráficos e geocronológicos. *Boletim do Museu Paraense Emílio Goeldi*, **7:**199-235.

Craveiro, G.S, Villas, R.N. da Costa Silva. A.R. 2012. Depósito Visconde, Carajás (PA): geologia e alteração hidrotermal das rochas encaixantes. *Revista Brasileira de Geociências*, **42:**453-470.

Craveiro, G.S., Xavier. R.P., Villas, R.N.N. 2018a (Accepted). The Cristalino IOCG deposit: an example of multi-stage events of hydrothermal alteration and copper mineralization. *Brazilian Journal of Geology*.

Cunha, I.R.V., Dall'Agnol, R., Feio, G.R.L. 2016. Mineral chemistry and magnetic petrology of the Archean Planalto Suite, Carajás Province – Amazonian Craton: Implications for the evolution of ferroan Archean granites. *Journal of South American Earth Sciences*, **67:**100-121.

Dall'Agnol, R., Oliveira, D.C., Lamarão, C.N. 2013. Magmatismo granitoide arqueano e evolução geológica do Subdomínio de Transição da Província Carajás, sudeste do Cráton Amazônico, Brasil. *Boletim do Museu Emílio Goeldi*, **8(3):**251-256.

Dall'Agnol, R., Teixeira, N.P., Rämö, O.T., Moura, C.A.V., Macambira, M.J.B., Oliveira, D.C. 2005, Petrogenesis of the Paleoproterozoic, rapakivi, A-type granites of the Archean Carajás Metallogenic Province, Brazil. *Lithos*, **80:** 101–129.

Deer W.A., Howie R.A., Zussman J. 1997. *Rock-forming minerals: double-chain silicates*, v. 2B, 2nd ed., The Geological Society, London, 771p.

DOCEGEO, 1988. Revisão litoestratigráfica da Província Mineral de Carajás – Litoestratigrafia e principais depósitos minerais. *In*: 35° Congresso Brasileiro de Geologia, 35. Belém, *Expanded abstract*, 11-54.

Driesner, T., Seward, T.M., Tironi, I.G. 1998. Molecular dynamics simulation study of ionic hydration and ion association in dilute and 1 molal aqueous sodium chloride solutions from ambient to supercritical conditions. *Geochimica et Cosmochimica Acta*, **62:**3095-3107.

Ercit, T.S. 2002. The mess that is "allanite". *The Canadian Mineralogist*, **40:**1411-1419.

Feio, G.R.L., Dall'Agnol, R., Dantas, E.L., Macambira, M.J.B., Gomes, A.C.B., Sardinha, A.S., Oliveira, D.C., Santos, R.D., Santos, P.A. 2012b, Geochemistry, geochronology, and origin of the Neoarchean Planalto Granite suite, Carajás, Amazonian craton: A-type or hydrated charnockitic granites? *Lithos*, **151:**57-73.

Feio, G.R.L., Dall'Agnol R., Dantas E.L., Macambira M.J.B., Santos J.O.S., Althoff F.J., and Soares J.E.B., 2013. Archean granitoid magmatism in the Canaã dos Carajás area: Implications for crustal evolution of the Carajás province, Amazonian craton, Brazil. *Precambrian Research*, **227:**157-186.

Ferreira Filho, C.F., Cançado, F., Correa, C., Macambira, E.M.B., Junqueira-Brod, T.C., Siepierski, L. 2007. Mineralizações estratiformes de PGE-Ni associadas a complexos acamadados em Carajás: os exemplos de Luanga e Serra da Onça. *In*: Rosa-Costa, L. T., Klein, E.L., Viglio, E.P. (Ed.). *Contribuições à geologia da Amazônia*. Belém: Sociedade Brasileira de Geologia, v.5:1-14.

Galarza, M.A. and Macambira, M.J.B. 2002. Geocronologia e evolução crustal da área do depósito de Cu-Au Gameleira, Província Mineral de Carajás (Pará), Brasil. *Revista do Instituto de Geociências da USP*, **2:**143-159.

Gibbs, A.K., Wirth, K.R., Hirata, W.K., Olszewski Jr., W.J. 1986. Age and composition of the Grão Pará Group volcanics, Serra dos Carajás. *Revista Brasileira de Geociências*, **16:**201–211.

Giesting, P.A. and Filiberto J. 2015. Crystal chemistry and formation mechanisms of the potassic-chloro-hastingsite in MIL03346 and paired stones. *In*: 46th Lunar and Planetary Science Conference.

Grainger, C.J., Groves, D.I., Tallarico, F.H.B., Fletcher, I.R. 2008. Metallogenesis of the Carajás Mineral Province, southern Amazon Craton: Varying styles of Archean through Paleoproterozoic to Neoproterozoic base- and precious-metal mineralization. *Ore Geology Reviews*, **33:**451-489.

Greré, R. and Sorensen, S. S. 2004. Allanite and other REE-rich epidote-group minerals. *Review in Mineralogy & Geochemistry*, **56:**431-493.

Groves, D. I., Bierlein, F.P. Meinert. L.D, Hitzman, M.W. 2010. Iron oxide cooper-gold (IOCG) deposits through Earth history: Implications for origin, lithospheric setting, and distinction from other epigenetic iron oxide deposits. *Economic Geology*, **105:**641-654.

Henry, D.J and Daigle, N.M. 2018. Chlorine incorporation into amphibole and biotite in high-grade iron formations: interplay between crystallography and metamorphic fluid. *American Mineralogist*, **103:**55-68.

Henry, D.J, Novák, M., Hawthorne, F.C., Ertl, A., Dutrow, B.L., Uher, P., Pezzotta, F. 2011. Nomenclature of the tourmaline-supergroup minerals. *American Mineralogist*, **96:**895-913.

Huhn, S.R.B., Souza, C.I.J., Albuquerque, M.C., Leal, E.D., Brustolin, V. 1999b. Descoberta do depósito Cu (Au) Cristalino: Geologia e mineralização associada região da Serra do Rabo - Carajás – PA. In: SBG/NO, Simpósio de Geologia da Amazônia, Manaus, *Proceedings...* **6:**140–143.

Hunger, R.B. 2017. O depósito de óxido de ferro cobre-ouro (IOCG) Grota Funda, Domínio Carajás (pa): alteração hidrotermal, regime de fluidos e idade da mineralização. Masters dissertation. IG-UNICAMP, 182p.

Kranidiotis, P., MacLean, W.H. 1987. Systematic of chlorite alteration at the Phelps Dodge massive sulfide deposit, Matagami, Quebec. *Economic Geology*, **82:**1898-1911.

Leake, B.E., Woolley, A.R., Arps, C.E.S., Birch, W.D., Gilbert,M.C., Grice, J.D., Hawthorne, F.C., Kato, A., Kisch, H., Krivovichev., V.G., Linthout. K., Laird. J., Mandarino., J., Maresch, W., Nickel, E.H., Rock, N.M.S., Shumacher, J.C., Smith, D.C., Stephenson, N.C.N., Ungaretti, L., Whittaker, E.J.W., Youzhi. G. Nomenclature of amphiboles: report of the subcommittee on the amphiboles of the International Mineralogical Association, commission on new minerals and minerals names. *The Canadian Mineralogist*, **35:**219-246.

Léger, A., Rebbert, C., Webstrer, J. 1996. Cl-rich biotite and amphibole from Black Forest, Cornwall, New York. *American Mineralogist*, **81:**495-504.

Lindenmayer, Z. G., Fleck, A., Gomes, C.H., Santos, A.B.S., Caron, R., Paula, F.C., Laux, J.H., Pimentel, M.M., Sardinha, A.S. 2005. Caracterização geológica do alvo estrela (Cu-Au), Serra dos Carajás, Pará In: Caracterização de *Depósitos Minerais em Distritos Mineiros da Amazônia*. DNPM, CT-Mineral / FINEP, ADIMB, 2005, cap. IV, 1, 137-205.

Lindenmayer, Z.G., Laux, J.H., Teixeira, J.B.G. 2001. Considerações sobre a origem das Formações Ferríferas da Formação Carajás, Serra dos Carajás. *Revista Brasileira de Geociências*, **31(1):**21-28.

Lobato, L.M., Rosière, C.A., Silva, R.C.F., Zucchetti, M., Baars, F.J., Seoane, J.C.S., Rios, F.J., Pimentel, M., Mendes, G.E., Monteiro, A.M. 2005. A mineralização hidrotermal de ferro da Província Mineral de Carajás - controle estrutural e contexto na evolução metalogenética da Província. In: Marini, J.O.; Queiróz, E.T.; Ramos, W.B. (eds.), *Caracterização de distritos mineiros da Amazônia*. DNPM-CT-Mineral-ADIMB, 25–92.

Macambira, E.M.B. and Vale, A.G. 1997. São Félix do Xingu: folha SB.22-Y-B, Estado do Pará, escala 1:250.000. Texto Explicativo. Brasília: CPRM. 344 p., il. Programa Levantamentos Geológicos Básicos do Brasil (PLGB).

Macambira, J.B., 2003. O ambiente deposicional da Formação Carajás e uma proposta de modelo evolutivo para a Bacia Grão Pará. Doctoral thesis, IG-UNICAMP, 217p.

Machado, N., Lindenmayer, Z.G., Krogh, T.E., Lindenmayer, D. 1991. U–Pb geochronology of Archean magmatism and basement reactivation in the Carajás area, Amazon shield, Brazil. *Precambrian Research*, **49:**329–354.

Makino, K., Tomita, K., Suwa, K. 1993. Effect of chlorine on the crystal structure of a chlorine-rich hastingsite. *Mineralogical Magazine*, **57:**677-685.

Meirelles, M.R. and Dardenne, M.A. 1991. Vulcanismo basáltico de afinidade shoshonítica em ambiente de arco arqueano, Grupo GrãoPará, Serra dos Carajás, PA. *Revista Brasileira de Geociências*, **21:**41-50.

Melo, G.H.C., Monteiro, L.V.S., Xavier, R.P., Moreto, C.P.N., Santiago, E.S.B., Dufrane, E.A., Aires, B. 2017. Temporal Evolution of the giant Salobo IOCG deposit, Carajás Province (Brazil): constrains from paragenesis of hydrothermal alteration and U-Pb geochronology. *Mineralium Deposita*, **52:**709-732.

Melo, G.H.C., Monteiro, L.V.S, Moreto, C.P.N, Xavier, R.P., Silva, M.A.D. 2014. Paragenesis and Evolution of the hydrothermal Bacuri iron-oxide-copper-gold deposit, Carajás Province (PA). *Brazilian Journal of Geology*, **44(1):** 73-90.

Monteiro, L.V.S., Xavier, R.P., Carvalho, E.R., Hitzman, M.W., Johnson, C.A., Souza Filho, C.R., and Torresi, I. 2008a. Spatial and temporal zoning of hydrothermal alteration and mineralization in the Sossego iron oxide- copper-gold deposit, Carajás Mineral Province, Brazil: Parageneses and stable isotope constraints. *Mineralium Deposita*, **43:**129−159.

Monteiro, L.V., Xavier. R.P., Hitzman, M.W., Juniani, C., Souza Filho, C.R., Carvalho, E.R. 2008b. Mineral chemistry of ore and hydrothermal alteration at the Sossego iron oxide-copper-gold deposit, Carajás Mineral Province, Brazil. *Ore Geology Reviews*, **34:**317-336.

Moreto, C.P.N., Monteiro L.V.S., Xavier R.P., Amaral W.S., Santos T.J.S., Juliani C., Souza Filho, C.R. 2011. Mesoarchean (3.0 and 2.86 Ga) host rocks of the iron oxide-Cu-Au Bacaba deposit, Carajás Mineral Province: U-Pb geochronology and metallogenetic implications. *Mineralium Deposita*, **46:**789-811.

Moreto, C.P.N., Monteiro, L.V.S., Xavier, R.P., Creaser, R.A., Dufrane, S.A., Melo, G.H.C., Delinardo da Silva, M.A., Tassinari, C.C.G., Sato, K. 2015a. Timing of multiple hydrothermal events in the iron oxide–copper–gold deposits of the Southern Copper Belt, Carajás Province, Brazil. *Mineral Deposita*, **50:**517–546.

Moreto, C.P.N., Monteiro, L.V.S., Xavier, R.P., Creaser, R.A., Dufrane, S.A., Tassinari, C..CG., Sato, K., Kemp, A.I.S., Amaral, W.S. 2015b. Neoarchean and Paleoproterozoic iron oxide-copper-gold events at the Sossego deposit, Carajás Province, Brazil, Re-Os and U-Pb geochronological evidence. *Economic Geology*, **110:**809–835.

Mougeot, R., Respaut, J.P., Briqueu, L., Ledru, P., Milesi, J.P., Lerouge, C., Marcoux, E., Huhn, S.B., Macambira, M.J.B. 1996b. Isotope geochemistry constrains for Cu, Au mineralizations and evolution of the Carajás Province (Para, Brazil). *In*: SBG, Congresso Brasileiro de Geologia, *Anais*... Salvador, **7:**321–324.

Nogueira, A.C.R., Truckenbrodt, W., Pinheiro, R.V.L. 1995. Formação Águas Claras, Pré-Cambriano da Serra dos Carajás: redescrição e redefinição litoestratigráfica. *Boletim Museu Paraense Emílio Goeldi,* **7:**177–277.

Oberti, R., Ungaretti, L., Cannillo, E., Hawthorne, F.C. 1993. The mechanism of Cl incorporation in amphibole. *American Mineralogist*, **78:**746-752.

Ohmoto, H. 2003. Nonredox transformations of magnetite-hematite in hydrothermal systems. *Economic Geology*, **98:**157-161.

Ollila, J.T. 1984. Partitioning of barium between coexisting K-feldspars and plagioclases in Bushveld granites from Zaaiplaats area, South Africa. *Bulletin of the Geological Society of Finland*, **56(1-2)**: 53–75.

Pe-Piper, G. 1988. Calcic amphiboles of mafic rocks of the Jeffers Brook plutonic complex, Nova Scatia, Canada. *American Mineralogist*, **73:**993-1006.

Pichavant, M. 1981. An experimental study of the effect of boron on a water saturated haplogranite at 1 kbar vapor pressure. *Contribution to Mineral Petrology*, **76:**430-439.

Pinheiro R.V.L. and Holdsworth, R.E. 2000. Evolução tectonoestratigráfica dos sistemas transcorrentes Carajás e Cinzento, Cinturão Itacaiúnas, na borda leste do Cráton Amazônico, Pará. *Revista Brasileira de Geociências*, **30(4):**597-606.

Pinto, A. 2012. Salobo Copper Mine Feasibility in Carajás, Pará State. *In*: ADIMB, V Brazilian Symposium on Mineral Exploration. 2012. Ouro Preto - MG, Brazil.

Previato, M., 2016. Evolução paragenética e regime de fluidos hidrotermais no sistema Borrachudo: Implicações para a metalogênese e cobre na Província Carajás. Masters dissertation. IG-USP. 131p.

Rämö, O.T., Dall'Agnol, R., Macambira, M.J.B., Leite, A.A.S., Oliveira, D.C. 2002. 1.88g. oxidized a-type granites of the Rio Maria Region, eastern Amazonian Craton: positively anorogenic! *Journal of Geology*. **110:**603-610.

Reis, F.N. 2001. Estudo isotópico do depósito cupro-aurífero de Serra Verde, Província Mineral de Carajás, Pará. In: Simpósio de Geologia da Amazônia, 7., 2001, Belém. Proceedings..., Belém: SBG, 2001. 1 CD-ROM.

Réquia, K., Stein, H., Fontboté, L., Chiaradia, M. 2003. Re–Os and Pb–Pb geochronology of the Archean Salobo iron oxide copper–gold deposit, Carajás Mineral Province, northern Brazil. *Mineralium Deposita*, **38:**727–738.

Ribeiro, A.A., Suíta, M.T.F., Sial, A.N., Fallick, A.E., Eli, F., Goulard, A.E. 2009. Geoquímica de isótopos estáveis (C, S e O) das rochas encaixantes e do minério de Cu (Au) do depósito Cristalino, Província Mineral de Carajás, Pará. *Geochimica Brasiliensis*, **23:**159-176.

Rosenberg P.E., Foit F. 1977. Fe2+-F avoidance in silicates. *Geochimica et Cosmochimica Acta*, **41**: 345-346.

Sardinha, A.S., Barros, C.E.M. & Krymsky, R. 2006. Geology, geochemistry and U–Pb geochronology of the Archean (2.74 Ga) Serra do Rabo granite stocks, Carajás Metallogenic Province, northern Brazil. *Journal of South American Earth Sciences*, 20:327-339.

Seward, T.M. and Driesner, T. 2004. Hydrothermal solution structure: experiments and computer simulations. In: Palmer, D. A., Fernández-Prime, Harvey, A.H; (editors) *Aqueous systems at elevated temperature and pressures: physical chemistry in water, steam and hydrothermal solutions*. 2004. Chapter 5, 149–182. 753p.

Siepierski, L. 2016. Geologia, Petrologia e potência para mineralizações magmáticas dos corpos máfico-ultramáficos da região de Canaã dos Carajás, Província Mineral de Carajás. Doctoral Thesis. IG-UnB, 158p.

Silva, A.R, Villas, R.N., Lafon, J., Craveiro, G.S., Ferreira, V.P. 2015.Stable isotope systematics and fluid inclusion studies in the Cu-An Visconde deposit, Carajás Mineral Province, Brazil: implications for fluid source generation. *Mineralium Deposita*, **50:**547-569.

Soares, A.D.V., Macambira, M.J.B., Santos, M.G.S., Vieira, E.A., Masotti, F.S., Souza, C.I.J., Padilha, J.L., Magni, M.C.V. 2001. Depósito Cu (Au) Cristalino, Serra dos Carajás PA: Idade da Mineralização com base em Análises Pv-Pb em sulfetos (Dados Preliminares). *In*: SBG, 7° Simpósio de Geologia da Amazônia, Belém, *Proceedings...* CD-ROM.

Soares, A.D.V., Ronzê, P.C., Santos, M. G.S., Leal, E.D., Barreira, C.F. 1999. Geologia e mineralizações do depósito de Cu-Au Alemão − Província Mineral de Carajás (PA). In: SBG, 5° Simpósio de Geologia da Amazônia. *Resumos expandidos...* Manaus, p. 144-147.

Tallarico, F.H.B., Figueiredo B.R., Groves D.I., Kositcin N., McNaughton N.J., Fletcher I.R., Rego J.L. 2005. Geology and SHRIMP U–Pb geochronology of the Igarapé Bahia deposit, Carajás copper–gold belt, Brazil: an Archean (2.57 Ga) example of iron–oxide Cu–Au–(U– REE) mineralization. *Economic Geology*, **100:**7–28.

Tavares, F.M. 2015. Evolução geotectônica do nordeste da Província Carajás. Doctoral Thesis. IG-UFRJ. 115p.

Teixeira, A.S., Ferreira Filho, C.F., Giustina, M.E.S.D., Araújo, S.M., Silva, H.H.A.B. 2015. Geology, petrology and geochronology of the Lago Grande layered complex: evidence for a PGE-mineralized magmatic suíte in the Carajás Mineral Province, Brazil. *Journal of South American Earth Sciences*, **64:**116-138.

Teixeira, J.B.G., 1994. Geochemistry, petrology, and tectonic setting of Archean basaltic and dioritic rocks from the N4 Iron deposit, Serra dos Carajás, Pará, Brazil. Doctoral thesis. IG-USP. 161p.

Tindle, A.G., Breaks, F.W., Selway, J.B. Tourmaline in petalite-subtype granitic pegmatites: evidence of fractionation and contamination from the Pakeagama Lake and Separation Lake areas of northwestern Ontario, Canada. *The Canadian Mineralogist*, **40:**753-788.

Torresi, I. Xavier, R.P., Bortholoto, D.F.A., Monteiro, L.V.S. 2011. Hydrothermal alteration, fluid inclusions and stable isotope systematics of the Alvo 118 iron-oxide-copper-gold deposit, Carajás Mineral Province (Brazil): Implications for ore genesis. *Mineralium Deposita*, **47:**299-323.

Trendall, A.F., Basei, M.A.S., De Laeter, J.R., and Nelson, D.R., 1998, SHRIMP U-Pb constraints on the age of the Carajás formation, Grão Pará Group, Amazon Craton. *Journal of South American Earth Sciences*, **11:**265-277.

Vasquez, L.V., Rosa-Costa, L.R., Silva, C.G., Ricci, P.F., Barbosa, J.O., Klein, E.L., Lopes, E.S., Macambira, E.B., Chaves, C.L., Carvalho, J.M., Oliveira, J.G., Anjos, G.C., Silva, H.R., 2008. *Geologia e Recursos Minerais do Estado do Pará: Sistema de Informações Geográficas–SIG: Texto Explicativo dos Mapas Geológico e Tectônico e de Recursos Minerais do Estado do Pará*. Organizers: M.L Vasquez, L.T. Rosa Costa. Scale1:1.000.000. Belém: CPRM.

Wesolowski, D.J., Ziemniak, S.E., Anovistz, L.M., Machesky, M.L. Bénéseth, P., Palmer, D.A. 2004. Solubility and surface adsorption characteristics of metal oxides. In: Palmer, D. A., Fernández-Prime, Harvey, A.H; (editors) *Aqueous systems at elevated temperature and pressures: physical chemistry in water, steam and hydrothermal solutions*. 2004. Chapter **14:**493–586, 753p.

Williams, P.J., Barton, M.D., Johnson, D.A., Fontboté, L., Haller, A., Mark, G., Oliver, N.H.S., Marschik. R. 2005. Iron oxide copper-gold deposits: Geology, space-time distribution, and possible modes of origin. *Economic Geology 100th Anniversary Volume*. 371-405.

Xavier, R.P., Monteiro, L.V.S., Moreto, C.P.N., Pestilho, A.L.S., Melo, G.H.C., Silva, M.A.D., Aires, B., Ribeiro, C., Silva, F.H.F. 2012. The iron oxide copper-gold system of the Carajás Mineral Province, Brazil. *Economic Geology*, Special Publication, 16, Chapter X.

Xavier, R.P., Moreto, C.P.N., de Melo, G.H.C., Toledo, P., Hunger, R., Deminardo, M., Faustinoni, J., Lopes, Ananda. 2017. Geology and metallogeny of Neoarchean and Paleoproterozoic copper systems of the Carajás Domain, Amazonian Craton, Brazil. Proceedings of the *14th BiennialSGA Meeting of the Society for Geology Applied to Mineral Deposits*, Quebec, Canada. 20-23 August,pp. 899-902.

Xavier, R.P., Moreto, C.P.N., de Melo, G.H.C., Toledo, P., Hunger, R., Delinardo, M., Faustinoni, J., Lopes, Ananda. 2017. Geology and metallogeny of Neoarchean and Paleoproterozoic copper systems of the Carajás Domain, Amazonian Craton, Brazil. *Proceedings of the 14th Biennial SGA Meeting of the Society for Geology Applied to Mineral Deposits*, Quebec, Canada. 20-23 August, 899-902.

Xavier, R.P., Wiedenbeck, M., Trumbell, R.B., Dreher, A.M., Monteiro, L.V.S., Rhede, D., Araújo, C.E.G., Torresi, I. 2008. Tourmaline B-isotopes fingerprint marine evaporites as the source of high-salinity ore fluids in iron-oxide-copper-gold deposits, Carajás Mineral Province (Brazil). *Geology*, **36:**743–74

4 A FLUID INCLUSION AND STABLE ISOTOPE (O, H, S AND C) STUDY OF THE ARCHEAN IOCG CRISTALINO DEPOSIT, CARAJÁS PROVINCE, BRAZIL: IMPLICATIONS TO ORE GENESIS.

Gustavo Souza Craveiro

Raimundo Netuno Nobre Villas

Roberto Perez Xavier

Successfully received: submission A Fluid Inclusion and Stable Isotope (O, H, S and C) study of the Archean IOCG Cristalino deposit, Carajás Mineral Province, Brazil: Implications to ore genesis. for Ore Geology Reviews

2 mensagens

Ore Geology Reviews <EviseSupport@elsevier.com>   2 de setembro de 2018 02:32
Responder a: oregeo@elsevier.com
Para: craveiro@ufpa.br

This message was sent automatically. Please do not reply.

Ref: ORGEO_2018_696
Title: A Fluid Inclusion and Stable Isotope (O, H, S and C) study of the Archean IOCG Cristalino deposit, Carajás Mineral Province, Brazil: Implications to ore genesis.
Journal: Ore Geology Reviews

Dear Mr. Souza Craveiro,

Thank you for submitting your manuscript for consideration for publication in Ore Geology Reviews. Your submission was received in good order.

To track the status of your manuscript, please log into EVISE® at: http://www.evise.com/evise/faces/pages/navigation/NavController.jspx?JRNL_ACR=ORGEO and locate your submission under the header 'My Submissions with Journal' on your 'My Author Tasks' view.

Thank you for submitting your work to this journal.

Kind regards,

Ore Geology Reviews

Have questions or need assistance?
For further assistance, please visit our Customer Support site. Here you can search for solutions on a range of topics, find answers to frequently asked questions, and learn more about EVISE® via interactive tutorials. You can also talk 24/5 to our customer support team by phone and 24/7 by live chat and email.

A Fluid Inclusion and Stable Isotope (O, H, S and C) study of the Archean IOCG Cristalino deposit, Carajás Mineral Province, Brazil: Implications to ore genesis.

Gustavo Souza Craveiro, Raimundo Netuno Nobre Villas, Roberto Perez Xavier

Abstract

The hydrothermal history of the Archean Cu-Au Cristalino deposit evolved from ~550°C to ~150°C along which its host rocks were moderately to intensely altered. Sodic, calcic-ferric, potassic, propylitic and carbonatic alterations developed successively, as well as two main ore types: an earlier chalcopyrite-pyrite-magnetite-Au associated with the calcic-ferric assemblages, and a later chalcopyrite-Au±pyrite±hematite related to the potassic and propylitic alteration zones. Estimated pressures (0.6 to 2. 6 kbar) are consonant with the brittle and brittle-ductile deformational environments where alteration and mineralization took place. The ore fluid was hot, acidic and hypersaline and chemically approached by the system H_2O-NaCl-$CaCl_2$-CO_2±$MgCl_2$±$FeCl_2$. Salinity might have exceeded 55 wt. % NaCl equiv. in the early alteration stages but decreased progressively to 7.9 wt. % NaCl equiv. from 250° C, after incursion of surficial water into the system. Initially ^{18}O-enriched/D-depleted ($\delta^{18}O_{vsmow}$ =+9.73 to +6.48‰; δD_{vsmow}= -30.17 to -40.25‰) and most likely derived from magmatic sources, the fluid became relatively ^{18}O-depleted/D-enriched ($\delta^{18}O_{vsmow}$ =+5.57 to -0.28‰; δD_{vsmow}= -19.15 to -22.24‰) as result of dilution caused by mixing with meteoric water. $\delta^{13}C_{VPDB}$ values for vein and breccia calcite (-6.5 to -3.8‰) are consistent with a deep source for CO_2, which was probably released from an underlying magma chamber. The $\delta^{34}S_{VCDT}$ values for chalcopyrite show narrow variation (+1.6 to +3.5 ‰) and indicate a homogeneous reservoir for sulfur, which was likely of igneous origin. Although most data point to a magmatic affiliation, a few samples reveal significant influence of sedimentary rocks on their isotope composition. Mostly transported as chloride complexes (>350°C), Cu and Au precipitated in response to decrease in temperature and Cl⁻ activity and increase in pH. The chalcopyrite-Au±pyrite±hematite ore assemblage was additionally favored by f_{O2} increase in the late stages of the hydrothermal alteration. An aqueous, colder (200-150° C) and less saline (21-3.1 wt. % NaCl equiv.) seems to have circulated in the Cristalino deposit area, being trapped as secondary fluid inclusions. The origin is unknown, but it could be related to a nearby Paleoproterozoic granitic intrusion. The data presented here support previous interpretations that consider Cristalino as of IOCG typology. In comparison with other

Archean Carajás IOCG deposits, particularly those that lie in the southern sector of the Carajás Domain, the Cristalino deposit shows many similarities regarding ore fluid composition and evolution, as well as the isotopic signature of sulfides and carbonates.

*G. S. Craveiro, e-mail: craveiro@ufpa.br; (corresponding author)
G. S. Craveiro; R. N. N. Villas,
Graduate Program in Geology and Geochemistry, Geoscience Institute, Federal University of Pará-UFPA, Rua Augusto Corrêa, 01 Guamá, P.O. Box 1611, 66075-110 Belém, PA, Brazil.
R. N. N. Villas, e-mail: netuno@ufpa.br

R. P. Xavier, e-mail: xavier@ig.unicamp.br
Instituto de Geociências, Universidade Estadual de Campinas, R. João Pandiá Calógeras, 51, CEP 13083-970, Campinas, SP, Brazil.

INTRODUCTION

The iron oxide copper-gold (IOCG) deposits of the Carajás Domain (CD) present many similarities, in particular those that lie in the southern sector, such as Alvo 118, Sossego, Cristalino, Bacaba, Castanha, Visconde, Borrachudo, among others. Hosted in volcano-sedimentary units of the Itacaiúnas Supergroup as well as in intrusive rocks of the basement, these deposits bear evidence of coeval granitic magmatism and general tectonic control (Grainger *et al*. 2008, Xavier *et al*. 2012, 2017). Large volumes of the host rocks are sodic-altered and typically affected by proximal sodic-calcic/calcic-sodic, potassic and propylitic alterations, in which the sulfide-rich mineralization generally post-dates the iron-oxide formation.

Both Neoarchean and Paleoproterozoic IOCG systems exhibit similar trends in fluid evolution. Initially hypersaline and hot (>500°C), the metalliferous brines acquire moderate to low salinity at lower temperatures (ca. 250°C), and aqueous-carbonic fluids also circulate through the rocks (Xavier *et al*. 2012). Ore-forming fluids have been interpreted as having magmatic derivation in the early hydrothermal stages, while in the late stages they become $\delta^{18}O$ depleted and δD enriched, indicative of fluid mixing, possibly with seawater and/or meteoric water (Monteiro *et al*. 2008a, Ribeiro *et al*. 2009, Torresi *et al*. 2012, Silva *et al*. 2015). This scenario reproduces fairly well what has been observed in other IOCG deposits worldwide, such as Olympic Dam and Ernest Henry, Australia (Williams *et al*. 2005, 2010; Groves *et al*. 2010) and Candelaria in the Chilean iron belt (Mathur *et al*. 2002).

In spite of numerous and important advances in the knowledge of IOCG deposits (Hitzman *et al*. 1992, Barton and Johnson 1996, Pollard 2001, Williams *et al*. 2005, Grainger

et al. 2008, Groves *et al.* 2010, Xavier et al. 2012), many issues require more research to give more vigorous support to interpretative models. At the center of the discussions are, for example, the origin of the high salinity fluids, sulfur, and metals. Another important issue is the role of granite intrusion, whether restricted or not to provide heat for the circulation of fluids for the IOCG mineralization (Pollard 2001, Groves *et al.* 2010).

The world-class Cristalino deposit (379 Mt @ 0.66 wt.% Cu; 0.3 g/t Au; Pinto 2012) is an example of IOCG deposit still little investigated. It is located in the Serra do Rabo region (Fig. 1B), about 40 km east of the Sossego mine and immediately south of the Estrela copper-polymetallic deposit, at the eastern termination of the Carajás fault, in the CD southern sector.

Despite the valuable contribution of previous works (Huhn *et al.* 1999, Soares *et al.* 2001, Ribeiro *et al.* 2009, among others), the nature and sources of the fluids and metals of the Cristalino hydrothermal system need to be constrained. To throw some light on the genesis of the Cristalino deposit, this study aims to define the potential sources of the hydrothermal fluids and the P-T conditions under which alteration and mineralization took place based on stable isotopes (O, H, S and C) and fluid inclusion data.

GEOLOGICAL SETTING OF THE CARAJÁS DOMAIN

The Carajás Domain (CD) to the north and the Rio Maria Domain (RMD) to the south are two tectonically distinct crustal blocks that make up the Carajás Province (Vasquez *et al.* 2008) located in the east-southeast of the Amazon Craton (Fig. 1A).

The basement of the CD (Fig. 1B) consists of TTG-like gneisses-migmatites, orthogranulites and calc-alkaline granitoids with ages within the range of 3.0-2.83 Ga and is overlain by the Rio Novo Group (>2.76 Ga) and Itacaiúnas Supergroup (2.76-2.73 Ga) as well as the Águas Claras Formation (> 2.65 Ga), all built in the so-called Carajás basin (Vasquez *et al.* 2008).

The rocks of the Rio Novo Group crop out in the Serra Pelada region and form part of a mafic/ultramafic volcano-sedimentary sequence with intercalations of banded iron formations (BIF) and metaquartzites (Araújo and Maia 1991, Oliveira 1994, Vasquez *et al.* 2008). The minimum age of this group is constrained by the intrusive Luanga mafic-ultramafic and the Estrela granitic complexes, both dated at 2763±7 Ma (Machado *et al.* 1991; Barros *et al.* 2001).

The Itacaiúnas Supergroup encompasses the Igarapé Salobo, Grão Pará, Igarapé Bahia and Igarapé Pojuca groups, which host several world-class metallic deposits. Their lower

units consist dominantly of bi-modal volcanic rocks, whereas the upper ones include metasiltstones, metargilites and BIF associated with minor metabasalts and metadacites. The intermediate units comprise thick layers of BIF (DOCEGEO 1988, Soares *et al*. 1999, Ronzê *et al*. 2000, Lindenmayer *et al*. 2001, Vazquez *et al*. 2008).

Mafic-ultramafic layered igneous intrusions represented by the Serra Leste and the Cateté Intrusive suites transect the basement and the Itacaiúnas Supergroup. Both suites consist of elongated bodies that form clusters of PGE-, Cr- and Ni-bearing mafic-ultramafic rocks (Macambira and Vale 1997, Ferreira Filho *et al*. 2013, Siepierski 2016). The chromite-bearing Luanga and Lago Grande complexes are part of the Serra Leste Suite and have been dated, respectively, at 2763±7 Ma (Machado *et al*. 1991) and 2722±53 Ma (Teixeira *et al*. 2015).

The Estrela Complex, Serra do Rabo, Igarapé Gelado and Old Salobo intrusions are Archean high potassium subalkaline granites that have been emplaced only into the Carajás basin rocks (Feio *et al*. 2013) at a time interval spanning from 2763 to 2573 Ma.

The Águas Claras and Rio Fresco Formations are Archean sedimentary covers which overlie unconformably the Itacaiúnas Supergroup and the Rio Novo Group, respectively, the latter hosting the epigenetic Au-PGE Serra Pelada deposit (Nogueira *et al*. 1995, Grainger *et al*. 2008). The Águas Claras deposition age is uncertain, ranging from 2.70 to 2.65 Ga, according to U-Pb dating on zircon monocrysts from crosscutting mafic dikes (Dias *et al*. 1996), Mougeot *et al*. 1996, Trendall *et al*. 1998).

The Paleoproterozoic is essentially represented by a number of granitic intrusions that crosscut the basement and the metavolcano-sedimentary sequences with ages varying from 1883±2 to 1874±2 Ma (Machado *et al*. 1991, Rämö *et al*. 2002, Dall'Agnol *et al*. 2005). They are metaluminous to peraluminous A-type granites that have been assembled in the Serra dos Carajás Intrusive Suite (Dall'Agnol *et al*. 2005) including the Serra dos Carajás, Cigano, Pojuca, Rio Branco and Breves intrusions. The Breves granite hosts a Cu±Au± (Mo, W- Sn) hydrothermal deposit whose complex evolution involved the interaction of magmatic and meteoric fluids with pre-existing oxidized rocks (Botelho *et al*. 2005).

Detrital zircon crystals with U-Pb ages up to 3.20 Ga (Galarza and Macambira 2002, Dall'Agnol *et al*. 2005) are thought to be vestiges of a Paleoarchean crust in the CD. Accretional and collisional processes involving consolidated crustal segments between 3.08-2.93 and 2.87-2.83 Ga are related to the agglutination of the basement assemblage (Feio *et al*. 2013). A new tectonic activity took place in the Carajás Domain from 2.76 to 2.70 Ga and

was marked by both the deposition of the volcano-sedimentary sequences of the Itacaiúnas Supergroup and mafic/ultramafic and granitic plutonism. The Carajás basin has its origin attributed to an intracontinental rift (Gibbs *et al*. 1986, DOCEGEO 1988, Macambira 2003, Tallarico *et al*. 2005) or to a magmatic arc (Meirelles and Dardenne 1991, Teixeira 1994, Lindenmayer *et al*. 2005, Lobato *et al*. 2005). The most remarkable CD structures are considered coeval with the 2.76-2.71 Ga type-A granite intrusions (Barros *et al*. 2009), a hypothesis also shared by Feio *et al*. (2013) and Dall'Agnol *et al*. (2013). These structures have resulted from a NE-SE crustal shortening, being related to strike-slip and oblique shear zones present in the Itacaiúnas Group rocks and evidenced by an E-W sub-vertical foliation in the basement units. Reactivation occurred at least three times from the Archean to the Paleoproterozoic (Costa *et al*. 1995, Araújo *et al*. 1988, Pinheiro and Holdsworth 2000).

MATERIALS AND METHODS

Core samples from nine drill holes (FD-58, FD-96, FD-107, FD-155, FD-209, FD-224, FD-266, FD-325 and DH-00003) in various locations within the Cristalino deposit area were used in the present investigation. Fluid inclusions analyses were carried out in laboratories housed at the Geosciences Institute of the Federal University of Pará (IG-UFPA). Over 20 doubly polished 100-200 μm-thick thin sections from mineralized samples were prepared for petrographical examination under transmitted light, using a Zeiss Axioplan 40 microscope. Fluid inclusion description and documentation followed the procedures recommended by Shepherd *et al*. (1985), van den Kerkhof and Hein (2001), Wilkinson (2001) and Samson *et al*. (2003), among others. Microthermometric runs were done in a Linkam THSMG600 heating-freezing stage capable of attaining temperatures from -180° to +650ºC. The stage was periodically calibrated using the triple point for pure CO_2 (-56.6ºC) and H_2O (0.0 ºC). Fluid composition were estimated from eutectic temperatures experimentally obtained in simple chemical systems by Borisenko (1977, 1982), Davis *et al*. (1990) and Spencer *et al*. (1990).

For stable isotopic analyses, pure mineral fractions were handpicked with aid of binocular loupe from the groundmass of volcanic rocks and from mineralized veins and breccias. The mineral fractions consisted of silicates (12), oxides (5), carbonates (10), and sulfides (10). Analyses in actinolite, tourmaline and chlorite (oxygen and hydrogen), epidote (oxygen), magnetite (oxygen), chalcopyrite and pyrite (sulfur) were performed in the Queen's Facilities for Isotope Research, Department of Geological Sciences, Queen's University,

Canada. Oxygen in silicates was extracted from samples heated at 550-600°C according to the method recommended by Clayton and Mayeda (1965) and its isotopic composition determined in a Thermo-Finnigan Delta^{Plus} XP isotope-ratio mass spectrometer (IRMS). For hydrogen analyses in silicates, the samples were degassed at 100°C in silver capsules for one hour, then loaded in a zero-black auto-sampler. The isotopic composition was measured using a Thermo-Finnigan thermo-combustion elemental analyzer (TC/EA) coupled with a Thermo-Finnigan Delta^{Plus} continuous flow isotope-ratio mass spectrometer (CF-IRMS). $\delta^{18}O$ and δD values are presented relative to the V-SMOW (Vienna Standard Mean Ocean Water) with precision of 0.1‰.

The isotopic composition of sulfur was obtained using a MAT 253 stable isotope ratio mass spectrometer coupled with a Costech ECS 4010 elemental analyzer. $\delta^{34}S$ values are noted relative to the V-CDT (Vienna Canyon Diablo Troilite) standard and reproductible to 0.2 ‰.

Additionally, isotopic ratios of carbon and oxygen were determined in ten fractions of pure calcite. After reaction with H_3PO_4 @ 100% at 25°C for 12 hours and evaporated, the samples were analyzed in a Finnigan Delta-E at the Stable Isotope Laboratory (LABISE) of the Geology Department of the Federal University of Pernambuco. $\delta^{13}C$ values are given relative to the V-PDB (Vienna Pee Dee Belemnite) standard.

GEOLOGY OF THE CRISTALINO DEPOSIT

Lithostratigraphy

The following lithostratigraphic units have been recognized in the Cristalino deposit area (Fig. 2): Cruzadão granite, Grão Pará Group, the Serra do Rabo granite and mafic dikes (Huhn *et al.* 1999b, Soares *et al.* 2001, Ribeiro *et al.* 2009, Tavares 2015, Craveiro *et al.* submitted a). Figure 2 depicts the geological map and an N60ºE geological section with ore projections.

The Cruzadão granite (2831± 6 Ma, 2848 ± 5 Ma, U-Pb in zircon, Moreto *et al.* 2011) represents the basement and is dominantly composed of monzogranitic rocks. It does not outcrop in the area but has been intercepted at depth by drill holes where it shows sharp contact with the Parauapebas Formation (lower volcanic rocks of the Grão Pará Group) and the Serra do Rabo granite. The Parauapebas Formation consists of basaltic and rhyolitic volcanic rocks. According to Craveiro *et al.* (submitted a), the mafic varieties display aphanitic to vesicular texture and amphibole, magnetite, allanite, and chlorite as the main

constituents. The felsic varieties are less abundant and have been altered to tourmaline, amphibole, K-feldspar, and chlorite-epidote-calcite.

Intrusive into the Parauapebas Formation rocks, the Serra do Rabo pluton is a sub-alkaline granite that occurs in the NE portion of the area dated at 2743 ± 1.6 Ma (Sardinha *et al.* 2006). NNW-SSE-trending gabbro dikes, probably related to the Neoproterozoic Rio da Onça Gabbro (Tavares 2015), crosscut both volcanic rocks of the Grão Pará Group and the Serra do Rabo granite.

The volcanic rocks show different degrees of alteration and are transected by mm- to cm-thick shear zones and veins with variable compositions. Some rocks are mildly to strongly deformed and developed locally proto-mylonitic fabric. The Cu-Au mineralization is hosted mostly by the Parauapebas Formation and, to lesser extent, by banded iron formations (Carajás Formation).

Hydrothermal Alteration and mineralization

The volcanic rocks of Parauapebas Formation were strongly affected by hydrothermal alteration, especially along lithological contacts and NW-SE second order shear zones. The alteration processes evolved under ductile-brittle to dominantly brittle regime. Earlier products are mainly observed in the rock groundmass in which they partially replaced igneous minerals, whereas later products tend to occur in dilatant structures and corresponding halos, overprinting previously altered zones.

Initially, the rocks experienced a distal sodic alteration characterized by chessboard albite (Fig. 3A, 3G), tourmaline (Fig. 3B), allanite and minor quartz, monazite and calcite that substituted preferentially for primary felsic minerals preserving much of the original texture. Though related to the sodic alteration, scapolite is only recorded in the Cruzadão granite. More pervasive, the ensuing calcic-ferric alteration produced actinolite, magnetite and allanite (Fig. 3C, 3H) in addition to minor apatite (Fig. 3J), epidote and rare uraninite, chiefly in the mafic volcanic rock as a textural destructive process.

The end of the Ca-Fe alteration coincided with the change of the deformational regime from ductile-brittle to essentially brittle, when the potassium alteration enters the scene. Biotite was produced in small amounts associated with minor magnetite (Fig.3I) and soon dominated by K-feldspar together with subordinate quartz (Fig. 3D, 3J), titanite, allanite, hematite and calcite. The KF-rich assemblages occur mainly in veins and breccia-bodies (Fig.3F) whose cm-thick halos overprinted zones previously affected by sodic and calcic-ferric alterations.
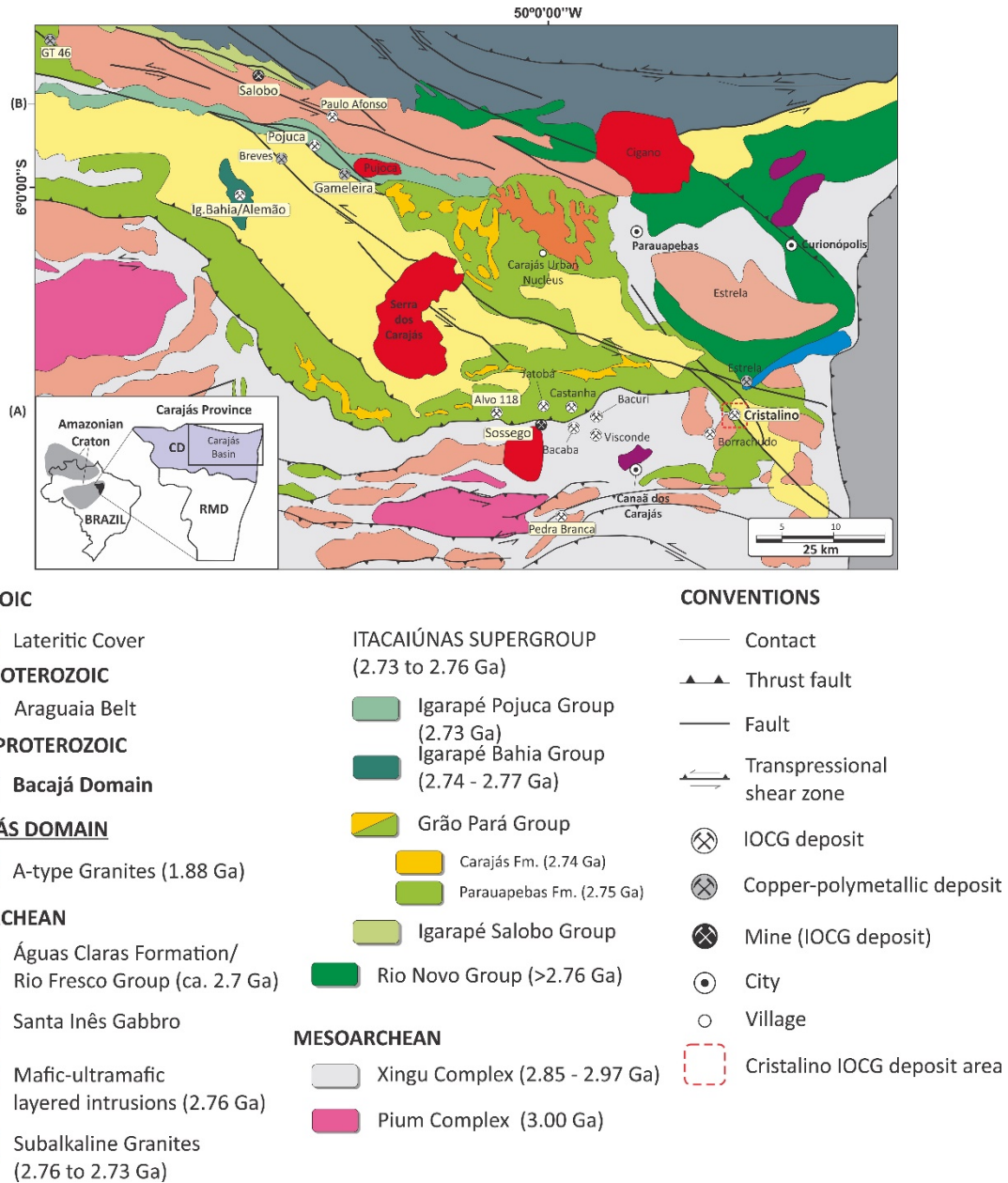
Figure 1. (A) Tectonic compartmentation of the Amazonian Craton (Santos et al. 2000); (B) Main tectono-stratigraphic units of the Carajás Domain (compiled and modified from Vasquez *et al*. 2008, Xavier *et al*. 2012, Dall'Agnol *et al*. 2013, Feio *et al*. 2013, Tavares 2015).
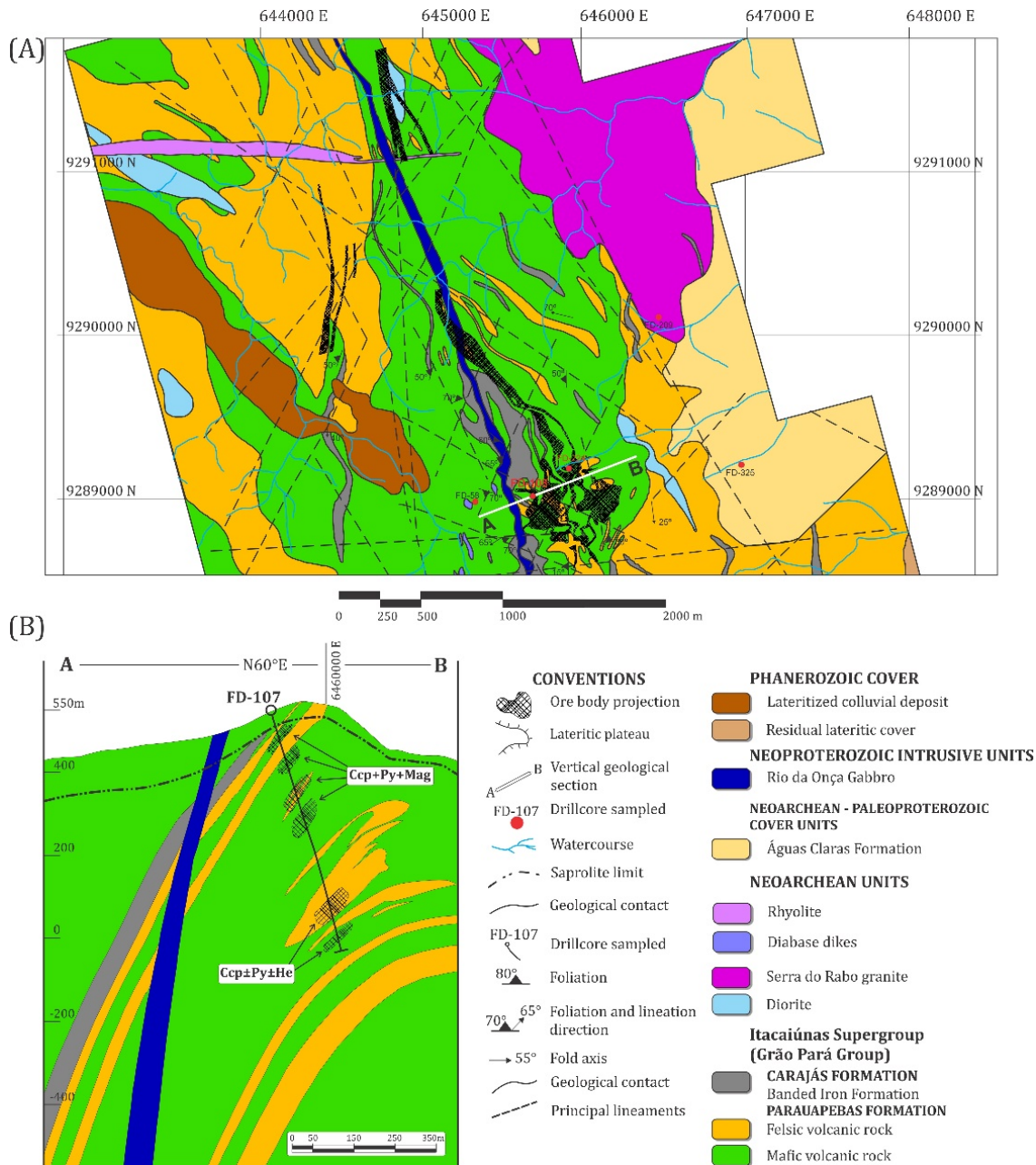
Figure 2. Geology of Cristalino deposit: (A) Geological map (1:5.000 scale), modified from Soares *et al.* (2001) and Vale (2003); (**B**) Geological section modified from vale 2003.

Tourmaline is chiefly observed in felsic volcanic rocks and seems to have been formed early during the sodic alteration (Fig.3B), and later as tourmaline-bearing veins and aggregates, in zones formerly altered by hydrothermal K-feldspar.

Propylitization/carbonation followed the potassic alteration and accounted for the generation of chlorite-epidote-calcite (Fig. 3F) with minor quartz, allanite and hematite. In veins and in the groundmass, this alteration affects all previous alteration phases in the volcanic rocks and portions of the BIF (Fig. 3K) near lithological contacts. Though it is best developed in mafic volcanic rock (Fig. 3E, 3L).

In the final stages of the Cristalino hydrothermal system, K-feldspar-rich and calcite-rich veins were formed, both with variable proportions of quartz, allanite, chalcopyrite, hematite, chlorite and epidote. The KF-rich veins show generally straight walls with cm-thick halos and represent a second phase of the potassic alteration. The multi-directional calcite-rich veins (Fig. 3E) are related to late phases of the propylitic when the system became chemically dominated by carbonates, and then characterized carbonation. Many breccias were formed by the interlocking of this array of veins (Fig. 3F), cemented different generations of minerals, chiefly composed by K-feldspar, and calcite, chlorite, epidote, hematite and musketovite (magnetite after hematite, Fig. 3F).
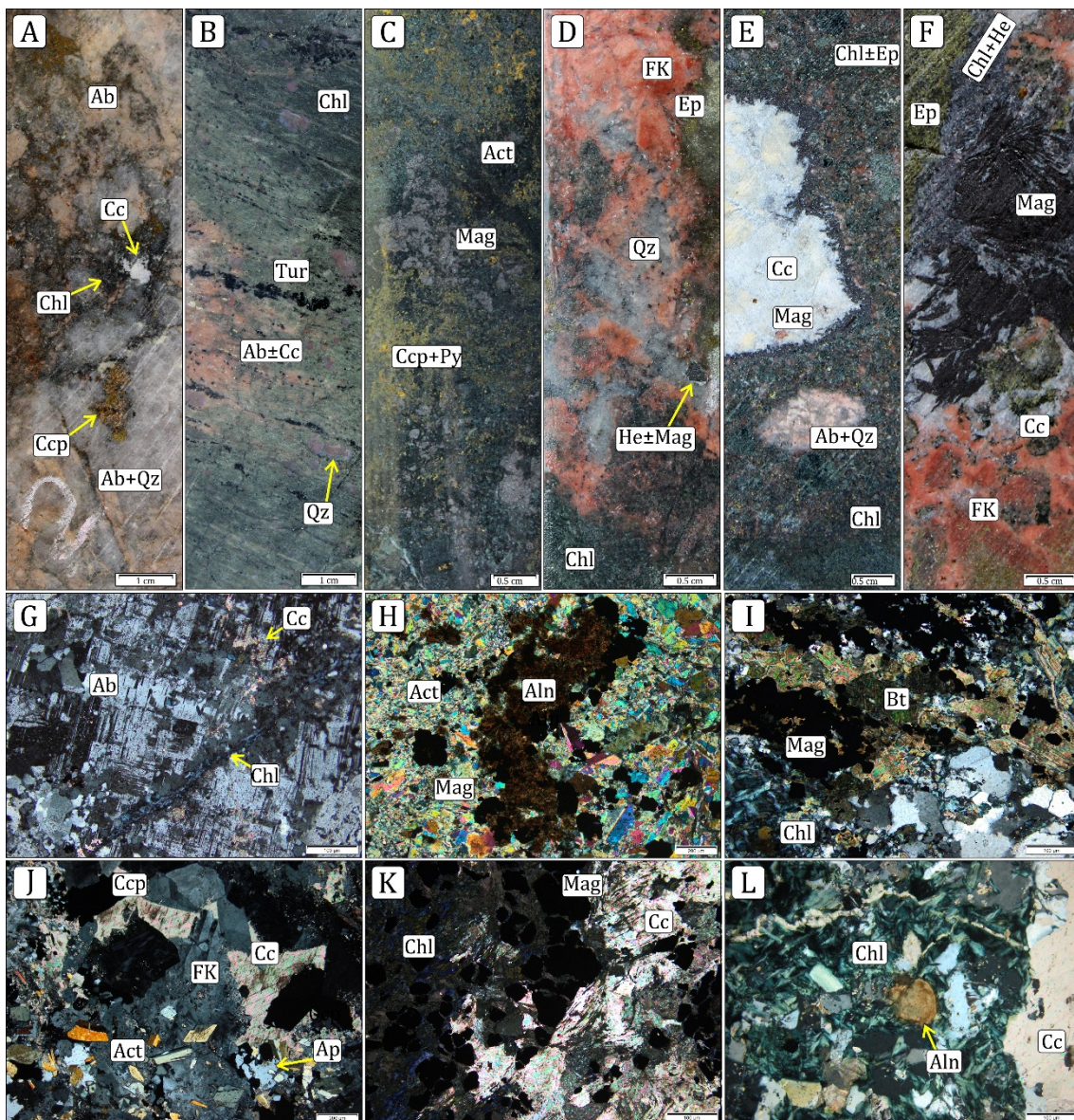
Figure 3. Principal alteration products of the Cristalino deposit, depicted in photographs (A-F) and photomicrographs in crossed polarized light (G to L). (**A**) Felsic volcanic rock affected pinkish albite as product of sodic alteration. Calcite, chlorite and chalcopyrite in veinlets, as late alteration products from propylitization. (**B**) Tourmaline crystals defining mineral lineation along blue quartz, in felsic

volcanic rock affected respectively by sodic and propylitic alteration; (**C**) Mafic volcanic rock altered by pervasive calcic-ferric alteration with actinolite, magnetite, chalcopyrite and pyrite; (**D**) Reddish K-feldspar and quartz as potassic alteration product in felsic volcanic rock. Zone partially disrupted by chlorite and epidote; (**E**) Prevalent propylitic alteration with chlorite and minor epidote over mafic volcanic rock with altered amygdaloidal cavities. In the middle, a calcite-bearing vein with thin layer magnetite in the walls; (**F**) Breccia in severely altered felsic volcanic rock, cemented by K-feldspar, calcite, epidote, hematite and magnetite (magnetite after hematite); (**G**) Chessboard albite associated with minor calcite in felsic volcanic rock, and a veinlet of chlorite; (**H**) Actinolite, allanite and magnetite as products of the calcic-ferric alteration, which replaced zones of mafic volcanic rock; (**I**) Biotite and magnetite association related to potassic alteration grown in felsic volcanic rock; (**J**) K-feldspar, and minor calcite and chalcopyrite, from potassic alteration affecting felsic volcanic rock previously altered by actinolite and minor apatite, from calcic-ferric alteration. (**K**) Chlorite and calcite as propylitic alteration minerals in BIF, near contact with volcanic rocks; (**L**) Chlorite and calcite-rich veins and veinlets as major alteration mineral in mafic volcanic rock previously affected by Ca-Fe alteration. Abbreviations: Ab: albite; Act: actinolite; Aln: allanite; Ap: apatite; Bt: biotite; Cc: calcite; Ccp: chalcopyrite; Chl: chlorite; Ep: epidote; FK: K-feldspar; He: hematite, Mag: magnetite; Qz: quartz; Py: pyrite.

The Cristalino deposit comprises a major ~N15°W-trending ore body, hosted in the bimodal volcanic rocks of Parauapebas Formation and subordinately in banded iron formation (BIF) of the Grão Pará Group (Carajás Formation). According to its modes of occurrence, the following types of ore can be recognized: (1) disseminations; (2) breccias; and (3) sulfide-rich veins.

Disseminations of chalcopyrite and pyrite coexisting with magnetite (up to 50%) and minor allanite and uraninite occur chiefly in mafic volcanic rocks (Fig. 3C). As the alteration progressed towards the end of the Ca-Fe stage, chalcopyrite behaved as a substitutive mass (Fig. 4A, 4E, 4F) over the alteration minerals. Other sulfides, like galena and millerite (Fig. 4H) also occur as minor phases.

In felsic volcanic rocks disseminations also occur but consist of chalcopyrite (Fig. 4G) with minor pyrite and hematite. When present, the scarce magnetite is usually partially replaced by hematite (Fig. 4J). The chalcopyrite-pyrite-magnetite-Au association (Fig. 3C, 4A) is coeval with the calcic-ferric alteration, whereas the chalcopyrite-Au±pyrite±hematite ore association (Fig. 4B, 4G) is related mainly to the potassic and propylitic alterations.

Highly mineralized zones are represented by substitution and infill bodies, which could be distinguished in: (**1**) chalcopyrite-pyrite-magnetite-Au breccia-like bodies, with minor galena, millerite and Au (Fig.4A, 4E, 4F), in which sulfides behave as substitutive mass mainly over the mafic volcanic rocks previously affected by calcic-ferric alteration; and (**2**) chalcopyrite±pyrite±hematite breccias, with minor native Au (Fig. 4B), in which chalcopyrite occurs as breccia matrix cementing clasts, generally in zones previously affected by potassic alteration and propylitization/carbonation.

Calcite-chalcopyrite- and chalcopyrite-bearing veins (Fig. 4D) and veinlets (Fig. 4I) are often related to chalcopyrite±hematite breccia bodies and crosscut the volcanic rocks in multiple directions, varying in composition and proportion of sulfides. The most common assemblages are chalcopyrite-hematite-K-feldspar and chalcopyrite-calcite (Fig. 4C) containing minor amounts of pyrite, hematite and musketovite. A representation of the hydrothermal mineral paragenesis is shown in the figure 5.

RESULTS

Fluid Inclusion Petrography

Fluid Inclusions (FI) have been described in the rock groundmass, veins and breccias. In the groundmass they are scarce and only a few aqueous FI could be identified in quartz crystals associated with early tourmaline in felsic volcanic rock. In contrast, FI are plenty in quartz and calcite crystals from mineralized veins and breccias that occur in mafic and felsic volcanic rocks.

All observed FI are aqueous in nature, except for the single-phase ones, which are carbonic. In the groundmass, they are two-phase inclusions (L+G) and occur as isolated cavities showing ~5 μm in diameter, rounded to irregular shapes and estimated degree of fill (F) between 0.7 and 0.9. It was not possible to distinguish safely whether the host quartz is igneous or hydrothermal.

Within quartz and calcite crystals from mineralized veins and breccias, three types of FI have been identified: (1) gaseous single-phase (G); (2) two-phase (L+G); and (3) three-phase (L+S+G). Rare multi-phase (S1+S2+L+G) FI were additionally described, but only in quartz.

The gaseous single-phase FI (Fig. 6F) occur along inter-granular trails and as isolated cavities, mostly found in calcite crystals. They are dark and show in general elongated shapes and diameter ranging from 2 to 5 μm.
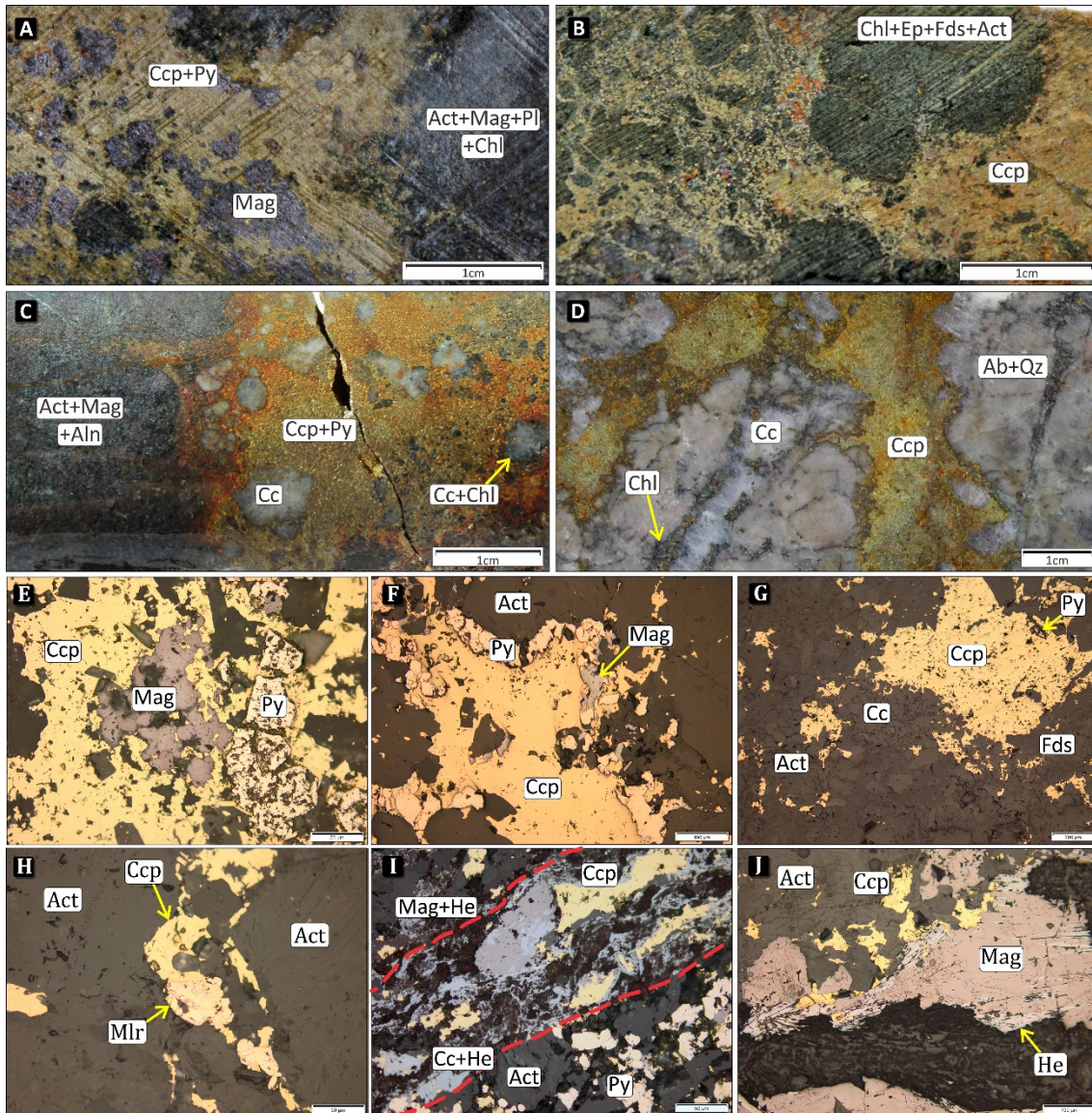
Figure 4. Main features of the Cristalino deposit ore. Photographs of drill-hole samples (A to D), photomicrographs under reflected light (E to J). (A) Chalcopyrite-pyrite-magnetite breccia-like body in Ca-Fe altered mafic volcanic rock. (B) Chalcopyrite±hematite±pyrite breccia and veinlets, in felsic volcanic rock harshly altered to chlorite, epidote, K-feldspar and actinolite. (C) Chalcopyrite-calcite breccia developed in a Ca-Fe altered mafic volcanic rock. (D) Chalcopyrite- and calcite-rich veins crosscutting a Na-altered felsic volcanic rock. (E) Magnetite and pyrite replaced by chalcopyrite in a chalcopyrite-magnetite breccia hosted by a mafic volcanic rock. (F) In late stages of Ca-Fe alteration in volcanic rocks, chalcopyrite as substitution mass over pyrite, magnetite and actinolite in breccia-like body; (G) A magnetite-free, chalcopyrite-rich dissemination in Ca-Fe and K-altered felsic volcanic rock (same sample depicted in Fig. 3J); (**H**) Millerite associated with disseminated chalcopyrite in Ca-Fe altered volcanic rock; (I) A calcite-chalcopyrite-hematite±magnetite veinlet, outlined by dashed red lines, in a felsic volcanic rock. Magnetite crystals are partially martitized; (J) Magnetite crystal being altered by hematite in mafic volcanic rock affected by propylitization. Ab: albite, Act: actinolite, Cc: calcite, Ccp: chalcopyrite, Chl: chlorite, Fds: K-feldspar, He: hematite; Mag: magnetite; Py: pyrite; Qz: quartz.
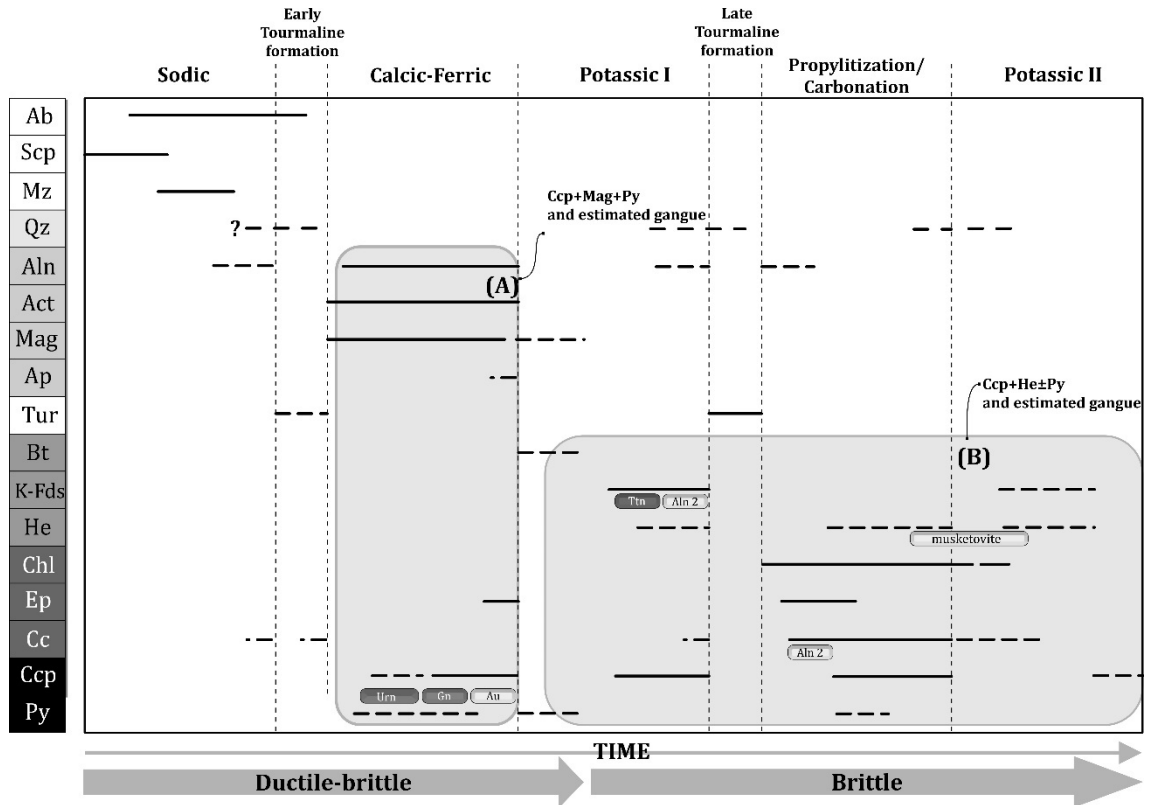
Figure 5. Paragenetic sequence of the Cristalino hydrothermal system. Ab: albite, Act: actinolite, Aln: allanite; Ap: apatite, Bt: biotite, Cc: calcite, Chl: chlorite, Ccp: chalcopyrite, Ep: epidote, He: hematite, Gn: galena, K-fds: K-feldspar, Mag: magnetite, Mz: monazite, Py: pyrite, Qz: quartz, Scp: scapolite, Urn: uraninite, Ttn: titanite.

The two-phase FI are found on cleavage planes of calcite and along intra-granular and trans-granular trails. Along intra-granular trails, the FI display rounded to occasional negative crystal shapes, 5 to 20 μm in diameter and estimated F between 0.8 and 0.9. They coexist with three-phase FI in quartz and calcite (Fig. 6A, 6B, 6E). Along trans-granular trails and on cleavage planes of calcite crystals, the FI show regular to elongated and occasional negative crystal shapes, diameter of ~5 μm, F between 0.7 and 0.9 and wobble bubble at room temperature (Fig. 6E, 7I).

The three-phase FI hosted by quartz (Fig. 6A, 6B and 6C) exhibit rounded to regular shapes and subordinate negative crystal forms. Dimensions vary from 5 to 20 μm and F estimated between 0.8 and 0.9. The solids are cubic with edge up to 4 μm. These FI occur as isolated cavities or along short intra-granular trails. In calcite crystals, rare three-phase FI (Fig. 6G. 7H) present variable F, shapes (cubic and parallelepiped) and dimensions (5 to 15 μm) (Fig. 6G, 6H). The multi-phase FI have irregular shapes and diameters around 10 μm. The solids are cubic (opaque and translucent) and correspond to more than 50% of the cavity volume (Fig. 6D).
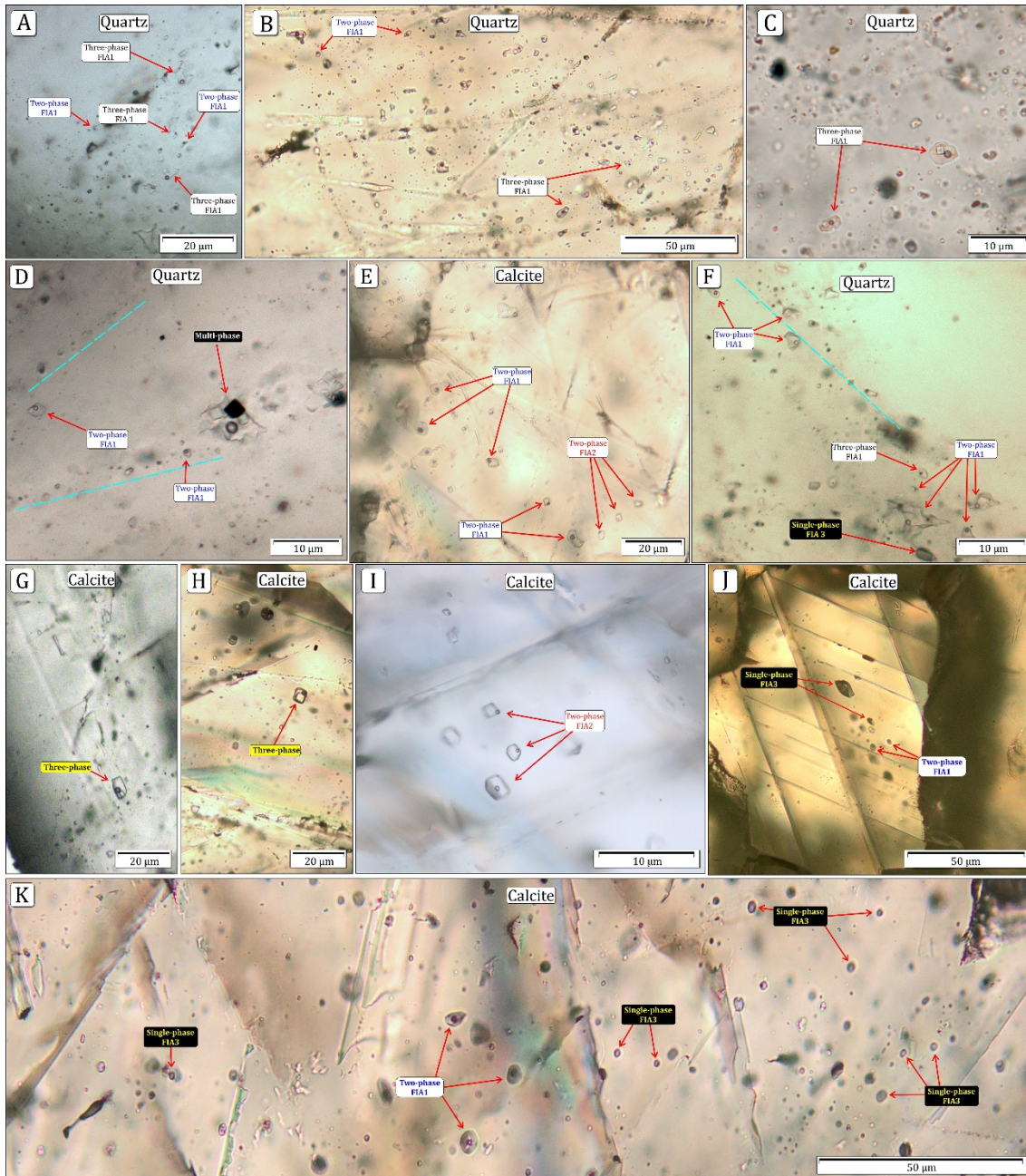
Figure 6. Photomicrographs recording, at room temperature and in plane polarized light (PPL), the principal types of fluid inclusions (FI) hosted in quartz and calcite crystals from the breccias and veins containing the chalcopyrite±Au±pyrite±hematite ore association of the Cristalino deposit. (A) Inclusions belonging to FIA1 in a quartz crystal. (B) Growth zones of a quartz crystal where inclusions of FIA1 were trapped. (C) Along an intra-granular trail in a quartz crystal, three-phase FI of FIA1 presenting similar volumetric ratios among solid (halite?), vapor and liquid phases. (D) In a quartz crystal host, a rare multi-phase FI showing irregular shape and cubic opaque (magnetite? pyrite?) and translucent (halite?) solids together with two-phase FI of FIA1 and FIA2. (E) Two-phase inclusions of FIA1 with diameter of ~10 μm and slightly darker bubbles that differ from two-phase inclusions of FIA2 with ~5 μm in diameter and clear wobble bubble trapped in a calcite crystal. (F) In a quartz crystal, short intra-granular trails containing two-phase inclusions of FIA1. More commonly trapped in calcite crystals, single-phase inclusions (FIA 3) were also found in quartz. (G and F) Rare three-phase inclusions present in calcite crystals. Observe that they differ in dimensions, shape of solid and phase volumetric ratios. (I) Typical two-phase inclusions of FIA2 trapped in a calcite crystal, presenting high volumetric phase ratios (> 0.90) and clear bubbles; (J) Single-phase inclusion, from

FIA3 as negative crystal in calcite from mineralized vein; (K) Growth zones in calcite crystal in mineralized breccia, with inclusions of FIA1 (two-phase) and FIA3 (single-phase).

Taking into account the concept of fluid inclusion assemblages (Goldstein and Reynolds 1994), the documented fluid inclusions of the Cristalino deposit may be grouped as (FIA1) - the coexisting two- and three-phase FI hosted by quartz and calcite crystals (Fig. 6B) from mineralized veins and breccias -, (FIA2) - the isolated two-phase FI present along trans-granular trails (Fig. 6E, 6I), and (FIA3) - the gaseous single-phase FI trapped in quartz (Fig. 6F) and calcite (Fig. 6J, 6K) crystals of breccias and veins. The variable shapes and degree of fill observed in the scarce FI hosted by quartz from the groundmass may indicate they have undergone physical changes after trapping, what made them inappropriate to be adequately studied.

The coexistence of saturated aqueous and gaseous carbonic inclusions may be indicative of fluid immiscibility (Roedder and Bodnar 1980, Ramboz *et al.* 1982, Hurai *et al.* 2015), although the occurrence of aqueous-carbonic inclusions was to be expected. It is possible, however, that they do occur but with an imperceptible thin film of water surrounding a large gas bubble, preventing them from being recognized. In addition to the ex-solution of two distinct fluids (aqueous saline and carbonic), immiscibility may have provided conditions for heterogeneous fluid entrapment.

Microthermometric data

Freezing runs

The microthermometric data indicated eutectic temperatures ranging from -55.9 to -18.4º C which, according to Borisenko (1977, 1982), Davis *et al.* (1990) and Spencer *et al.* (1990), may correspond to the following chemical systems: H_2O-NaCl-$CaCl_2$ (-51.6°C) and H_2O-NaCl-$FeCl_2$ (-37.0°C), recognized in FIA1, and H_2O-NaCl-KCl (-23.1, -22.9 °C) and H_2O-NaCl (-21.2°C), only recognized in FIA2. In quartz from the groundmass, eutectic temperatures ranged from -50 to -40°C, suggesting chemical systems similar to those of AIF1.

Ice-melting temperatures (T_{im}) obtained for two-phase FI covered the interval from -20.0º to -1.8º C and are distributed as follows: FIA1 (-20.0º to –5.0º C), FIA2 (-19.0º to – 1.8º C) and matrix quartz (-15.5º to – 14.0º C).

Once frozen, the gaseous single-phase inclusion of FIA3 confirmed a carbonic system with CO_2 melting temperature (T_{CO2m}) between -56.8 and -54.9° C, most close to that of pure CO_2 (-56.6°C, Diamond 2001). The depression of the CO_2 melting point may be accounted for minor amounts of CH_4 and/or N_2 in the gas phase. Values higher than -56.6º C are more difficult to explain and may result from solid solution with another component (CO?, SO_2?),

thermal gradients in the sample causing delaying melting, nature of phases present at the melting point, among other factors (see www.geology.wisc.edu/flincs/fi/disc/co2melt.html - discussion during January and February 1999).

Heating runs

Total homogenization of the two-phase FI in quartz from the rock groundmass occurred by the disappearance of the vapor bubble into the liquid state at temperatures of 320°-$155°C$. As only 10 measurements could be made in the scarce FI that were found, this large interval does not have much meaning and, therefore, the data were not even plotted in the histograms of figure 7.

For the FIA1 inclusions, T_{TH} range from 465° to $120°$ C and refer to about 120 measurements. Three-phase FI homogenized into the liquid state by dissolution of the daughter mineral (halite?) at the 465°-$214°C$ interval (Fig. 7B), along the vapor-unsaturated halite liquidus, taking as reference the H_2O-$NaCl$ system. Only two T_{TH} reached values above 460° C, while the other values spread from 338° to 214° C, noting that in three cases homogenization occurred at 338°, 336° and $328°C$ by the simultaneous disappearance of the vapor bubble and solid into the liquid state, i.e. $T_{hd} = T_{vd}$ (Fig. 7D). Just one three-phase FI homogenized into the liquid state by disappearance of the vapor bubble (245° C), after the dissolution of the solid (225° C).

The multi-phase FI trapped in quartz of FIA1 decrepitated at temperatures below ~600° C before homogenization, probably indicating leakage and/or necking-down.

Homogenization in two-phase inclusions of FIA1 and FIA2 occurred by vapor disappearance into the liquid state at temperature ranges of, respectively, $250°$-$120°$ C and 184°-124° C (Fig. 7B). Significantly, most T_{TH} in inclusions of FIA2 fall in the narrow interval of 180°-160° C.
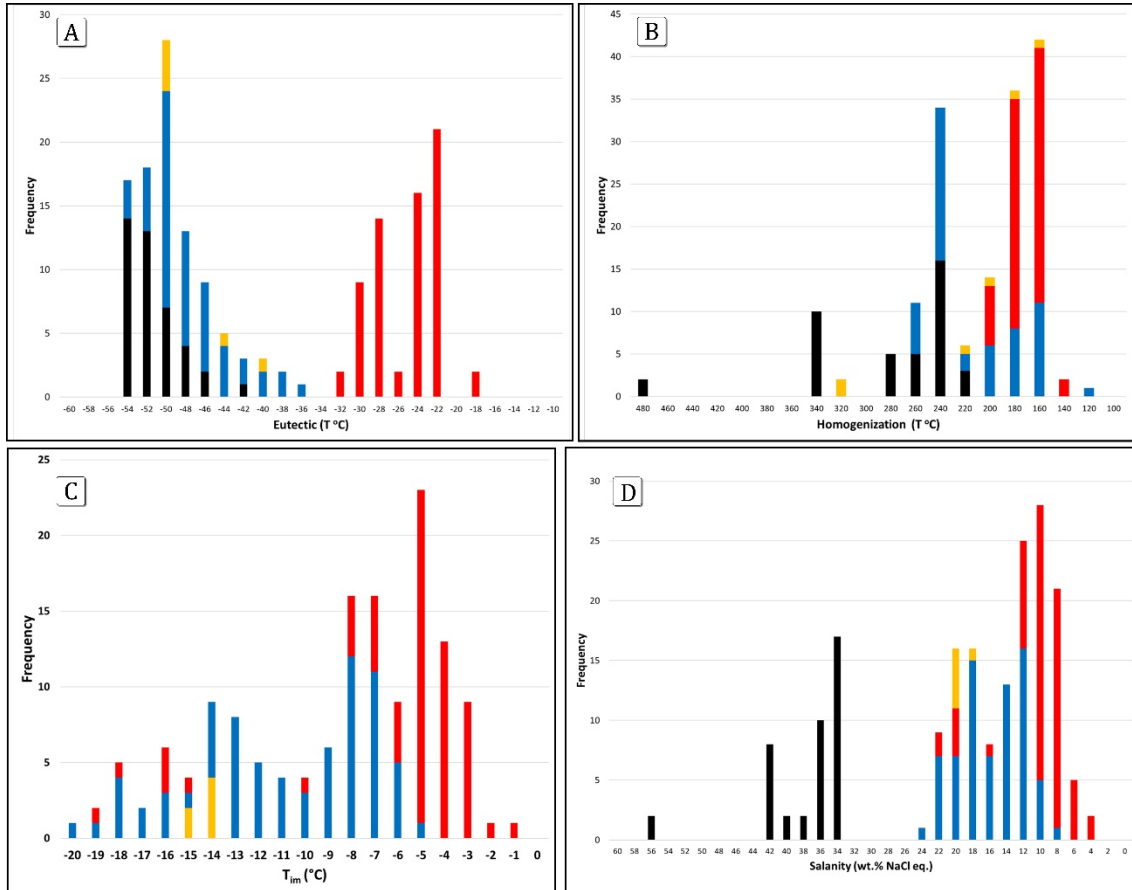
Figure 7. Histograms and binary plot summarizing fluid inclusion data of the Cristalino deposit. Black columns and dots: three-phase inclusions of FIA1; blue columns: two-phase inclusions of FIA1; and red columns: two-phase inclusions of FIA2; orange columns: two-phase inclusion in quartz from groundmass. (A) Histogram of eutectic temperatures. (B) Histogram of total homogenization temperatures. (C) Histogram of ice melting temperatures for two-phase inclusions. (D) Histogram of salinities.

Salinity

Salinity data, expressed in weight percent of NaCl equivalent (% wt. NaCl equiv.) are shown in Figure 7C. Values for three-phase FI were obtained based on the temperature of the halite dissolution (T_{hd}), using the equations of Sterner *et al*. (1988) for $T_{hd} \leq T_{vd}$ and Lecumberri-Sanchez *et al*. (2012) for $T_{hd} \leq T_{vd}$. For the two-phase FI, salinity was calculated from temperature of ice melting (T_{im}), using the equation proposed by Bodnar (1993).

Fluid salinity values spread from 55.1 to 3.0 wt. % NaCl equiv. The highest values (55.1 to 32.5 wt. % NaCl equiv.) refer to three-phase inclusions of FIA1, intermediate values (21.7 to 7.9 wt. % NaCl equiv.) to two-phase inclusions of FIA1 and the lowest values (21.6 to 3.1 wt. % NaCl equiv.) to inclusions of FIA2. For fluid trapped in quartz of the groundmass, the few measurements of the T_{im} indicate values around 17-18 % wt. NaCl equiv. Higher salinities were estimated in FI from FIA1, involving more complex salt-water

systems, while lower saline fluids (FIA2) show simpler composition with sodium and potassium as major cations (Fig. 8).
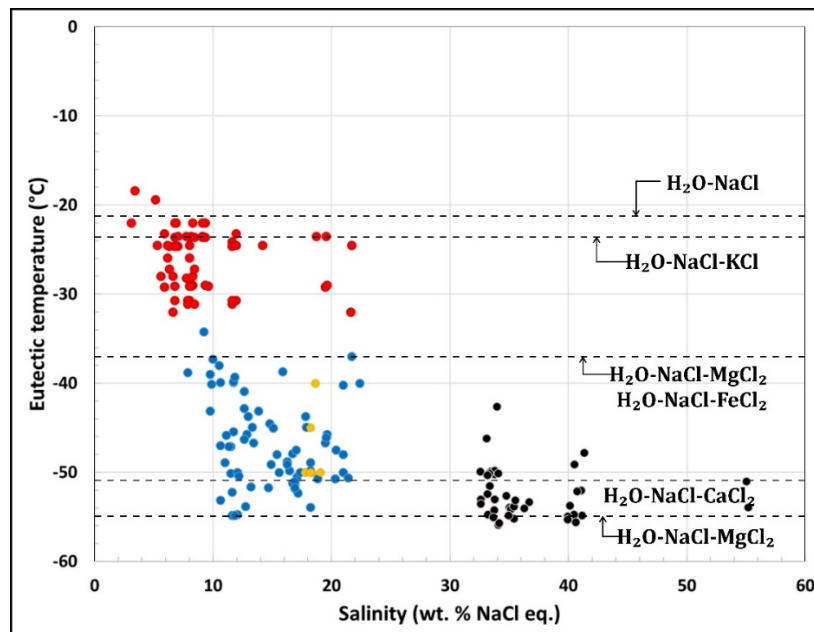
Figure 8. Diagram salinity versus eutectic temperature showing the most relevant salt-water systems which occur in the Cristalino deposit. Black dots: three-phase inclusion from FIA1; blue dots: two-phase inclusion from FIA1; red dots: two-phase inclusions from FIA2; orange dots: two-phase inclusions trapped in quartz from the groundmass.

Density

Fluid density was calculated using the equations of Bodnar (1983) and Bodnar and Vityk (1994) both having as reference the H_2O-NaCl system (Isoc from Fluids Package, Bakker 2003). Density values vary from 1.12 to 0.87 g/cm³. The three-phase inclusions of FIA1 contain the densest fluid (1.08 to 1.12 g/cm³, average of 1.10 g/cm³) with positive slope dP/dT between 17.05 and 19.03 °C/bar along the curve L + G + halite (Bodnar 1994). The fluid trapped in inclusions of FIA2 show density that varies from 0.90 to 1.08 g/cm³ (average of 0.98 g/cm³).

The densities found in two-phase FI in quartz crystals from the groundmass varied from 0.87 to 1.05 g/cm³. For reasons already discussed above, data on such inclusions will no longer be considered.

Attempts to measure the homogenization of the carbonic phase failed due to non-nucleation of the liquid phase below room temperature. As a result, densities of the carbonic fluid could not be calculated.

Table 1 summarizes fluid inclusion data obtained in minerals of the Cristalino deposit.

Table 1. Summary of microthermometric data of fluid inclusions of Cristalino deposit.

Type	Two-phase	Three-phase	Two-phase	Two-phase	Single-phase	Multi-phase
AIF	none	I		II	III	none
Size (μm)	~5	5 to 10	5 to 20	~5	2 - 5	10 to 20
f	0.7 to 0.9	0.8 to 0.9	08 to 0.9	0.7 to 0.9	-	~0.9
T_e (°C)	-50 to -40	-58 to -42	-55 to -34	-32 to -18	-	-50 to -40
$T_{m\ CO2}$ (°C)	-	-	-	-	-57 to -55	
$T_{m\ ice}$ (°C)	-15.5 to -14.0	-	-5.0 to -20	-19.9 to -1.80	No ice	
T_{Clath} (°C)	-	-	-	-	No clathrate	
T_{vd}	155 to 320	120 to 335	120 to 240	124 to 183	-	200 to 300
T_{TH} (°C)	155 to 320	213 to 465	120 to 240	124 to 183	-	-
$T_{halite\ diss.}$ (°C)	-	213 to 465	-	-	-	-
Homogenization mode	vapor disappearance	Halite melting and vapor disappearance.	vapor disappearance	Vapor disappearance		
Salinity (wt.% NaCl eq.)	19.0 to 17.8	55.1 to 32.3	21.7 to 7.9	21.6 to 3.1	-	-
Density (g/cm³)	0.87 to 1.05	1.08 to 1.12	1.08 to 0.90	1.08 to 0.92	-	-

Stable Isotopes

Oxygen, hydrogen, carbon and sulfur stable isotope compositions from selected silicates, oxides, carbonates and sulfides helped constraining the diverse hydrothermal alteration stages in the Cristalino deposit, besides providing insights into potential sources of the hypersaline hydrothermal fluid and its components.

Oxygen isotopes

Oxygen isotopic data of minerals from different alteration zones of the Cristalino deposit are shown in Table 2. In quartz associated with tourmaline from the sodic alteration, $\delta^{18}O_{V\text{-SMOW}}$ varies from +10.9 to +11.5 ‰, slightly higher than +9.8 ‰ measured in quartz associated with chlorite from the propylitized rocks and more than two-fold the values of +5.0 to +5.2 ‰ found for actinolite from the calcic-ferric zones, where it is associated with magnetite and chalcopyrite-pyrite-magnetite ore. In tourmaline associated with chessboard albite and quartz from the sodic alteration, $\delta^{18}O_{V\text{-SMOW}}$ falls between +7.7 and +9.2 ‰.

Values of $\delta^{18}O_{V\text{-SMOW}}$ for magnetite from the Ca-Fe alteration zone and for vein magnetite (musketovite) related to the propylitic assemblage are quite distinct. While in the former $\delta^{18}O_{V\text{-SMOW}}$ is close to zero (+0.8 ‰), in the latter it covers the interval of -3.7 to -5.5 ‰. Also distinct are the $\delta^{18}O_{V\text{-SMOW}}$ found in chlorites from veins (+1.1 ‰) and matrix (+5.6 ‰), both produced during the propylitic alteration. Epidote from a calcite-rich vein recorded +5.57 ‰, a value comparable to that of the matrix chlorite.

Calcite from mineralized veins, which crosscut mafic volcanic rocks, has slightly lower $\delta^{18}O_{V\text{-SMOW}}$ values (+8.8 to +10.2 ‰) compared to calcite from mineralized breccias

(+9.0 to +11.1 ‰), in felsic volcanic rocks. A late calcite vein, which crosscuts calcite-rich breccias, has a $\delta^{18}O$ V-SMOW = 16.4 ‰. Higher values (+21.7 to +25.3 ‰) were found in calcite from mm-thick veins that also contain chalcopyrite and crosscut BIF near the contact with volcanic rock.

Hydrogen isotopes

Hydrogen isotopic data (δD_{VSMOW}) for hydroxyl-bearing silicates (tourmaline, actinolite and epidote) vary from -69.2 to -43.2 ‰ (Table 2), but each mineral shows a distinct range, so that there is no overlap. The highest values are registered in tourmaline (-48.7 to -43.2 ‰) no matters the stage of its formation, whereas the lowest interval (-69.2 to -63.2 ‰) is measured in actinolite from the Ca-Fe alteration zones. In turn, chlorites from propylitic assemblage present intermediate values (-60.8 and -56.2 ‰).

Temperature Conditions

Mineral pairs in equilibrium were used to estimate the Cristalino thermal conditions based on oxygen isotope fractionation factors, according to equations proposed by Chiba *et al.* (1989), Zheng (1993) and Zheng *et al.* (1993) (Table 3).

The quartz-tourmaline pair, generated in felsic volcanic rocks during the sodic alteration yielded a temperature of 540°C, accounting for the early tourmaline formation, associated with sodic alteration. A slightly higher temperature (549°C) was calculated with the actinolite-magnetite pair present in an altered mafic volcanic rock, which hosts the chalcopyrite-pyrite-magnetite ore. This value is consistent with the average temperature of 540 °C estimated by the plagioclase-amphibole geothermometer and considered the temperature at which actinolite formed (Craveiro *et al.* submitted b).

The thermal conditions of the propylitic alteration were constrained by temperatures obtained with the quartz-chlorite (207° C), calcite-chlorite (251° C) and calcite-magnetite (246°, 377 ° and 407 ° C) pairs, drawing attention to the ~130° C gap between 377° and 251° C. These temperatures are in general agreement with those obtained by the chlorite geothermometer most of which estimated between 290° and 350°C (Craveiro *et al.* submitted b).

At 235 ± 24°C (interval based on the lower temperatures obtained with minerals pairs of the propylitic zone), the fluid presents $\delta^{18}O_{VSMOW}$ = +5.57‰ and δD_{VSMOW} = -22.24‰ (quartz-chlorite pair) and $\delta^{18}O_{VSMOW}$ = -0.28‰ and δD_{VSMOW} = -19.15‰ (calcite-chlorite pair).

Carbon and Sulfur Isotopes

$\delta^{13}C_{V-PDB}$ values for calcite from mineralized veins, veins crosscutting BIF and breccias hosted by Grão Pará Group rocks vary, respectively, from -6.3 to -4.2 ‰, from -6.4 to -5.9 ‰ and from -4.9 to -3.8 ‰ (Tab. 3). These values do not differ significantly, so much so that the variation between the highest and the lowest value does not exceed 2.6 ‰.

Isotopic Composition of the hydrothermal fluids

Temperatures calculated for each alteration stage were used to estimate the hydrogen and oxygen isotopic composition of the fluids (Table 3), using the fractionation factors and respective equations for actinolite-H_2O, epidote-H_2O, tourmaline-H_2O, chlorite-H_2O, magnetite-H_2O and quartz-H_2O (Wennner and Taylor 1971, Matsuhisa *et al.* 1979, Grahan *et al.* 1984, 1987, Zheng 1991, Zheng 1993).

The fluid in equilibrium with quartz and tourmaline from the sodic alteration, at 540ºC, presents $\delta^{18}O_{VSMOW}$ between +9.73 and +7.81 ‰, and δD_{VSMOW} between -35.91 and -30.17 ‰. Less enriched in ^{18}O ($\delta^{18}O_{VSMOW}$ = +8.01 to +6.48 ‰) and in D (δD_{VSMOW} = -40.25 to -34.18 ‰), the fluid at 549ºC equilibrated with actinolite and magnetite from the Ca-Fe alteration zones.

All S isotopic analyses refer to chalcopyrite (Tab. 4) and $\delta^{34}S_{V-CDT}$ values range from +1.6 to +3.5 ‰. Coexisting with magnetite from the Ca-Fe alteration zones, chalcopyrite presents relatively less uniform $\delta^{34}S_{V-CDT}$ values (+1.6 to +2.3 ‰) comparable to those determined in chalcopyrite from magnetite-poor breccias hosted by potassic and propylitic altered volcanic rocks (+2.0 and +2.2 ‰).

Table 2 – Oxygen and hydrogen isotope composition of the minerals of Cristalino deposit and calculated fluid composition.

Sample	Alteration stage	Mode of occurrence	Minerals	$\delta^{18}O_{min}$ (VSMOW) ‰	δD_{min} (VSMOW) ‰	T (°C)[a]	$\delta^{18}O_{H2O}$ (VSMOW) ‰[b]	δD_{H2O} (VSMOW) ‰[c]
23-155-I	Early Na alteration	Volcanic Felsic rock	Tur	9.2	-48	540.0	9.3	-35.4
23-155-II	Early Na alteration	Volcanic Felsic rock	Tur	--	-45	540.0	-	-31.5
44-58	Early Na alteration	Tourmaline vein	Tur	8.2	-49	540.0	8.3	-35.9
17-96	Early Na alteration	Tourmaline vein	Tur	7.7	-43	540.0	7.8	-30.2
23-155-I	Early Na alteration	Volcanic Felsic rock	Qz	11.1		540.0	9.4	
23-155-II	Early Na alteration	Volcanic Felsic rock	Qz	10.90		540.0	9.2	
23-155-III	Early Na alteration	Volcanic Felsic rock	Qz	11.3		540.0	9.6	
44-58	Early Na alteration	Tourmaline vein	Qz	11.5		540.0	9.7	
107-04-I	Ca-Fe alteration	Mafic volcanic rock	Act	6.2	-63.5	549.0	8.0	-34.5
04-107-II	Ca-Fe alteration	Mafic volcanic rock	Act	5.2	-63.2	549.0	7.0	-34.2
04-107-III	Ca-Fe alteration	Mafic volcanic rock	Act	5.0	-63.9	549.0	6.8	-35.0
DH03-17	Ca-Fe alteration	Ore I (Maf. Vol. Rck)	Act	5.8	-69.2	549.0	7.6	-40.2
DH03-17	Ca-Fe alteration	Ore I (Maf. Vol. Rck)	Mag	0.8		549.0	7.6	
14-155-I	Propylitic	Cc+Chl±He±Ccp Breccia (Ore II)	Mag	-3.7		393.0	4.2	
14-155-B	Propylitic	Cc+Chl±He±Ccp Breccia (Ore II)	Mag	-5.3		393.0	2.6	
14-155-II	Propylitic	Cc+Chl±He±Ccp Breccia (Ore II)	Mag	-5.5		234.6	3.1	
DH03-02	Propylitic	BIF	Mag	4.8		234.6	13.4	
12-96	Propylitic	Mafic volcanic rock	Chl	5.6	-61	234.6	4.3	-22.5
04-107	Propylitic	Cc-Chl vein	Chl	1.1	-58	234.6	-0.1	-19.2
DH03-02	Propylitic	Cc-Ep vein	Ep	5.6		234.6	2.9	

a = Temperature calculate from pairs of minerals in equilibrium, presented in table 3;
b = oxygen isotopes fractionation: Matsuhisa et al. (1979) for quartz; Zheng (1991) for magnetite; Zheng (1993) for actinolite, tourmaline and epidote; Wenner and Taylor (1971) for chlorite;
c = hydrogen isotopes fractionation: Graham et al. (1984) for actinolite and chlorite; Kotzer et al. (1993) for tourmaline
Abbreviations: Act: actinolite; Chl: chlorite; Ep: epidote; Mag: magnetite; Qz: quartz; Tur: tourmaline

Vein chalcopyrite reveals quite distinct values: +1.58 to +1.63 ‰ in a vein that crosscuts mafic volcanic rock and +3.2 to +3.5 ‰ in a calcite-bearing vein that transects a felsic volcanic rock. Highly impoverished in heavy sulfur, is the chalcopyrite from a mm-thick vein that crosscuts a BIF layer, with $\delta^{34}S_{VCDT}$ = -32.6 ‰.

DISCUSSION

Stable isotope (O, H, C, and S) and fluid inclusion data can be used to place a number of constraints on the source of mineralizing fluids and estimate the conditions of ore formation (Ohmoto and Rye 1979, Roedder 1984, Shepherd *et al*. 1985, O`Neil 1986, Kerrich 1987, Ohmoto and Goldhaber 1979, Samson *et al*. 2003).

Table 3 – Calculated isotope temperatures from the oxygen isotope composition from mineral-pair in equilibrium using fractionation factors, and comparison with estimated temperature from independent geothermometers.

Alteration stage		Oxygen isotopes[a]	Mineral chemistry
Na alteration		540°C (Qz-Tur pair)	
Ca-Fe alteration and Ore I (Ccp+Py+Mag)		549°C (Act-Mag pair) ~400°C	645.4 to 401,5°C, 532.2°C average (Plag-Amp geothermometer of Holland and Blundy 1994)
Propylitic alteration and Ore II (Ccp±Py±He)	Mineralized breccia	409°C (Cc-Mag/Msk pair) 377°C (Cc-Mag/Msk pair) Mean = 393°C	353.2 to 217.4°C, 299.9°C average (Chlorite geothermometer of Cathelineau and Nieva 1985)
	Mineralized veins	246°C (Cc-Mag/Msk pair) 251°C (Cc-Chl pair) 207°C (Qz-Chl pair) Mean = 234.6°C	

[a] *Oxygen isotopes fractionation: Chiba et al. (1989), Zheng (1993) and Kotzer et al. (1993)*

P-T conditions of ore-forming fluid

The hydrothermal alteration of the host rocks of the Cristalino deposit took place between ~550°C and ~230°C, from the early sodic and calcic-ferric stages to the late propylitization and carbonation. The higher temperature, obtained by isotopic fractionation using actinolite-magnetite and quartz-tourmaline mineral pairs, is corroborated by the value of 532.2° C ± 55°C determined for actinolite formation with the amphibole-plagioclase geothermometer (Craveiro *et al.* submitted b). At this temperature, partial to complete replacement of the wall rock by calcic-ferric altered zones should have required high fluid/rock ratio and/or a long-lived hydrothermal system (Hedenquist and Lowenstern 1994, Pirajno 2009) in which a reactive, metalliferous fluid interacted with the wall rocks to radically change the original composition of mafic volcanic rocks. In these zones, calcic-ferric

infill assemblages have not been observed, implying that alteration occurred in a structural environment dominated by elevated confining pressures. It is not by chance that the associated chalcopyrite-pyrite-magnetite mineralization is chiefly represented by replacement bodies, as described in other Carajás IOCG deposits formed at deeper crustal levels (Monteiro *et al*. 2008a, Xavier et al. 2012, Moreto *et al* 2015a).

Table 4 – Carbon and oxygen composition of calcites from Cristalino deposit.

Sample	Mode of occurrence	$\delta^{18}O_{min}$ (VPDB)‰	$\delta^{13}C_{min}$ (VPDB)‰	$\delta^{18}O_{min}$ (VSMOW)‰	T (°C)	$\delta^{18}O_{H2O}$ (VSMOW)‰[a]
14 -155AI	Cc±He±Ccp Breccia	-21.2	-3.8	9.0	393.0	10.1
14-155 B	Cc+He+Ccp Breccia	-20.6	-4.2	9.7	393.0	10.8
14-155 C	Cc+He+Ccp Breccia	-18.3	-3.8	11.1	393.0	12.3
14-155 A II	Cc+He+Ccp Breccia	-14.1	-4.9	16.4	234.6	15.0
25-155 I	Cc-rich vein	-21.3	-6.5	8.8	393.0	10.0
25-155 II	Cc-rich vein	-20.9	-6.3	9.4	393.0	10.5
25-155 III	Cc-rich vein	-21.2	-6.3	9.1	393.0	10.2
04-107	Cc-Chl vein	-20.6	-4.2	10.2	393.0	11.4
DH 03 02 I	Cc-rich vein in BIF	-5.4	-5.9	25.3	234.6	23.9
DH 03 02 II	Cc-rich vein in BIF	-8.9	-6.4	21.7	234.6	20.3

a = *oxygen isotopes fractionation: Zheng (1994).*
b = *Temperature calculate from pairs of minerals in equilibrium, presented in table 3.*

By the time the chlorite-epidote-calcite assemblage overprinted most of the previous alteration zones, the fluid had become cooler. The thermal condition was constrained by isotopic fractionation of several mineral pairs from the propylitic zones, yielding a temperature interval from 392°C ± 15° C to 235°C ± 24°C. The higher value was obtained with two calcite-magnetite pairs from a mineralized breccia, while the lower value was provided by calcite-chlorite and quartz-chlorite pairs from chalcopyrite-bearing veins, and by a calcite-magnetite pair from a mineralized breccia.

In this interval falls the temperature of 300° ± 32 °C estimated for the chlorite formation with the chlorite geothermometer (Craveiro *et al*. submitted b). Likewise, it agrees with most total homogenization temperatures (340° to 220°C) obtained in fluid inclusions trapped in minerals directly associated with both the propylitic zones and chalcopyrite±pyrite±hematite ore. The abundance of open-space structures is consonant with lower confining pressures characteristic of shallower crustal levels that certainly favored the infiltration of surficial water and decrease in temperature of the mineralizing fluid after mixing (see below). Fissural structures host much of that late mineralization.

Based on the isochores calculated with fluid package programs (Bakker 2003) and using the formation temperature of the Cristalino chlorite (Craveiro *el al*. submitted b), the trapping pressures of the ore fluid associated with propylitic alteration were estimated between 353.2 °C at 2.61 Kbar and 217.4 °C at 0.59 Kbar (Fig. 9A). The brittle deformational regime dominates at depths up to 5 km from the ground surface (Passchier and Trouw 2005), so that only pressures corresponding to the 220°-300° C range (0.6 to 1.7 kbar) would be compatible with the regime that prevailed during the propylitic alteration of the Cristalino volcanic rocks. It turns out that this temperature range is not very representative, which leads to the conclusion that the more frequent ranges of temperature would indicate pressures higher than those expected for the brittle regime, yet coherent with the transition to brittle-ductile conditions.

Apparently, heterogeneous trapping occurred at temperatures close to 250°C as indicated by a group of saturated FI that show not only $T_{hd} > T_{vd}$ but also scattering and increasing bulk salinity (Fig. 9B) (Ramboz *et al*. 1982).

Table 5 -Sulfur isotope composition of chalcopyrite from Cristalino deposit.

Sample	$\delta^{34}S_{sulfide(PDB)}$‰	Ore Assemblage	Lithotype
44-155-I	1.9	Ccp from Ccp+Py+Mag (Ore I)	Mafic volcanic rock
44-155-II	1.8	Ccp from Ccp+Py+Mag (Ore I)	Mafic volcanic rock
DH03-24_I	1.6	Ccp in Ccp±Py+Cc vein (Ore II)	Mafic volcanic rock
DH03-24-II	1.6	Ccp in Ccp±Py+Cc vein (Ore II)	Mafic volcanic rock
107-03	2.3	Ccp from Ccp+Py+Mag (Ore I)	Mafic volcanic rock
107-25	2.0	Ccp in Cc+Ccp rich vein (Ore II)	Felsic volcanic rock
14-155C	2.2	Ccp + He in breccia (Ore II)	Felsic volcanic rock
26-155-I	3.5	Ccp in Cc-rich vein (Ore II)	Felsic volcanic rock
26-155-II	3.2	Ccp in Cc-rich vein (Ore II)	Felsic volcanic rock
DH03_02	-32.6	Ccp in Cc-rich vein in BIF (Ore II)	BIF

Fluid sources and evolution

In the Carajás IOCG deposits, especially those from the CD southern sector, magmatic fluids have been pointed out to be responsible for the early stages of the hydrothermal alteration (Monteiro *et al*. 2008a, Silva *et al*. 2015, Xavier *et al*. 2012). Moreover, at high temperature, the fluid composition does not differ significantly suggesting the predominance of similar reservoirs. Regarding the Cristalino hydrothermal system, at temperatures as high as 550° C, the sodic and calcic-ferric assemblages are related to a fluid with a narrow range of both $\delta^{18}O_{H2O}$ (+8.4 ± 1.3 ‰) and δD_{H2O} (-34.6 ± 3.0 ‰) (Fig. 10A), consistent with water exsolved from magmas (Hedenquist and Lowenstern 1994, Taylor 1997) (Fig. 10B).

It should be added that variations in $\delta^{18}O_{H2O}$ and δD_{H2O} values may reflect also the influence the host rock composition. Actinolite samples from mafic volcanic rocks afforded $\delta^{18}O_{H2O}$ slightly lower (+7.37 ± 0.54 ‰) than those of tourmaline samples (8.46 ± 0.75 ‰) extracted from felsic volcanic rocks. Lower δD_{H2O} values, more typical of magmatic water released by felsic magmas (Taylor 1997), are found for the fluid in equilibrium with tourmaline. Therefore, these values could indicate an exchange between primary minerals and a more O^{18}- enriched fluid. Monteiro *et al.* (2008a) suggest that a similar combination of $\delta^{18}O_{H2O}$ and δD_{H2O} values in the Sossego deposit could have resulted from high temperature equilibration of deep circulation of basinal or formational/meteoric waters with the host rocks.

No suitable study could be performed on fluid inclusions of minerals from the earlier alteration zones. Most microthermometric data are not reliable, starting with the uncertainty as to the magmatic or hydrothermal nature of the host quartz. However, minerals with relatively high chlorine content were documented in the sodic and calcic-ferric assemblages. Allanite, a mineral generally devoid of Cl, presents contents of this halogen up to 0.6 wt. % and even higher contents (up to 2.94 wt. % Cl) occur in Fe-edenite (Craveiro *et al.* submitted b), suggesting high chlorine activity in the fluid that circulated during the earlier stages of the Cristalino hydrothermal system.

At higher temperatures, this hypersaline and relatively oxidized (presence of Fe^{3+}-allanite and abundant magnetite) fluid may have leached considerable amounts of metals from the wall rock, then flowed through second order shear zones and lithological contacts into the volcanic rocks where the chalcopyrite-pyrite-magnetite ore association was formed. This stage lasted until the calcic-ferric alteration faded away at ca. 400°C (Craveiro *et al.* submitted b).

As temperature dropped (<400° to ~200º C), the fluid not only became gradually depleted in ^{18}O (Fig. 10A) but also less saline (55.1 to 7.9 wt. % NaCl eq.). The trend of dilution is shown by curve a-a' (Fig. 11). Calcite and BIF magnetite samples are not part of this trend and fall on the right side of the magmatic water field. In addition to the ^{18}O depletion, the fluid shows D enrichment as well demonstrates the chlorite samples that are shifted toward the meteoric water line (Fig. 10B), due to mixing of magmatic water with externally-derived fluids.

It is plausible to assume from the spatial relationships between aqueous and carbonic inclusions (Fig. 6F, 6J, 6K) that the rock-altering fluid might have been aqueous-carbonic, which, by unmixing, would have produced immiscible phases that were trapped in these two

distinct inclusions. Aqueous-carbonic fluids have been reported in Salobo, Igarapé Bahia and Borrachudo deposits (Réquia and Fontboté 2001, Dreher *et al*. 2005, Previato 2016) and in other IOCG deposits worldwide (see Niiranen *et al*. 2007, Benavides *et al*. 2007).
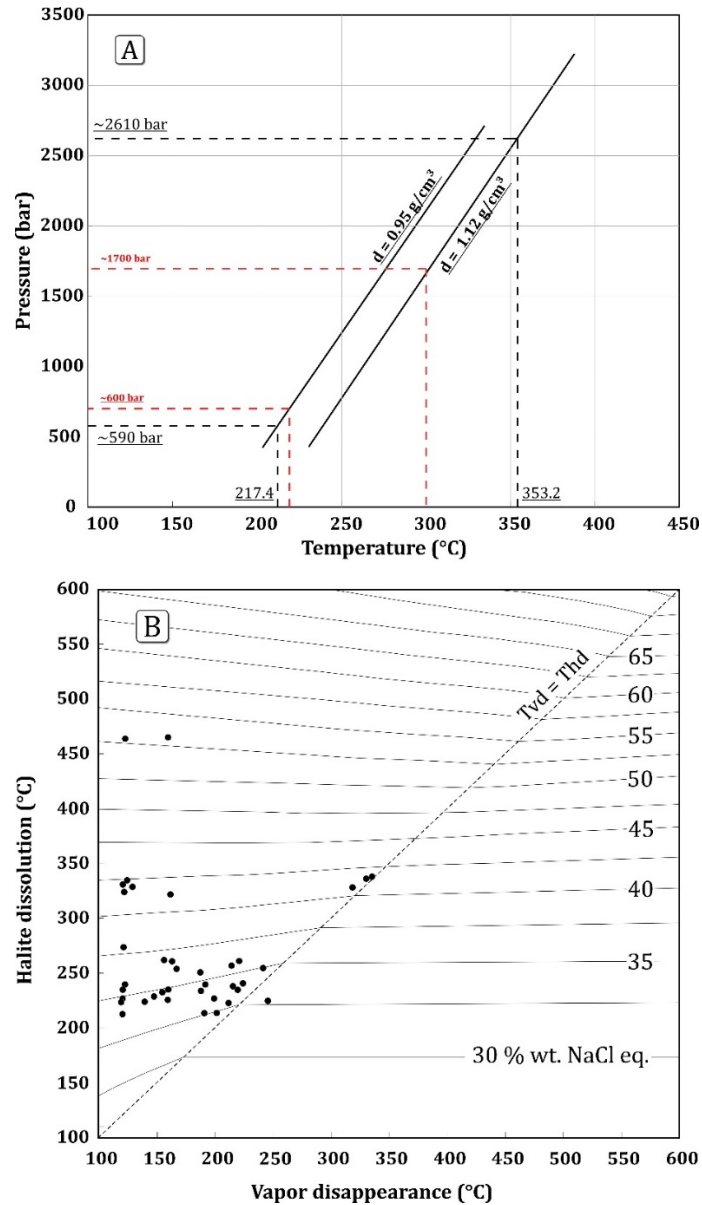
Figure 9. (A) Temperature-Pressure diagram where isochores are drawn according to Fluids package (Bakker 2003). Density (d) figures represent the end-members of the ore fluid that circulated during the propylitic alteration. Temperatures are based on the chlorite geothermometer.; (B) T_{hd}-T_{vd} diagram (after Lecumberr-Sanchez *et al*. 2012) for three-phase inclusions of FIA1. Black dashed lines: estimated PT conditions based on density variation of fluid 1 and thermal amplitude of chlorite formation (Craveiro et al. submitted b). Red lines: expected PT conditions for a brittle dominated structural regime (Passchier and Trouw, 2005).

The imprecise data obtained with the FI related to the earlier stages of the hydrothermal alteration do not allow knowing the characteristics of the fluid, although it is supposed that it should have been hot, acidic and hypersaline. This fluid could have been

derived, at least in part, from the magmas that generated the Serra do Rabo (2741 ± 1.6 Ma, U-Pb in zircon, Sardinha *et al*. 2006) and/or Planalto (2747 ± 2 Ma, U-Pb in zircon, Huhn *et al*. 1999a) granites, which crop out in the Cristalino deposit area and surroundings. In favor of this hypothesis plays the dating of the chalcopyrite-pyrite-magnetite ore association at 2719 ± 36 Ma (Pb-Pb leaching in chalcopyrite, Soares *et al*. 2001), comparable, within the limits of error, to the emplacement ages of those granitic intrusions.
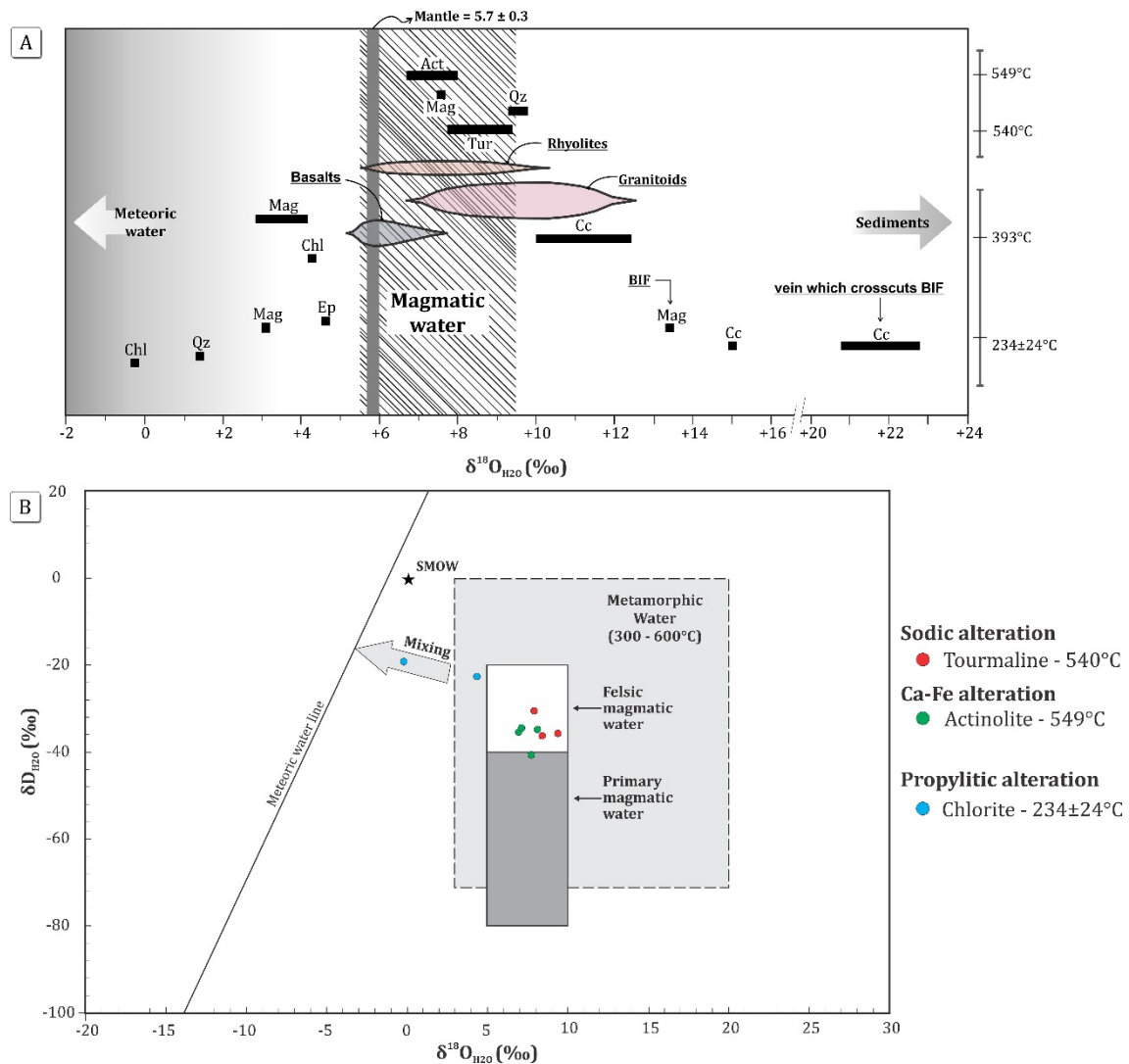
Figure 10. (A) Range of oxygen isotope compositions of the fluids (black bars) related to the hydrothermal alteration and mineralization of the Cristalino deposit. On the right side, are recorded the temperatures used in the calculations. Magmatic water field and directions towards meteoric water and sediments are from Taylor (1997). Oxygen isotope compositions of rhyolites, granitoids and basalts were taken from Taylor (1974). Act: actinolite, BIF: banded iron formation, Cc: calcite, Chl: chlorite, Ep: epidote, Mag: magnetite, Qz: quartz. (**B**) Oxygen and hydrogen isotope composition of fluids responsible for the alteration and mineralization of Cristalino deposit. Metamorphic, primary magmatic and felsic magmatic waters are respectively from Sheppard (1986), Taylor (1974) and Taylor (1992).

On the other hand, considering the late alteration assemblages, FI data reveal that two fluids circulated through the rocks: a metal-rich aqueous-carbonic (H_2O-$NaCl$-$CaCl_2$ ± CO_2 ± KCl ± $MgCl_2$ ± $FeCl_2$) and an aqueous (H_2O-$NaCl$-KCl ± $MgCl_2$) referred to hereafter, respectively, as fluids 1 and 2.

Fluid 1 — most likely the same fluid responsible for the early stages of alteration and mineralization — would have been unmixed (as assumed above) and the resulting phases would be then represented by primary inclusions in quartz and calcite from mineralized veins and breccias. Its aqueous counterpart would have been responsible for the late alteration processes and chalcopyrite±pyrite±hematite ore.

In turn, fluid 2 was trapped as secondary inclusions along crystal boundaries and micro-fracture planes. It is a colder saline fluid that experienced a practically isothermal dilution (21 to 3.1 wt. % NaCl eq.) indicated by trend c-c' in Fig. 11 due to mixing with surficial water. It probably represents a late fluid of restrict circulation and unknown origin. Could it be related to any Paleoproterozoic granitic intrusion that occurs in the neighborhood of the Cristalino area? Similar fluids have been described in several Carajás IOCG deposits (Torresi *et al.* 2011, Previato 2016, Silva *et al.* 2012).

Sources of Carbon and Sulfur

Calcite is commonly described as a late hydrothermal product in several IOCG deposits all over the world (Groves *et al.* 2001, Williams *et al.* 2010, and references herein), a finding that is also recognized in Carajás (Monteiro *et al.* 2008a, Pestilho 2011, Moreto *et al.* 2015a, Silva *et al.* 2015, Xavier *et al.* 2017). The carbon isotopic composition ($\delta^{13}C_{V\text{-}PDB}$) is dependent on temperature, f_{O2} and pH during mineral precipitation, as well as the $\delta^{13}C_{\Sigma C}$ of the fluids (Ohmoto 1972, Ohmoto and Rye 1979, Ohmoto and Goldhaber 1997).

The $\delta^{13}C_{VPDB}$ values of calcite from the Cristalino deposit range between -6.5 and -3.8‰ and show relatively little variation with respect to how it occurs, whether in breccias or veins hosted by felsic volcanic rocks. These rather uniform values point to a large-scale hydrothermal system with a homogeneous source and are consistent with $\delta^{13}C_{VPDB}$ values in carbonatites, diamonds and kimberlites (-3 to -8‰, Taylor 1986). They thus may indicate a deep source for CO_2, most likely related to fluids released from an underlying magma chamber. The less negative results (> -5‰) are also projected in the field of marine limestones (Perry and Tan 1972), but these rocks have not yet been described in the CD and are for the moment discarded as a potential source for carbon of the Cristalino calcite.

Most results show also a tight range of $\delta^{18}O_{VSMOW}$ values (+8.8 to +11.1‰) that fall in the interval from +7.0 to +12.0 ‰ determined in rhyolites, dacites, and granitoids (Taylor 1974). Three samples, however, from calcite-rich veins that crosscut BIF (DH 03 02I and DH 03 02II) and a breccia (14-155AII) are distinctly enriched in ^{18}O (Tab. 2). The former may have incorporated a great deal of ^{18}O from the BIF whose sedimentary or diagenetic oxygen isotope composition is highly enriched in heavy oxygen, whereas the latter may reflect exchange isotope disequilibrium or local interaction with an aqueous fluid that was either ^{18}O-rich or had a relatively low temperature.
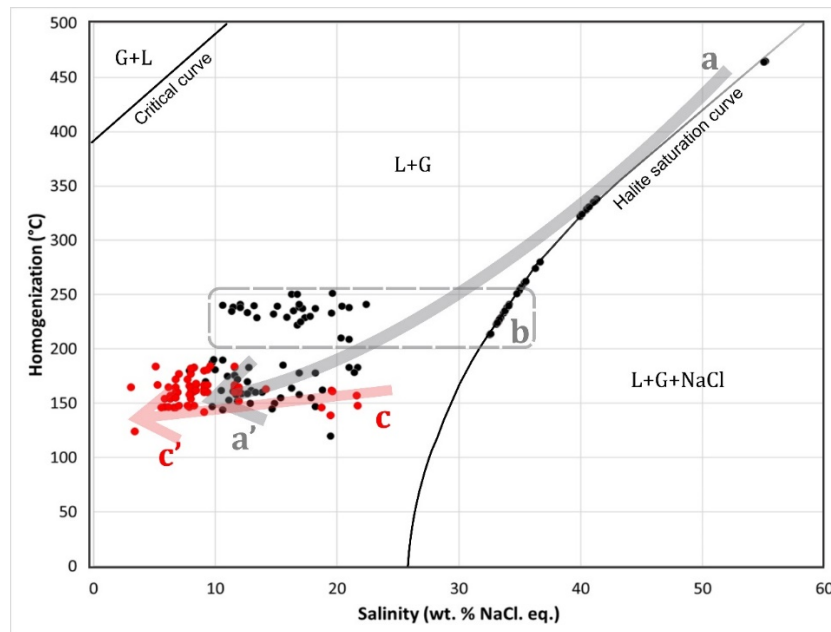
Figure 11. Salinity versus total homogenization temperature diagram in which are plotted data of inclusions representing fluids 1 and 2. Halite saturation and critical curves, as well as the stability fields of G + L, L + G, L + G + NaCl, according to Bodnar *et al*. (1985). The grey arrow **a-a'** indicates the dilution trend for fluid 1 (black filled circles). FI in rectangle "**b**" suggest heterogeneous trapping of fluid 1. The red arrow **c-c'** indicates the dilution trend for fluid 2 (red filled circles).

The isotope composition of most Cristalino calcite is in good agreement with previous data obtained by Ribeiro *et al*. (2009) in this deposit (Fig. 12). In comparison to other Carajás IOCG deposits, $\delta^{13}C_{VPDB}$ values are consistent with those of carbonates present in mineralized breccias of the Sossego and Alvo 118 (Monteiro *et al*. 2008a, Torresi *et al*. 2012), but quite distinct from those of the Igarapé Bahia, located in the CD northern sector (Dreher *et al*. 2005). On the other hand, the abnormally high $\delta^{18}O_{VSMOW}$ values in mineralized vein calcites may suggest a trend of contamination by sedimentary rocks that include some Igarapé Bahia calcite.
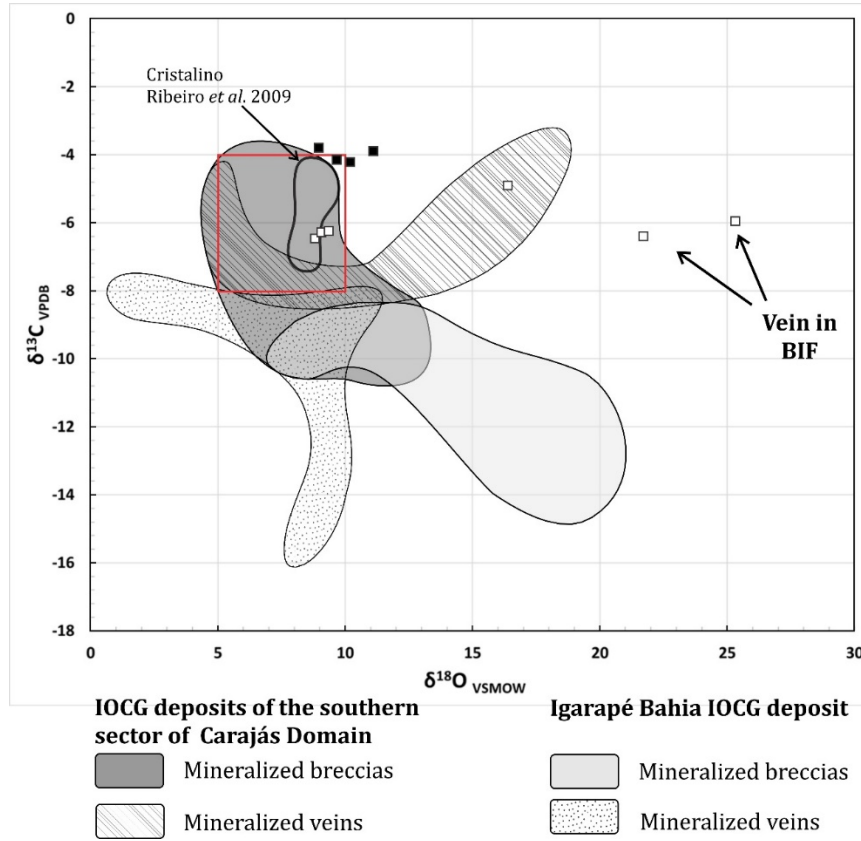
Figure 12. Oxygen and carbon isotopic data of carbonates from the Cristalino deposit compared to those of other Carajás IOCG deposits. Black squares: mineralized breccias; white squares: mineralized veins. Sources for Carajás IOCG deposits: southern sector (Torresi *et al*. 2012), Sossego deposit (Monteiro *et al*. 2008a, (4) Cristalino (Ribeiro et al. 2009). Igarapé Bahia: Dreher *et al*. (2005). Red square – primary carbonatite (Taylor *et al*. 1967).

Sulfur isotope compositions of sulfides in hydrothermal systems are controlled by the isotopic compositions of the fluids, as well as temperature, Eh and pH at the site of ore deposition, the first parameter being characteristic of the source of sulfur and the other three relate to the conditions of deposition (Ohmoto 1986, Ohmoto and Goldhaber 1997).

The $\delta^{34}S_{VCDT}$ values of chalcopyrite from the Cristalino deposit range from +1.6 to +3.5‰ and show a narrow variation regardless of its location in the deposit. These values are rather uniform, and indicate a homogeneous source of sulfur, which was likely of magmatic origin. A single sample (DH03 02), however, reveals an abnormally ^{34}S depleted composition (-32.6‰) and may reflect sedimentary sulfur contributed by the BIF that hosts the chalcopyrite-bearing vein.

Values closer to the sulfur isotope composition of the mantle (Fig. 13) have been obtained in sulfides from the Cristalino (Ribeiro *et al.* 2009), Borrachudo (Previato 2016), Salobo (Réquia *et al.* 2001), Bacuri (Pestilho 2011) and Castanha (Monteiro *et al.* 2007,

Pestilho 2011) and interpreted to have had less influence of sulfur leached from the host igneous rocks.

Other Carajás IOCG deposits show a broader range of $\delta^{34}S_{VCDT}$ results, notably Igarapé Bahia, Sequeirinho and Sossego ore bodies, Bacaba, Visconde and Alvo 118 (Fig.11), some with sulfides distinctly enriched in ^{34}S that points to sulfur possibly derived from the host igneous rocks or even evaporites.
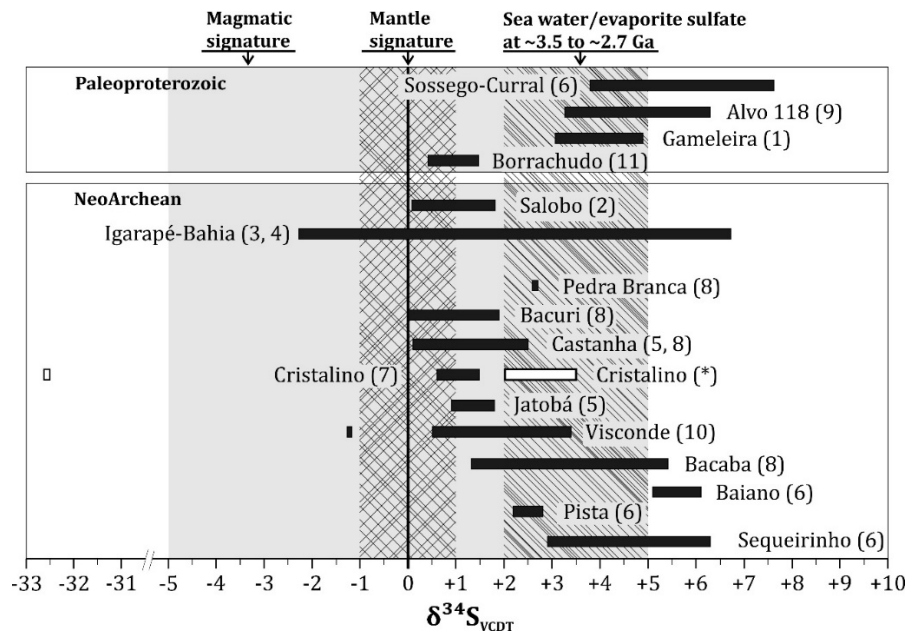
Figure 13. Sulfur isotope compositions of sulfides from the Cristalino deposit compared with other cooper deposits of Carajás domains. 1 – Lindenmayer et al. 2001, 2 - Réquia et al. 2001, 3 – Villas *et al*. 2001, 4 – Dreher 2004, 5 - Monteiro et al. 2007, 6 - Monteiro et al. 2008a, 7 - Ribeiro et al. 2009, 8 – Pestilho 2011, 9 - Torresi et al. 2012, 10 - Silva et al. 2015, 11 – Previato 2016, (*) this work. Magmatic field (grey field) and Archean sulfate (dashed field) are from Ohomoto and Goldhaber (1997); mantle signature (crossed dashed field) is from Eldridge *et al*. (1991).

Ore deposition processes

The rich Cu-Au ore of the Cristalino deposit bear evidence for an unusually effective mechanism of ore deposition, which may have caused substantial metal saturation and precipitation mainly in calcic-ferric altered mafic volcanic rocks. At temperatures > 350º C, both Cu and Au are chiefly carried by chloride complexes, and metal precipitation as native Au and sulfide can be induced by a decrease in temperature, ligand (chloride) activity and pH. The fluid-rock interaction, which accompanied ore deposition at Cristalino, produced actinolite-rich zones and is considered to have influenced ore precipitation (chalcopyrite-pyrite-Au-magnetite) since such alteration decreases the acidity of the fluid.

Structural evidence for a transition from a closed to an open vein system, and a concomitant change from lithostatic to hydrostatic conditions, implies that immiscibility may

have taken place. Unmixing would have oxidized the ore fluid, decreased its temperature and significantly increased its pH due to the loss of acidic volatiles. Thus, it would have promoted the precipitation of chalcopyrite with minor pyrite, Au and hematite. However, vapor-rich fluid inclusions are rare. If unmixing occurred during the late stage of mineralization, it was probably of limited extent.

By contrast, the coincidence of the late mineralization stage with the opening of the vein system and the widespread appearance of cooler, much more dilute fluids are readily explained by incursion of meteoric water which mixed with magmatic fluids. Further evidence of mixing is given by the evolution of the oxygen isotope composition of the ore fluid. Mixing of magmatic with meteoric waters should lead to progressive decreases in the $\delta^{18}O$ values of the ore fluid. Unmixing, on the other hand, increases the $\delta^{18}O$ of the remaining liquid because of preferential partitioning of the light isotope into the vapor, and this is reflected in the paragenesis by a gradual increase in $\delta^{18}O$ with time.

CONCLUSION

1. Hydrothermal alteration and mineralization in the Archean Cu-Au Cristalino deposit occurred at temperatures that ranged from ~550º to ~250º C and pressures between 2.6 and 0.6 Kbar, consistent with the brittle and brittle-ductile regimes under which these processes developed.

2. The hydrothermal fluid responsible for the alteration and mineralization was metal-rich, acidic and hypersaline, showing expressive contribution from magmatic sources, as supported by O and H isotope data ($\delta^{18}O_{vsmow}$ =+9.73 to +6.48‰; δD_{vsmow}= -30.17 to -40.25‰.

3. Ore fluid salinity vary from > 55 to 7.9 wt. % NaCl equiv., the higher values being most likely prevalent during the earlier pervasive sodic and calcic-ferric alterations and mineralization (chalcopyrite-pyrite-magnetite-Au ore).

4. Below 350-300ºC, at the time the deformational regime changed from brittle-ductile to brittle, the later alteration zones formed and chalcopyrite-Au±pyrite±hematite ore association precipitated in veins and breccias. The transition from a closed to an open space system favored the infiltration of surficial water causing dilution. Salinity decreased to 7.9 wt. % NaCl equiv. and the fluid became progressively ^{18}O-depleted and D-enriched ($\delta^{18}O_{vsmow}$ =+5.57 to -0.28‰; δD_{vsmow}= -19.15 to -22.24‰).

5. $\delta^{13}C_{VPDB}$ values for vein and breccia calcite (-6.5 to -3.8‰) are consistent with a deep source for CO_2, which was probably released from an underlying magma chamber. The $\delta^{34}S_{VCDT}$ values for chalcopyrite show narrow variation (+1.6 to +3.5 ‰) and indicate a homogeneous reservoir for sulfur, which was likely of igneous origin. Although most data point to a magmatic affiliation, a few samples reveal significant influence of sedimentary rocks on their isotope composition.

6. Mostly transported as chloride complexes (>350ºC), Cu and Au precipitated in response to decrease in temperature and Cl⁻ activity and increase in pH. The chalcopyrite-Au±pyrite±hematite ore assemblage was additionally favored by f_{O2} increase in the late stages of the hydrothermal alteration.

7. An aqueous, colder (200-150º C) and less saline (21-3.1 wt. % NaCl equiv.) seems to have circulated in the Cristalino deposit area, being trapped as secondary fluid inclusions. The origin is unknown, but it could be related to a nearby Paleoproterozoic granitic intrusion.

8. The data presented here support previous interpretations that consider Cristalino as of IOCG typology. In comparison with other Archean Carajás IOCG deposits, particularly those that lie in the southern sector of the Carajás Domain, the Cristalino deposit shows many similarities regarding ore fluid composition and evolution, as well as the isotopic signature of sulfides and carbonates.

REFERENCES

Araújo, O.J.B., Maia, R.G.N., Jorge-João, X.S. Costa, J.B.S. 1988. A megaestruturação da folha Serra dos Carajás. *In*: SBG, Congresso Latino Americano de Geologia, *Anais...*, **7**:324-333.

Araújo, O.J.B., and Maia, R.G.N. 1991. Programa de levantamentos geológicos básicos do Brasil, Serra dos Carajás, folha SB-22-Z-A, Estado do Pará. *Texto explicativo*, Brasília, DNPM/CPRM. 164p.

Bakker, R.J. 2003. Package FLUIDS 1. Computer programs for analysis of fluid inclusion data and for modelling bulk fluid properties. *Chemical Geology*, **194**:3-23.

Barros, C.E.M., Barbey, P., Boullier, A.M., 2001. Role of Magma Pressure, Tectonic Stress and Crystallization Progress in the Emplacement of Syn-tectonic Granites. The A-type Estrela Granite Complex (Carajás Mineral Province, Brazil). *Tectonophysics*: **343**:93–109.

Barros, C.E.M., Sardinha, A.S., Barbosa, J.P.O., Macambira, M.J.B., Barbey, P., Boullier, A.M. 2009. Structure, petrology, geochemistry and zircon U/Pb and Pb/Pb geochronology of the synkinematic Archean (2.7 Ga) A-type granites from the Carajás Metallogenic Province, northern Brazil. *The Canadian Mineralogist*, **47**:1423-1440.

Barton, M.D. and Johnson, D.A., 1996. Evaporitic Source Model for Igneous Related Fe Oxide–(REE–Cu–Au–U) Mineralization. *Geology*, **24**:259–262.

Benavides, J.A., Kyser, T.K., Clark, A.H., Oates, C., Zamora, R., Tarnovschi, R., Castillo, B. 2007, The Mantoverde iron oxide coppergold district, III Región, Chile: The role of regionally derived, nonmagmatic fluids in chalcopyrite mineralization. *Economic Geology*, **102**: 415-440.

Bodnar, R.J. 1983. A method of calculating fluid inclusion volumes based on vapor bubble diameters and P - V - T - X properties of inclusion fluids. *Economic Geology,* **78**:535–542.

Bodnar, R.J., 1993. Revised equation and table for determining the freezing point depression of H_2O–NaCl solutions. *Geochimica et Cosmochimica Acta,* **57**:683–684.

Bodnar, R.J., 1994. Synthetic fluid inclusions: XII. The system H_2O-NaCl. Experimental determination of the halite liquidus and isochores for a 40 wt.% NaCl solution. *Geochimica et Cosmochimica Acta,* **58**:1053–1063.

Bodnar, R.J., Burnham, C.W., Sterner, S.M. 1985. Synthetic fluid inclusions in natural quartz. III. Determination of phase equilibrium properties in the system H_2O–NaCl to 1000°C and 1500 bars. *Geochimica et Cosmochimica Acta,* **49**:1861–1873.

Bodnar, R.J. and Vityk, M.O. 1994, Interpretation of Microthermometric Data for H2O-NaCl Fluid Inclusions. In: De Vivo, B. and Frezzotti, M.L., Eds., *Fluid Inclusions in Minerals: Methods and Application*, Pontignsno-Siena, 117- 130.

Borisenko, A.S., 1977. Study of salt composition of fluid inclusions in minerals using cryometric technique. *Geologiya i Geofizica*. **8**:16–27 (in Russian).

Borisenko, A.S. 1982. Analysis of salt content of solutions in gas-liquid inclusions in minerals using cryometric methods. In: Laverov, N.P. (Ed.), *Ispolzovaniye metodov termobarogeokhimiyi pri poiskach i izucheniyi rudnych mestorozhdeniy*. Nedra, Moskva, pp. 37–46 (in Russian).

Botelho, N.F., Moura, M.A., Teixeira, L.M., Olivo, G.R., Cunha, L.M., Santana, M.U. 2005. Caracterização geológica e metalogenética do depósito de Cu±(Au, W, Mo, Sn) Breves, Carajás. *In*: Matini, O.J., Queiroz, E.T., Ramos, B.W. (Ed.). *Caracterização de depósitos minerais em distritos mineiros da Amazônia*. Brasília: DNPM –CT/MINERAL–ADIMB, 2005. cap. VI, p 339- 389.

Cathelineau, M. and Nieva, D. 1985. A chlorite solid solution geothermometer. The Los Azufres (Mexico) geothermal system. *Contribution to Mineral Petrology*. **91**:235-244.

Clayton, R. N. and Mayeda, T. 1963. The use of bromine pentafluoride in the extraction of oxygen from oxides and silicates for isotopic analysis. *Geochimica et Cosmochimica Acta*, **27**:47-52.

Chiba, H., Chacko, T., Clayton, R.N., Goldsmith, J.R. 1989. Oxygen isotope fractionations involving diopside, forsterite, magnetite, and calcite: Application to geothermometry. *Geochimica et Cosmochimica Acta,* **53**: 2985-2995.

Craveiro, G.S., Xavier, R.P., Villas, R.N.N. (*in revision*). The Cristalino IOCG Deposit: an example of multi-stage events of hydrothermal alteration and copper mineralization. *Brazilian Journal of Geology.*

Craveiro, G.S., Xavier, R.P., Villas, R.N.N. 2018. Mineral chemistry and geothermometry of alteration zones, IOCG Cristalino Deposit, Carajás Mineral Province, Brazil. *Manuscript submitted for publication.*

Costa, J.B.S., Araújo, O.J.B., Santos, A., Jorge João, X.S., Macambira, M.J.B., Lafon, J.M. 1995. A Província Mineral de Carajás: aspectos tectono-estruturais, estratigráficos e geocronológicos. *Boletim do Museu Paraense Emílio Goeldi*, **7**:199-235.

Dall'Agnoll, R., Oliveira, D.C., Lamarão, C.N. 2013. Magmatismo granitoide arqueano e evolução geológica do Subdomínio de Transição da Província Carajás, sudeste do Cráton Amazônico, Brasil. *Boletim do Museu Emílio Goeldi,* **8(3)**: 251-256.

Dall'Agnol, R., Teixeira, N.P., Rämö, O.T., Moura, C.A.V., Macambira, M.J.B., Oliveira, D.C. 2005, Petrogenesis of the Paleoproterozoic, rapakivi, A-type granites of the Archean Carajás Metallogenic Province, Brazil. *Lithos,* **80**:101–129.

Davis, D.W., Lowenstein, T.K., Spencer, R.J., 1990, Melting behavior of fluid inclusions in laboratory-grown halite crystals in the systems $NaCl – H_2O$, $NaCl – KCl – H_2O$, $NaCl – MgCl_2 – H_2O$ and $NaCl – CaCl_2 – H_2O$. *Geochimica et Cosmochimica Acta,* **54**: 591 – 601.

Dias, G.S., Macambira, M.J.B., Dall'Agnol, R., Soares, A.D.V., Barros, C.E.M. 1996. Datação de zircões de sillmetagabro: comprovação da idade arqueana da Formação Águas Claras, Carajás, Pará. *In*: SBG 5° Simp. Geol. da Amazônia, Belém, *Resumos Expandidos*. p. 376-379.

DOCEGEO, 1988. Revisão litoestratigráfica da Província Mineral de Carajás – Litoestratigrafia e principais depósitos minerais. In: Congresso Brasileiro de Geologia, 35. Belém, *Expanded abstract*, 11-54.

Dreher, A.M., Xavier, R.P., Taylor, B.E., Martini., S.L. 2007. New geologic, fluid inclusion and stable isotope studies on the controversial Igarapé Bahia Cu–Au deposit, Carajás Province, Brazil. *Mineralium Deposita*. DOI 10.1007/s00126-007-0150-6.

Eldridge, C.S., Compston, W., Williams, I.S., Harris, J.W., Bristow, J.W., 1991. Isotope evidence for the involvement of recycled sediments in diamond formation. *Nature,* **353:** 649–653.

Feio, G.R.L., Dall'Agnol R., Dantas E.L., Macambira M.J.B., Santos J.O.S., Althoff F.J., and Soares J.E.B., 2013. Archean granitoid magmatism in the Canaã dos Carajás area: Implications for crustal evolution of the Carajás province, Amazonian craton, Brazil. *Precambrian Research*, **227:**157-186.

Ferreira Filho, C.F., Cunha, E.M., Lima, A.C., Cunha, J.C., 2013. *Depósito de Níquel-Cobre Sulfetado de Santa Rita, Itagibá, Bahia, Brasil*. Série arquivos abertos vol. 39. Companhia Baiana de Pesquisa Mineral, Salvador – Bahia, p. 59.

Galarza, M.A. and Macambira, M.J.B. 2002. Geocronologia e evolução crustal da área do depósito de Cu-Au Gameleira, Província Mineral de Carajás (Pará), Brasil. *Revista do Instituto de Geociências da USP,* **2:**143-159.

Gibbs, A.K., Wirth, K.R., Hirata, W.K., Olszewski Jr., W.J. 1986. Age and composition of the Grão Pará Group volcanics, Serra dos Carajás. *Revista Brasileira de Geociências*, **16:**201–211.

Goldstein, R.H. and Reynolds, T. J., 1994. Systematics of fluid inclusions in diagenetic minerals SEMP. Short Course, v. 31, SOc, *Sediment Geology*, Tulsa, Oklahoma, 198p.

Graham, C.M., Harmon, R.S., Sheppard, S.M.F., 1984. Experimental hydrogen isotope studies: Hydrogen isotope exchange between amphibole and water; *American Mineralogist,* **69:** 128-138.

Graham, C.M., Viglino, J.A., Harmon, R.S. 1987. Experimental study of hydrogen-isotope exchange between aluminous chlorite and water and of hydrogen diffusion in chlorite. *American Mineralogist,* **72:**566-579.

Grainger, C.J., Groves, D.I., Tallarico, F.H.B., Fletcher, I.R. 2008. Metallogenesis of the Carajás Mineral Province, southern Amazon Craton: Varying styles of Archean through Paleoproterozoic to Neoproterozoic base- and precious-metal mineralization. *Ore Geology Reviews*, **33:**451-489.

Groves, D. I., Bierlein, F.P. Meinert. L.D, Hitzman, M.W. 2010. Iron oxide cooper-gold (IOCG) deposits through Earth history: Implications for origin, lithospheric setting, and distinction from other epigenetic iron oxide deposits. *Economic Geology*, **105**:641-654.

Hedenquist, J. W. and Lowenstern, J. B., 1994. The role of magmas in the formation of hydrothermal ore deposits. *Nature,* **370:**519–527.

Hitzman, M.W., Oreskes, N., Einaudi, M.T. 1992. Geological characteristics and tectonic setting of Proterozoic iron oxide (Cu-U-Au-REE) deposits. *Precambrian Research,* **58:**241 – 287.

Holland, T. and Blundy, J. 1994. Non-ideal interactions in calcic amphiboles and their bearing on amphibole-plagioclase thermometry. *Contribution to Mineral Petrology,* **116:**433-47.

Huhn, S.R.B., Macambira, M.J.B., Dall'Agnol, R., 1999a. Geologia e Geocronologia Pb/Pb do Granito Alcalino Arqueano Planalto, Região da Serra do Rabo, Carajás – PA. *In*: SBG, 11° Simp. Geol. da Amazônia. *Anais*. Manaus/AM, p. 463-466.

Huhn, S.R.B., Souza, C.I.J., Albuquerque, M.C., Leal, E.D., Brustolin, V. 1999b. Descoberta do depósito Cu (Au) Cristalino: Geologia e mineralização associada região da Serra do Rabo - Carajás – PA. *In*: SBG, 11° Simpósio de Geologia da Amazônia, Manaus, *Proceedings*. **6:**140–143.

Hurai, V., Huraiova, M., Slobodnik, M., Thomas, W., 2015. *Geofluids. Developments in Microthermometry, Spectroscopy, Thermodynamics, and Stable Isotopes*. Elsevier, 489 p.

Kerrich R. 1987. The stable isotope geochemistry of Au-Ag vein deposits in metamorphic rocks. Mineral. Assoc. Canada, Short Course Handbook, **13:**287-336.

Kotzer, T.G.; Kyser, T.K.; King, R.W.; and Kerrich, R. (1993) An empirical oxygen- and hydrogen-isotope geothermometer for quartz-tourmaline and tourmaline-water. *Geochimica et Cosmochimica Acta,* **57:**3421-3426

Lecumberri-Sanchez, P., Steele-MacInnis, M., Bodnar, R.J., 2012. A numerical model to estimate trapping conditions of fluid inclusions that homogenize by halite disappearance. *Geochimica et Cosmochimica Acta,* **92:**14–22.

Lindenmayer, Z. G., Fleck, A., Gomes, C.H., Santos, A.B.S., Caron, R., Paula, F.C., Laux, J.H., Pimentel, M.M., Sardinha, A.S. 2005. Caracterização geológica do alvo estrela (Cu-Au), Serra dos Carajás, Pará *In*: *Caracterização de Depósitos Minerais em Distritos Mineiros da Amazônia*. DNPM, CT-Mineral / FINEP, ADIMB, 2005, cap. IV, 1, 137-205.

Lindenmayer, Z.G., Laux, J.H., Teixeira, J.B.G. 2001. Considerações sobre a origem das Formações Ferríferas da Formação Carajás, Serra dos Carajás. *Revista Brasileira de Geociências*, **31(1)**:21-28.

Lobato, L.M., Rosière, C.A., Silva, R.C.F., Zucchetti, M., Baars, F.J., Seoane, J.C.S., Rios, F.J., Pimentel, M., Mendes, G.E., Monteiro, A.M. 2005. A mineralização hidrotermal de ferro da Província Mineral de Carajás - controle estrutural e contexto na evolução metalogenética da Província. In: Marini, J.O.; Queiróz, E.T.; Ramos, W.B. (eds.), *Caracterização de distritos mineiros da Amazônia*. DNPM-CT-Mineral-ADIMB, 25–92.

Macambira, E.M.B. and Vale, A.G. 1997. *São Félix do Xingu: folha SB.22-Y-B, Estado do Pará, escala 1:250.000. Texto Explicativo*. Brasília: CPRM. 344 p., il. Programa Levantamentos Geológicos Básicos do Brasil (PLGB).

Macambira, J.B., 2003. O ambiente deposicional da Formação Carajás e uma proposta de modelo evolutivo para a Bacia Grão Pará. Doctoral thesis, IG-UNICAMP, 217p.

Machado, N., Lindenmayer, Z.G., Krogh, T.E., Lindenmayer, D. 1991. U–Pb geochronology of Archean magmatism and basement reactivation in the Carajás area, Amazon shield, Brazil. *Precambrian Research*, **49:**329–354.

Mathur R, Marschik R, Ruiz J, Munizaga F, Leveille RA, Martin W. 2002. Age of mineralization of the Candelaria Fe oxide Cu–Au deposit and the origin of the Chilean iron belt, based on Re–Os isotopes. *Economic Geology,* **97:**59–71.

Matsuhisa, Y., Goldsmith, J.R., Clayton, R.N. 1979. Oxygen isotopic fractionation in the system quartz-albite-anorthite-water. *Geochimica et Cosmochimica Acta,* **43:**1131-1140

Meirelles, M.R. and Dardenne, M.A. 1991. Vulcanismo basáltico de afinidade shoshonítica em ambiente de arco arqueano, Grupo GrãoPará, Serra dos Carajás, PA. *Revista Brasileira de Geociências*, **21:**41-50.

Monteiro, L.V.S., Xavier, R.P., Souza Filho, C.R., Augusto, R.A., 2007. Aplicação de isótopos estáveis ao estudo dos padrões de distribuição das zonas de alteração hidrotermal

associados ao sistema de óxido de ferro-cobre-ouro Sossego, Província Mineral de Carajás. In: SBGq, *Congresso Brasileiro de Geoquímica*, 8, Atibaia, CD-Rom.

Monteiro, L.V.S., Xavier, R.P., Carvalho, E.R., Hitzman, M.W., Johnson, C.A., Souza Filho, C.R., and Torresi, I. 2008. Spatial and temporal zoning of hydrothermal alteration and mineralization in the Sossego iron oxide- copper-gold deposit, Carajás Mineral Province, Brazil: Parageneses and stable isotope constraints. *Mineralium Deposita*, **43:**129−159.

Moreto, C.P.N., Monteiro L.V.S., Xavier R.P., Amaral W.S., Santos T.J.S., Juliani C., and Souza Filho C.R. 2011. Mesoarchean (3.0 and 2.86 Ga) host rocks of the iron oxide-Cu-Au Bacaba deposit, Carajás Mineral Province: U-Pb geochronology and metallogenetic implications. *Mineralium Deposita*, **46:**789-811.

Moreto, C.P.N., Monteiro, L.V.S., Xavier, R.P., Creaser, R.A., Dufrane, S.A., Melo, G.H.C., Delinardo da Silva, M.A., Tassinari, C.C.G., Sato, K. 2015. Timing of multiple hydrothermal events in the iron oxide–copper–gold deposits of the Southern Copper Belt, Carajás Province, Brazil. *Mineralium Deposita*, **50:**517–546.

Mougeot, R., Respaut, J.P., Briqueu, L., Ledru, P., Milesi, J.P., Lerouge, C., Marcoux, E., Huhn, S.B., Macambira, M.J.B. 1996. Isotope geochemistry constrains for Cu, Au mineralizations and evolution of the Carajás Province (Para, Brazil). In: Congresso Brasileiro de Geologia, Salvador. *Anais...* Salvador, SBG, **7:**321–324.

Niiranen, T., Poutiainen, M., Mänttäri, I. 2007. Geology, geochemistry, fluid inclusion characteristics, and U–Pb age studies on iron oxide–Cu–Au deposits in the Kolari region, northern Finland. *Ore Geology Reviews*, **30(2):**75-105.

Nogueira, A.C.R., Truckenbrodt, W., Pinheiro, R.V.L. 1995. Formação Águas Claras, Pré-Cambriano da Serra dos Carajás: redescrição e redefinição litoestratigráfica. *Boletim Museu Paraense Emílio Goeldi,* **7:**177–277.

O`Neil, J.R. 1986. Theoretical and experimental aspects of isotope fractionation. *Reviews in Mineral*. **16:**1-40.

Ohmoto, H., and Goldhaber, M.B. 1997. Sulfur and carbon isotopes. In: Barnes HL (ed) *Geochemistry of hydrothermal ore deposits*, 3rd edn. Wiley, New York, pp. 517 – 611.

Ohmoto, H. 1972. Systematics of sulfur and carbon isotopes in hydrothermal ore deposits. *Economic Geology,* **67:**551-578.

Ohmoto, H. and Rye, R.O. 1979. Isotopes of sulfur and carbon. In: Barnes H.L (ed), *Geochemistry of hydrothermal ore deposits*, 2nd ed. New York, Wiley Interscience, p. 509-567.

Oliveira, J.R. 1994**.** *Programa Levantamentos Geológicos Básicos do Brasil: Folha Serra Pelada (Folha SB.22-Z-A).* Estado do Pará. Brasília, DNPM/CPRM, 248p.

Passchier, C.W. and Trouw, R.A. 2005, *Microtectonics*. Springer-Verlag Berlin Heidelberg. 366 p.

Perry, E.C. and Tan, F.C. 1972. Significance of oxygen and carbon isotope variations in Early Precambrian cherts and carbonate rocks of Southern Africa. *Geological Society of America Bulletin,* **83:**647-664.

Pestilho, A.L.S. 2011. Sistemática de isótopos estáveis aplicada à caracterização da evolução dos paleosistemas hidrotermais associados aos depósitos cupríferos Alvo Bacaba e Alvo Castanha, Província Mineral de Carajás, PA. PhD thesis, University of Campinas.

Pinheiro R.V.L. and Holdsworth, R.E. 2000. Evolução tectonoestratigráfica dos sistemas transcorrentes Carajás e Cinzento, Cinturão Itacaiúnas, na borda leste do Cráton Amazônico, Pará. *Revista Brasileira de Geociências*, **30(4):**597-606.

Pinto, A. 2012. Salobo Copper Mine Feasibility in Carajás, Pará State. In: V Brazilian Symposium on Mineral Exploration. 2012. Ouro Preto - MG, Brazil.

Pirajno, F., 2009. *Hydrothermal processes and mineral systems*. Springer-Verlag, New York. p.101-123.

Pollard, P.J. 2001. Sodic(-calcic) alteration in Fe oxide-Cu-Au districts: An origin via unmixing of magmatic H_2O-CO_2-NaCl $CaCl_2$-KCl fluids. *Mineralium Deposita*, **36**:93–100.

Previato, M., 2016. Evolução paragenética e regime de fluidos hidrotermais no sistema Borrachudo: Implicações para a metalogênese e cobre na Província Carajás. Masters dissertation. IG-USP. 131p.

Ramboz, C., Pichavant, M., Weisbrod, A. 1982. Fluid immiscibility in natural processes: use and mixture of fluid inclusion data. *Chemical Geology*, **37:**29-48.

Rämö, O.T., Dall'Agnol, R., Macambira, M.J.B., Leite, A.A.S., Oliveira, D.C., 2002. 1.88 Ga. oxidized a-type granites of the Rio Maria Region, eastern Amazonian Craton: positively anorogenic. *Journal of Geology*. **110:**603-610.

Requia, K. and Fontboté, L. 2001. The Salobo iron oxide copper – gold hydrothermal system, Carajás Mineral Province, Brazil. GSA Annual Meeting, Boston, *Abstracts with programs*, 33(6), p A-2.

Ribeiro, A.A., Suíta, M.T.F., Sial, A.N., Fallick, A.E., Eli, F., Goulard, A.E. 2009. Geoquímica de isótopos estáveis (C, S e O) das rochas encaixantes e do minério de Cu (Au) do depósito Cristalino, Província Mineral de Carajás, Pará. *Geochimica Brasiliensis*, **23:**159-176.

Roedder, E. 1984. Fluid inclusions. Mineral. Soc. America. *Reviews in Mineralogy*, 12, 644p.

Roedder, E. and Bodnar, R.J. 1980. Geologic pressure determinations from fluid inclusion studies. Annu. Rev. *Earth and Planetary Science Letters*, **8:**263-301.

Ronzê, P.C. Soares, A.D.V., Santos, M.G., Barreira, C.F. 2000. Alemão copper-gold (U-REE) deposit, Carajás, Brazil. *In*: Porter, T.M. (Ed.). *Hydrothermal iron oxide copper-gold & related deposits: a global perspective.* V. 1. PGC Publishing, Adelaide, pp 191-202.

Samson I, Anderson A. and Marshall D. (ed.) 2003. Fluid Inclusions – Analysis and Interpretation. Mineral. Assoc. *Canada, Short Course Series* v. 32, 374p.

Santos, J.O., Hartmann, L.A., Gaudette, H.E., Groves, D.I., McNaughton, N.J., Fletcher, I.R. 2000. A new understanding of the provinces of the Amazon Craton based on integration of field mapping and U-Pb and Sm-Nd geochronology. *Gondwana Research,* **3:**453-488.

Sardinha, A.S., Barros, C.E.M. & Krymsky, R. 2006. Geology, geochemistry and U–Pb geochronology of the Archean (2.74 Ga) Serra do Rabo granite stocks, Carajás Metallogenic Province, northern Brazil. *Journal of South American Earth Sciences*, **20:**327-339.

Shepherd, T.J., Rankin, A.H., Alderton, D.H.M. 1985. *A practical guide to fluid inclusion studies*. Blackie & Son Ltd., Glasgow, 239p.

Sheppard, S.M.F., 1986. Characterization and isotopic variations in natural waters, in: Valley, J.W., Taylor, H.P.J., O'Neil, J.R. (Eds.), *Stable Isotopes in High Temperature Geological Processes*. Mineralogical Society of America, Chelsea, pp.165-183.

Siepierski, L. 2016. *Geologia, Petrologia e potência para mineralizações magmáticas dos corpos máfico-ultramáficos da região de Canaã dos Carajás, Província Mineral de Carajás.* Tese de Doutorado. IG-UnB, 158p.

Silva, A.R.C., Villas, R.N., Lafon, J.M., Craveiro, G.S. 2012. Idade da alteração e mineralização do depósito de Cu-Au Visconde, Província Mineral de Carajás (Pará), Brasil. *In*: Congresso Brasileiro de Geologia, 46, Brazil, September 30-October, 6, 2012, *Proceedings*, p. 1–2.

Silva, A.R, Villas, R.N., Lafon, J., Craveiro, G.S., Ferreira, V.P. 2015. Stable isotope systematics and fluid inclusion studies in the Cu-Au Visconde deposit, Carajás Mineral Province, Brazil: implications for fluid source generation. *Mineralium Deposita*, **50:**547-569.

Soares, A.D.V., Macambira, M.J.B., Santos, M.G.S., Vieira, E.A., Masotti, F.S., Souza, C.I.J., Padilha, J.L., Magni, M.C.V. 2001. Depósito Cu (Au) Cristalino, Serra dos Carajás PA: Idade da Mineralização com base em Análises Pv-Pb em sulfetos (Dados Preliminares). In: Simpósio de Geologia da Amazônia, 7, Belém, *Proceedings...* SBG. CD-ROM.

Soares, A.D.V., Ronzê, P.C., Santos, M. G.S., Leal, E.D., Barreira, C.F. 1999. Geologia e mineralizações do depósito de Cu-Au Alemão − Província Mineral de Carajás (PA). In: Simpósio de Geologia da Amazônia, 5, 1999. Manaus. *Resumos expandidos...* Manaus: SBG, 1999, p. 144-147.

Spencer, R.J., Moller, N., Weare, J.H., 1990. The prediction of mineral solubilities in natural waters: a chemical equilibrium model for the Na-K-Ca-Mg-Cl-SO$_4$-H$_2$O systems at the temperatures below 25 ° C. *Geochimica et Cosmochimica Acta,* **54:**575–590.

Sterner S.M., Hall D.L., Bodnar R.J. 1988. Synthetic fluid inclusions. V. Solubility relations in the system NaCl-KCl-H$_2$O under vapor-saturated conditions. *Geochimica et Cosmochimica Acta*, **52:**989-1005.

Tallarico, F.H.B., Figueiredo B.R., Groves D.I., Kositcin N., McNaughton N.J., Fletcher I.R., Rego J.L. 2005. Geology and SHRIMP U–Pb geochronology of the Igarapé Bahia deposit, Carajás copper–gold belt, Brazil: an Archean (2.57 Ga) example of iron–oxide Cu–Au–(U− REE) mineralization. *Economic Geology*, **100:**7–28.

Tavares, F.M. 2015. Evolução geotectônica do nordeste da Província Carajás. Tese de doutorado. IG-UFRJ. 115p.

Taylor, H. P. Jr., 1974. The application of oxygen and hydrogen studies to problems of hydrothermal alteration and ore deposition, *Economic Geology*, **69:**843-883.

Taylor, B.E. 1986. Magmatic volatiles: isotopic variation of C, H, and S. *Reviews in Mineralogy*, **16**:185-225.

Taylor, B.E. 1992. Degassing of H$_2$O from rhyolitic magma during eruption and shallow intrusion, and the isotopic composition of magmatic water in hydrothermal systems. *Geological Survey of Japan Report,* **279:**190–194.

Taylor, H.P. Jr. 1997, Oxygen and hydrogen isotope relationships in hydrothermal mineral deposits. In: Barnes HL (ed) *Geochemistry of hydrothermal ore deposits*, Wiley, New York, pp 229 − 302.

Taylor, II.P., Frechen, J., Dcgens, E.T. 1967, Oxygen and carbon isotope studies of carbonatites from the Laacher See District, West Germany and the Alno District, Sweden. *Geochimica et Cosmochimica Acta*, **31:**407-30.

Teixeira, A.S., Ferreira Filho, C.F., Giustina, M.E.S.D., Araújo, S.M., Silva, H.H.A.B. 2015. Geology, petrology and geochronology of the Lago Grande layered complex: evidence for a PGE-mineralized magmatic suíte in the Carajás Mineral Province, Brazil. *Journal of South American Earth Sciences*, **64**:116-138.

Teixeira, J.B.G., 1994. Geochemistry, petrology, and tectonic setting of Archean basaltic and dioritic rocks from the N4 Iron deposit, Serra dos Carajás, Pará, Brazil. Doctoral thesis. IG-USP. 161p.

Torresi, I. Xavier, R.P., Bortholoto, D.F.A., Monteiro, L.V.S. 2012. Hydrothermal alteration, fluid inclusions and stable isotope systematics of the Alvo 118 iron-oxide-copper-gold deposit, Carajás Mineral Province (Brazil): Implications for ore genesis. *Mineralium Deposita*, **47:**299-323.

Trendall, A.F., Basei, M.A.S., De Laeter, J.R., and Nelson, D.R., 1998, SHRIMP U-Pb constraints on the age of the Carajás formation, Grão Pará Group, Amazon Craton. *Journal of South American Earth Sciences*, **11:**265-277.

Vale, 2003. Projeto Cu-Au Cristalino. *Internal report*.

van den Kerkhof, A.M. and Hein, U. 2001. Fluid inclusion petrography. *Lithos* 55, 27–47.

Vasquez, L.V., Rosa-Costa, L.R., Silva, C.G., Ricci, P.F., Barbosa, J.O., Klein, E.L., Lopes, E.S., Macambira, E.B., Chaves, C.L., Carvalho, J.M., Oliveira, J.G., Anjos, G.C., Silva, H.R., 2008. *Geologia e Recursos Minerais do Estado do Pará: Sistema de Informações Geográficas–SIG: Texto Explicativo dos Mapas Geológico e Tectônico e de Recursos Minerais do Estado do Pará.* Organizers: M.L Vasquez, L.T. Rosa Costa. Scale1:1.000.000. Belém: CPRM.

Villas, R.N.N. and Galarza, M.A.T., Almada, M.C.O., Viana, A.S., Ronzé, P.C. 2001. Geologia do depósito Igarapé Bahia/Alemão, Província Carajás, Pará. In: Jost H, Brod JA, Queiroz ET (eds) *Caracterização de depósitos auríferos em distritos mineiros brasileiros*, DNPM/ADIMB, Brasília, DF, pp 215 – 240.

Wenner, D.B. and Taylor, H.P. Jr., 1971. Temperatures of serpentinization of ultramafic rocks based on 18O/16O fractionation between coexisting serpentine and magnetite. *Contribution to Mineral Petrology,* **32:**165-185.

Wilkinson, J.J., 2001. Fluid inclusions in hydrothermal ore deposits. *Lithos*: **55**, 229-272.

Williams, P.J., Barton, M.D., Johnson, D.A, Fontboté, L., de Haller, A., Mark, G., Oliver, N.H.S., Marschik, R., 2005. Iron oxide-copper-gold deposits: Geology, space-time distribution, and possible modes of origin. *Economic Geology 100th Anniversary* Volume, p. 371−405.

Williams, P.J., Kendrick, M.A., Xavier, R.P., 2010. Sources of ore fluid components in IOCG deposits. In: Porter TM (ed.) *Hydrothermal Iron Oxide Copper–Gold and Related Deposits: A Global Perspective*, Adelaide: PGC Publishing. pp. 107–116.

Xavier, R.P., Monteiro, L.V.S., Moreto, C.P.N., Pestilho, A.L.S., Melo, G.H.C., Silva, M.A.D., Aires, B., Ribeiro, C., Silva, F.H.F. 2012. The iron oxide copper-gold system of the Carajás Mineral Province, Brazil. *Economic Geology*, *Special Publication*, 16, Chapter X.

Xavier, R.P., Moreto, C.P.N., de Melo, G.H.C., Toledo, P., Hunger, R., Deminardo, M., Faustinoni, J., Lopes, Ananda. 2017. Geology and metallogeny of Neoarchean and Paleoproterozoic copper systems of the Carajás Domain, Amazonian Craton, Brazil. *Proceedings* of the 14th BiennialSGA Meeting of the Society for Geology Applied to Mineral Deposits, Quebec, Canada. 20-23 August, pp. 899-902.

Zheng, Y.F. 1991. Calculation of oxygen isotope fractionation in metal oxides. *Geochimica et Cosmochimica Acta,* **55:**2299-2307

Zheng, Y.F. 1993. Calculation of oxygen isotope fractionation in hydroxyl-bearing silicates. *Journal of South American Earth Sciences,* **120:**247-263.

Zheng, Y.F. 1994. Oxygen isotope fractionation in metal monoxides. *Mineralogical Magazine*, **58a**:1000-1001.

5 CONCLUSÕES E CONSIDERAÇÕES FINAIS

O depósito cupro-aurífero Cristalino, de idade arqueana, consiste de corpo de minério principal de direção ~N15°W, hospedado principalmente em rochas vulcânicas da Formação Parauapebas e, mais restritamente, em formações ferríferas bandadas da Formação Carajás. As rochas vulcânicas mostram-se moderada a intensamente alteradas, sendo reconhecidas as alterações sódica, cálcio-férrica, potássica, propilítica e carbonática, as duas primeiras desenvolvidas a temperaturas mais altas (410°->550° C) sob regime dúctil-rúptil, e as demais a temperaturas mais baixas (220°-410° C), sob regime essencialmente rúptil.

A alteração sódica produziu albita tabuleiro de xadrez quase pura, quantidades menores de turmalina schorlítica e minerais ricos em ETRL (Ce-allanita, monazita). Ela foi seguida pela alteração cálcico-férrica que gerou abundante actinolita (X_{Mg}=0,87–0,69, Cl = até 0,59 % em peso) além de Ce-allanita e magnetita associadas a disseminações e corpos brechoides compostos de calcopirita-pirita-magnetita-Au (associação de minério precoce). Localmente, Fe-edenita (X_{Mg}=0,67-0,42, Cl = até 2,94 % em peso) substitui as assembleias cálcico-férricas dentro de restritos halos de alteração sódico-cálcica.

As alterações potássicas (K-feldspato±biotita) e propilítica/carbonatação (clorita-epidoto-calcita) entram em cena a seguir, superpondo-se a assembleias hidrotermais previamente formadas. K-feldspato é praticamente estoiquiométrico, porém contém algumas impurezas notadamente BaO (até 1,21 % em peso). Clorita mostra a maior variação composicional dentre todos os minerais e sua composição parece ter sido particularmente controlada pelo tipo de rocha encaixante, química do fluido hidrotermal e temperatura. Tanto chamosita como clinocloro (X_{Fe}=0,37-0,80) estão presentes, a primeira sendo mais comum. Os teores de cloro são em geral < 0.02 % em peso e um pouco mais significativo em clorita que substitui albita tabuleiro de xadrez (até 0,06 % em peso).

Contemporaneamente às alterações potássica e propilítica ocorreu nova mineralização, quando foi precipitada a associação de minério tardia constituída de calcopirita-Au±pirita ±hematita na forma de matriz de brechas e em veios.

A história hidrotermal do depósito Cristalino evoluiu de ~550° a 150° C sob pressões estimadas de 0,6 a 2,6 Kbar consistentes com o regime deformacional rúptil e transição para o regime rúptil-dúcitl. Inicialmente o fluido mineralizador era quente, hipersalino e de composição aproximada pelo sistema H_2O-NaCl-$CaCl_2$-CO_2±$MgCl_2$±$FeCl_2$. Salinidades podem ter ultrapassado 55.1 % em peso equiv. NaCl, mas se reduziram progressivamente a 7.9 % em peso NaCl equiv., de 250° C em diante após a incursão de águas superficiais no

sistema. Inicialmente enriquecido em ^{18}O e empobrecido em D ($\delta^{18}O_{vsmow}$ =+9,73 a +6,48‰; δD_{vsmow}= -30,17 a -40,25‰) e muito provavelmente derivado de fontes magmáticas, o fluido se tornou relativamente empobrecido em ^{18}O e enriquecido em D ($\delta^{18}O_{vsmow}$ =+5,57 a -0,28‰; δD_{vsmow}= -19,15 a -22,24‰) em decorrência de diluição causada pela mistura com água meteórica.

O fluido mineralizador pode ter recebido, pelo menos em parte, contribuição de água emanada de magmas que geraram granitos neoarqueanos, tais com os Granitos Serra do Rabo e Planalto (2,74 Ga). Em favor dessa hipótese, há a datação da associação de minério precoce em 2719 ±39 Ma (Pb-Pb, por lixiviação em calcopirita, Soares *et al.* 2001).

Valores de $\delta^{13}C_{VPDB}$ em calcita de veios e brechas (-6,5 a -3,8‰) indicam uma fonte profunda para CO_2, provavelmente liberado de alguma câmara magmática subjacente. Por seu turno, valores de $\delta^{34}S_{VCDT}$ em calcopirita (+1,6 a +3,5 ‰) sugerem uma fonte homogênea e provavelmente de origem ígnea para o enxofre. Embora a maioria dos dados apontem para uma filiação magmática, algumas amostras de calcita e sulfeto revelam expressiva influência de rochas sedimentares em suas composições isotópicas.

Provavelmente transportados em grande parte como complexos de cloreto (> 350º C), Cu e Au foram precipitados em resposta à diminuição de temperatura e da atividade de Cl⁻, e ao aumento do pH. A formação da associação de minério tardia foi adicionalmente favorecida pelo aumento de f_{O2} nos estágios mais tardios da alteração hidrotermal.

Um fluido aquoso independente, mais frio (200-150º C) e menos salino (21-3,1 % peso NaCl equiv.) parece ter circulado na área do depósito, tendo sido aprisionado como inclusões fluidas secundárias. Sua origem é desconhecida, porém ele poderia estar relacionado a alguma intrusão granítica paleoproterozoica que ocorre nas circunvizinhanças do depósito.

Os dados aqui apresentados ratificam interpretações anteriores que consideram a tipologia IOCG para o depósito Cristalino. Comparando-o com outros depósitos IOCG de Carajás, notadamente aqueles que ocorrem no setor sul do Domínio Carajás, o depósito Cristalino mostra muitas similaridades em relação ao ambiente tectônico, composição e evolução do fluido mineralizador, bem como às assinaturas isotópicas da calcita e sulfetos.

REFERÊNCIAS

Almada M.C.O. & Villas, R.N. 1999. O depósito Bahia: um possível exemplo de depósito vulcanogenênico tipo Besshi arqueano em Carajás. *Revista Brasileira de Geociências*, **29:** 579-592.

Almeida J.A.C., Dall'Agnol R., Dias S.B., Althoff F.J. 2010. Origin of the Archean leucogranodiorite–granite suites: evidence from the Rio Maria terrane and implications for granite magmatism in the Archean. *Lithos*, **120**: 235–257.

Almeida J.A.C., Dall'Agnol R., Oliveira M.A., Macambira M.J.B., Pimentel M.M., Rämö O.T., Guimarães F.V., Leite A.A.S. 2011. Zircon geochronology and geo-chemistry of the TTG suites of the Rio Maria granite-greenstone terrane: implications for the growth of the Archean crust of Carajás Province, Brazil. *Precambrian Research,* **187:** 201–221.

Althoff F.J., Barbey P., Boullier A.M. 2000. 2.8 - 3.0Ga plutonism and deformation in the SE Amazonian craton: the Archean granitoids of Marajoara (Carajás Mineral Province, Brazil). *Precambrian Research*, **104:**187-206.

Araújo O.J.B., Maia R.G.N., Jorge-João X.S., Costa J.B.S. 1988. A megaestruturação da folha Serra dos Carajás. *In*: SBG, 7º Congresso Latino Americano de Geologia, *Anais...* p. 324-333.

Araújo O.J.B. & Maia R.G.N. 1991. *Serra dos Carajás, folha SB-22-Z-A, Estado do Pará. Texto explicativo*. Brasília,DF, DNPM/CPRM. 164p. (Programa de Levantamentos Geológicos Básicos do Brasil).

Augusto R.A., Monteiro L.V.S., Xavier R., Souza Filho C.R. 2008. Zonas de alteração hidrotermal e paragênese do minério de cobre do Alvo Bacaba, Província Mineral de Carajás (PA). *Revista Brasileira de Geociências,* **38**(2): 263-277.

Avelar V.G., Lafon J.M., Correia Jr. F.C., Macambira E.M.B. 1999. O magmatismo arqueano da região de Tucumã – Província Mineral de Carajás: Novos resultados geocronológicos. *Revista Brasileira de Geociências*, **29(**4): 453-460.

Barros C.E.M., Barbey P., Boullier A.M. 2001. Role of Magma Pressure, Tectonic Stress and Crystallization Progress in the Emplacement of Syn-tectonic Granites. The A-type Estrela Granite Complex (Carajás Mineral Province, Brazil). *Tectonophysics,* **343:** 93– 109.

Barros C.E.M., Macambira M.J.B., Barbey P., Scheller T. 2004. Dados isotópicos Pb-Pb em zircão (evaporação) e Sm-Nd do Complexo Granítico Estrela, Província Mineral de Carajás, Brasil: Implicações petrológicas e tectônicas. *Revista Brasileira de Geociências*, 34(1): 531-538.

Barros C.E.M., Sardinha A.S., Barbosa J.P.O., Macambira M.J.B., Barbey P., Boullier A.M. 2009. Structure, petrology, geochemistry and zircon U/Pb and Pb/Pb geochronology of the synkinematic Archean (2.7 Ga) A-type granites from the Carajás Metallogenic Province, northern Brazil. *The Canadian Mineralogist*, **47**: 1423-1440.

Barton M.D. & Johnson D.A. 2004. Footprints of Fe oxide (-Cu-Au) system. *University of Western Australia Special Publication*, **33**: 12-116.

Barton M.D. & Johnson D.A. 1996. Evaporitic source model for igneous related fe oxide– (REE–Cu–Au–U) mineralization. *Geology,* **24:** 259–262.

Beisiegel V.R., Bernardelli A.L., Drummond N.F., Ruff A.W., Tremaine J.W. 1973. Geologia e recursos minerais da Serra dos Carajás. *Revista Brasileira de Geociências*, **3**(4): 215-242.

Borisenko A.S. 1982. Analysis of salt content of solutions in gas-liquid inclusions in minerals using cryometric methods. In: Laverov, N.P. (Ed.), *Ispolzovaniye metodov*

Borisenko A.S. 1977. Study of salt composition of fluid inclusions in minerals using cryometric technique. *Geologiya i Geofizica*. **8:**16–27.

Botelho N.F., Moura M.A., Teixeira L.M., Olivo G.R., Cunha L.M., Santana M.U. 2005. Caracterização geológica e metalogenética do depósito de Cu±(Au, W, Mo, Sn) Breves, Carajás. *In*: Matini, O.J., Queiroz, E.T., Ramos, B.W. (Ed.). *Caracterização de depósitos minerais em distritos mineiros da Amazônia*. Brasília, DF: DNPM – CT/MINERAL–ADIMB, 2005. Cap. 6, p 339-389.

Brito Neves B.B. & Cordani U.G. 1991. Tectonic evolution of South America during the Late Proterozoic. *Precambrian Research*, **53**: 23-40.

Cathelineau, M. & Nieva D. 1985. A chlorite solid solution geothermometer. The Los Azufres (Mexico) geothermal system. *Contribution to Mineral Petrology*. **91:**235-244.

Clayton R. N. & Mayeda T. 1963. The use of bromine pentafluoride in the extraction of oxygen from oxides and silicates for isotopic analysis. *Geochimica et Cosmochimica Acta*, **27**:47-52.

Costa J.B.S., Araújo O.J.B., Santos A., Jorge João X.S., Macambira M.J.B., Lafon J.M. 1995. A Província Mineral de Carajás: aspectos tectono-estruturais, estratigráficos e geocronológicos. *Boletim do Museu Paraense Emílio Goeldi*, **7:** 199-235.

Craveiro G.S., Villas R.N.N., Xavier R.P. 2018. A Fluid Inclusion and Stable Isotope (O, H, S and C) study of the Archean IOCG Cristalino Deposit, Carajás Province, Brazil: Implications to ore genesis. *Manuscrito submetido para publicação*.

Dall'Agnol R., Teixeira N.P., Rämö O.T., Moura C.A.V., Macambira, M.J.B., Oliveira D.C.O. 2005. Petrogenesis of the Paleoproterozoic Rapakivi A-type granite of the Archean Carajás Metallogenetic Province, Brazil. *Lithos,* **80:**101-129.

Dall'Agnol R., Oliveira M.A., Almeida J.A.C., Althoff F.J., Leite A.A.S., Oliveira D.C., Barros C.E.M. 2006. Archean and Paleoproterozoic granitoids of the Carajás Metallogenic Province, eastern Amazonian Craton. *In*: Dall'Agnol, R., Rosa-Costa, L.T., Klein, E.L. (Ed.), *Symposium on Magmatism, Crustal Evolution, and Metallogenesis of the Amazonian Craton*. Belém, PRONEX-UFPA-SBGNO, pp. 99–150 (Volume and Field Trip Guide).

Dall'Agnoll R., Oliveira D.C., Lamarão C.N. 2013. Magmatismo granitoide arqueano e evolução geológica do Subdomínio de Transição da Província Carajás, sudeste do Cráton Amazônico, Brasil. *Boletim do Museu Emílio Goeldi*, **8**(3): 251-256.

Dall'Agnol R., Teixeira N.P., Rämö O.T., Moura C.A.V., Macambira M.J.B., Oliveira D.C. 2005. Petrogenesis of the Paleoproterozoic, rapakivi, A-type granites of the Archean Carajás Metallogenic Province, Brazil. *Lithos*, **80**: 101–129.

Davis D.W., Lowenstein T.K., Spencer R.J. 1990. Melting behavior of fluid inclusions in laboratory-grown halite crystals in the systems NaCl – H_2O, NaCl – KCl – H_2O, NaCl – $MgCl_2$ – H_2O and NaCl – $CaCl_2$ – H_2O. *Geochimica et Cosmochimica Acta,* **54:** 591 – 601.

Dias G.S., Macambira M.J.B., Dall'Agnol R., Soares A.D.V., Barros C.E.M. 1996. Datação de zircões de sill metagabro: comprovação da idade arqueana da Formação Águas Claras,

Carajás, Pará. *In*: SBG, 5° Simpósio de Geologia da Amazônia, Belém. *Resumos Expandidos...* p. 376-379.

DOCEGEO (Rio Doce Geologia e Mineração S.A) 1988. Revisão litoestratigráfica da província mineral de Carajás. *In*: SBG, 35° Congresso Brasileiro de Geologia, Belém. *Anais...* **1**: 11-54.

Dreher A.M., Xavier R.P., Taylor B.E., Martini S.L. 2007. New geologic, fluid inclusion and stable isotope studies on the controversial Igarapé Bahia Cu–Au deposit, Carajás Province, Brazil. *Mineralium Deposita*. DOI 10.1007/s00126-007-0150-6.

Ercit T.S. 2002. The mess that is "allanite". *The Canadian Mineralogist*, **40**:1411-1419.

Feio G.R. L. 2011. *Magmatismo granitoide arqueano da área de Canaã dos Carajás: Implicações para a evolução crustal da Província Carajás*. Tese de Doutorado, Universidade Federal do Pará, Belém. 205 p.

Feio G.R.L., Dall'Agnol R., Dantas E.L., Macambira M.J.B., Santos J.O.S., Althoff F.J., Soares J.E.B. 2013. Archean granitoid magmatism in the Canaã dos Carajás area: Implications for crustal evolution of the Carajás province, Amazonian craton, Brazil. *Precambrian Research*, **227**: 157-186.

Feio G.R.L., Dall'Agnol R., Dantas E.L., Macambira M.J.B., Gomes A.C.B., Sardinha A.S., Oliveira D.C., Santos R.D., Santos P.A. 2012. Geochemistry, geochronology, and origin of the Neoarchean Planalto Granite suite, Carajás, Amazonian craton: A-type or hydrated charnockitic granites? *Lithos*, **151**: 57-73.

Ferreira Filho C.F., Cunha E.M., Lima, A.C., Cunha J.C., 2013. Depósito de Níquel-Cobre Sulfetado de Santa Rita, Itagibá, Bahia, Brasil. *Série arquivos abertos* (Companhia Baiana de Pesquisa Mineral, Salvador – Bahia), **39**: 1-59.

Galarza M.A. & Macambira M.J.B. 2002. Geocronologia e evolução crustal da área do depósito de Cu-Au Gameleira, Província Mineral de Carajás (Pará), Brasil. *Revista do Instituto de Geociências da USP*, **2**: 143-159.

Galarza M.A., Macambira M.J.B., Villas R.N. 2008. Dating and isotopic characteristics (Pb and S) of the Fe oxide-Cu-Au-U-REE Igarapé Bahia ore deposit, Carajás mineral province, Pará state, Brazil. *Journal of South Earth Sciences*, **25**: 377–397.

Gibbs A.K., Wirth K.R., Hirat W.K., Olszewsk W.J. 1986. Age and composition of the Grão-Pará group volcanics, Serra dos Carajás. *Revista Brasileira de Geociências*, **16**(2): 201-211.

Goldstein R.H. & Reynolds T. J. 1994. Systematics of fluid inclusions in diagenetic minerals SEMP. Short Course, v. 31, SOc, *Sediment Geology*, Tulsa, Oklahoma, 198p.

Gomes A.C.B. & Dall'Agnol R. 2007. Nova associação tonalítica-trondhjemítica Neoarqueana na região de Canaã dos Carajás: TTG com altos conteúdos de Ti, Zr e Y. *Revista Brasileira de Geociências*: **37**, 182-193.

Gomes A.C.B., 2003. *Geologia, petrografia e geoquímica dos granitoides de Canaã dos Carajás, SE do Estado do Pará*. Dissertação de Mestrado, Universidade Federal do Pará, Belém, 160p.

Gomes C.B., Cordani U.G., Basel M.A.S. 1975. Radiometric ages from the Serra dos Carajás Area, Northern Brazil. *Geological Society of America*, **86**:939-945.

Grainger C. J., Groves D. I., Tallarico F. H. B., Fletcher I. R. 2008. Metallogenesis of the Carajás Mineral Province, Southern Amazon Craton, Brazil: Varying styles of Arquean

through Paleoproterozoic to Neoproterozoic base- and precious-metal mineralization. Ore *Geology Reviews*: **33**, 451–489.

Groves D.I., Bierlein F.P., Meinert L.D., Hizman M.W. 2010. Iron oxide copper-gold (IOCG) deposits through earth history: implications of origin, lithospheric setting, and distinction from other epigenetic iron oxide deposits. *Economic Geology*, **105**: 641-654.

Haller A. & Fontboté L. 2009. The Raúl-Condestable iron oxide copper-gold deposit, central coast of Peru: ore and related hydrothermal alteration, sulfur isotopes, and thermodynamic constrains. *Economic Geology*, **104**: 365-384.

Hirata W.K., Rigon J.C., Kadekaru K., Cordeiro A.A.C., Meireles E.A. 1982. Geologia Regional da Província Mineral de Carajás. *In*: SBG/NO, 1º Simpósio de Geologia da Amazônia, Belém, *Anais...* p. 100–110.

Hitzman M.W., Oreskes N., Einaudi M.T. 1992. Geological characteristics and tectonic setting of Proterozoic iron oxide (Cu-U-Au-REE) deposits. *Precambrian Research* **58**:241 – 287.

Holland T. & Blundy J. 1994. Non-ideal interactions in calcic amphiboles and their bearing on amphibole-plagioclase thermometry. *Contribution to Mineral Petrology,* **116**:433-47.

Huhn S.B., Macambira M.J.B., Dall'Agnol R. 1999a. Geologia e geocronologia Pb-Pb do Granito Alcalino Planalto, Região da Serra do Rabo, Carajás-PA. *In*: SBG, 6° Simpósio de Geologia da Amazônia, Belém, *Resumos expandidos...* p.463-466.

Huhn S.R.B., Souza C.I.J., Albuquerque M.C., Leal E.D., Brustolin V. 1999b. Descoberta do depósito Cu(Au) Cristalino: geologia e mineralização associada - Região da Serra do Rabo – Carajás (PA). *In*: : SBG, 6° Simpósio de Geologia da Amazônia, Belém, *Resumos expandidos...* p. 140-143.

Kranidiotis P. & MacLean W.H. 1987. Systematic of chlorite alteration at the Phelps Dodge massive sulfide deposit, Matagami, Quebec. *Economic Geology*, **82**:1898-1911.

Kyser T.K. & O'Neil J.R. 1984. Hydrogen isotope systematics of submarine basalts. *Geochimica et Cosmochimica Acta*, **48**: 2123-2133.

Lancaster-Oliveira J.A., Fanton J., Almeida A.J., Leveille R.A., Vieira S. 2000. Discovery and geology of the Sossego copper – gold deposit, Carajás District, Pará State, Brazil. *In*: IUGS, 31th International Geologial Congress, Precedings…[CD-ROM].

Leite A.A.S., Dall'Agnol R., Althoff F.J. 1999. Geoquímica e aspectos petrogenéticos do Granito Xinguara, Terreno Granito-Greenstone de Rio Maria–Cráton Amazônico. *Revista Brasileira de Geociências*, **23** (3):429–436.

Leite A.A.S., Dall'Agnol R., Macambira M.J.B., Althoff F.J. 2004. Geologia e Geocronologia dos granitoides Arqueanos da região de Xinguara (PA) e suas implicações na evolução do Terreno Granito-Greenstone de Rio Maria. *Revista Brasileira de Geociências*, **34**:447–458.

Lindenmayer Z. G., Fleck A., Gomes C.H., Santos A.B.S., Caron R., Paula F.C., Laux J.H., Pimentel M.M., Sardinha A.S. 2005. Caracterização geológica do alvo estrela (Cu-Au), Serra dos Carajás, Pará *In*: Marini O.J., Queiroz E.T., Ramos B.W (Ed.) *Caracterização de Depósitos Minerais em Distritos Mineiros da Amazônia*. DNPM, CT-Mineral / FINEP, ADIMB, 2005, cap. IV, 157-226.

Lindenmayer Z.G., Laux J.H., Teixeira J.B.G. 2001. Considerações sobre a origem das Formações Ferríferas da Formação Carajás, Serra dos Carajás. *Revista Brasileira de Geociências*, **31**(1):21-28.

Lobato L.M., Rosière C.A., Silva R.C.F., Zucchetti M., Baars F.J., Seoane J.C.S., Rios F.J., Pimentel M., Mendes G.E., Monteiro A.M. 2005. A mineralização hidrotermal de ferro da Província Mineral de Carajás - controle estrutural e contexto na evolução metalogenética da Província. *In*: Marini O.J., Queiroz E.T., Ramos B.W (Ed.). *Caracterização de Depósitos Minerais em Distritos Mineiros da Amazônia*. DNPM, CT-Mineral / FINEP, ADIMB, 2005, cap II, 25–92.

Macambira E.M.B., Ricci P.S.F., Anjos G.C. 2013. Contexto geológico e potencial mineral da Folha Repartimento (SB.22-X-A) - Estado do Pará. *In*: SBG, 13° Simpósio de Geologia da Amazônia, Belém, Anais... [CD-ROM].

Macambira, E.M.B., Vale, A.G. 1997. *São Félix do Xingu: folha SB.22-Y-B, Estado do Pará, escala 1:250.000. Texto Explicativo*. Brasília, DF, DNPM/CPRM. 344 p., il. (Programa Levantamentos Geológicos Básicos do Brasil).

Macambira, J.B. 2003. *O ambiente deposicional da Formação Carajás e uma proposta de modelo evolutivo para a Bacia Grão Pará*. Tese de doutorado, Campinas-SP, Universidade Estadual de Campinas, 217p.

Macambira J.B., Macambira M.J.B., Scheller T., Gomes A.C.B. 1996. Geocronologia Pb/Pb e tipologia de zircões de rochas vulcânicas da Formação Carajás-Pará: indicador da idade dos BIFs. *In*: SBG/NE, 39° Congresso Brasileiro de Geologia, *Resumos Expandidos...* pp. 516–518.

Macambira M.J.B. & Lafon, J.M. 1995. Geocronologia da Província Mineral de Carajás: síntese dos dados e novos desafios. *Boletim Museu Paraense Emílio Goeldi*, *(Série Ciências da Terra),* **7:**263–288.

Macambira M.J.B. & Lancelot J. 1996. Time constraints for the formation of the Archean Rio Maria crust, southeastern Amazonian Craton, Brazil. *International Geology Review*, **38**:1134–1142.

Machado N., Lindenmayer Z., Krogh T.H., Lindenmayer Z.G. 1991. U-Pb geochronology of Archaean magmatism and basement reactivation in the Carajás area, Amazon shield, Brazil. *Precambrian Research*, **49:**329-354.

Mansur E.T. & Ferreira Filho C.F. 2016. Magmatic structure and geochemistry of the Luanga Mafic-Ultramafic Complex: Further constrains for the PGE-mineralized magmatism in Carajás. *Lithos* **266/267**:28-43.

Medeiros Neto F.A. & Villas, R.N.N. 1985. Geologia da jazida de Cu-Zn do corpo 4E-Pojuca, Serra dos Carajás. *In*: SBG/Norte, 3° Simpósio de Geologia da Amazônia. Belém, Anais..., p. 97-112.

Meireles E. De M., Hirata W.K., Amaral A.F., Medeiros Filho C.A., Gato W. 1984. Geologia das Folhas Carajás e Rio Verde, Província Mineral dos Carajás, Estado do Para. *In*: SBG, 5° Congresso Brasileiro de Geologia, Rio de Janeiro. *Anais...* p :2164-2174.

Meirelles M.R. & Dardenne M.A. 1991. Vulcanismo basáltico de afinidade shoshonítica em ambiente de arco arqueano, Grupo GrãoPará, Serra dos Carajás, PA. *Revista Brasileira de Geociências*, **21**:41-50.

Monteiro L.V.S., Xavier R.P., Carvalho E.R., Hitzman M.W., Johnson C.A., Souza Filho C.R., Torresi I. 2008. Spatial and temporal zoning of hydrothermal alteration and mineralization in the Sossego iron oxide- copper-gold deposit, Carajás Mineral Province, Brazil: Parageneses and stable isotope constraints. *Mineralium Deposita*, **43**:129−159.

Moreto C.P.N., Monteiro L.V.S., Xavier R.P., Amaral W.S., Santos T.J.S., Juliani C., Souza Filho C.R. 2011. Mesoarchean (3.0 and 2.86 Ga) host rocks of the iron oxide-Cu-Au Bacaba deposit, Carajás Mineral Province: U-Pb geochronology and metallogenetic implications. *Mineralium Deposita*, **46**:789-811.

MoretoC.P.N., MonteiroL.V.S., Xavier R.P., Creaser R. A., DuFrane A., Tassinari C. G., Sato K., Kemp A., Amaral W. S. 2015. Neoarchean and Paleoproterozoic Iron Oxide-Copper-Gold Events at the Sossego Deposit, Carajás Province, Brazil: Re-Os and U-Pb Geochronological Evidence. *Economic Geology and the Bulletin of the Society of Economic Geologists*, **110**:809-835.

Mougeot R., Respaut J.P., Briqueu L., Ledru P., Milesi J.P., Lerouge C., Marcoux E., Huhn S.B., Macambira M.J.B. 1996. Isotope geochemistry constrains for Cu, Au mineralizations and evolution of the Carajás Province (Para, Brazil). *In*: SBG, 7° Congresso Brasileiro de Geologia, Salvador. Anais... p, 321–324.

Neves M.P., Villas R.N., Galarza M.A. 2006. Datação e avaliação da fonte dos metais do Depósito Sossego, Região de Carajás: Evidências isotópicas de Pb e Sm-Nd. *In*: SBG, 43° Congresso Brasileiro de Geologia, Belém, Anais...[CD-ROM].

Nogueira A.C.R., Truckenbrodt W., Pinheiro R.V.L. 1995. Formação Águas Claras, Pré-Cambriano da Serra dos Carajás: redescrição e redefinição litoestratigráfica. *Boletim Museu Paraense Emílio Goeldi*, 7:177–277.

Oliveira J.R. 1994. *Serra Pelada, folha SB.22-Z-A, Estado do Pará. Texto explicativo*. Brasília,DF, DNPM/CPRM. 248p. il. (Programa de Levantamentos Geológicos Básicos do Brasil).

Oliveira M.A., Dall'Agnol R., Althoff F.J., Leite A.A.S. 2009. Mesoarchean sanukitoid rocks of the Rio Maria Granite-Greenstone Terrane, Amazonian craton, Brazil. *Journal of South American Earth Sciences*, **27**:146–160.

Oliveira M.A., Dall'Agnol R., Scaillet B. 2010. Petrological constraints on crystallization conditions of Mesoarchean Sanukitoid Rocks, Southeastern Amazonian Craton, Brazil. *Journal of Petrology*, **51**:2121–2148.

Olszewski W.J., Wirth K.R., Gibbs A.K., Gaudette H.E. 1989. The age, origin and tectonics of the Grão Pará Group and associated rocks, Serra dos Carajás, Brazil: Archean continental volcanism and rifting. *Precambrian Research*, **42**: 229-254.

Pereira R.M.P., Rosière C.A., Santos J.O.S., Lobato L.M., Figueiredo e Silva R.C., McNaughton N.J. 2009. Unidade Caninana: sequência clástica paleoproterozoica revelada por datação U em zircões detríticos da Província Mineral Carajás. *In*: SBG, 11° Simpósio de Geologia da Amazônia, Manaus, Anais... [CD-ROM].

Pimentel M.M., Lindenmayer Z.G., Laux J.H., Armstrong R., Araujo J.C. 2003. Geochronology and Nd isotope geochemistry of the gameleira Cu–Au deposit, Serra dos Carajás, Brazil: 1.8–1.7 Ga hydrothermal alteration and mineralization**.** *Journal of South American Earth Sciences*, **15**, 803-813.

Pinheiro R.V.L & Holdsworth R.E. 2000. Evolução tectonoestratigráfica dos sistemas transcorrentes Carajás e Cinzento, Cinturão Itacaiúnas, na borda leste do Cráton Amazônico, Pará*. Revista Brasileira de Geociências*: **30**(4), 597-606.

Pinto, A. 2012. Salobo Copper Mine Feasibility in Carajás, Pará State. *In*: ADIMB, 5th Brazilian Symposium on Mineral Exploration. 2012. Ouro Preto - MG, Brazil.

Pollard P.J. 2001. Sodic(-calcic) alteration in Fe oxide-Cu-Au districts: An origin via unmixing of magmatic H_2O-CO_2-NaCl $CaCl_2$-KCl fluids. *Mineralium Deposita*, **36**:93–100.

Pollard P.J., Mark G., Mitchell L. 1998. Geochemistry of post-1540 Ma granites in the Cloncurry district. *Economic Geology*, **93**:1330–1344.

Pollard P.J. 2006. An intrusion-related origin. For Cu-Au mineralization in iron oxide-copper-gold (IOCG) provinces. *Mineralium Deposita*, **41**:179-187.

Previato M., 2016. *Evolução paragenética e regime de fluidos hidrotermais no sistema Borrachudo: Implicações para a metalogênese e cobre na Província Carajás*. Dissertação de Mestrado. São Paulo/SP, Instituto de Geociências, Universidade de São Paulo. 131p.

Rämö O.T., Dall'Agnol R., Macambira M.J.B., Leite A.A.S., Oliveira D.C. 2002. 1.88Ga oxidized a-type granites of the Rio Maria Region, eastern Amazonian Craton: positively anorogenic! *Journal of Geology*, **110**: 603-610.

Réquia K. & Xavier R.P. 1995. Fases fluidas na evolução metamórfica do depósito polimetálico de Salobo, Província Mineral de Carajás, Pará. *Revista de Escola Minas*, Ouro Preto, **49(2):**117–122.

Ricci P.S.F. & Carvalho M.A. 2003. Rocks of the Pium-Area, Carajás Block, Brazil – A deep seated High-T Gabbroic Pluton (Charnockitoid-like) with xenoliths of enderbitic gneiss dated at 3002 Ma – The basement problem revisited. *In*: SBG, 8° Simpósio de Geologia da Amazônia, Manaus, Anais... [CD-Rom].

Ronzê P.C. Soares A.D.V., Santos M.G., Barreira C.F. 2000. Alemão copper-gold (U-REE) deposit, Carajás, Brazil. *In*: Porter, T.M. (Ed.). *Hydrothermal iron oxide copper-gold & rela ed deposits: a global perspective*. V. 1. PGC Publishing, Adelaide, pp 191-202.

Rosière C.A., Baars F.J., Seoane J.C.S., Lobato L.M., Silva L.L.da, Souza S.R.C.de, Mendes G.E. 2006. Structure and iron mineralization of the Carajás Province. *Applied Earth Science: IMM Transactions section B*, **115**:126-133.

Samson I, Anderson A., Marshall D. (eds.) 2003. *Fluid Inclusions – Analysis and Interpretation*. Mineral. Association of Canada, Short Course Series **32**, 374p.

Santos J.O.S. Geotectônica do Escudo das Guianas e Brasil-Central. 2003. *In*: Bizzi, L.A. et al. (Ed.). *Geologia, tectônica e recursos minerais do Brasil: texto, mapas e SIG. Brasília,* CPRM-Serviço Geológico do Brasil, p. 169-226.

Santos J.O.S., Hartmann L.A., Faria M.S., Riker S.R., Souza M.M., Almeida M.E., McNaugthon N.J. 2006. A compartimentação do cráton amazonas em províncias: avanços ocorridos no período 2000–2006. *In*: SBG-NO, 9° Simpósio de Geologia da Amazônia. Belém. *Anais...*[CD-ROM].

Santos J.O.S., Hartmann L.A., Gaudette H.E., Groves D.I., McNaughton N.J., Fletcher I.R., 2000. A new understanding of the provinces of the Amazon Craton based on integration of field mapping and U–Pb and Sm–Nd geochronology. *Gondwana Research*, **3**:453–488.

Santos J.O.S., Van Breemen O.B., Groves D.I., Hartmann L.A., Almeida M.E., Macnaughton N.J., Fletcher I.R. 2004. Timing and evolution of multiple Paleoproterozoic magmatic arcs in the Tapajós Domain, Amazon Craton: constraints from SHRIMP and TIMS zircon, baddeleyite and titanite U–Pb geochronology. *Precambrian Research*, **131**:73–109.

Sardinha A.S., Barros C.E.M., Krymsky R. 2006. Geology, geochemistry and U-Pb geochronology of the Archean (2.74 Ga) Serra do Rabo granite stocks, Carajás Metallogenetic Province northern Brazil. *Journal of South American Earth Sciences*: **20**, 327-339.

Shepherd T.J., Rankin, A.H., Alderton D.H.M. 1985. *A practical guide to fluid inclusion studies*. Blackie & Son Ltd., Glasgow, 239p.

Siepierski L. 2016. *Geologia, Petrologia e potência para mineralizações magmáticas dos corpos máfico-ultramáficos da região de Canaã dos Carajás, Província Mineral de Carajás*. Braísilia/DF, Tese de doutorado. Instituto de Geociências, Universidade de Brasília, 158p.

Sillitoe R.H. 2003. Iron oxide-copper-gold deposits: an Andean view. *Mineralium Deposita*, **38**, 787-812.

Silva M.G., Teixeira J.B.G., Pimentel M.M., Vasconcelos P.M., Arielo A., Rocha W.J.S.F. 2005. Geologia e mineralizações de Fe-Cu-Au do Alvo GT46 (Igarapé Cinzento, Carajás). *In*: Matini, O.J., Queiroz, E.T., Ramos, B.W. (Ed.). *Caracterização de depósitos minerais em distritos mineiros da Amazônia*. Brasília, DF: DNPM – CT/MINERAL–ADIMB, 2005 cap III. p: 94-151.

Silva A.R.C., Villas R.N., Lafon J., Craveiro G.S., Ferreira V.P. 2015. Stable isotope systematics and fluid inclusion studies in the Cu-An Visconde deposit, Carajás Mineral Province, Brazil: implications for fluid source generation. *Mineralium Deposita*, **50**:547-569.

Silva A.R.C., Villas R.N., Lafon J.M., Craveiro G.S. 2012. Idade da alteração e mineralização do depósito de Cu-Au Visconde, Província Mineral de Carajás (Pará), Brasil. *In*: SGB, 46° Congresso Brasileiro de Geologia, Santos, *Anais...*[CD-ROM].

Silva G.G., Lima J.J.C., Andrade A.R.F., Issler R.S., Guimarães G. 1974. *Geologia da Folha SC.22 – Tocantins, texto explicativo*. DNPM, Rio de Janeiro, 143p.

Soares A.D.V., Macambira M.J.B., Santos M.G.S., Vieira E.A., Masott F.S., Souza C.I.J., Padilha J.L., Magni M.C.V. 2001. Depósito Cu (Au) Cristalino, Serra dos Carajás PA: Idade da Mineralização com base em Análises Pv-Pb em sulfetos (Dados Preliminares). *In*: SBG, 7° Simpósio de Geologia da Amazônia, Belém, *Anais...* [CD-ROM].

Soares A.D.V., Ronzê P.C., Santos M. G.S., Leal E.D., Barreira C.F. 1999. Geologia e mineralizações do depósito de Cu-Au Alemão – Província Mineral de Carajás (PA). *In*: SGB, 5° Simpósio de Geologia da Amazônia, Manaus. *Resumos expandidos...* p.144-147.

Souza Z.S., Potrel A., Lafon J.M., Althoff F.J., Pimentel M.M., Dall'Agnol R., Oliveira C.G. 2001. Nd, Pb and Sr isotopes in the Identidade Belt, an Archean green- stone belt of Rio Maria region (Carajás Province, Brazil): implications for the geodynamic evolution of the Amazonian Craton. *Precambrian Research*, **109**:293–315.

Spencer R.J., Moller N., Weare J.H., 1990. The prediction of mineral solubilities in natural waters: a chemical equilibrium model for the Na-K-Ca-Mg-Cl-SO4-H2O systems at the temperatures below 25 °C. *Geochimica et Cosmochimica Acta,* **54**:575–590.

Tallarico F.H.B., Figueiredo B.R., Groves D.I., Kositcin N., McNaughton N.J., Fletcher I.R., Rego J.L. 2005. Geology and SHRIMP U–Pb Geochronology of the Igarapé Bahia Deposit, Carajás Copper–Gold Belt, Brazil: an Archean (2.57 Ga) example of iron–oxide Cu–Au–(U–REE) mineralization. *Economic Geology*, **100**:7-28.

Tassinari C.C.G. & Macambira M.J.B. 2004. A evolução tectônica do Cráton Amazônico. *In*: Mantesso-Neto, V., Bartorelli A., Carneiro, C.D.R., Brito-Neves, B.B. (Ed.). *Geologia do continente Sul-americano: evolução da obra de Fernando Flávio Marques de Almeida*. São Paulo: Beca, 2004. p. 471–485.

Tassinari C.C.G., Macambira, M.J.B. 1999. Geochronological provinces of the Amazonian Craton. *Episodes*, **22:**174-182.

Tassinari C.C.G., Mellito M.K., Babinski M. 2003. Age and origin of the Cu (Au-Mo-Ag) Salobo 3A ore deposit, Carajás mineral province, Amazonian craton, northern Brazil. *Episodes*, **26**:2−9.

Tavares F.M. 2015. *Evolução geotectônica do nordeste da Província Carajás*. Tese de doutorado. Rio de Janeiro/RJ. Instituto de Geociências, Universidade Federal do Rio de Janeiro. 115p.

Tavaza E. & Oliveira C.G. 2000. The Igarapé Bahia Au-Cu-(REE-U) deposit, Carajás Mineral Province, Northern Brazil. *In*: Porter T.M. (Ed.) *Hydrothermal iron oxide copper – gold & related deposits: a global perspective*. Australia Mineral Foundation, Adelaide, pp 203 – 212

Teixeira A.S., Ferreira Filho C.F., Giustina .E.S.D., Araújo S.M., Silva H.H.A.B. 2015. Geology, petrology and geochronology of the Lago Grande layered complex: evidence for a PGE-mineralized magmatic suíte in the Carajás Mineral Province, Brazil. *Journal of South American Earth Sciences*, **64 (2015)**: 116-138.

Teixeira J.B.G. 1994. *Geoquímica, petrologia e ambiente tectônico das rochas basálticas e dioríticas arqueanas do depósito de Fe N4, Serra dos Carajás, Pará, Brasil*. Tese de doutorado. São Paulo/SP. Instituto de Geociências, Universidade de São Paulo. 161p.

Tindle A.G., Breaks F.W., Selway J.B. 2002. Tourmaline in petalite-subtype granitic pegmatites: evidence of fractionation and contamination from the Pakeagama Lake and Separation Lake areas of northwestern Ontario, Canada. *The Canadian Mineralogist*, **40:**753-788.

Torresi I., Xavier R.P., Bortholoto D.F.A, Monteiro L.V.S. 2012. Hydrothermal alteration, fluid inclusions of the Alvo 118 iron-oxide-copper-gold deposit, Carajás Mineral Province (Brazil): Implications of ore genesis. *Mineralium Deposita*: DOI 10.1007/s00126-011-0373-4.

Trendall A.F., Basei M.A.S., De Laeter J.R., Nelson D.R. 1998. SHRIMP U-Pb constraints on the age of the Carajás formation, Grão Pará Group, Amazon Craton. *Journal of South American Earth Sciences*, **11**:265-277.

van den Kerkhof A.M. Hein, U. 2001. Fluid inclusion petrography. *Lithos* **55**, 27–47.

Vasquez L.V., Rosa-Costa L.R., Silva C.G., Ricci P.F., Barbosa J.O., Klein E.L., Lopes E.S., Macambira E.B., Chaves C.L., Carvalho J.M., Oliveira J.G., Anjos G.C., Silva H.R. (Org). 2008 . *Geologia e Recursos Minerais do Estado do Pará: Sistema de Informações Geográficas–SIG: Texto Explicativo dos Mapas Geológico e Tectônico e de Recursos Minerais do Estado do Pará. Escala 1:1.000.000*. Belém, CPRM, 328p.

Villas R.N. & Santos M.D. 2001. Gold deposits of the Carajás Mineral Province: deposit types and metallogenesis. *Mineralium Deposita*, **36**: 300-331.

Wilkinson J.J. 2001. Fluid inclusions in hydrothermal ore deposits. *Lithos*: **55**, 229-272.

Williams P.J., Barton M.D., Johnson D.A, Fontboté L., de Haller A., Mark G., Oliver N.H.S., and Marschik R. 2005. Iron oxide-copper-gold deposits: Geology, space-time distribution, and possible modes of origin. *Economic Geology 100th Anniversary* Volume, p. 371−405.

Williams P.J. & Skirrow R.G. 2000. Overview of IOCG deposits in the Curnamona Province and Cloncurry district (eastern Mount Isa block), Australia, *In*: Porter, T. M., (Ed.)., *Hydrothermal iron oxide copper-gold and related deposits: A global perspective:* Adelaide, Australian Mineral Foundation, p. 105–122.

Wirth K.R., Gibbs,A.K., Olszewski W.J. 1986. U-Pb ages of zircons from the Grão Pará Group and Serra dos Carajás granite, Pará, Brazil. *Revista Brasileira de Geociências*, **16**:195–200.

Xavier R.P., Monteiro L. V. S., Souza Filho C. R., Torresi I., Carvalho E. R., Dreher A. M., Wiedenbeck M., Trumbull R. B., Pestilho A. L. S., Moreto C. P. N. 2010. The Iron Oxide Copper-Gold Deposits of the Carajás Mineral Province, Brazil: An Update and Critical Review. *In*: Porter, *T. M.,* (Ed), *Hydrothermal Iron Oxide Copper-Gold & Related Deposits: A Global Perspective*, v. 3 – *Advances in the Understanding of IOGC Deposits*, PGC Publishing, Adeleide., p 1-22.

Xavier R.P., Monteiro L.V.S., Moreto C.P.N., Pestilho A.L.S., Melo G.H.C., Silva M.A.D., AiresB., Ribeiro C., Silva F.H.F. 2012. The iron oxide copper-gold system of the Carajás Mineral Province, Brazil. *Economic Geology, Special Publication*, **16**, Chapter X.

Xavier R.P., Moreto C.P.N., Melo G.H.C., Toledo P., Hunger R., Deminardo M., Faustinoni J., Lopes. A. 2017. Geology and metallogeny of Neoarchean and Paleoproterozoic copper systems of the Carajás Domain, Amazonian Craton, Brazil. *In*: 14th Biennial SGA Meeting of the Society for Geology Applied to Mineral Deposits, Quebec, Canada *Proceedings…* p. 899-902.

Xavier R.P., Wiedenbeck M., Trumbull R.B., Dreher A.M., Monteiro L.V.S., Rhede D., Araújo C.E.G., Torresi I. 2008. Tourmaline B-isotopes fingerprint marine evaporites as the source of high-salinity ore fluids in iron oxide-copper-gold deposits, Carajás mineral province (Brazil): *Geology*: **36**, 743−746.
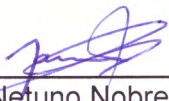
PARECER

Sobre a Defesa Pública da Tese de Doutorado de
GUSTAVO SOUZA CRAVEIRO

A banca examinadora da Tese de Doutorado de **GUSTAVO SOUZA CRAVEIRO** orientando do Prof. Dr. Raimundo Netuno Nobre Villas (UFPA), composta pelos professores doutores, Lena Virgínia Monteiro (USP), José Haroldo da Silva Sá (UFBA), Régis Munhóz Kras Borges (UFPA) e Candido Augusto Veloso Moura (UFPA) após apresentação da sua tese intitulada **"GEOLOGIA, ALTERAÇÃO HIDROTERMAL E GÊNESE DO DEPÓSITO IOCG CRISTALINO, PROVÍNCIA MINERAL DE CARAJÁS, BRASIL"**, emite o seguinte parecer:

O candidato realizou sua apresentação de forma satisfatória. Na arguição mostrou domínio da temática abordada e respondeu às perguntas formuladas pela banca. O trabalho foi apresentado na forma artigos, escritos na língua inglesa, sendo todos os três manuscritos submetidos a periódicos especializados. A tese foi considerada de bom nível e atende plenamente as exigências para uma tese de doutorado.

Finalmente, a banca examinadora decidiu por unanimidade aprovar a tese de doutorado.
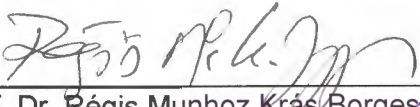
Belém, 22 de outubro de 2018.

_____
Prof. Dr. Raimundo Netuno Nobre Villas (Orientador – UFPA)

_____
Prof.ª Dr.ª Lena Virgínia Monteiro (USP)

_____
Prof. Dr. José Haroldo da Silva Sá (UFBA)

_____
Prof. Dr. Régis Munhoz Krás Borges (UFPA)

_____
Prof. Dr. Candido Augusto Veloso Moura (UFPA)